/
Article / Book Information

( )	
Title(English)	Seismic Performance and Preliminary Design Procedure for Low-Rise Wooden Horizontal Hybrid Structure with Rigid Core
( )	WuDi
Author(English)	Di Wu
( )	: ( ), : , : 11097 , :2019 3 26 , : , : , , , ,
Citation(English)	Degree:Doctor (Engineering), Conferring organization: Tokyo Institute of Technology, Report number: 11097 , Conferred date:2019/3/26, Degree Type:Course doctor, Examiner:,,,,
( )	
Type(English)	Doctoral Thesis

Doctoral Dissertation for Year 2019

Seismic Performance and Preliminary Design Procedure for Low-Rise Wooden Horizontal Hybrid Structure with Rigid Core

Supervisor

Professor Sakata Hiroyasu

Department of Architecture and Building Engineering
Tokyo Institute of Technology

Wu Di

Abstract

In 2010, Japanese government issued a law to promote the utility of large-scale wooden structure in public facilities, such as schools, gyms and libraries. Such facilities are generally low-rise buildings with large inner space and require critical disaster prevention, for instance, fire and seismic scenario, which challenges the traditional wooden building techniques. In the past few decades, the utility of such large-scale wooden structure has been constrained compulsively by the building codes in many countries. Although the wooden structure has shown some good seismic performance on account of its light-weight, flexibility and ductility, those terms substantially restrict the building area size and structural stories, considering that the smaller the area, the lower risk of the fire.

Comfortingly, the situation now is changing with the development of new fireproofing and construction techniques. One alternative method to lift the inherent limitation of the wood is using the hybrid structure. Hybrid construction allows the designer to combine the best attributes of wood and other material to improve performance, economics and occupant satisfaction in a way that might not be possible using only one of the material and its associated construction techniques. In 2012, Architectural Institute of Japan (AIJ) presented a prototype of horizontal wood-concrete hybrid building in school construction to explore the feasible techniques and implementation of the large-scale wooden structure, also as a response to the issued law in 2010. Since the seismic activity in Japan is above the average, the seismic performance of the prototype is highly worthy of note. Take it as an opportunity, the seismic performance of such horizontal hybrid structure is then studied in this research.

The thesis is organized into six chapters as follows:

Chapter 1 introduces the background of the application of wooden hybrid structure and conducts relative literature review. The main objects of the study is highlighted and the scope of the studied structure is delineated.

Chapter 2 introduces the shaking table tests on three 1/3-scale specimen of wooden horizontal hybrid structure. In this chapter, a target-drift-based design process is proposed and the influence of the diaphragm stiffness is investigated as well as the influence of the shear wall configuration. In addition, the engineering interested parameters such as shaking mode, maximum displacement, story drift, peak acceleration and force distribution are also studied. From the test results, the basic characteristic of the wooden horizontal hybrid structure is reviewed.

Chapter 3 builds a 3D discrete numerical model in *OpenSees*. A modified subroutine material was proposed to simulate the wood shear wall and diaphragm. The accuracy of the numerical model was confirmed by the comparison between the analytical results and the shaking table tests

in Chapter 2.

Chapter 4 extends the numerical model proposed in Chapter 3, by changing some concerned design features, such as the stiffness ratio between the core part and the wood part and the stiffness ratio between the diaphragm and the wood shear wall. A quantitative evaluation on the concerned design feature is provided. Some specified values for the design features were suggested and a simple method to evaluate the shear distribution between the diaphragm and the shear wall was proposed.

Chapter 5 proposes a simple design procedure for determining the concerned seismic shear force of the wooden horizontal hybrid structure in the preliminary linear design. The dual equivalent lateral force (DELF) method is presented that permits the extension of the equivalent lateral force (ELF) method by separating the hybrid structure into two independent substructures. The prediction of the DELF method is reasonable when compared with the result of modal response spectrum (MRS) method.

Chapter 6 presents the conclusions drawn from this study, the conclusions from each chapter are outlined.

Contents

Notation

Chapter 2

A_i	vertical distribution factor of *i*-story
C_i	seismic shear coefficient of *i*-story
C_o	standard shear coefficient
FEMA	Federal Emergency Management Agency
F_{tot}	total base shear derived from accelerometer
M_i	seismic mass of *i*-story in wood part
M_{tot}	seismic mass of wood part
PGA	peak ground acceleration
P_i	shear strength at design drift
P_y	design shear force of shear wall at one frame
Q	total design base shear force of wood part
Q'	modified design base shear force of wood part
$Q_{diap,n}$	maximum seismic shear force transferred to the core part by diaphragm of *n*-story
Q_{real}	recorded base shear force of wood part
Q_{tot}	total base shear recorded by force transducer
$Q_{wall,i}$	maximum seismic shear force sustained by wood shear wall of *i*-story
R_i	percentage of shear force sustained by wood shear wall
R_t	vibration characteristic factor
W_C	design weight of additional concrete mass
W_{tot}	total design weight of wood part
$W_{tot,real}$	real weight of wood part
W_W	design weight of wood part
Z	seismic zone factor
λ	ratio between Q and Q_{real}

Chapter 3

a, b, c	stiffness degradation parameter in *MSAWS* material
C	damping matrix in *OpenSees*
D_y	displacement at the yield strength
F	strength of *MSAWS* material
F_0	intercept strength of MSAWS material for the asymptotic line to the envelope curve

F_I	intercept strength of *MSAWS* material for the pinching branch of the hysteretic curve
K_{comm}	committed stiffness matrix
$K_{current}$	current stiffness matrix
K_{init}	initial stiffness matrix
K_p	stiffness of the reload branch to the envelope curve in *MSAWS* material
K_q	stiffness of the pinching branch in *MSAWS* material
M	mass matrix in *OpenSees*
MSAWS	modified *SAWS*
OpenSees	Open System for Earthquake Engineering Simulation
P_y	yield strength
$Q_{dia,n}$	maximum seismic shear force transferred to the core part by the diaphragm of *n*-story
$Q_{wall,i}$	maximum seismic shear force sustained by the wood shear wall of *i*-story
R_i	percentage of shear force sustained by wood shear wall
S_0	initial stiffness of the envelope curve in *MSAWS* material
S_1	stiffness of the asymptotic line to the envelope curve in *MSAWS* material
S_2	stiffness of the descending branch in the envelope curve in *MSAWS* material
S_3	stiffness of the unloading branch off the envelope curve in *MSAWS* material
S_4	stiffness of the pinching branch at Δ_u in *MSAWS* material
SAWS	seismic analysis of wood frame structures
S_q	stiffness of the tangent of the envelope curve through the pinching point in *MSAWS* material
α_M	mass coefficient of Rayleigh damping
β_K	stiffness coefficient of Rayleigh damping
Δ	displacement of *MSAWS* material
Δ_F	final displacement of *MSAWS* material
Δ_{max}	displacement at the intersection point of the reloading branch and the envelope curve in *MSAWS* material
Δ_u	displacement of *MSAWS* material at ultimate strength
ξ_i	damping ratio of *i*-mode
ω_i	circular frequency of *i*-mode

Chapter 4

k_C'	stiffness of the core part normalized by the mass ratio β
k_0	series stiffness of the diaphragm and the core part
k_C	initial stiffness of the core frame
k_D	initial stiffness of the diaphragm
k_S	initial stiffness of the wood shear wall
m_C	lumped mass of the core part
m_W	lumped mass of wood part
Mw	moment magnitude scale
PGA	peak ground acceleration
PGV	peak ground velocity
Q_D	shear force transferred to the core part through the diaphragm
Q_i	lateral shear force of the wood part in i-story
Q_S	shear force transferred to the ground through the wood shear wall
R_jb	fault-source distance
Vs30	average seismic shear-wave velocity from the surface to a depth of 30 meters
α	core-wood stiffness ratio
β	core-wood mass ratio
γ	core-wood formal frequency ratio
δ	diaphragm-wall stiffness ratio
ρ	seismic force percentage sustained by the wood shear wall

Chapter 5

C_n	vertical distribution factor of n-story
$C_{n,\mathrm{A}}$	vertical distribution factor of n-story in Substructure A
C_p	participation factor of the total weight of the structure
C_s	seismic response coefficient of hybrid structure
d_r	displacement of the roof
$F''_{n,\mathrm{C}}$	seismic force of the node at n-story in the core part calculated using ELF method
F_n	lateral seismic force of n-story
$F_{n,\mathrm{A}}$	lateral seismic force of n-story in Substructure A
$F_{n,\mathrm{C}}$	combined seismic force of the node at n-story in the core part
F_{nx}	combined seismic force of the node at m-story, x-frame in the original structure
$F_{nx,\mathrm{A}}$	lateral seismic force of the node at n-story, x-frame in Substructure A

g   gravity acceleration, set to 9.8m/s^2 in this paper

h_n height of n-story

$h_{n,A}$ height of n-story in Substructure A

$\boldsymbol{k}$ stiffness matrix of the linear model

K_d stiffness of the diaphragm

K_s stiffness of the wood shear wall

$\boldsymbol{m}$ mass matrix of the linear model

M_i seismic mass of node i

m_{mx} seismic mass of node at m-story, x-frame

N number of stories

N_A number of stories in Substructure A

Q_n shear force transferred to the core part though the diaphragm of n-story

$R_{A/B}$ weighting factor of Substructure A/B

S total maximum response

S_a spectral acceleration of the concerned ground motion

$Sa(T_j)$ spectral acceleration at the period of mode j

S_j maximum response of mode j

T_1 natural period of the structure

V total design base shear

V_W total design base shear

W total effective seismic weight

W_n seismic weight of n-story

$w_{n,A}$ seismic weight of n-story of the wood part in Substructure A

w_{nx} seismic weight of the node at n-story, x-frame

W_W total effective seismic weight of the wood part

γ_j participation factor for mode j

ω_j frequency of jth mode of the linear model

Φ_j jth mode of the linear model

1   Introduction

1.1   Back ground and motivation

In 2010, Japanese government issued a law ("the Act for Promotion of Use of Wood in Public Buildings," Law No. 36 of 2010) to promote the utility of large-scale wooden structure in public facilities, such as schools, gyms and libraries. Such facilities are generally low-rise buildings with large inner space and require critical disaster prevention, for instance, fire and seismic scenario, which challenges the traditional wooden building techniques. In the past few decades, the utility of such large-scale wooden structure has been constrained compulsively by the building codes in many countries (BCJ 2016; Ministry of Construction 2003; NRCC 2005). Although the wooden structure has shown some good seismic performance on account of its light-weight, flexibility and ductility, those terms substantially restrict the building area size and structural stories, considering that the smaller the area, the lower risk of the fire.

Comfortingly, the situation now is changing with the development of new fireproofing and construction techniques. One alternative method to lift the inherent limitation of the wood is using the hybrid structure. Hybrid construction allows the designer to combine the best attributes of wood and other material to improve performance, economics and occupant satisfaction in a way that might not be possible using only one of the material and its associated construction techniques (Canada Wood Group 2017). Wooden hybrid structure is usually built in different levels: element level and system level. The element level means the wood and other material are combined in a structural member, that is, hybrid beam, column, joint, diaphragm and wall. Studies have indicated that the hybrid members generally have superior performance than the one made of single material (Ahmadi and Saka 1993; Gelfi *et al.* 2002; Steinberg *et al.* 2003; Goertz *et al.* 2017).

Furthermore, the system level signifies that the relatively independent systems composed of different materials work cooperatively in a coherent building. Existing wooden hybrid structure of system level generally consist of three types: vertical type, horizontal type and composite type. Fig. 1.1 illustrates the representative structural design of the three types. The vertical hybrid structure usually comprises a wooden superstructure and a supporting concrete podium. The horizontal hybrid structure signifies that a ground-based wood structure is connected to an adjacent rigid core structure which is usually built with concrete or steel. While the composite type has both the characteristics of the former two types. The basic design idea of the wooden hybrid structure is to decrease the structural mass by using lightweight wood instead of concrete or steel, thereby reduce the seismic force when subjected to earthquakes. Also, for certain types,
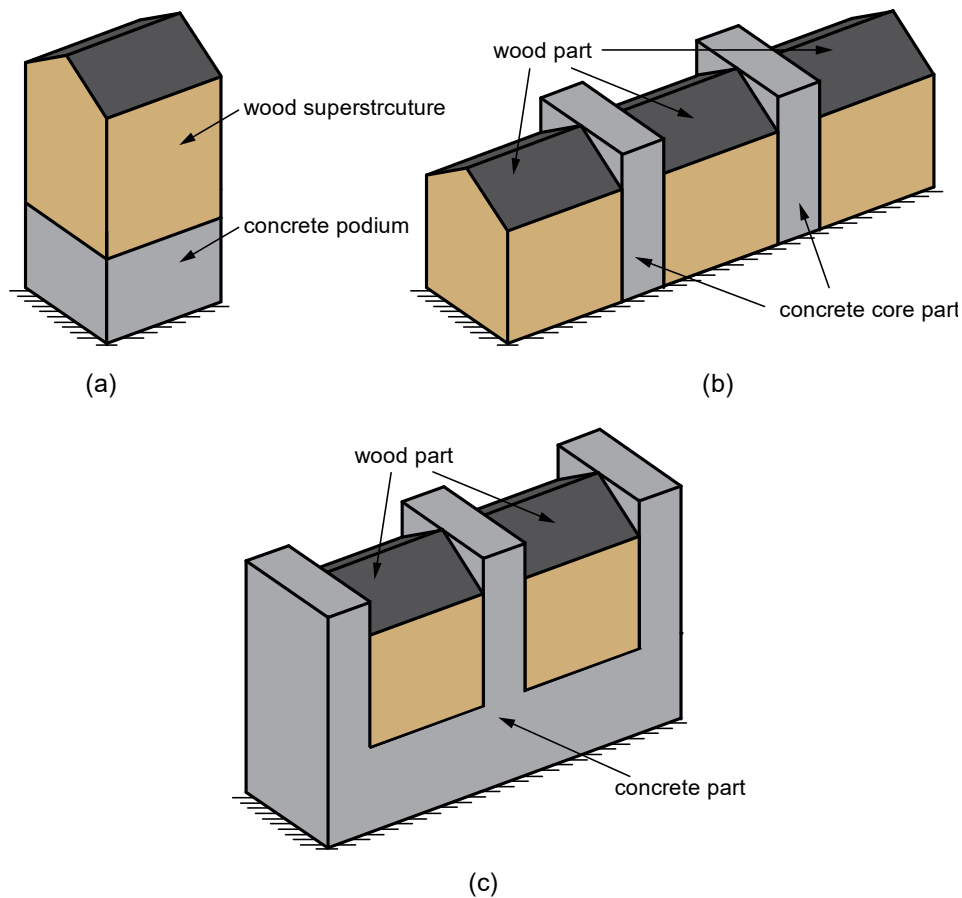
Fig. 1.1 Typical design of wood based hybrid structure (a) vertical type, (b) horizontal type, (c) composite type

such as horizontal and composite type, the flammable wood part is physically separated by the fireproof concrete part which is favorable for the fire prevention design.

Several engineering practices of wooden hybrid structure have been built around the world. Fig. 1.2 is a typical vertical hybrid building in America, comprised of concrete-built retail spaces in the ground story and 46 residential units in the upper five wood-frame stories (Canada Wood Group 2017). Fig. 1.3 shows the OGAL Plaza in Iwata, Japan. It is a large public facility with two stories. Benefitting from the wood-concrete horizontal hybrid design, the dimension in the span direction reaches 28 meters which could provide huge indoor space. Fig. 1.4 demonstrates a variant of wooden vertical hybrid structure in Canada. The concrete cores are placed in the middle of the building rather than at one side as the horizontal type shown in Fig. 1.1(b). The location of the concrete resisting system is designed for maximizing the resistance to torsion under lateral loads (Christian Dagenais&ref15). Fig. 1.5 illustrates the teaching building

Fig. 1.2 Vertical hybrid type in Cornerstone Condominiums, Portland, OR: Innovative Housing, Inc.*
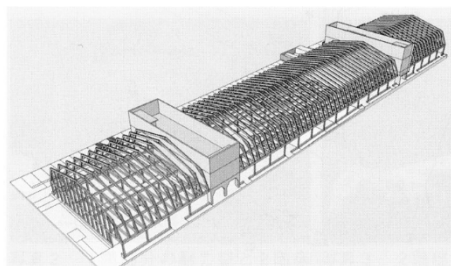
| (a) | (b) |

Fig. 1.3 Horizontal hybrid type in Iwata, Japan: OGAL Plaza (a) structural drawing, (b) interior view*

| (a) | (b) |

Fig. 1.4 Horizontal hybrid type in Quebec, Canada: FondAction CSN office building (a) exterior picture, (b) structural drawing*

---

* see Appendix A

(a)

(b)

Fig. 1.5 Composite hybrid type in Kamakura, Japan: Eiko Gakuen High School (a) front view, (b) back view*
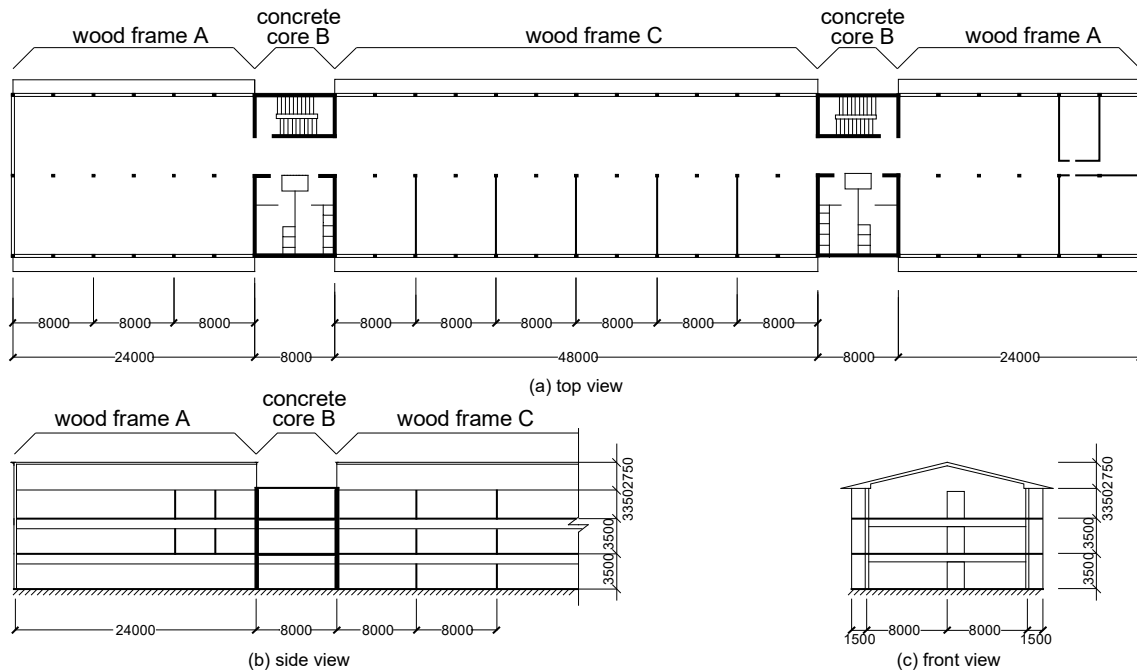

Fig. 1.6 Design prototype of horizontal hybrid structure proposed by AIJ (dimension in millimeters)
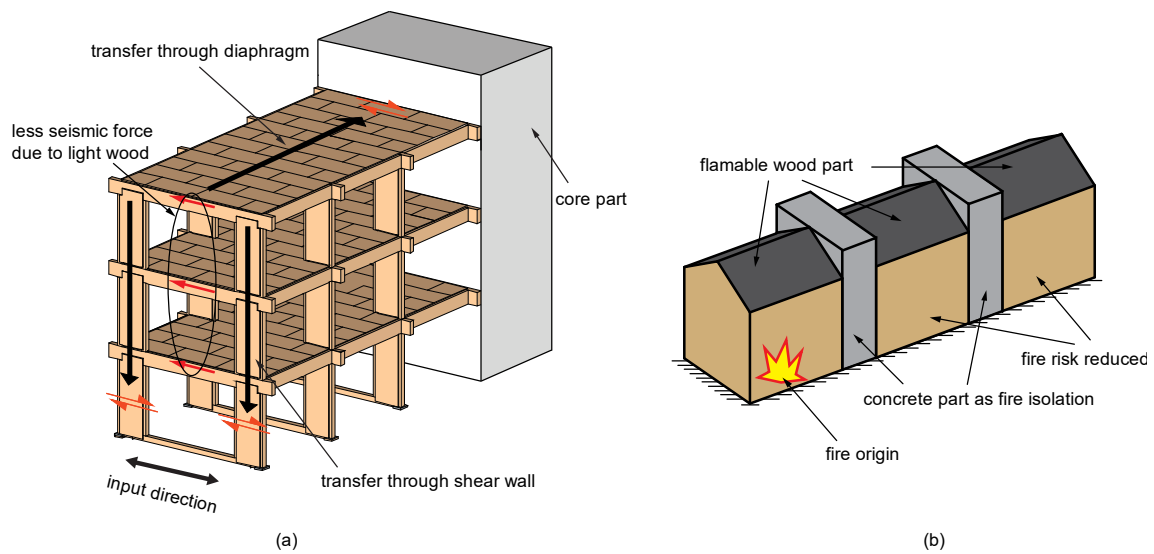
---

* see Appendix A

Fig. 1.7 Advantages of wooden horizontal hybrid structure (a) seismic resistance, (b) fireproofing

of Eiko Gakuen High School in Kamakura, Japan. The two-story building is a composite type hybrid structure. The first floor and the staircase are built with reinforced concrete while the second floor is built with wood discontinuous beam and wood-wrapped steel column. In this case, the wood part on the second floor is encircled on three sides by the concrete part. In 2012, Architectural Institute of Japan (AIJ) presented a prototype of horizontal wood-concrete hybrid building (Fig. 1.6) in school construction to explore the feasible techniques and implementation of the large-scale wooden structure (Inayama *et al*. 2012), also as a response to the issued law in 2010. Since the seismic activity in Japan is above the average, the seismic performance of the prototype is highly worthy of note. Take it as an opportunity, the seismic performance of such horizontal hybrid structure is then studied in this research.

1.2 Advantage of wooden horizontal hybrid structure

The idea of the hybrid structure is to utilize the advantages of various building material while overcome the disadvantages. The used materials usually have opposite characters, hence the materials could be complementary to each other rather than intensifying the disadvantages. For the wooden horizontal hybrid structure in this research, wood material and concrete material have multiple opposite characters: 1. wood is light-weight and concrete is heavy; 2. wood is ductile and concrete is fragile; 3. wood is flammable and concrete is fire-resistant; 4. wood has low strength and concrete has high strength. In the prototype, the wood part could light the weight of the whole building to reduce the total seismic force during earthquake (Fig 1.7(a)). The concrete part could sustain the shear force transferred through the diaphragm to mitigate the demands of

the wood part and hence provide large inner space in the wood part. On the other hand, the wood part is separated into several independent section by the concrete part. In case of fire alarm, the fire-resistant concrete part could slow the spread of fire and make time to minimize the damage (Fig 1.7(b)).

1.3 Previous study on system level wooden hybrid structure

To study the properties of system level hybrid structure, several efforts have been made:

Xiong and Jia (2008) presented a full-scale shaking table test on vertical wood-concrete hybrid structure consists of a 2-story wooden superstructure supported by a concrete base floor. Five specimens have different lateral story stiffness ratio varying from 2 to 12 between the concrete part and the wood part. The specimens were subjected to earthquake input with PGA up to 0.5g. The results showed that as the story stiffness ratio of the concrete to wood increased, the response of structure decreased. It is also found that the simplified natural period evaluation equation for normal structure can be used on hybrid structure with symmetric and regular configuration.

Zhou *et al*. (2014) analyzed numerical models of a 6-story light wooden frame with connection to a reinforced masonry core. The masonry core was in the middle of the building and surrounded by the wood shear wall subsystem. The numerical model of the wood shear wall and the masonry shear wall were elastic-perfectly plastic curve which has the equivalent energy with test results. The nonlinear response indicated that the existence of the masonry core significantly reduced the building story drift at the cost of an increase in the total base shear demand. For models with masonry core stiffness designed to be 25, 50 and 100% of the wood subsystem, the maximum lateral drift of the wood subsystem reduced to 79, 62 and 48% of the drift of a pure wood duplicate.

Yamazaki and Sakata (2016) proposed a simplified modeling method of wooden horizontal hybrid structure. The wood part and the core part were considered to be independent in vibration because of the difference of their fundamental periods. The basic vibration properties of the wood part in the hybrid structure was simulated by the two-dimensional continuous body. Based on the method, the vibration mode and member forces of the hybrid structure were predicted and evaluated. Conventional formula of seismic shear coefficient distribution was also developed for horizontal hybrid structure and the accuracy was reasonable compared with earthquake response analysis.

Isoda *et al*. (2016; 2017) conducted a series of shaking table tests on wooden frame-reinforced concrete core horizontal hybrid structure. Three specimens were tested: a one-story building with flexible plywood diaphragm, a one-story building with rigid RC diaphragm and a two-story building with flexible plywood diaphragm. The tests found that the performance of the wood

frame was governed by the inelastic deformation of the connections and the damage to the wood frame could be reduced by increasing the rigidity of the floor diaphragm since the shear force will be concentrating at the RC core. However, due to the inherent plan irregularity, the connection was vulnerable to several earthquake during which pounding may happen at the connection.

Mortazavi *et al*. (2016; 2017) investigated the seismic performance of a single-story building with a nonlinear flexible roof diaphragm which was made of steel decks or wooden deck panels and also proposed design expressions for such type of buildings. In the proposed approach, the flexible diaphragm was designed to act as the energy dissipating system and the nonlinearity of the diaphragm did not make a significant difference in the magnification of the internal forces.

Kaushik and Tannert (2017) studied a 30-story wood-concrete composite hybrid system using linear numerical simulation. In the model, concrete slabs at every third story provided the necessary stiffness and strength to resist gravity and lateral loads while the intermediate floors were constructed using light-frame wood to create the living spaces. A reduction of 41% in roof displacement was observed in the hybrid model due to the lower weight of the wooden part.

1.4 Research scope and objective

Previous research has demonstrated several advantages of the wooden hybrid structure. However, due to the absence of engineering practices and design process for the wooden hybrid structure in seismic region, the existing research mainly focused on numerical simulation. Meanwhile, those which included specimen tests usually addressed qualities required by a specific solution rather than considering various structural configurations and characteristics. Accordingly, there still has been a lack of empirical and experimental data especially on the wooden horizontal hybrid structure. Therefore, the main objects of this research are:

- Investigate the seismic performance of the wooden horizontal hybrid structure;
- Investigate the influence of different structural configurations of the wooden horizontal hybrid structure, such as stiffness ratio between the core part and the wood part, location of wood shear wall and stiffness of diaphragm;
- Propose a simplified approach to evaluate the seismic shear force distribution for the hybrid structure.

For the reason of simplicity and existing engineering practice, as well as the empirical test conducted by previous researchers, the wooden hybrid structures investigated in this study are limited to the following:

(1) The total number of stories of the structure is not greater than 3. Considering the potential application of such hybrid structure in large-scale public facilities, such as station, school and

hospital, the structure is designed to be low-rise and have a relatively small aspect ratio.

(2) The rigid core in the hybrid structure is connected to the wood part only on one side horizontally. Alternative design such as the prototype with rigid core intervals between wood parts, as shown in Fig. 1.1(b), is also acceptable since the symmetrical design of the prototype makes the Part A and half of the Part C have a similar seismic performance (Inayama *et al*. 2012). In that condition, only one group of wood part and core part is studied in this paper.

(3) The detailed design and deformation demand of the connection part is not the focus of this study since the design of the connection may vary in a wide range following the configuration of the wood part and the core part, resulting in manifold pending questions of the performance of the connection itself. Although the connection could affect the performance of the horizontal hybrid structure seriously, the scope of this study focus on the overall interaction between the wood part and the part due to the dynamic difference between the two parts. Therefore, in the numerical simulation, when the core part and wood part are fixed connected, the connection part is assumed to be rigid and efficient to transfer the internal force between the wood part and the core part.

1.5 Thesis organization

The thesis is organized into six chapters as follows:

- Chapter 2 introduce the shaking table tests on three 1/3-scale specimen of wooden horizontal hybrid structure. In this chapter, a target-drift-based design process is proposed and the influence of the diaphragm stiffness is investigated as well as the influence of the shear wall configuration. In addition, the engineering interested parameters such as shaking mode, maximum displacement, story drift, peak acceleration and force distribution are also studied. From the test results, the basic characteristic of the wooden horizontal hybrid structure is reviewed.

- Chapter 3 builds a 3D discrete numerical model in *OpenSees*. A modified subroutine material was proposed to simulate the wood shear wall and diaphragm. The accuracy of the numerical model was confirmed by the comparison between the analytical results and the shaking table tests in Chapter 2.

- Chapter 4 extends the numerical model proposed in Chapter 3, by changing some concerned design features, such as the stiffness ratio between the core part and the wood part and the stiffness ratio between the diaphragm and the wood shear wall. A quantitative evaluation on the concerned design feature is provided. Some specified values for the design features were suggested and a simple method to evaluate the shear distribution between the diaphragm and

the shear wall was proposed.

- Chapter 5 proposes a simple design procedure for determining the concerned seismic shear force of the wooden horizontal hybrid structure in the preliminary linear design. The dual equivalent lateral force (DELF) method is presented that permits the extension of the equivalent lateral force (ELF) method by separating the hybrid structure into two independent substructures. The prediction of the DELF method is reasonable when compared with the result of modal response spectrum (MRS) method.

- Chapter 6 presents the conclusions drawn from this study. Recommendations for the future research about the wooden horizontal hybrid structure are outlined.

2   Seismic performance of wooden horizontal hybrid structure

2.1   Introduction

In 2012, Architectural Institute of Japan (AIJ) presented a prototype of horizontal wood-concrete hybrid building (Fig.1.6) in school construction to explore the feasible techniques and implementation of the large-scale wooden structure (Inayama *et al*. 2012), also as a response to the issued law in 2010. In that research, static and dynamic analyses were conducted using a simplified 2D linear model. The force and deformation demand of the prototype was studied. Since the model was linear, the failure mechanism of the hybrid structure was not clearly presented. Inspired by the design of the prototype, a series of tests were conducted in this research to study the seismic performance of wooden horizontal hybrid structure. As a pilot experiment, wood shear wall and diaphragm were tested first by quasi-static experiment to evaluate their strength. The quasi-static experiment is conducted by Hiyama (2015) and relative test information is present in Appendix B. Based on the pilot experiment, the specimens of the shaking table test were designed and tested under different input magnitudes. Sawada (2016) reported the detailed design and test procedure of the shaking table test and described the basic seismic performance of the test specimen, for instance, the description of the frequency and damping ratio, the displacement and story drift. Then the evaluation method of the seismic force for the horizontal hybrid structure is discussed, which was proposed by Yamazaki (2016). In this Chapter 2, the shaking table test on three 1/3-scale specimen is presented including part of the detailed design procedure of the specimen, the test observation and the corresponding assessment of the test result, most of which is not covered in the research of Sawada (2016)

2.2   Specimen design and test setup

2.2.1 Detailed design of specimen and test input

The detailed design and test procedure of the shaking table test is depicted in Appendix C. Only the design procedure of the additional weight is covered in this section.

2.2.2 Calculation of the additional weight

Several concrete bricks were fastened on each floor as additional mass, with a total weight of 19kN. The value derived from a series of pilot experiment (Hiyama 2016) in which the shear walls and the diaphragms were tested through quasi-static tests, individually. The detailed design of the pilot experiment is depicted in Appendix B. The design of the specimens in the pilot

experiment was the same with the 1/3-scale specimens in this shaking table test except for one difference, which was that the nail spacing of the shear wall in the pilot experiment is 33mm rather than 50mm in S1, S2 and S3. Hence, the design shear force of the shear wall P_y in S1 was estimated by simply multiplying the design shear strength P_i recorded in the pilot experiment by the factor $\alpha = 33/50$, which seemed to be reasonable compared with the shaking table results. Fig. 2.1 demonstrates the force-drift response of the tested shear wall in the pilot experiment and the shear strength P_i at the drift of 1/120.

The complete calculation procedure of the additional mass is as follows:

1. The revised Japanese seismic code featured a two-phase seismic design for earthquakes:
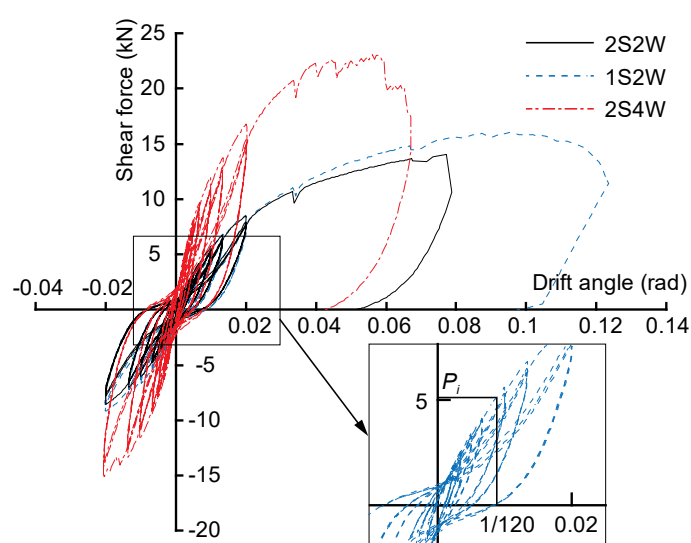

Fig. 2.1 Force –drift response of the shear wall and the shear strength at the design drift
in the pilot experiment

Table 2.1 Calculation for the weight of additional mass

Design	Level	Drift	P_i (kN)	$P_y = \alpha \times P_i$ (kN)	$Q = m \times P_y$ (kN)	C	W_{tot} (kN)	W_W (kN)	W_C (kN)	$W_{C,real}$ (kN)
Primary	IO	1/120	5	3.3	6.6	0.25	26.4	5	21.4	19

P_i : the shear strength of one wood shear wall frame recorded in pilot experiment with drift of 1/120

P_y : the design shear strength of one wood shear wall frame estimated for the specimen in this paper

m : the equivalent number of frame for the first floor, equaled to 2 for S1

primary seismic design for moderate earthquake scenario and secondary seismic design for severe one (Ministry of Construction 1980). According the seismic code, the relationship between seismic shear force and the structure weight used in this paper is presented in Eqs. (2.1-2.3)

$$Q = W_{tot} \times C_1 \tag{2.1}$$

$$W_{tot} = W_C + W_W \tag{2.2}$$

$$C_i = Z \times R_t \times A_i \times C_o \tag{2.3}$$

Where Q = the total design seismic shear force of the wood part; W_{tot} = the total design weight of the wood part; W_W = the design weight of wood frame; W_C = the design weight of the additional concrete mass; C_i = the seismic shear coefficient of i-story; Z = the seismic zone factor set to 1; R_t = vibration characteristic factor set to 1; A_i = vertical distribution factor of i-story (A$_1$ set to 1); C_o = the standard shear coefficient set to 0.25 for primary design.

2. In this paper, the primary design was conducted and, as a benchmark, S1 was supposed to reach the immediate occupancy (IO) level when subjected to moderate earthquake scenario. The IO level is defined by FEMA at which the story drift is around 1/100 radian (1/120 in this paper) and the structure begins to enter the inelastic range (FEMA 2000). According to the pilot experiment results (Hiyama 2016), the Q was determined firstly by the target story drift 1/120. When reached the IO level, the shear force distribution of the first floor was assumed to be triangle along the Y direction as shown in Fig. C.1. Therefore, the equivalent number of shear wall frame m =1/3+2/3+1=2 for the first floor. Then by Eqs. (2.1-2.3), the weight of additional concrete mass W_C attached to the specimens was calculated in Table 2.1. On account of the limits of the shaking table, mostly the allowed turning moment, 19kN was set to be the real weight of additional concrete mass $W_{C,real}$ in this test.

Several design features were worth noting. In the three specimens, S1 was the standard template and the shear force was designed based on it. In fact, the total weights of the wood part were nearly the same in the three specimens, 22.75, 22.73 and 24.25kN for S1, S2 and S3, individually. When subjected to same inputs, the specimens were supposed to sustain the approximate seismic shear force, which made it possible to compare the performance of the different design specimens. In addition, when calculating the design shear force of the specimen, the seismic force transferred to the core part by the diaphragm was not taken into consideration. For that reason, the overall design of the specimens was supposed to be conservative compared to a non-hybrid counterpart and therefore the additional concrete mass was implicitly insufficient for the specimens to reach the IO level in moderate earthquake scenario. The influence of the design features as well as its rationality was discussed in the following part.

2.3 Test observation

2.3.1 Low-amplitude test

Ground motions with PGA of 0.1, 0.2 and 0.4g were used as inputs initially. Visual inspection indicated that there was no visible damage after the first three tests. Fig. 2.2 shows the variation of natural frequency and damping ratio of the three specimens during the experiment. The natural periods of the three specimens were quite close, to be specific, 0.115s, 0.109s and 0.112s for S1, S2 and S3, respectively. The values of natural frequency and damping ratio changed slightly throughout the first three tests which indicated the specimens basically maintained their elastic status when subjected to moderate seismic scenarios.

2.3.2 High-amplitude test

The value of natural frequency and damping ratio changed apparently after the test of 0.6g and 0.8g, which indicated the damage accumulation and stiffness degeneration of the specimens. The frequency of S3 dropped more rapidly than S1 and S2 after input with PGA of 0.6g, which depicted that S3 was more vulnerable to strong ground motions due to less number of shear walls. The stiffness degeneration was mainly caused by the failure of the nail joints of the shear walls. Failure modes basically consisted of edge breakout and withdraw as shown in Fig. 2.3. Those two failure modes were also observed sporadically on the diaphragms. Although the stiffness of diaphragm and the arrangement of shear walls were different for three specimens, their failure patterns were nearly the same, that is, the shear walls of first floor at X1 sustained the most severe damage. In addition, for S3, the bolt of the joint between beam and column at X1 suffered the strain relaxation as shown in Fig. 2.3(d). This was caused by the lack of shear walls at the middle frames of the structure, in this case, the shear force endured by the beam-column joint was much higher than the one of S1 and S2.

(a) frequency   (b) damping ratio
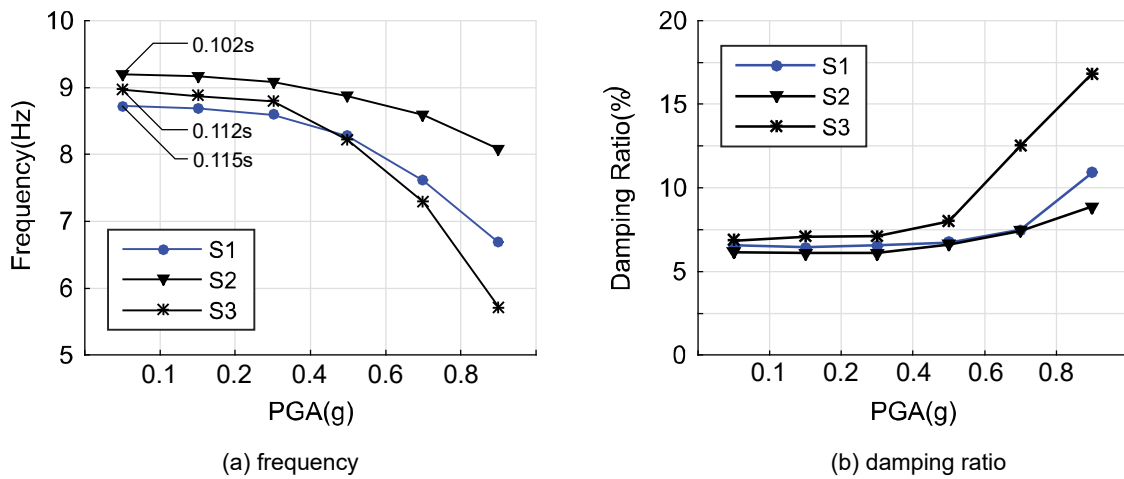
Fig. 2.2 Dynamic properties of fundamental mode of the specimens

(a) wall edge breakout   (b) diaphragm edge breakout

(c) nail withdraw   (d) bolt strain relaxation
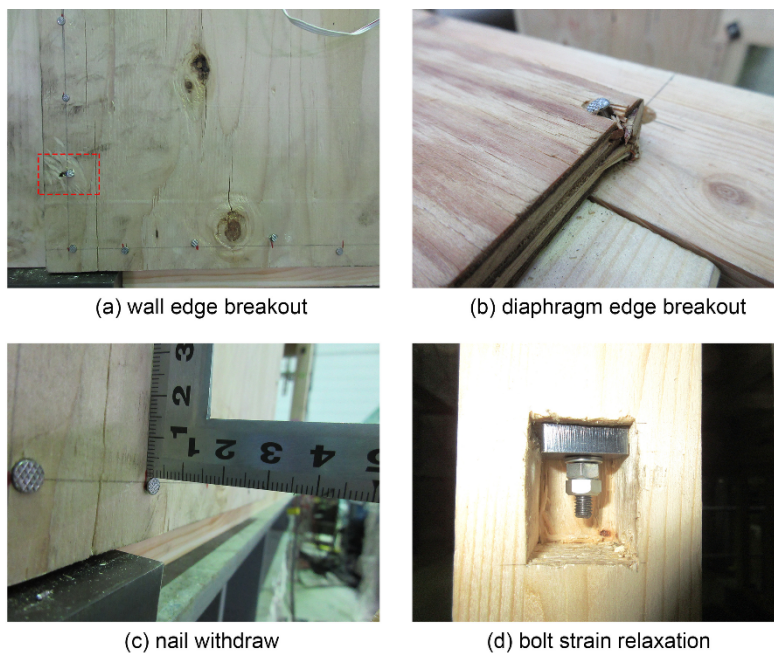
Fig. 2.3 Failure mode observed of the nail and the beam-column joint after input of 0.8g

2.3.3 Mode analysis

Fig. 2.4 demonstrates the vibration modes of S1 and S3 before the earthquake input. The vibration modes of S2 are mainly the same as S1 so they are omitted in the picture. It can be seen that the first modes of S1 and S3 were similar. The maximum displacement occurred at X1 of the third floor. The relative displacement decreased almost linearly from third floor to first floor and from X1 to X4. The vibration shape of the second and third mode shows several differences between the two specimens. The displacement of S3 was larger than S1 in the middle of the first floor. It is apparent that the lack of shear walls between middle studs made it easier for the X2 and X3 frames to participate into the vibration. Besides, although the core part was designed having a high lateral stiffness to simulate a rigid body, the mode analysis indicates that, to some extent, it participated in the vibration. However, since the response magnitude of the core part was minor contrasted with the flexible wood part, the following analysis would concentrate on the latter one. It is worth to point out that the specimen also sustained a lateral torsion during the tests. Considering its plane irregularity, the torsion was regarded as inevitable. This torsion could be derived from the twisting moment of the steel frame as well as the pullout of the connection joints between wood part and core part. Fig. 2.5 indicates that the torsion in first mode was coupling with the transverse vibration since they had the same dominant frequencies. The magnitude of the torsional movement was limited compared with the transverse vibration. Accordingly, the following study mainly focused on the response of the input direction and the torsion was omitted. The minor lateral and torsional response of the steel frame in the most concerned first mode also indicated that the steel frame was able to represent the concrete core of the prototype as expected in the design.

In all the three specimens, the first and third modes were mainly controlled by the wood part while the second mode was controlled by both the wood part and the steel part (Fig. 2.4). However, due to the different stiffness degeneration rates between the two parts, the order of the modes changed during the tests in S3. After the tests, the natural frequency of wood controlled modes (first and third mode) dropped from 8.7&16.4Hz to 5.1&11.9Hz, separately, meanwhile the frequency of steel controlled mode (second mode) dropped from 14.4 to 13.9Hz (Fig. 2.6). In this condition, the frequencies of wood controlled mode and steel controlled mode had a crossing, which caused a mix in vibration shape of the two parts. Fig. 2.7(a) depicts the second mode of S3 after the input of 0.8g, and the mode shape shows characteristics of the original third mode (Fig. 2.4(b)). Meanwhile, the third mode in Fig. 2.7(b) was highly alike with the original second mode (Fig. 13(b)). The influence of "frequency crossing" was not quite clear for now. A rough understanding was that it might slightly amplify the reaction of the wood part while mitigating
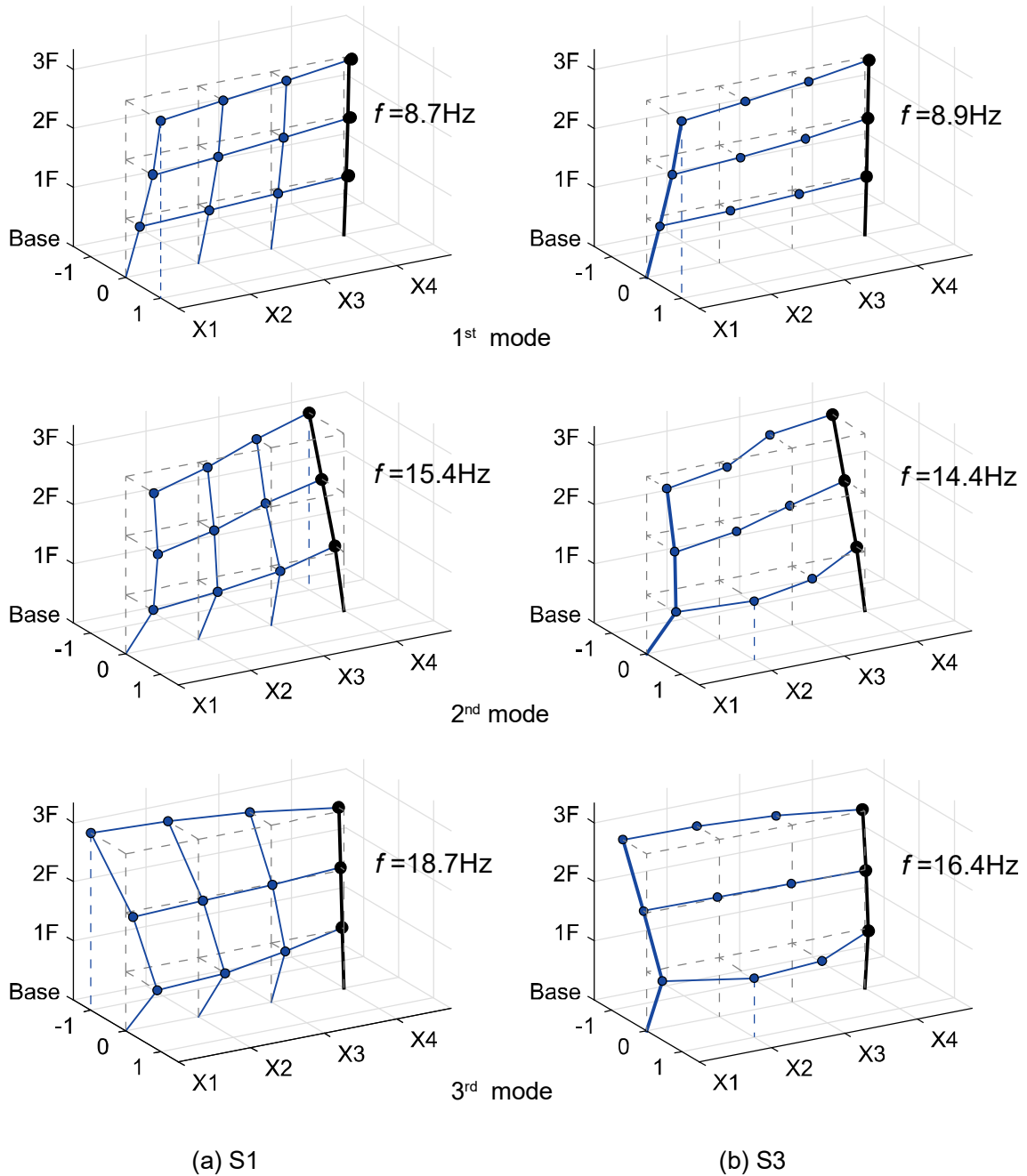
(a) S1   (b) S3
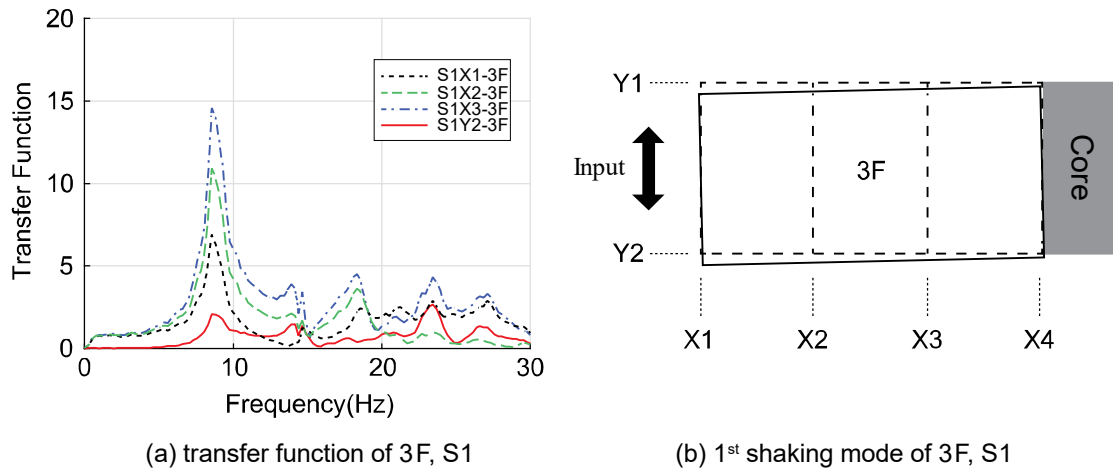
Fig. 2.4 First three vibration modes in S1 and S3 before input

(a) transfer function of 3F, S1   (b) 1st shaking mode of 3F, S1

Fig. 2.5 Transfer function of the roof acceleration and torsion component of the first vibration mode in S1

(a) transfer function of the wood part (X2) and core part (X4)   (b) mode frequency before the test and after 0.8g
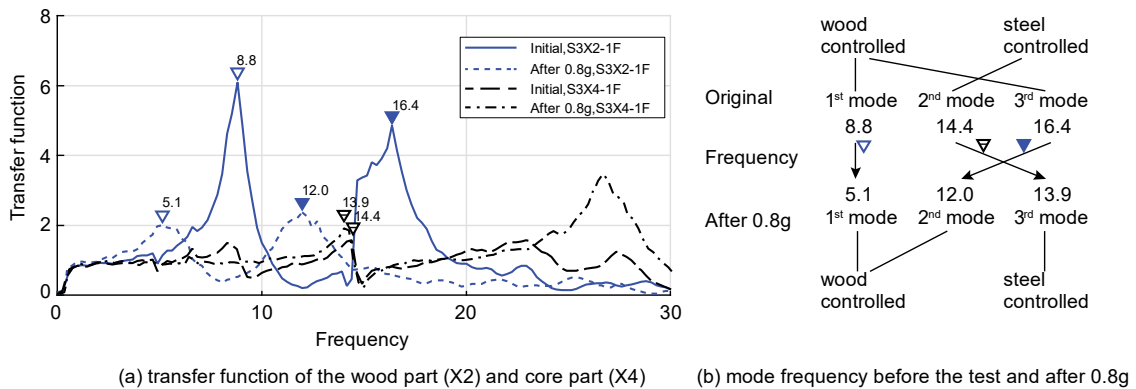
Fig. 2.6 Frequency crossing phenomenon observed in S3

the core part, since the crossing brought the wood controlled third mode forward to the second mode, which had a larger proportion in the vibration. However, it is noted that, in the prototype, the natural periods of the wood part and concrete core part were 0.51s and 0.08s respectively (Inayama *et al.* 2012). On account of the extreme high stiffness ratio between the two parts, the prototype was unlikely to sustain "frequency crossing". Despite that, the frequency approaching of the two parts might cause unexpected additional torsion to the hybrid system especially when the core part has a relative softer design than the specimen. Further study is needed on the

(a) 2nd mode   (b) 3rd mode
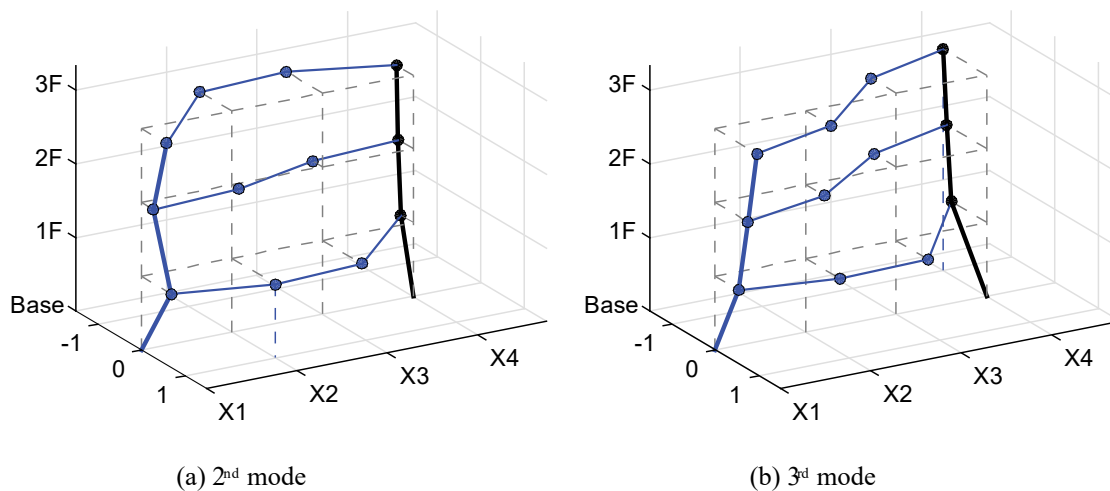
Fig. 2.7 Second and third mode of S3 after 0.8g when frequency crossing happened

influence of the frequency crossing phenomenon.

In normal conditions, the frequencies were discrete and independent for the different parts of hybrid structure, which made it possible to analyze the different part separately (Yamazaki and Sakata 2016). In spite of that, because of its unequal distribution of mass and stiffness, the horizontal hybrid structure might have vast degrees of freedom even with a few stories and small-scale, which made the natural frequency hard to identify as well as the vibration modes. Modal analysis was recommended to be conducted in multiple methods. Both transfer function and stochastic subspace identification method were used in this paper.

2.3.4 Displacement and story drift

The maximum relative displacement between wood part and shaking table during each test procedure is shown in Fig. 2.8 and Fig. 2.9. It can be inferred from the displacement shape that the vibration of the wood part at low-amplitude input was governed by the base mode, while at high-amplitude input the following mode started to participate in. Owing to its relatively rigid diaphragm, S2 manifested a good seismic performance during the whole test procedure with a slow and steady increment of node displacement. As a comparison, S1 and S3 both had a major increment of the displacement when the input rose from 0.6g to 0.8g. It also can be seen that S3 was the only specimen of which the maximum displacement occurred at the middle frame X2 rather than side frame X1. The lack of shear wall at the middle frame amplified the general displacement response in S3 especially for the severe inputs because the maximum roof displacement was -4.1%, 22.0% and 58.4% higher than S1 for 0.4g, 0.6g and 0.8g, separately. Table 2.2 is the detailed maximum inter-story drift angles during each test procedure. The influence of the conservative design was apparent. The specimens didn't reach the target drift (1/120) until the input raise to 0.6g while they were designed to reach that drift in moderate earthquake scenario whose PGA is around 0.2g. During the input of 0.8g, the maximum drift angle of the specimens were prevalently around 1/50, which is the significant damage (SD) level defined by FEMA (FEMA 2000).

Table 2.2 Maximum inter-story drift angle (unit: rad)

| | PGA | | | | | | | | |
| | 0.4g | | | 0.6g | | | 0.8g | | |
Floor	S1	S2	S3	S1	S2	S3	S1	S2	S3
3F	1/1049 X2	1/1022 X1	1/ 697 X2	1/ 597 X2	1/728 X1	1/365 X2	1/300 X2	1/499 X1	1/212 X2
2F	1/340 X1	1/288 X1	1/295 X2	1/212 X1	1/189 X1	1/120 X2	1/114 X1	1/137 X1	1/58 X2
1F	1/237 X1	1/191 X1	1/221 X2	1/112 X1	1/115 X1	1/97 X2	1/60 X1	1/85 X1	1/47 X2

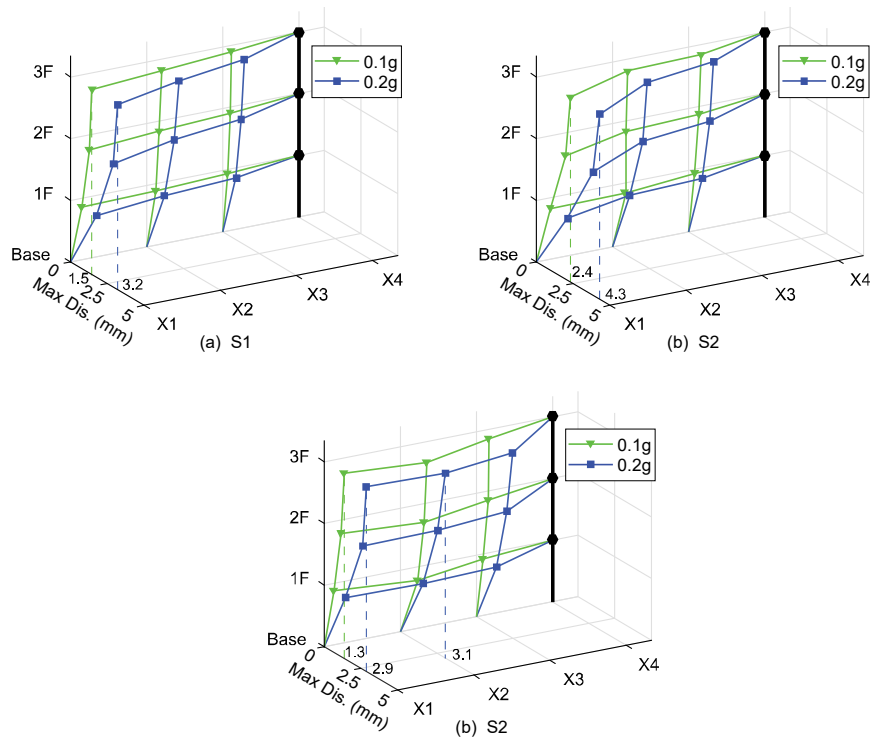Note: X# = grid where the maximum drift occurred

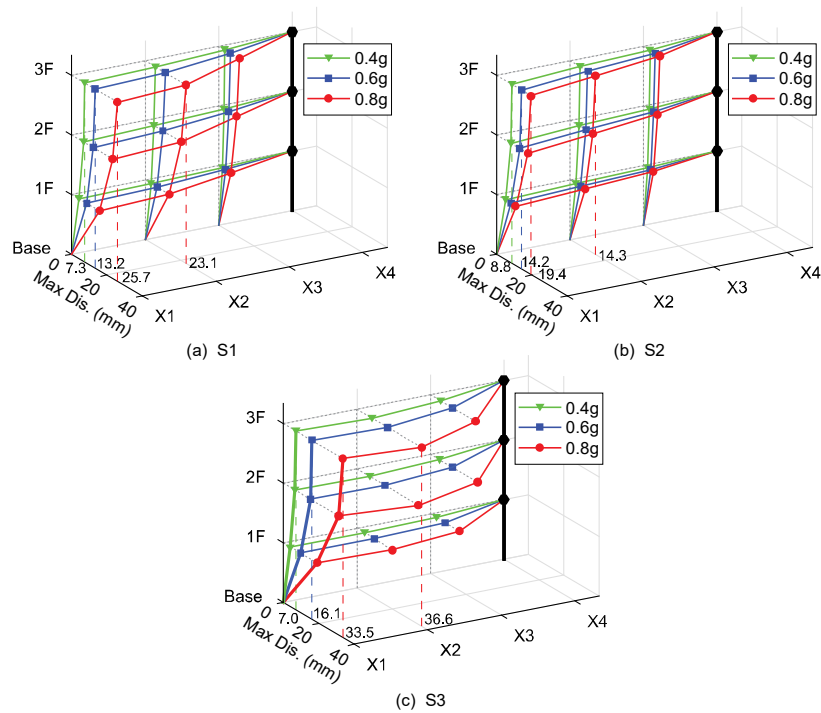Fig. 2.8 Maximum node displacement of the wood part with input of 0.1g and 0.2g

Fig. 2.9 Maximum node displacement of the wood part with input of 0.4g, 0.6g and 0.8g

2-11

2.3.5 Peak floor acceleration

Fig. 2.10 and Fig.2.11 presents the profile of maximum floor acceleration amplification calculated as the ratio between the floor acceleration (A_i) and the maximum table acceleration (PGA). For S1 and S3, the values of acceleration amplification fluctuated but overall, grew with the increasing PGA of the input. This was caused by the fact that the diaphragm connected to the steel frame was damaged and couldn't provide the constraint as it did in the low-amplitude input. In contrast, the amplification of S2 remained stable during the tests, which reflected that the force transfer system of S2 was not notably changed due to the rigid diaphragm. Meanwhile, towards the core direction, the acceleration amplification decreased from X1 to X3 on account of the constraint of the core part.

It is a notable fact that during the input of 0.2g, 0.6 and 0.8g, the maximum roof acceleration amplification at X1 in all three specimens exceeded 4 which was quite considerable compared
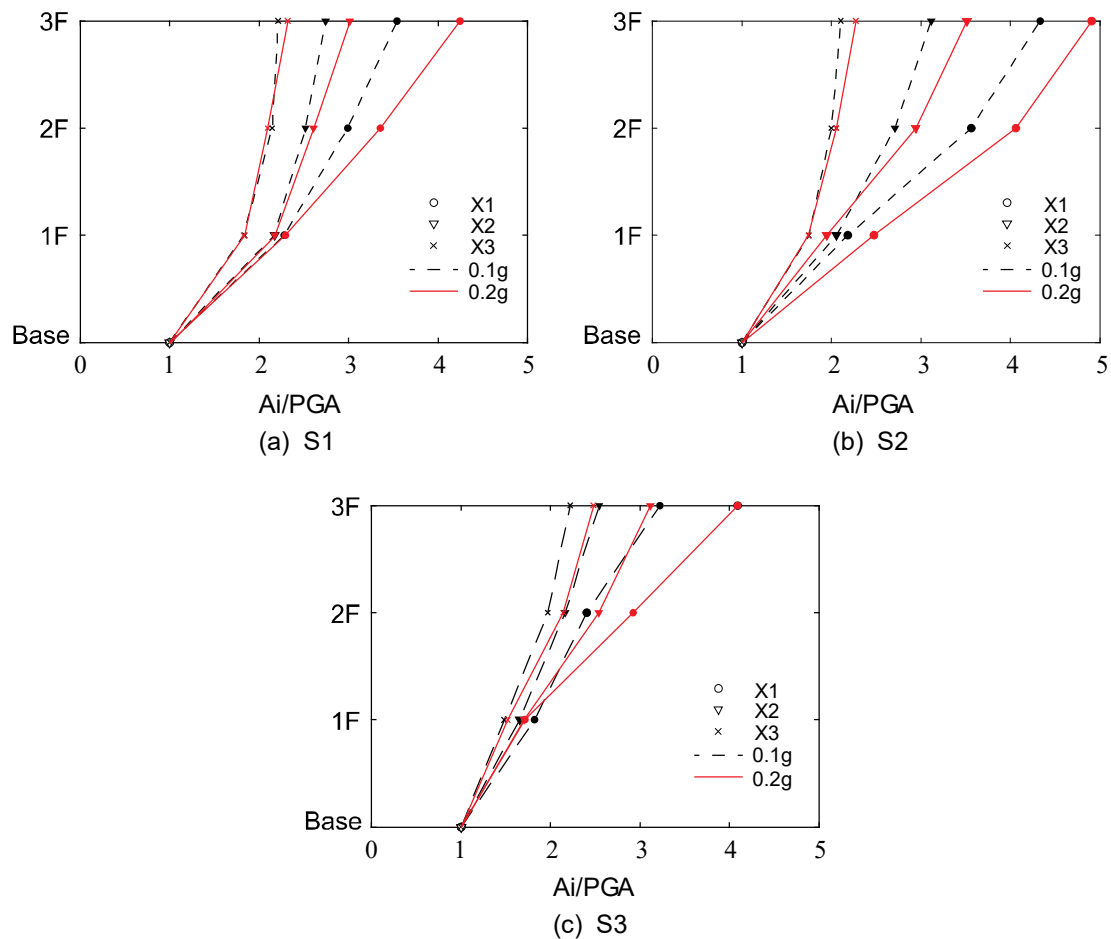

(a) S1   (b) S2

(c) S3

Fig. 2.10   Peak acceleration amplification along the height of the specimen with input of 0.1g and 0.2g
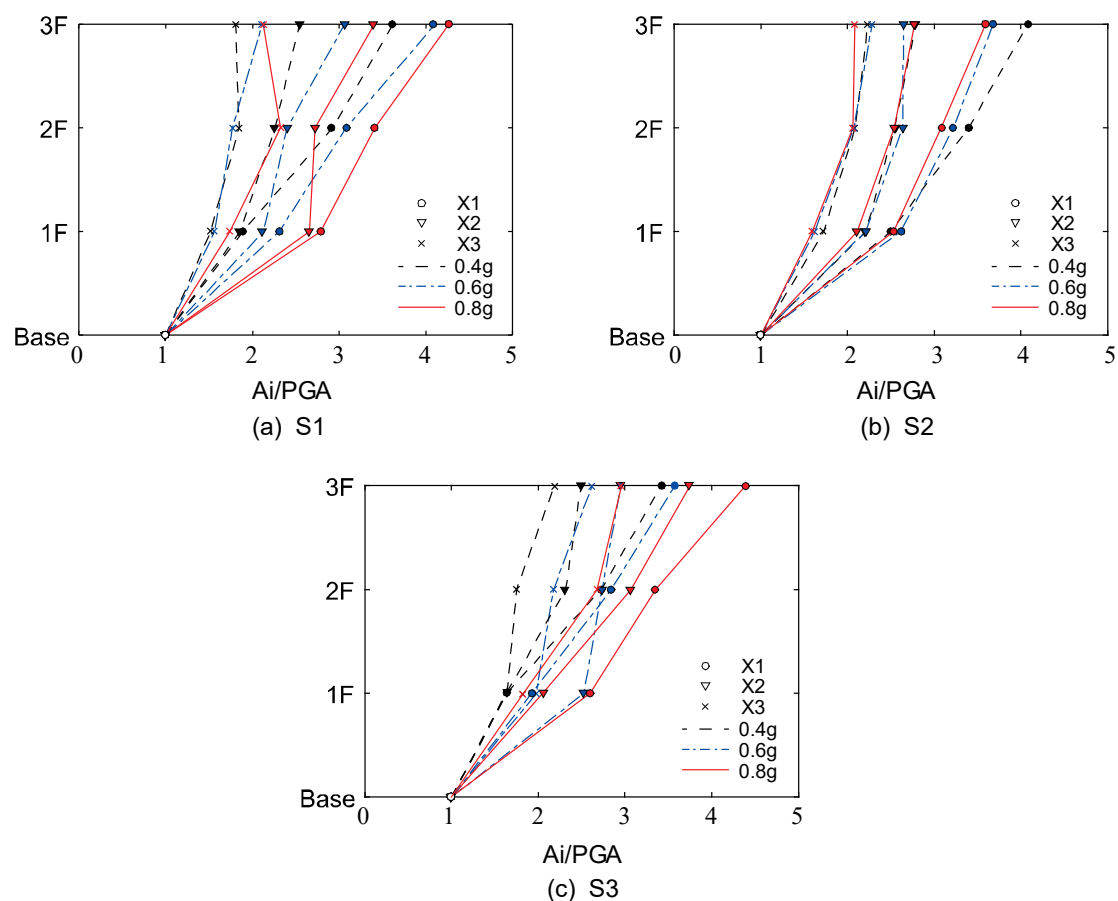
(a) S1

(b) S2

(c) S3

Fig. 2.11   Peak acceleration amplification along the height of the specimen with input of

0.4g, 0.6g and 0.8g

with the results of several existing shaking table experiments on non-hybrid wooden structures (Christovasilis *et al.* 2009; Filiatrault *et al.* 2009; Tomasi *et al.* 2015). Those previous full-scale experiments were conducted in a 2-story or 3-story building type and the recorded peak acceleration amplification varied from 1.2 to 2 with PGA from 0.84g to 1g. One major reason why the higher-than-normal amplification occurred in this paper was the fairly conservative design which made the seismic mass smaller than it should be. Although the scale factor of seismic acceleration was set to 1, the implicit factor was higher than 1 considering the reduced seismic mass in the specimen design (Table C.1). The other reason was the suddenly large lateral stiffness change between the wood part and the core part. On account of the similarity in the mechanism, potential bullwhip effect might happen when assuming the core part as a rigid base and the wood part as a soft superstructure. Consequently, the seismic response of the wood part

would be significantly amplified especially the top area far away from the core part. It should also be pointed out that the high height-width ratio accounted for the notable acceleration as well, since significant amplification was also recorded in a previous shaking table test of a seven-story wood structure (Ceccotti *et al*. 2013). As a matter of fact, high acceleration amplification was generally observed in the existing full-scale shaking table tests on system level wooden hybrid structure (Xiong and Jia. 2008; Isoda *et al*. 2017). Both in vertical hybrid and horizontal hybrid type, higher-than-normal acceleration amplification occurred even though the story drift and the damage of the structure were tolerable. Whether it was caused by the individual design or the inherent property of the wooden hybrid structure, on which further investigation was still needed. Up to now, the energy consumption system or seismic isolation system was expected to alleviate the high acceleration amplification by increasing the damping and confining the force transfer. In regard to the potential bullwhip effect, the limitation of the length to width ratio in the horizontal aspect was also supposed to mitigate the high acceleration amplification.

2.3.6 Hysteresis loop

To testify the accuracy of the shear force recorded by the force transducer, the total seismic force (F_{tot}) derived from the accelerometers on each floor is compared with the summation of shear force (Q_{tot}) recorded by the force transducers (Fig. 2.12). The result shows that they agreed well with each other, therefore, the shear force was accurate enough to evaluate the performance of the shear walls and diaphragms.

Fig. 2.13 to Fig. 2.16 show the force-displacement relationship of the shear walls and diaphragms. The loops have a clear backbone curve and typical pinched part at the origin point. When the PGA equaled to 0.4g, the linear relation of the curve indicated that both the shear wall and the diaphragm remained their elastic status well during the test.

With a shorter nail spacing, the rigid diaphragm of S2 shows a higher tangent stiffness than the one of S1. In both S1 and S2, when the input was 0.4g, the maximum shear forces of shear walls at frame X1 and X2 were nearly the same, yet the shear wall at X1 has higher deformation than the one at X2, whereas the demands of both shear force and deformation decrease at X3. The correlation remained constant when the PGA increased to 0.6g and 0.8g which implicitly indicated the transferred pattern of the shear force didn't change much during the test. It could also be found out that the middle columns bear a small amount of shear force in S3. Regardless of the core part, nearly 90% of the seismic force of the first floor was sustained by the shear walls in S3, which verified the assumption that the beam-column joint was nearly moment free.
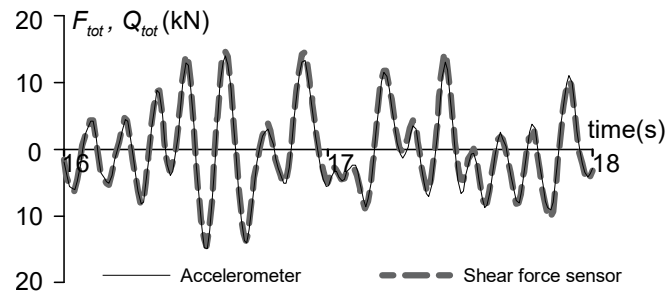
Fig. 2.12   Comparison of total seismic force derived from accelerometer (F_{tot}) and shear force sensor (Q_{tot})
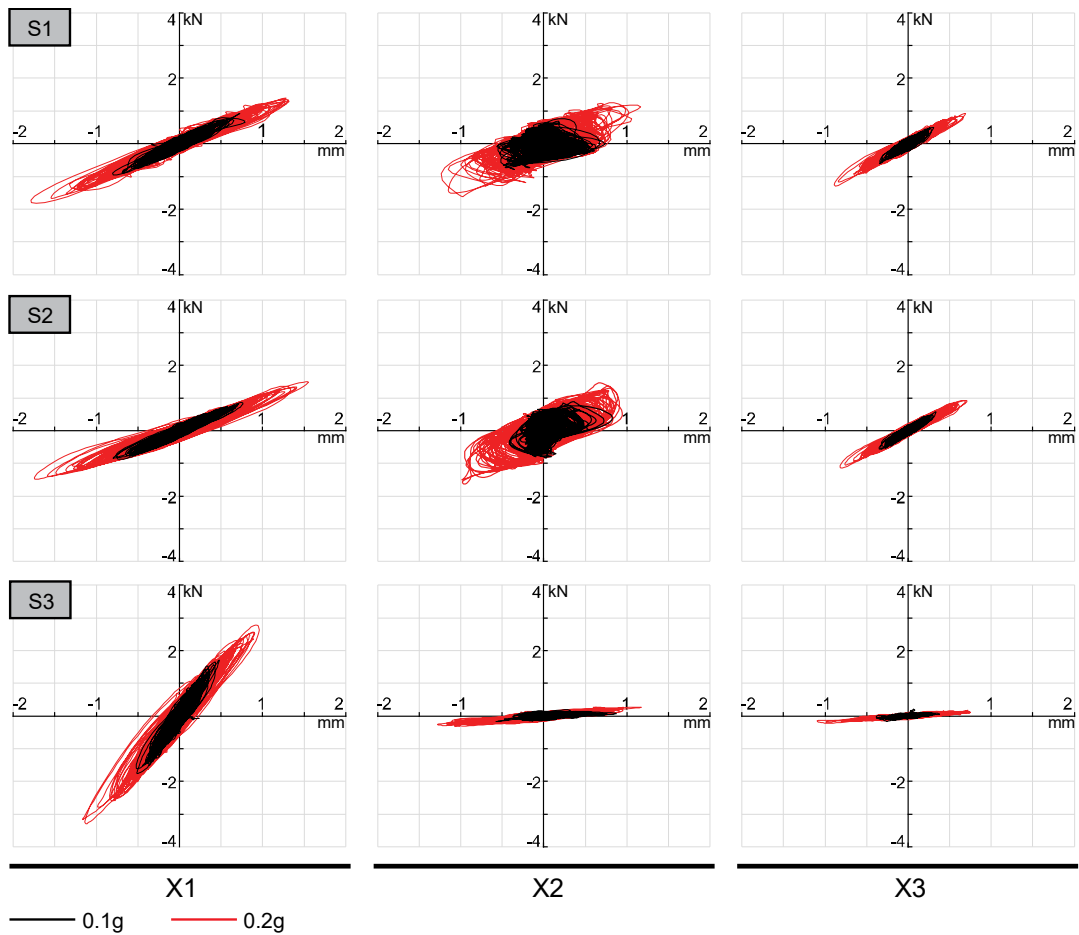
Fig. 2.13 Shear force-story displacement loops of shear walls on the first floor of S1, S2 and S3 with PGA=0.1g and 0.2g
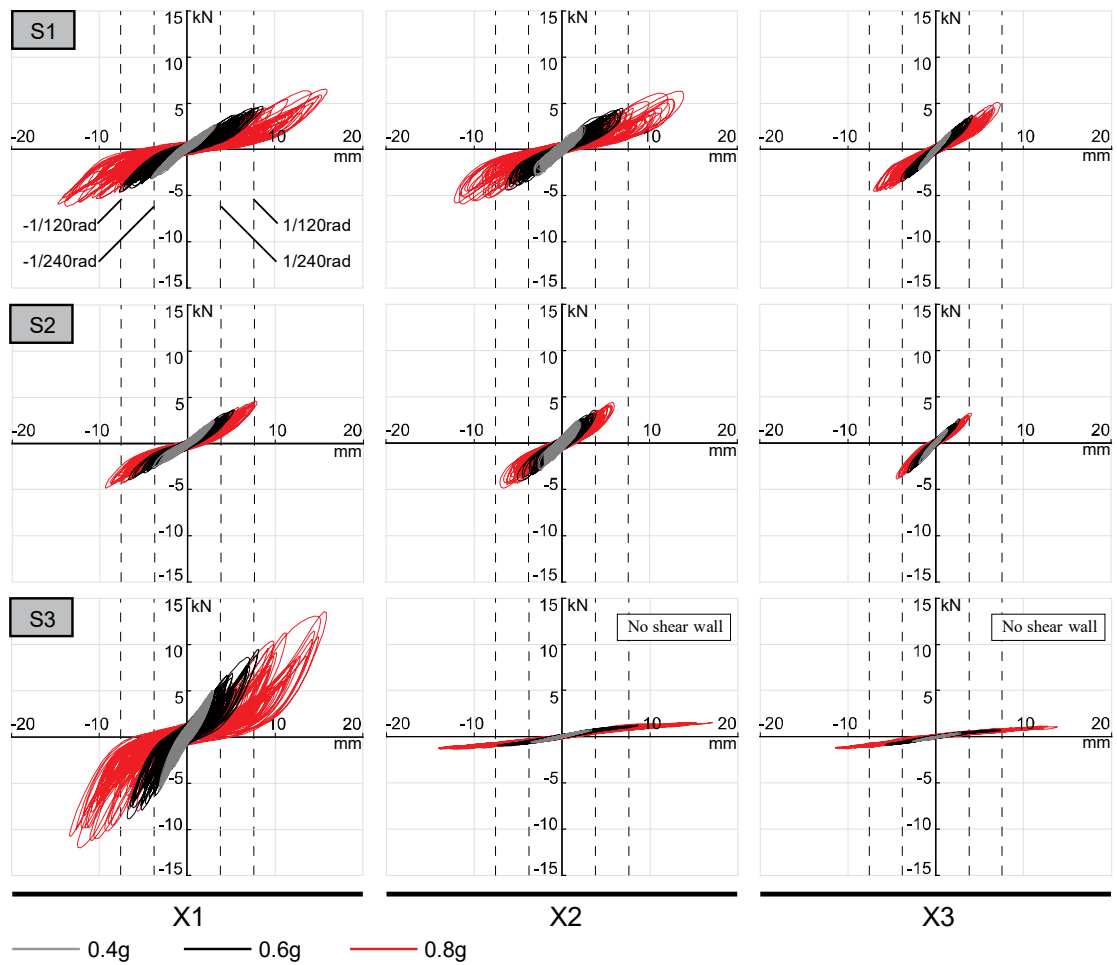
Fig. 2.14 Shear force-story displacement loops of shear walls on the first floor of S1, S2 and S3 with PGA=0.4g, 0.6g and 0.8g
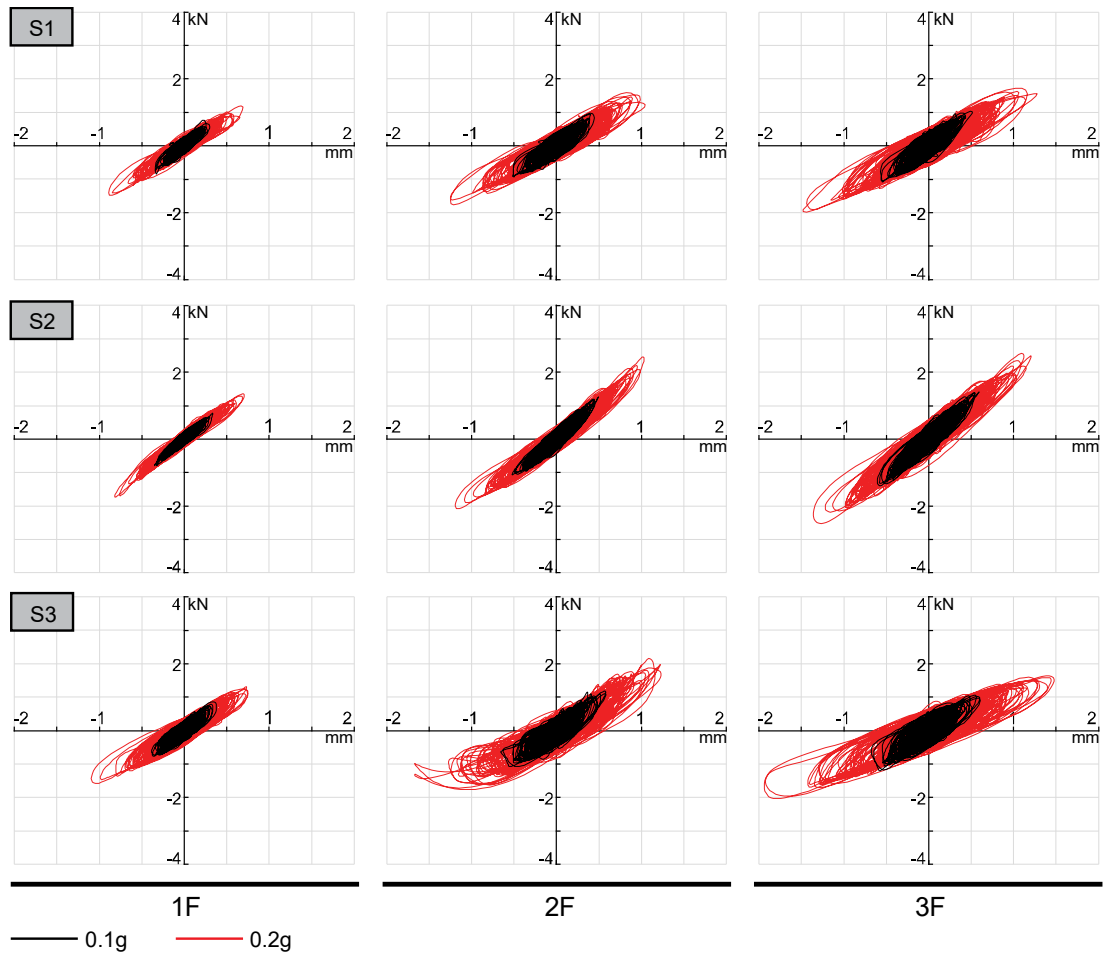
Fig. 2.15 Shear force-story displacement loops of diaphragms connected to the core part in S1, S2 and S3 with PGA=0.1g and 0.2g
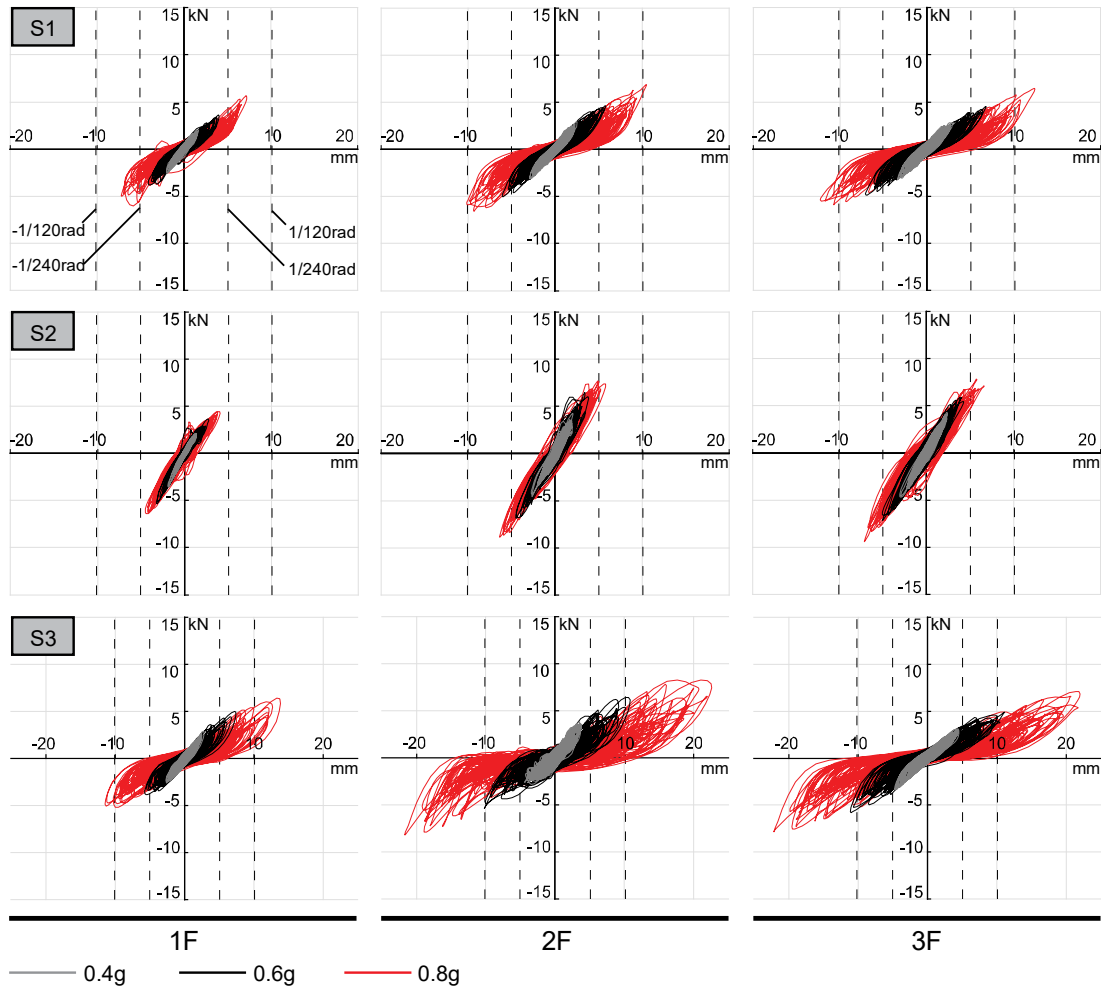
Fig. 2.16 Shear force-story displacement loops of diaphragms connected to the core part in S1, S2 and S3 with PGA=0.4g, 0.6g and 0.8g

2.3.7 Energy consumption

Fig. 2.17(a) shows the cumulative consumed energy of the constrained shear walls and diaphragms calculated from the hysteresis loops of S1. The constrained shear walls and diaphragms referred to the shear walls on the first floor and the diaphragms which are directly connected to the steel core. The major part of the energy was consumed on the constrained components where a large plastic deformation occurred due to the failure of the nails. It is also apparent that the energy consumed by the frame X1 and X2 was greater than the one consumed by X3, which formed a unique soft-segment rather than a soft-story compared to a normal structure. The same performance was observed in the constrained diaphragms (Fig. 2.17(b)). This gave the idea that the designer could reinforce the relative soft-segment on purpose using special technics such as consumption system or seismic isolation system to achieve functional and economic improvement. Those methods were also expected to reduce the high acceleration in the upper stories.
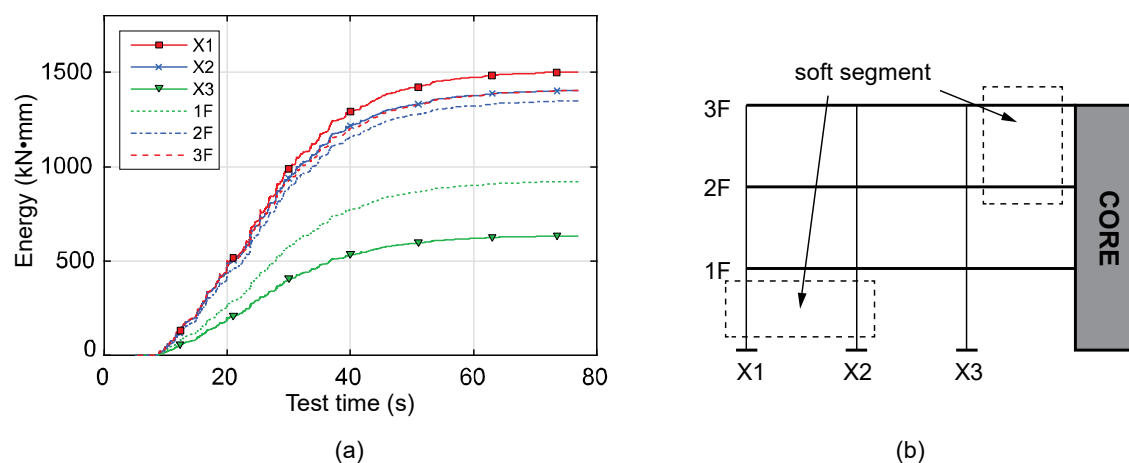
Fig. 2.17 (a) Accumulative energy dissipation curve during the input of 0.8g, and (b) the segment grid during the soft segment phenomenon of S1

2.4 Design implications

2.4.1 Shear force distribution

The one purpose of this experiment is to provide a seismic performance assessment of the wood horizontal hybrid structure which the engineering practice could consult. In this condition, the distribution of the seismic force is one of the main concerns in this research as well as in the

building seismic design. Considering the structural property of the hybrid specimen, the shear force generated from the seismic mass of the wood part was supposed to transfer in two ways, one by the vertical shear wall down to the ground, the other by the horizontal diaphragm sideways to the core part. The relative proportion of the peak shear force is illustrated in Fig. 2.18 and Fig 2.19. The shear force ratio R_i sustained by the shear wall of the i-story was calculated by Eq. (2.4),

$$R_i = \frac{Q_{wall,i}}{Q_{wall,i} + \sum_{n=i}^{3} Q_{diap,n}}$$ (2.4)

Where $Q_{wall,i}$ is the maximum seismic shear force sustained by the wooden shear wall of i-story, $Q_{diap,n}$ is the maximum seismic shear force transferred to the core part by the diaphragm of n-story. The ratio of the first floor represented the overall proportion of the base shear force sustained by the wooden shear wall to the total seismic shear force generated from the wood part. It is obvious that more than half of the seismic shear force was transferred to the core part, to be specific, average value 51.9%, 62.9%, 65.0% for S1, S2 and S3, separately. The values of the proportion were basically stable during the tests and believed to have a close correlation with the stiffness layout between the shear wall and the diaphragm, since the proportion rose whether when increase the stiffness of the diaphragm in S2 or reduce the stiffness of the shear wall in S3.

It should also be pointed out that on the third floor in S1 and S3, when the PGA of the ground motion rose gradually, the proportion of the core part decreased correspondingly. This stemmed from the fact that on the third floor the diaphragms was more seriously damaged than the shear walls, which limited their capacity to transfer the shear force from the wood part to the core part. As a comparison, the diaphragm connected to the core part in S2 remained its stiffness well, consequently the shear force distribution had no significant change through the tests (Fig. 2.19(b)).

Referring to the result of the shear force distribution, the target-drift-based design process could be improved. The specimen S1 was considered to be conservative due to the omission of seismic force transferred to the core part in the original design process. Assuming the transferred-to-core shear force was considered and had the same proportion with the test result as 51.9%. Then the modified design shear force Q' of S1 could be calculated by Eqs. (2.5-2.7):

$$Q' = Q / R_i$$ (2.5)

$$Q = \lambda \times Q_{real}$$ (2.6)

$$\lambda = W_{tot} / W_{tot,real}$$ (2.7)

where R_i =1-51.9%=48.1%; λ = the factor between the design shear force Q and the real shear force Q_{real}; W_{tot} = the total design weight of the wood part, equaled to 26.4kN according to Table.
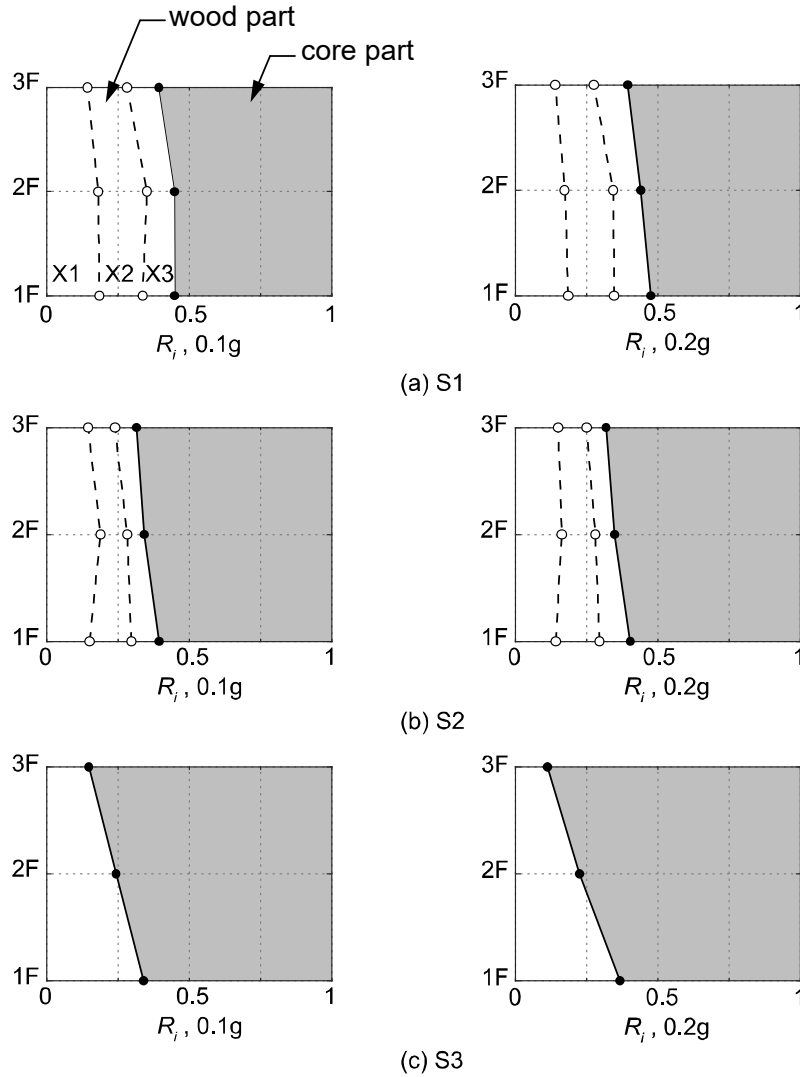
Fig. 2.18 Shear force ratio sustained by the shear wall along the height in S1, S2 and S3 during input of

0.1g and 0.2g

2.1; $W_{tot,real}$ = the real weight of the wood part used in S1, equaled to 22.75kN. Therefore, the relationship between the modified design shear force Q' and the real shear force recorded in the test Q_{real} was $Q'=2.41Q_{real}$. In the test of S1, when the PGA of the input was 0.2g, which equaled to the moderate earthquake scenario of the original design, the observed maximum shear force of the shear wall was 1.83kN with a drift around 1/390 at first floor, X1. The drift was apparently lower than the target drift of 1/120 referring to the conservative design. Then the factor 2.41 was used here to multiply the real shear force 1.83kN to get the modified shear force 4.41kN. According to the hysteresis property of the shear wall at first floor, X1 in S1 (Fig. 2.14), the
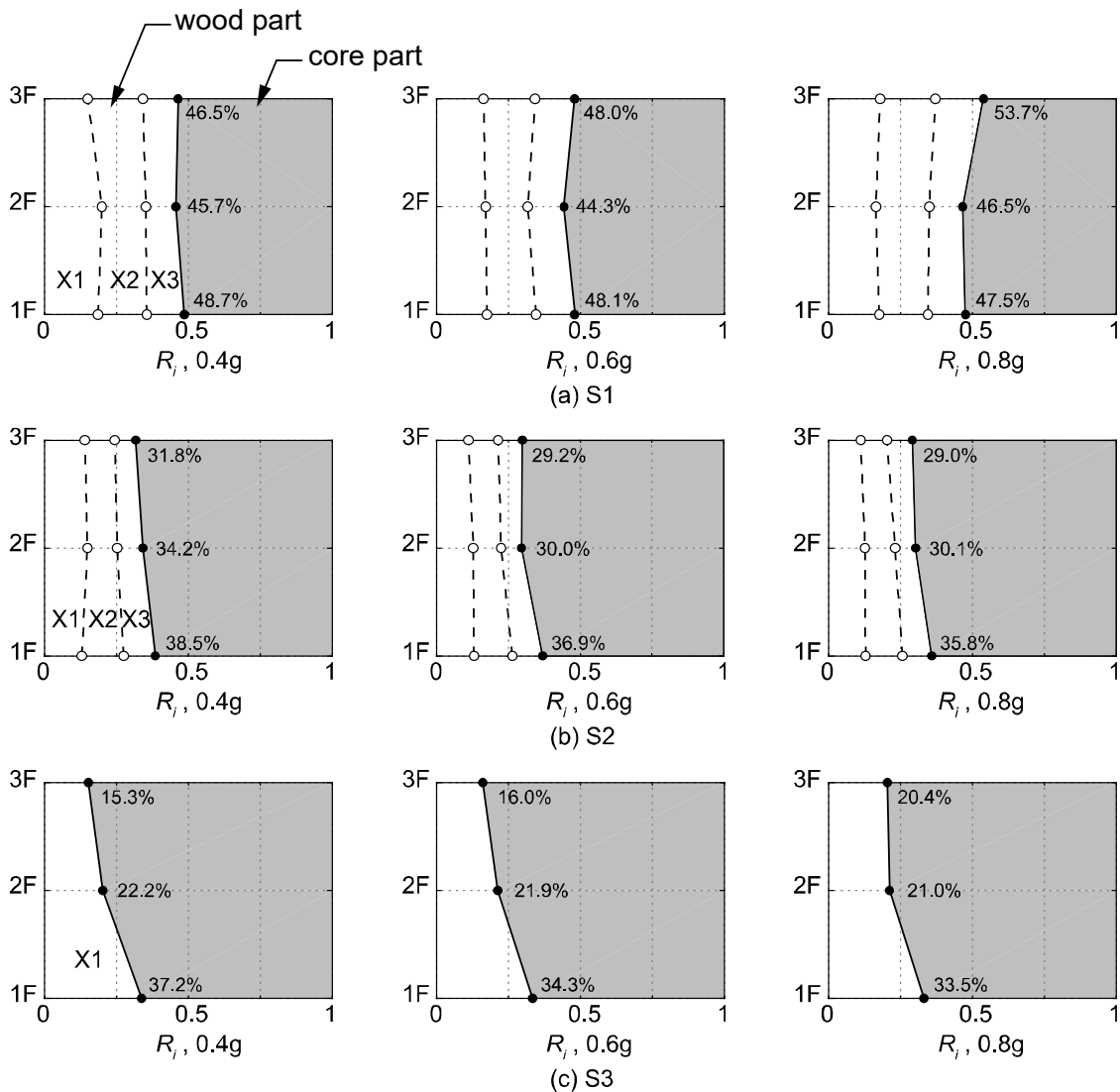
Fig. 2.19   Shear force ratio sustained by the shear wall along the height in S1, S2 and S3 during input of 0.4g, 0.6g and 0.8g

modified shear force 4.41kN was expected to reach a drift of 1/110, which is quite close to the target drift. The remarkable accordance between the modified shear force and the test result verified that the adopted design process in this test could be sufficient if appropriate transferred-to-core shear force was taken into consideration. This result highlighted the importance of the valid method to define the proportion of the shear force sustained between the shear wall and the diaphragm in the design stage. Relative quantification study is undergoing through numerical simulation and parameter analysis.

Fig. 2.20 presents the vertical distribution of the total story shear force as well as the seismic
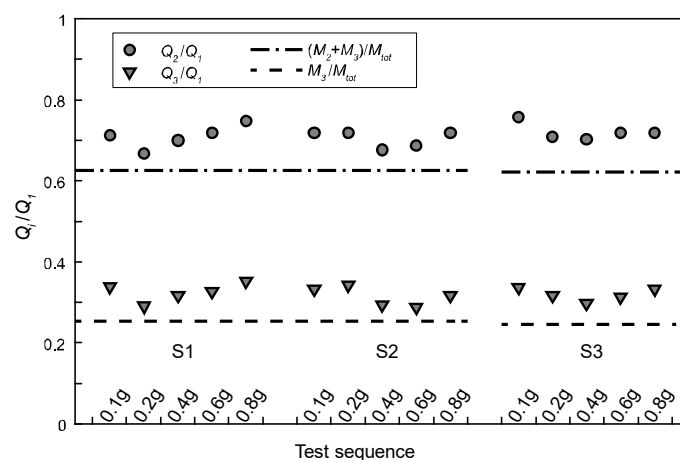
Fig. 2.20   Vertical distribution of peak story shear force and seismic mass in S1, S2 and S3

mass ratio along the height in the wood part, in other words, the seismic mass of the core part and accompanying shear force was not included in the figure. Q_i is the story shear force derived from the seismic mass above i-story. M_i is the seismic mass of the i-story in the wood part and $M_{tot} = M_1 + M_2 + M_3$. The ratios remained nearly constant throughout the tests. Obviously, the change of diaphragm stiffness and shear wall configuration didn't have a significant impact on the vertical distribution of seismic force. The ratio of the third floor to base shear was about 35% while that on the second floor was around 68% which gave the conjecture that the story shear force followed a nearly constant distribution along the height rather than the usual inverted triangular distribution. The vertical distribution could be used to estimate the demand of the diaphragms connected to the core part in the design stage. However, the rationality and accuracy of the constant distribution still need more inquiry.

2.4.2 Connection between wood part and core part

In a prior study by Isoda *et al*. (2017) on the shaking table test of wood-concrete hybrid structure, the connection between the wood part and the concrete part were severely damaged when subjected to high amplitude input. Considering the horizontal irregularity of this kind of hybrid structure, the designer should pay more attention to the connection performance. The connection of each floor used in this experiment consisted of a pair of thread steel bar at the main girder and several subordinate pairs along the connection beam (Fig. C.4). Fig. 2.21 and Fig. 2.22 illustrates the peak tensile force of the main bolt connections during the input of 0.1g to 0.8g. Apparently the forces of the side girder were greater than the ones in the middle. In S1 and S2, the tensile

force didn't show organized distribution along with the height. However, the tension of S3 increased according to the story height. The maximum tension for one steel bar was 4kN and hence the steel bars were deemed to be elastic throughout the test procedure. After the tests, the relative shifts between the two structural parts along the input direction were small and the maximum value was 0.2mm. Meanwhile, the residual increment of the gap between the two parts was under 0.005mm. In conclusion, the connection used in this experiment was reliable and adequate to transfer the shear force between the wood part and the core part.

As the prototype is a wood-concrete hybrid structure, its dynamic properties is not fully covered by the shaking table tests since the core part is simulated with steel frame rather than concrete structure. The main concern falls on the connection part. The connection between the two parts was supposed to be at tensile-shear stress status which is aggressive to the connection components. In the test specimens, the connection part is built with H-shaped steel. The connection part held well and remained elastic during the tests. No visual failure was observed for the connection part in the test specimen. For a wood-concrete horizontal hybrid structure, the circumstance may be more severe for the connection part since the significant tension will count against the concrete side in the connection. Existing experiment of the wood-concrete horizontal hybrid structure have shown that the concrete may suffer from heavy damage when subjected to severe input (Isoda 2016). Besides, the tension could decrease the strength of some connection type, for instance, the embedded steel bar connection (Ishida 2017).

Based on the existing research, several recommendations are made for the practice of wood-concrete horizontal hybrid structure:

1. The connection part in the concrete side should have mechanical connection with the main steel bar in the concrete part to prevent sudden failure due to the fracture of concrete around the connection.

2. The connection part in the wood side would not be the embedded adapting piece through the precast hold in the wood beam to avoid the split along the wood grain. External adapting piece is recommended for the connection part in the wood side.

3. Use seismic isolation device or damper in the connection part to protect the fragile concrete side. For instance, by using viscous or friction damper at the connection part, the shear transfer between the two parts could be more smooth and steady. Moreover, by changing the damper layout the proportion of the seismic force sustained by the wood part and the core part could be controlled.

(a) PGA=0.1g

(b) PGA=0.2g

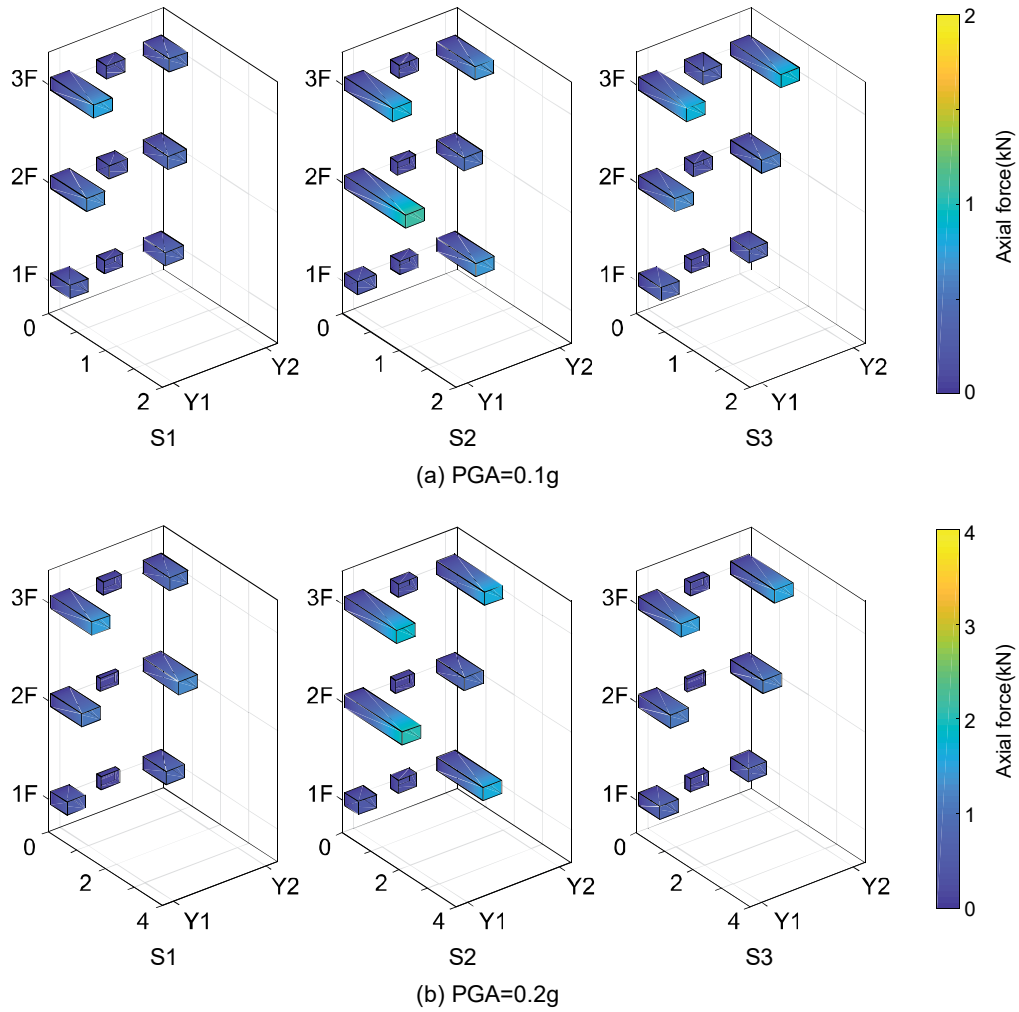Fig. 2.21　Vertical distribution of peak story shear force and seismic mass in S1, S2 and S3
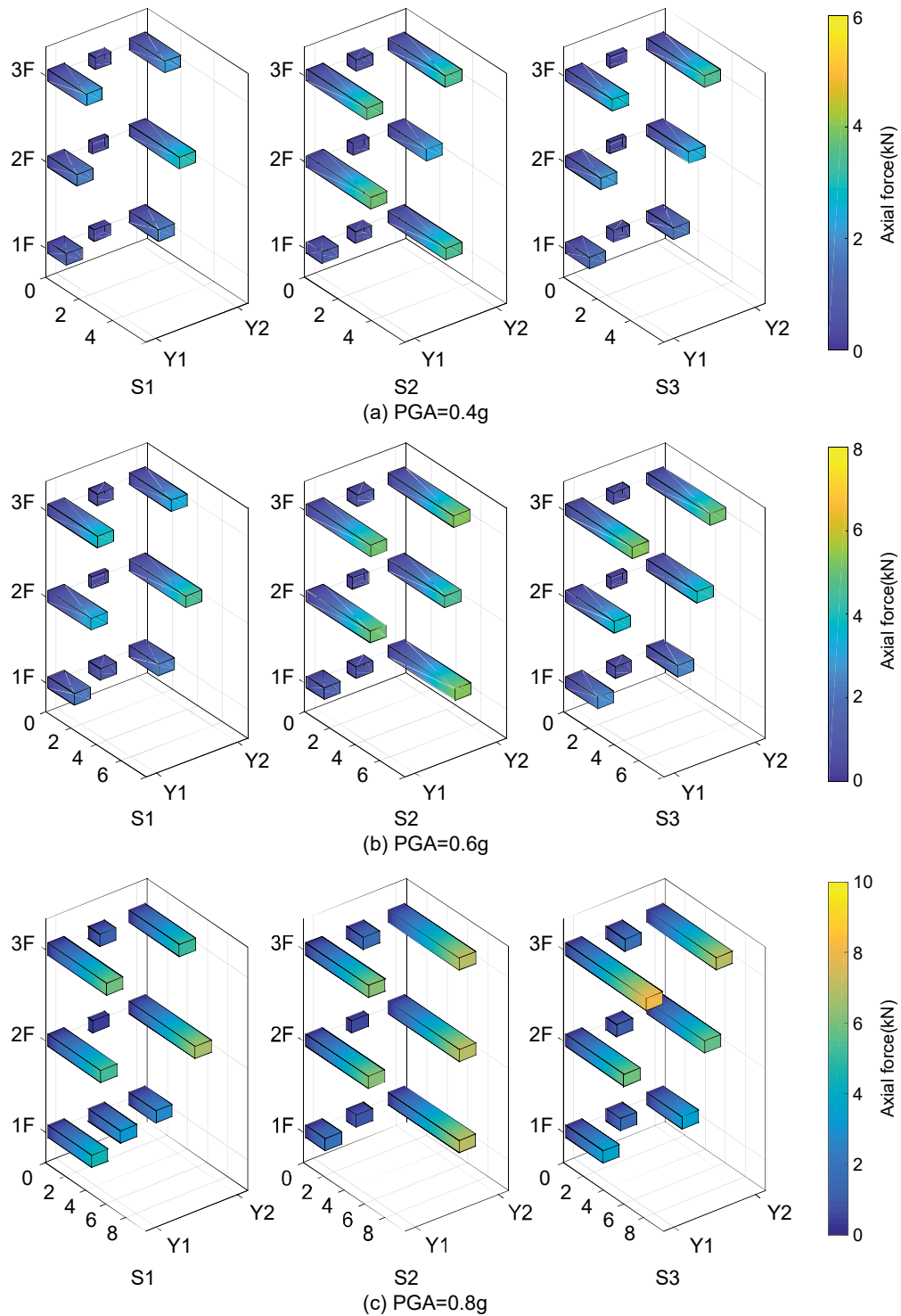
Fig. 2.22   Vertical distribution of peak story shear force and seismic mass in S1, S2 and S3

2.5 Conclusion

This chapter presented the shaking table tests of 1/3-scale wood horizontal hybrid structure, whose structural properties were in compliance with the prototype developed by AIJ. Three 3-story, 3-bay specimens were designed and tested, in which, S1 has 2 pieces of shear wall at each frame and a flexible diaphragm design; S2 has the same shear wall configuration with S1 yet a more rigid diaphragm with shorter nail spacing; S3 has 4 pieces of shear wall at the end frame but none at the middle ones and a same flexible diaphragm design with S1. All the specimens were connected to a rigid steel frame laterally. The objective of this study was to find out the feasibility of the proposed design process used in the horizontal hybrid structure, as well as the influence of the design features to the seismic performance of the wooden horizontal hybrid structure. Towards this end, the following conclusions could be drawn:

● Due to the limitation of the shaking table and the omission of the transferred-to-core shear force, the design of the specimens in this paper was verified to be relatively conservative. However, the proposed target-drift-based design process could be feasible if the transferred-to-core shear force was taken into consideration.

● The increase of the diaphragm stiffness substantially improved the seismic performance of the test specimen along with the higher demands for the connection and the core part. In addition, the concept of concentrated shear wall at one side was practicable and sufficient but the corresponding specimen was more vulnerable to severe earthquake scenarios. Furthermore, the influences of these design features also verified that the shear force transfer between the wood part and the core part was related to the stiffness layout of the shear wall and diaphragm.

● High-than-normal story acceleration amplification observed in the tests was caused by the conservative design and the potential bullwhip effect as well as the high height-width ratio in the input direction. The energy consumption system or seismic isolation system was expected to alleviate the high acceleration amplification and improve the seismic performance of the structure.

● The connection between the wood part and the core part was reliable and hold well in the tests. In view of the tensile-shear stress status, the stiffness layout of the shear wall and diaphragm as well as the eccentricity of the structure need to take into consideration to make a more comprehensive design for the connection.

In general, the performances of all the specimens were satisfactory during the tests. The seismic advantage of the wooden hybrid structure was evident. The characteristics of the wooden horizontal hybrid structure observed from the shaking table test is used to build the numerical model in Chapter 3.

3 Numerical modeling of the shaking table test

3.1 Introduction

In Chapter 2 several characteristics of the wooden horizontal hybrid structure has been revealed through the shaking table test. However, due to the limitation of the shaking table and the economic consideration, only three specimens were tested. The influence of the structural configuration on the performance of the wooden horizontal hybrid structure was not fully studied. To fill out the empirical results of this study, numerical analysis is conducted to explore the potential configuration of the wooden horizontal hybrid structure as well as the corresponding seismic performance. In this chapter, a 3D discrete model was built in *OpenSees* (PEER 2015) and a modified subroutine material was proposed to simulate the wood shear wall and diaphragm. The accuracy of the numerical model was confirmed by the comparison between the analytical results and the shaking table tests. As a benchmark, specimen S1 in the shaking table test of Chapter 2 is chosen to build the numerical model.

3.2 Building of numerical model

OpenSees is short for "The Open System for Earthquake Engineering Simulation", which is an open-source software framework for simulating the seismic response of structural and geotechnical systems. The modeling approach in *OpenSees* is very flexible which allows selection and various combinations of a number of different element formulations and material formulations, along with different approximations of kinematics to account for large-displacements and P-delta effects (PEER 2015). Also the open-source code allows the user to modify the subroutine easily to accomplish specific research demands. As a benchmark, Specimen S1 with interior wall of the shaking table test in Chapter 2 was firstly chosen to build the numerical model. Here in Section 3.2, the referred specimen means the Specimen S1 of the shaking table test.

3.2.1 Modeling of shear wall and diaphragm

The schematic configuration of the simplified 3D model is illustrated in Fig. 3.1. In this model, both the shear wall and the diaphragm were simulated by a pair of diagonal nonlinear spring, while the boundary elements (beam and column) were simulated by rigid truss element. Unlike the simulation of traditional structure in which the diaphragm is usually idealized as either rigid or flexible, the diaphragm of wooden horizontal hybrid structure was part of the force transfer
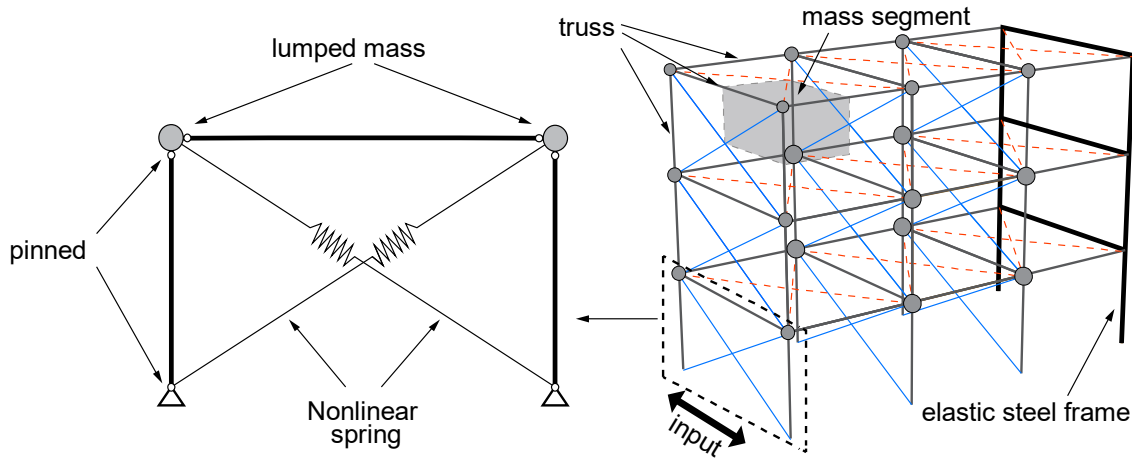
Fig. 3.1 Schematic configuration of the numerical model in *OpenSees*

and energy consumption system, therefore it was built the same way as the shear wall in the numerical model. The distinguishing feature of the numerical model derived from various aspects. In the pilot experiment, a series of wood shear wall and diaphragm which had the same configuration with the shaking table specimen were tested under quasi-static load (Hiyama 2016). Test observation indicated that the glulam beam and column kept sufficient rigidity while the lateral displacement was mostly caused by the rigid body shift of the frame along with the damage of the panel nails and beam-column joints (Fig. B.5-B.8). Therefore, the beam and column were considered as pinned rigid truss, and the lateral resistance of the frame in the input direction was only provided by the diagonal nonlinear springs.

3.3.2 Modified *SAWS* Material

To reproduce the hysteresis property of the shear wall and diaphragm, uniaxial *SAWS* material in *OpenSees* was used for the diagonal springs in the numerical model. *SAWS* material was developed to capture the nonlinear response of the individual sheathing-to-framing connectors, such as nail and bolt in wooden structure (Folz 2001). It was also designed to catch the typical pinching effect and stiffness degradation during hysteresis loadings. The relationship of the lateral force F and displacement Δ in Eq. (3.1)-(3.3) defines the piecewise exponential backbone curve,

$$F = \text{sgn}(\Delta) \cdot (F_0 + S_1 |\Delta|) \cdot [1 - \exp(-S_0 |\Delta| / F_0)], \quad |\Delta| \le |\Delta_u| \tag{3.1}$$

$$F = \text{sgn}(\Delta) \cdot F_u + S_2 [\Delta - \text{sgn}(\Delta) \cdot \Delta_u], \quad |\Delta_u| < |\Delta| \le |\Delta_F| \tag{3.2}$$

$$F = 0, \quad |\Delta| > |\Delta_F| \tag{3.3}$$
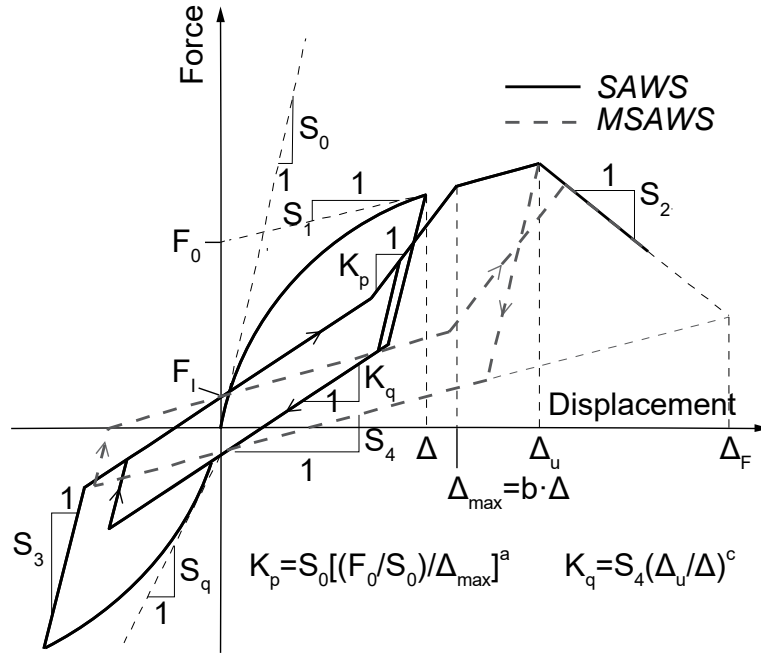
Fig. 3.2 Modified *SAWS* material

In the original *SAWS* material, the stiffness of the pinching part S_4 remains unchanged all through the displacement which is less accurate compared with the quasi-static experiment (Fig. B.3). On that account, the subroutine was modified by introducing a new parameter K_q (Fig. 3.2). The stiffness of the pinching part K_q is defined in Eq. (3.4)-(3.5),

$$K_q = \min[S_4(\Delta_u / \Delta)^c, S_q], \ |\Delta| \leq |\Delta_u| \tag{3.4}$$

$$K_q = S_4, \ |\Delta| > |\Delta_u| \tag{3.5}$$

The modified *SAWS* (*MSAWS*) material is supposed to have a better representation of the pinching effect than the original *SAWS* material, especially at the minor displacement.

Although the specimen design of the pilot quasi-static experiment and the shaking table tests were the same, the detailed nail spacing were different, which made the material parameters calibrated from the quasi-static experiment couldn't be used directly in the numerical simulation of the shaking table tests. As a solution, a two-step calibrating process was used in this study:

1. the *F*-Δ record of quasi-static experiment was scaled to match the envelope of the shaking table results (Fig. 3.3(a));

2. the parameters of *MSAWS* were then calibrated based on the scaled *F*-Δ record (Fig. 3.3(b)).

In step 1, only the magnitude of the shear force of the quasi-static curve was integrally scaled while the lateral displacement remained unchanged. In that way the stiffness of the quasi-static

(a) step 1   (b) step 2
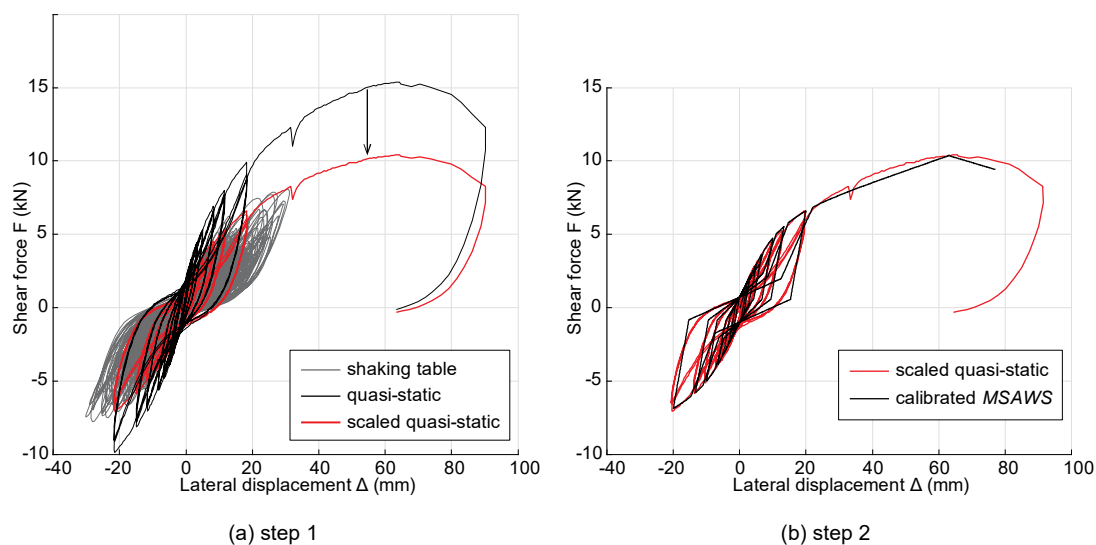
Fig. 3.3 Parameter calibration of the *MSAWS* material using experiment results

Table 3.1 Parameter of *MSAWS* material used in wood shear wall and diaphragm

Parameter	F_0(kN)	F_1(kN)	S_0(kN/m)	S_1	S_2	S_3	S_4	Δ_u(mm)	a	b	c
Shear wall	6.32	0.48	1250	32	-150	1190	15	90	0.5	1.1	1.2
Diaphragm	5.49	0.65	1313	143	-150	2000	30	50	0.3	1.1	1.2

curve was changed all through the test process, including the initial stiffness, yield stiffness, unloading stiffness and reloading stiffness. The scale procedure was conducted by the minimum mean squared error between the envelopes of the shaking table test and the quasi-static test. Although only the envelops were matched, considering the identical deformation mechanism between the shaking table and quasi-static test specimen, the internal stiffnesses were matched spontaneously. In step 2, each parameter of the *MSAWS* was calibrated separately according to the corresponding curve segment of the scaled quasi-static *F-Δ* record.

Table 3.1 shows the parameters used for the shear wall and diaphragm. The initial stiffness S_0 was derived from a series of geometrical calculation on the backbone curve of the scaled *F*-Δ record (Fig. 3.4):

1. Connect the two points with shear force magnitude of $0.1P_{max}$ and $0.4P_{max}$ on the backbone curve to get Line I, where the P_{max} is the ultimate strength of the wood shear wall or diaphragm;

2. Connect the two points with shear force magnitude of $0.4P_{max}$ and $0.9P_{max}$ on the backbone curve to get Line II;
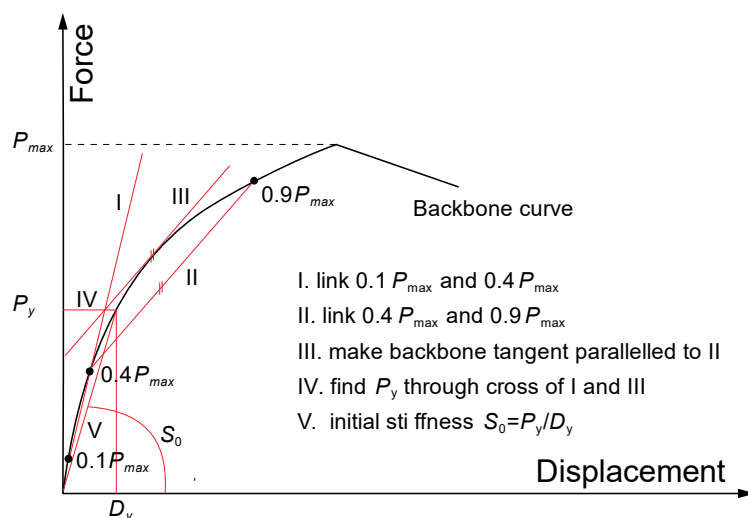
Fig. 3.4 Definition of the initial stiffness of the wood shear wall and diaphragm

3. Make a Line III which is paralleled to Line II and also the tangent of the backbone curve;

4. Make a horizontal Line IV through the intersection point of Line I and III, Line IV has an intersection point Y with the backbone curve;

5. The strength of point Y is defined as the yield strength P_y and the corresponding displacement is defined as the yield displacement D_y; Connect the origin and point Y to get the Line V whose tangent is defined as the initial stiffness $S_0 = P_y/D_y$.

The above procedure is recommended by Japan Housing and Wood Technology Center in the allowable shear strength design for the quasi-static test of the wood shear wall and diaphragm (JHWTC 2008). It uses the secant stiffness at the yield point as the initial stiffness. It is apparent that the secant stiffness S_0 is smaller than the actual tangent stiffness of the backbone curve at the origin, which made the initial rigidity of the numerical model smaller than the one of the shaking table specimen. As a consequence, the natural frequency of the numerical model was less than the one of the specimen as well. Apart from that, the underestimate of the initial stiffness for the specimen seems to have no further influence on the performance of the numerical model according to the analysis more hereof later.

It should be pointed out that the difference of the shear wall and diaphragm is embodied in the different parameters used in the *MSAWS* material as shown in Table 3.1. Fig. B.3(b) and Fig. B.4(b) demonstrates the force-drift response of the shear wall and diaphragm during the quasi-static test. The basic shapes of their hysteresis loops are similar, considering the same deformation and failure mechanism. In the shear wall and the diaphragm, although the configurations of the wood panels are different, the main shear stiffness is provided by the mechanical interlocking between the nails and wood panels. There is no essential difference for the performances of the

shear wall and diaphragm. Therefore, in the numerical model, the *MSAWS* material is calibrated separately to simulate the shear wall and diaphragm, separately. The difference including the initial stiffness and sharp of the backbone curve, the stiffness of unloading and reloading branch and the ratio of the stiffness degeneration for the reloading part.

3.2.3 Modeling of core part

The steel frame is supposed to be a relatively rigid core part in the hybrid structure. The results of the shaking table tests in Chapter 2 indicated that the core part remained elastic during the experiment even when subjected to severe input. Therefore, the core part was simulated with a
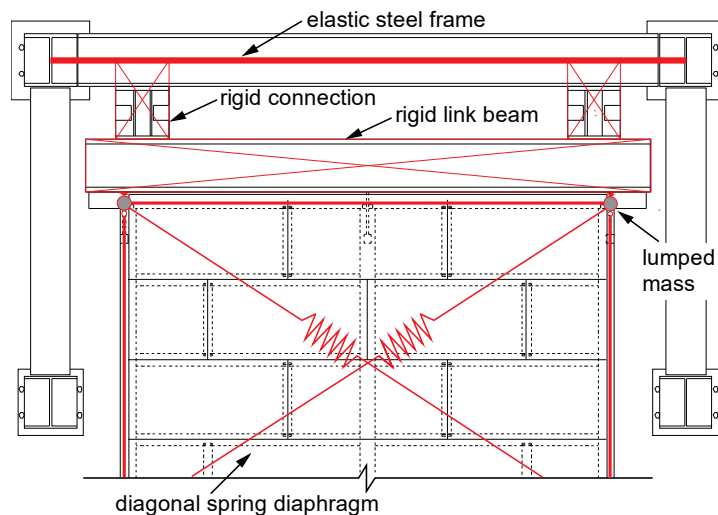
Fig. 3.5 Numerical model of the core part and the connection

simple elastic frame. The *elasticBeamColumn* element and *elasticUniaxial* material (Fig. 3.5) were used to build the core frame. The parameters of the material were adjusted to a certain level on which the numerical core frame would provide a similar shear resistance with the specimen steel core part. In the numerical model, the story shear stiffness of the core frame is nearly 23 times higher than the initial stiffness of the wood shear wall. The stiffness ratio was calibrated to keep the first three mode shape consistent between the numerical model and the shaking table test specimen. In fact, the lateral stiffness provided by the core part in the test specimen was

a series combination of: 1. the story stiffness of the steel frame; 2. the shear stiffness of the connection pieces. Instead of modeling the connection part intricately, the link beam and connecting pieces were represented by rigid body and the series stiffness was provided only by the elastic steel frame to promote the robustness and computational efficiency of the model.

3.2.4 Seismic mass and gravity load

Seismic mass of the numerical model was lumped at the beam-column joints at each floor, including the mass of the wooden frame and the concrete bricks in respectively tributary segment (Fig. 3.1). As for the core part, the lumped mass also included the mass of the connecting elements and the steel frame itself. The value was directly calculated from the test specimen. The gravity load was applied in accordance with the seismic mass at the beam-column joints using standard gravitational acceleration. The P-delta effect was implemented in the analysis considering the displacement ductility of the wood shear wall.

3.3 Validation of numerical model

Time history analysis was conducted in *OpenSees* using the built 3D numerical model. BCJ-L2 wave was used as the input and the magnitude of the PGA increased from 0.1g to 0.8g (Fig . C.6). The BCJ-L2 wave was scaled in time as the one used in the shaking table test. The duration and the input sequence of the BCJ-L2 wave were also exactly the same with the shaking table tests (Table C.3).

Rayleigh damping was assigned to the numerical model (Charney 2008). The damping matrix C in *OpenSees* is defined in Eq. (3.6),

$$C = \alpha_M \cdot M + \beta_K \cdot K_{\text{current}} + \beta_{K_{\text{init}}} \cdot K_{\text{init}} + \beta_{K_{\text{comm}}} \cdot K_{\text{comm}} \tag{3.6}$$

in which only α_M and β_K are considered here. It means that the mass matrix and current stiffness matrix are used to define the damping in the model. The damping ratio of the model in i-mode can be determined by Eq. (3.7),

$$\xi_i = \frac{\alpha_M}{2\omega_i} + \frac{\beta_K \omega_i}{2} \tag{3.7}$$

The coefficients α_M and β_K are determined by specifying damping ratios in any two modes, say m and n and writing Eq. (3.7) for each mode. These equations, solved simultaneously for α_M and β_K, are represented in matrix form in Eq. (3.8),

$$\left\{ \begin{array}{c} \xi_m \\ \xi_n \end{array} \right\} = \frac{1}{2} \begin{bmatrix} 1/\omega_m & \omega_m \\ 1/\omega_n & \omega_m \end{bmatrix} \left\{ \begin{array}{c} \alpha_M \\ \beta_K \end{array} \right\} \tag{3.8}$$

Which could be transformed into Eq. (3.9),

$$\left\{ \begin{array}{c} \alpha_M \\ \beta_K \end{array} \right\} = 2 \begin{bmatrix} 1/\omega_m & \omega_m \\ 1/\omega_n & \omega_m \end{bmatrix}^{-1} \left\{ \begin{array}{c} \xi_m \\ \xi_n \end{array} \right\} \tag{3.9}$$

Once two damping ratio in mode *m* and *n* are determined, the coefficient α_M and β_K can be calculated from Eq. (3.9). Then the calculated α_M and β_K can be used as input in the *OpenSees* script. The damping ratio of the first mode and second are used, and the Rayleigh damping ratio of the wood part and the steel core part are defined separately in the numerical model. The detailed parameter of Rayleigh damping ratio is shown in Table 3.2. The damping ratio came from the modal analysis of the shaking table tests and appeared to be reasonable according to the following comparison of the numerical analysis and shaking table tests.

Table 3.2 Parameter of Rayleigh damping ratio

Part	ξ_1	ξ_2	ω_1	ω_2	α_M	β_K
wood	0.06	0.06	47.10	91.68	3.7338	0.0009
steel core	0.02	0.02	47.10	91.68	1.2446	0.0003

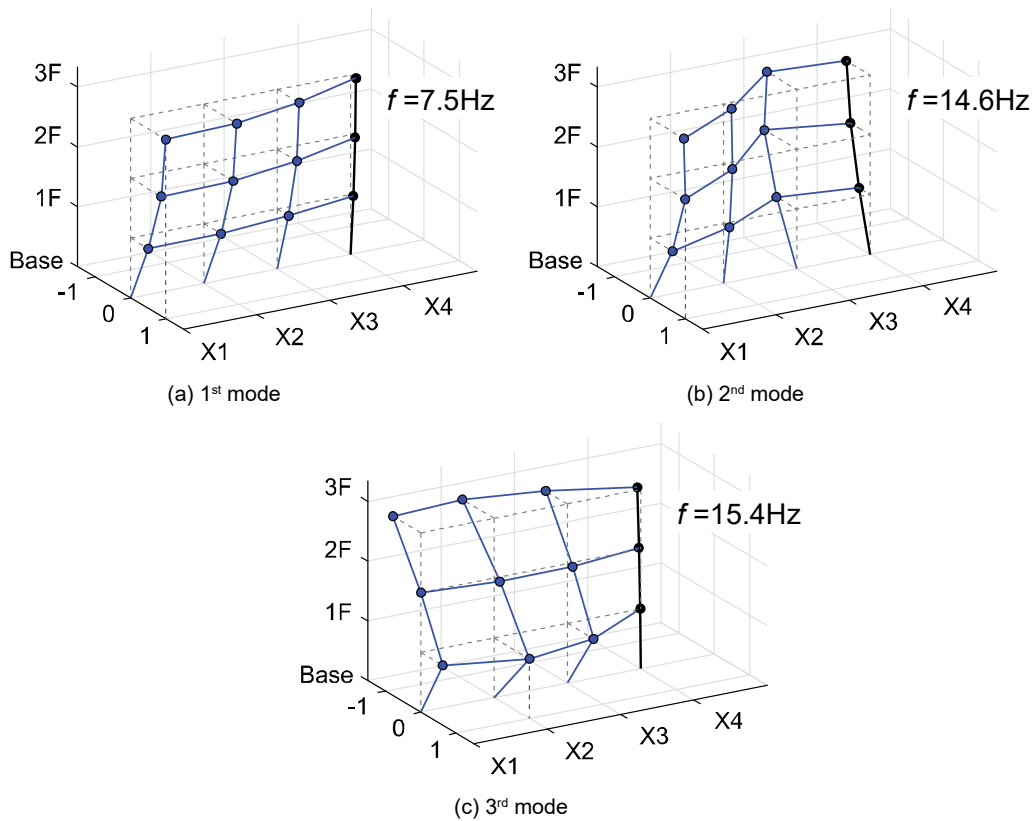(a) 1st mode

(b) 2nd mode

(c) 3rd mode

Fig. 3.6 Mode shape and frequency of the numerical model

3.3.1 Frequency and mode shape

Fig. 3.6 demonstrates the first three frequencies of the numerical model. Since the secant stiffness was used in the numerical model, the frequency of the model is smaller than the test specimen as expected. Comparison could be made between Fig. 3.6 and Fig. 2.4 which shows the mode shape and frequency of the test specimen. Although the frequency is underestimated, it is apparent that the numerical model is able to catch the characteristic of the vibration mode of the test specimen: the first mode is dominated by the wood part and the deformation decrease from the X1 to X3 and from 3F to 1F; the second mode is dominated by both the core part and the wood part while the third mode is dominated by the wood part only. It should be pointed out that the sharp of the second mode is closely connected to the story stiffness ratio between the wood part and the core part which will be, in some detail, discussed in Chapter 4.

3.3.2 Displacement and story drift

In seismic design, maximum displacement and the story drift is a critical indicator to evaluate the structure performance. Fig. 3.7 compares the displacement profile of the specimen and the model when the input PGA varies from 0.1g to 0.8g. The numerical model was able to catch the basic deformation pattern of the specimen. The displacement and story drifts decrease from X1 to X3, as a result of the constraint of the steel frame. Discrepancy happens when the input is minor: when the PGA equals to 0.1g, the numerical simulation overestimate the displacement of the whole wood part; when the PGA equals to 0.2g, the numerical simulation has a good prediction on the maximum displacement of frame X1 while overestimate the ones of frame X2 and X3. The discrepancy is caused by the conservative specified initial stiffness of the wood shear wall and diaphragm as shown in Fig. 3.4. On the other hand, the demands of the specimen is small when the input is minor, therefore, the records of the test may be more effected by the measurement error and processing method. In fact, Fig. 2.13 indicates that the displacement record of the shear wall X2 in S1 and S2 are not credible since their force-displacement loops are twisty compared with other elliptic curves. Hence the discrepancy of 0.1g and 0.2g is acceptable in this condition. For 0.4g to 0.8g, the deformations of the test and the numerical analysis have a good match: the maximum roof displacement and the maximum story drift are quite close. The detailed error of the maximum story drift is shown in Table 3.3 and the deviation is acceptable for varying magnitudes of the inputs. It is also worth noting that the predicted maximum story drift continually occurred at the 1st floor of X1, which is consistent with the tests of S1 (Table 2.2).

Table 3.3 Error of maximum story drift between test and numerical simulation (%)

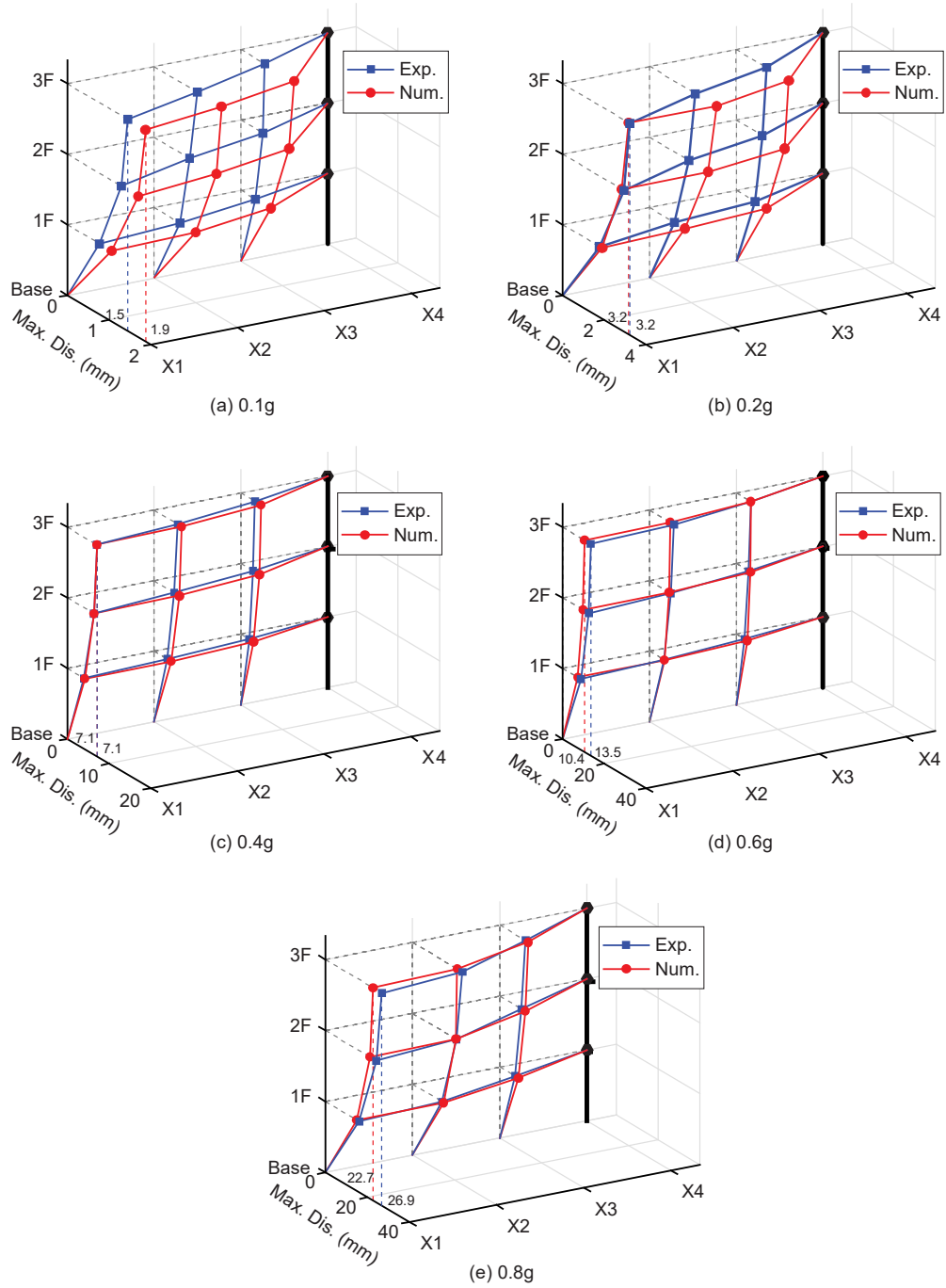| PGA	Story		
	1F	2F	3F
0.1g	31.3	6.1	7.3
0.2g	5.4	-3.6	7.2
0.4g	5.8	-10.8	21.0
0.6g	-9.0	-12.2	-7.4
0.8g	-7.7	-5.6	-22.5

Fig. 3.7 Comparison of displacement of the wood part between shaking table test and numerical simulation

3.3.3 Hysteresis loops

In addition to the amplitude values, the response time history for story displacement and the hysteresis loops offer intuition of the vibration properties. Fig. 3.8 to Fig. 3.12 demonstrate the displacement time history and hysteresis loops of the shear walls and diaphragms of the soft segment. Their vibration shared the same phase and the peak displacement basically occurred at the same time as well. When the input is 0.1g, the numerical model is able to catch the linear characteristic of the wood shear wall and diaphragm although the magnitude of the deformation and shear force is generally overestimated especially for the shear wall at the X2 and X3. It could be noticed that in Fig. 3.8(a) the stiffnesses of the specimen shear wall and the model are nearly the same but in Fig. 3.8(c) the stiffness of the specimen shear wall is higher than the numerical model. It means that although the performance of the structure is linear on the surface, when PGA equals to 0.1g, the stiffness of shear wall at X1 decrease more rapidly than the one at X3 due to underlying damage. The numerical model is not capable of distinguishing the slight stiffness degradation at the linear stage and as a consequence the prediction of the minor input is less accurate than the one of the severe input. When the input increases to 0.2g, the stiffness degradation expand and the prediction is more accurate than the one of 0.1g. There should be pointed out that the displacement gauge at the X2 suffered from unknown failure during the input of 0.1g and 0.2g therefore the relative records are not valid (Fig. 3.8 (b), Fig. 3.9(b)). For the input of 0.4g to 0.8g (Fig. 3.10-Fig. 3.12), the agreement between the prediction and the test is remarkable for different frame of the wood part. The *MSAWS* material is sufficient to simulate the approximately linear relationship during the 0.4g input and the plastic one during the input of 0.6g and 0.8g as well as the relative pinching effect and stiffness degradation. As for the displacement time history, the numerical simulation also has a good match with the test results. The value of the crests and trough are quite close. And the moments while the peak magnitude happens are also the same for the numerical simulation and the test results.

Fig. 3.8 Hysteresis loop and deformation time history of shear wall and diaphragm, PGA=0.1g

Fig. 3.9 Hysteresis loop and deformation time history of shear wall and diaphragm, PGA=0.2g

Fig. 3.10 Hysteresis loop and deformation time history of shear wall and diaphragm, PGA=0.4g
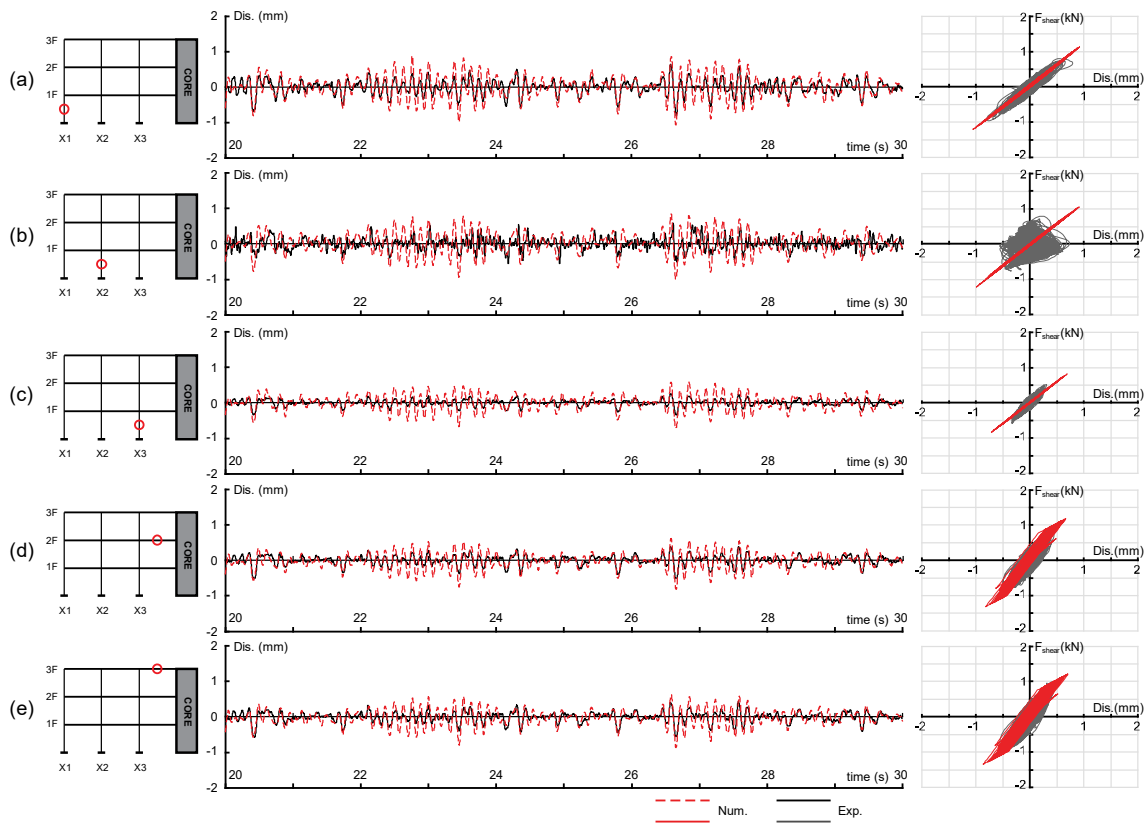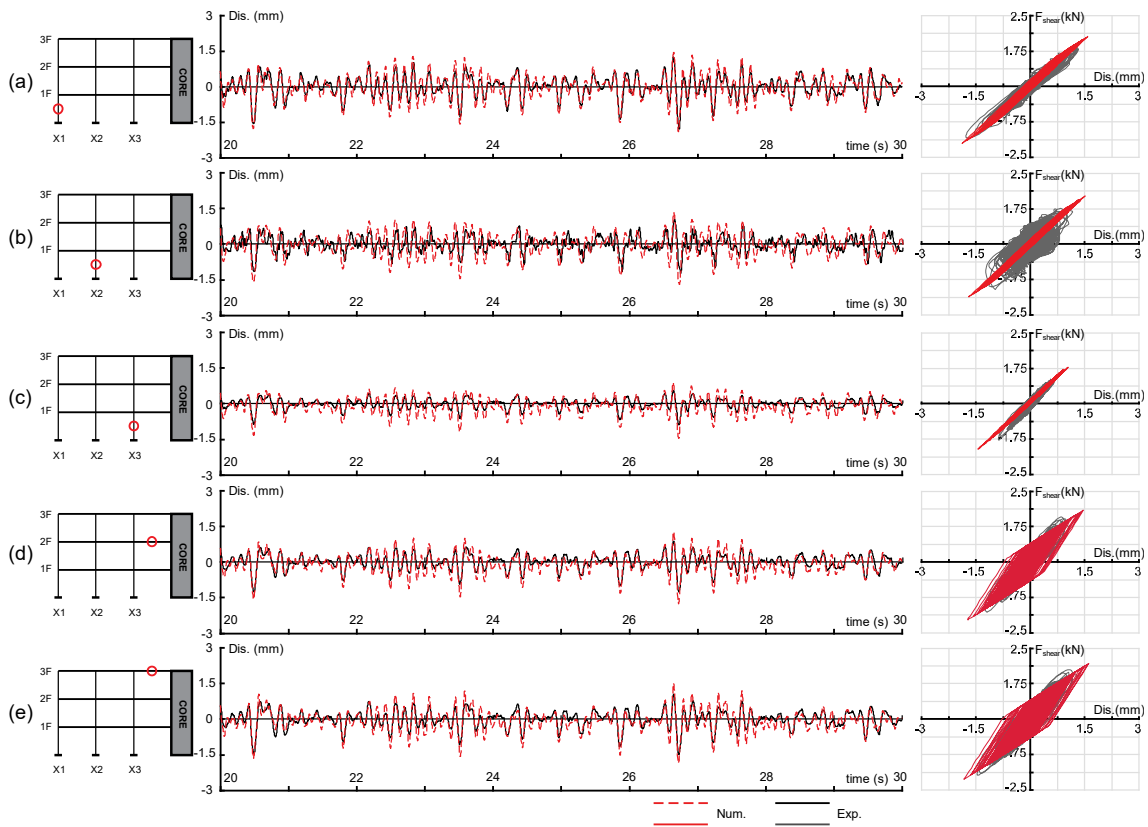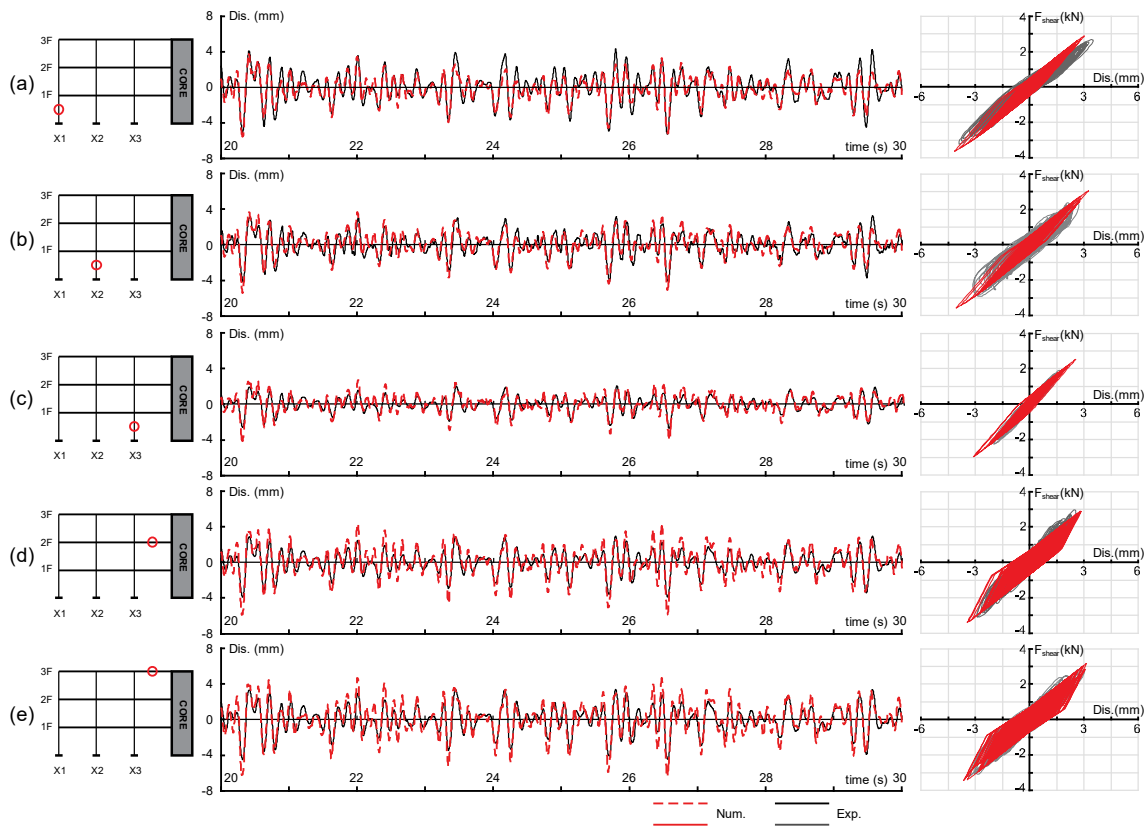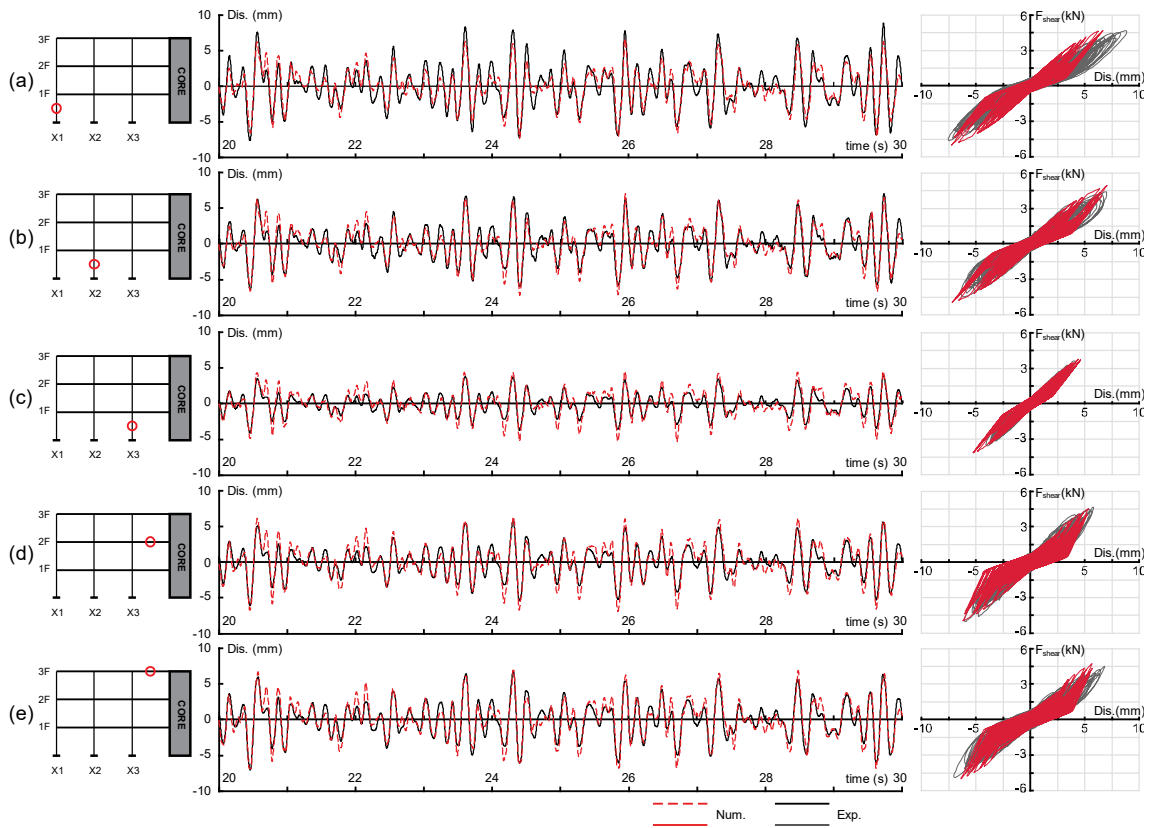
Fig. 3.11 Hysteresis loop and deformation time history of shear wall and diaphragm, PGA=0.6g
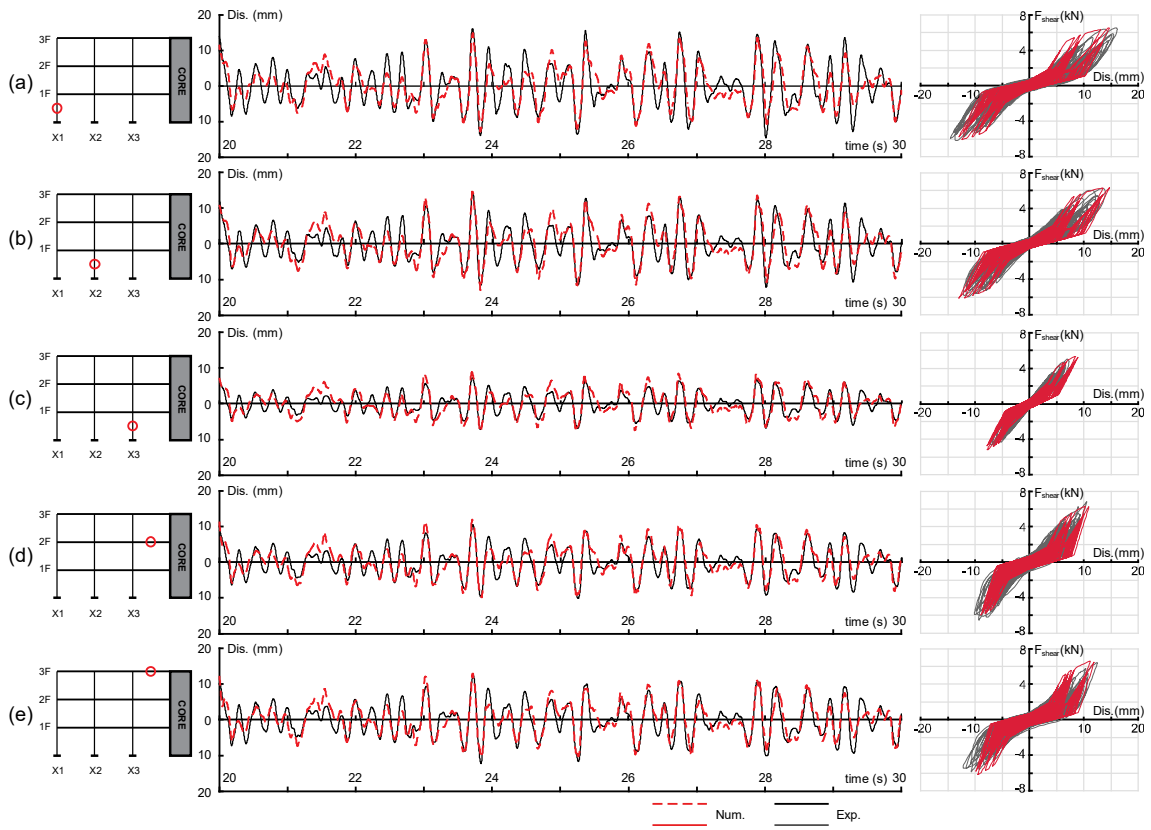
Fig. 3.12 Hysteresis loop and deformation time history of shear wall and diaphragm, PGA=0.8g

3.3.4 Shear force distribution

Another point of considerable interest in seismic evaluation is the distribution of seismic force, in this case, the proportion of the shear force sustained by wood shear walls and the core part. The relative proportion of the peak shear force is depicted in Fig. 3.13. The shear force ratio R_i sustained by the shear wall of the i-story was calculated by Eq. (3.10),

$$R_i = \frac{Q_{\text{wall},i}}{Q_{\text{wall},i} + \sum_{n=i}^{3} Q_{\text{dia},n}} \tag{3.10}$$

Where $Q_{\text{wall},i}$ is the maximum seismic shear force sustained by the wood shear wall of i-story, $Q_{\text{dia},n}$ is the maximum seismic shear force transferred to the core part by the diaphragm of n-story. The broken lines with solid circle define the percentage of lateral shear between the wood part and the core part. In the wood part, the width of between the broken lines means the percentage of the whole story shear sustained by each wood frame. It is apparent that when PGA equals to 0.1g, the numerical model underestimate the shear force sustained by the shear wall on the third floor (Fig. 3.13(a)). When PGA equals to 0.2g, the numerical model overestimate the shear force sustained by the frame X3 (Fig. 3.13(b)). The discrepancy is basically caused by the stiffness difference between the shear walls. The shear walls at X1 to X3 have the same design and are supposed to have the same performance during the experiment. However, due to construction error and measurement error, the shear walls at different frame shows different performance. Moreover, the damage of the outer wall is higher than the interior wall since it suffers from higher displacement even when the input is minor. The slight change of the stiffness differs the shear force distribution of the structure. For 0.4g to 0.8g, the agreement is more than satisfactory. At the 3rd floor, the decreased ratio of the core part indicates that the damage of the diaphragm due to increasing intensity of the input restrict the transmission of the seismic force from the wood part to the core part. In general, the numerical model is able to predict the lateral shear force distribution for severe input.
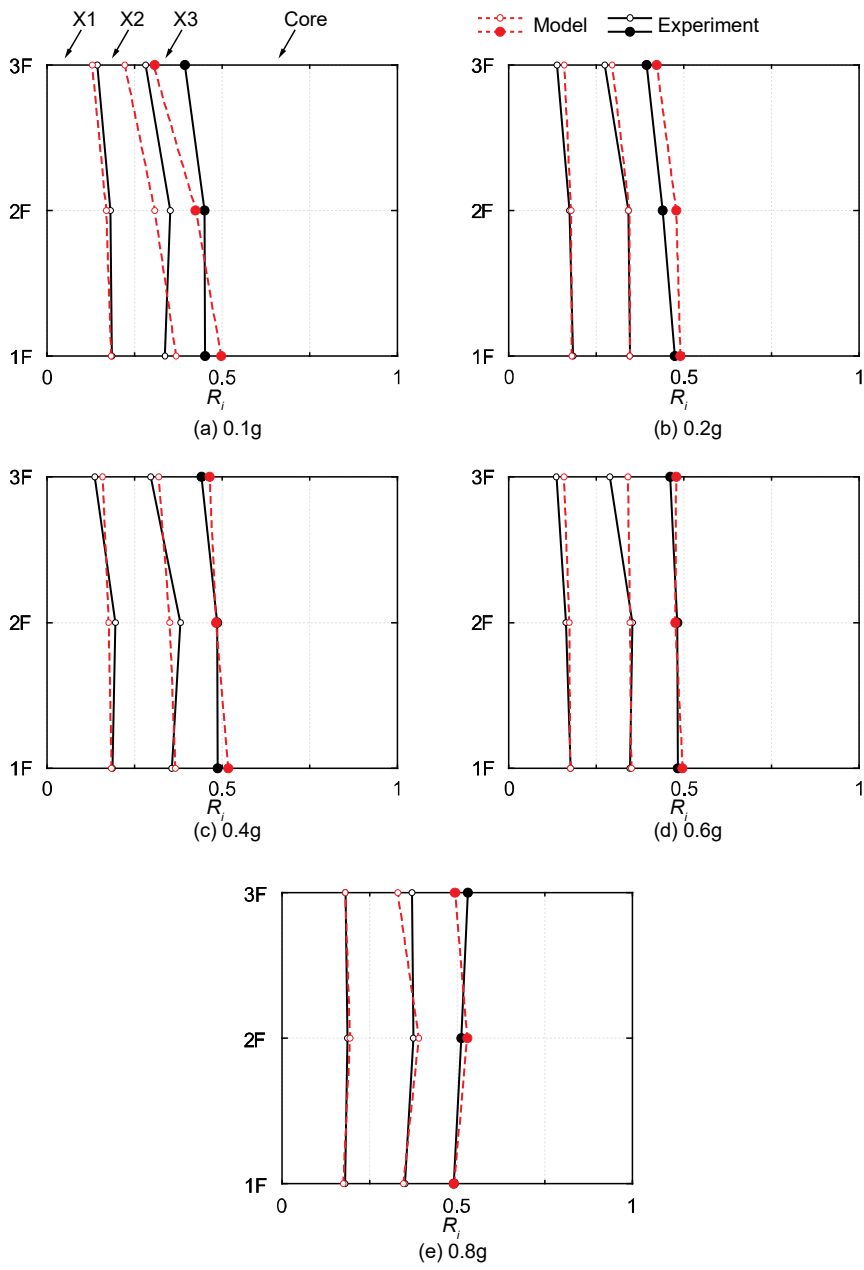
Fig. 3.13 Mode shape of the test specimen and the numerical model

3.3.5 Connection tension

Although the connection between the wood part and the core part was not subjected to any perceptible damage during the experiment, the complex stress condition of the connection is still noteworthy. Existing shaking table tests have revealed that the connection part may suffer from critical failure for the horizontal hybrid structure under severe ground motions (Isoda 2017). Table 3.4 presents axial tensile forces of the connection from the experiment and the numerical simulation. It is evident that the values computed by the analytical model are overstated compared with the experiment results. One distinct reason is that in the experimental specimen existed several subordinate connections while only the axial force of the main connection is measured during the tests (Fig. 3.14). Meanwhile in the numerical model only the main connection is simulated due to the thought of simplification. In this circumstance, the main connection in the numerical model sustains all the tension including the limited one which was apportioned by the subordinate connection in the test specimen. Therefore, the tension of the wood-core connection in the numerical model is overestimated.

(a)   (b)
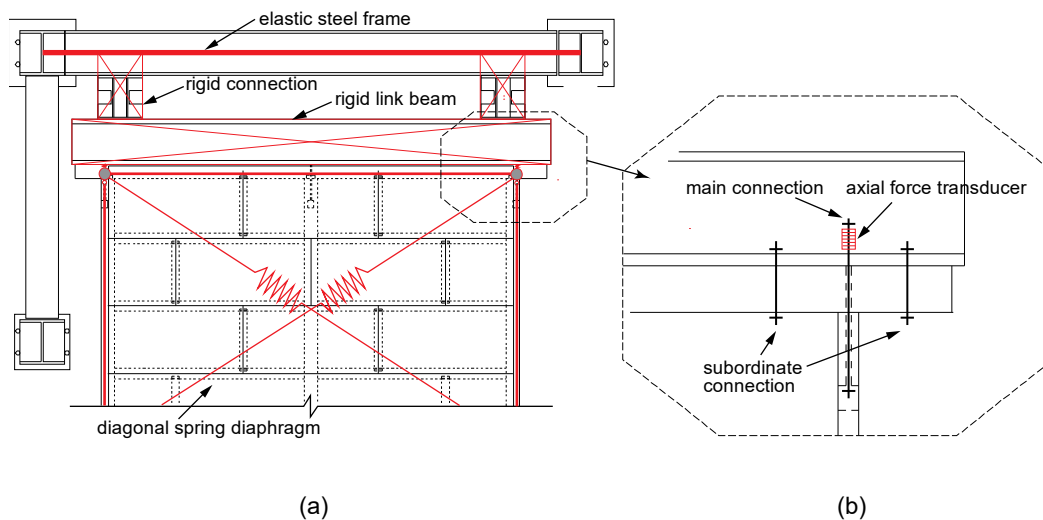
Fig. 3.14 Different design of connection between the (a) the numerical model and (b) the test specimen

Table 3.4 Maximum connection tension (kN)

PGA	Story								
	1F			2F			3F		
	Exp.	Num.	Error(%)	Exp.	Num.	Error(%)	Exp.	Num.	Error(%)
0.1g	0.34	0.54	58.8	0.63	1.23	95.2	0.75	1.29	72.0
0.2g	0.82	1.23	50.0	1.27	1.64	29.1	1.44	1.86	29.2
0.4g	1.77	1.88	6.2	3.01	3.20	6.3	2.31	2.94	27.2
0.6g	2.33	2.85	22.3	4.52	3.55	21.5	3.95	4.01	1.5
0.8g	4.71	5.4	24.6	7.20	6.62	–8.1	6.26	6.93	10.7

Error = (Num.-Exp.)/Exp.×100%

3.4 Conclusion

In this chapter, a numerical model is built in *OpenSees*. The model is composed of discrete beam and column while the shear wall and the diaphragm are simulated with linear springs. A user defined material is developed to simulate the performance of the shear wall and the diaphragm. The parameters of the material are calibrated base on the shaking table test in Chapter 2. In general, the built 3D numerical model was adequate to predict the seismic performance of the wooden horizontal hybrid structure, including the displacement and shear force demands during medium and severe earthquake scenarios. It is necessary to point out that the parameters used in the numerical model is calibrated directly from the experiment results, which is one of the major reasons why the accordance between the numerical simulation and the experiment are satisfactory. The purpose of the numerical simulation is not to predict the exact response of the test specimen, but to prove that the built numerical model, in which the wood shear wall and diaphragm are simulated with diagonal spring surrounded with rigid truss, is able to catch the dynamic characteristic of the wooden horizontal hybrid structure. Although discrepancies still exit, the numerical model is efficient to simulate the hybrid test specimen especially when subjected to moderate to severe ground motions. Therefore, using the built numerical model, parameter analysis is conducted in the next section to provide a better understanding of the response trend of the wooden horizontal hybrid structure with various design features.

4 Parameter study of concerned design feature

4.1 Introduction

Due to the force transfer mechanism between the core part and the wood part, the hybrid structure was susceptible to the dynamic difference between the two parts when subjected to the earthquake input paralleled to the connect section. Meanwhile, existing experiments indicated that the stiffness ratio between the shear wall and the diaphragm also had a major impact on the performance of the hybrid structure (Isoda *et al*. 2017). In the design stage of the test specimen, the stiffness of the core part was supposed to be rigid. Although the measured story lateral stiffness of the core part is 23 times of the wood part in the experiment, the design method is sufficient on specimen. The failure boundary of the proposed design method is not clear yet. Therefore, parameter study of the design feature for the wooden horizontal hybrid structure is conducted using time history analysis based on the built 3D numerical model in Chapter 3.

4.2 Concerned parameter

In the numerical model of the wooden horizontal hybrid structure, four concerned parameters which are supposed to have major influence on the dynamic property are defined as follows:

1. the stiffness ratio between the core part and the wood part (core-wood stiffness ratio)

$$\alpha = \frac{k_C}{k_S} \tag{4.1}$$

2. the mass ratio between the core part and the wood part (core-wood mass ratio)

$$\beta = \frac{m_C}{m_W} \tag{4.2}$$

3. the formal frequency ratio between the core part and the wood part (core-wood formal frequency ratio)

$$\gamma = \frac{\sqrt{k_C / m_C}}{\sqrt{k_S / m_W}} = \sqrt{\frac{\alpha}{\beta}} \tag{4.3}$$

4. the stiffness ratio between the wood diaphragm and shear wall (diaphragm-wall stiffness ratio)

$$\delta = \frac{k_D}{k_S} \tag{4.4}$$

where k_S, k_D and k_C are the initial stiffness of the wood shear wall, the diaphragm and the core frame; m_W and m_C are the lumped mass of wood part and the core part, respectively. Fig. 4.1 demonstrates the relative parameter in the profile of a simplified schematic model.

To make the results of the parameter analysis comparable and dependable, the numerical
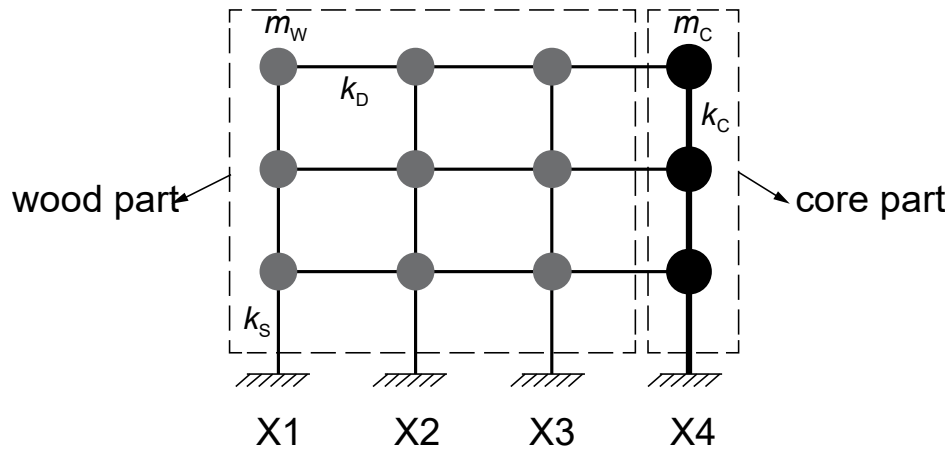
Fig. 4.1 Basic parameter used in the numerical model

investigation was performed by using the same model configuration with the S1 (Fig. C.2), with various concerned parameters. The core-wood stiffness ratio α was changing from 1 to 400, representing the design of the core part changing from a non-hybrid wood counterpart to a stiffer concrete or steel frame and then to a stiffest concrete shear wall structure. Meanwhile, the mass ratio β was changing from 1 to 8 in view of different design of the core part. The formal frequency ratio γ varied with the changing α and β automatically and was considered to be more representative of the inherent dynamic difference between the wood part and the core part. Besides, considering the use of flexible or rigid diaphragm, the diaphragm-wall stiffness ratio δ was changing from 1 to 200. It is worth noting that in the basic parameters, m_W and k_S were not changed during the analysis, in other words, the variation of the model configuration was focus on m_C, k_D and k_C.

4.3 Input ground motion

A total of 8 artificial and recorded earthquake ground motions with specified magnitude range of 6.7-8.3 and FEMA site class C or D (FEMA 2003) were chosen to examine the parameter influence of the hybrid structure. Detailed information of the ground motions is provided in Table 4.1 and the time history of acceleration is depicted in Fig. 4.2. The ground motions were a subset of the records set recommended by FEMA (FEMA 2009) and BCJ (Matushima 1995) in time history analysis. The BCJ set is 4 records provided by the Building Center of Japan to evaluate the seismic performance of high-rise buildings and earthquake-resistant buildings. The FEMA set is originally chosen to conduct nonlinear dynamic analysis and related collapse assessment of

archetype models. The set includes 22 far-field records and 28 near-field records. This paper chooses 7 representative records from the two sets to conduct the parameter analysis. The chosen criteria aim to cover a relative wide range of magnitude and rupture distance while including records with and without pulse. For each ground motion, only the horizontal record with the maximum PGA was used. To be consistent with the shaking table test, the time of the ground motions was firstly scaled to $1/\sqrt{3}$ of the original one. Then the magnitudes of the ground motions were scaled to a particular level on which their average 5% damping spectral acceleration equals to the design acceleration spectrum, namely spectrum of BCJ-L2, at the acceleration constant area, to be specific, from 0.1s to 0.4s in this study where the natural period of the S1 was also located in. Two level of input are tested in this chapter: moderate input with design PGA equals to 0.4g and severe input with design PGA equals to 0.8g. In Chapter 3, the built model is sufficient to predict the seismic performance of the wooden horizontal hybrid structure subjected to moderate and severe input. So the PGA of 0.4g and 0.8g are chosen to be the design PGA in this chapter. Fig. 4.3 shows the acceleration spectrum of the scaled ground motions with design PGA of 0.8g. There is one thing to point out that when the parameters of the 3D model changes, the natural period may change as well. In this condition, the natural period of the tested model could be out of the acceleration constant area. The scale factor in Table 4.1 is the PGA ratio between the used record and the original record. The chosen records are only scaled by the PGA and are supposed to provide a comparable results for the parameter analysis while without losing the discreteness of the various earthquakes. Therefore, the results of the parameter analysis are believed to be stable for various earthquake and design circumstance.
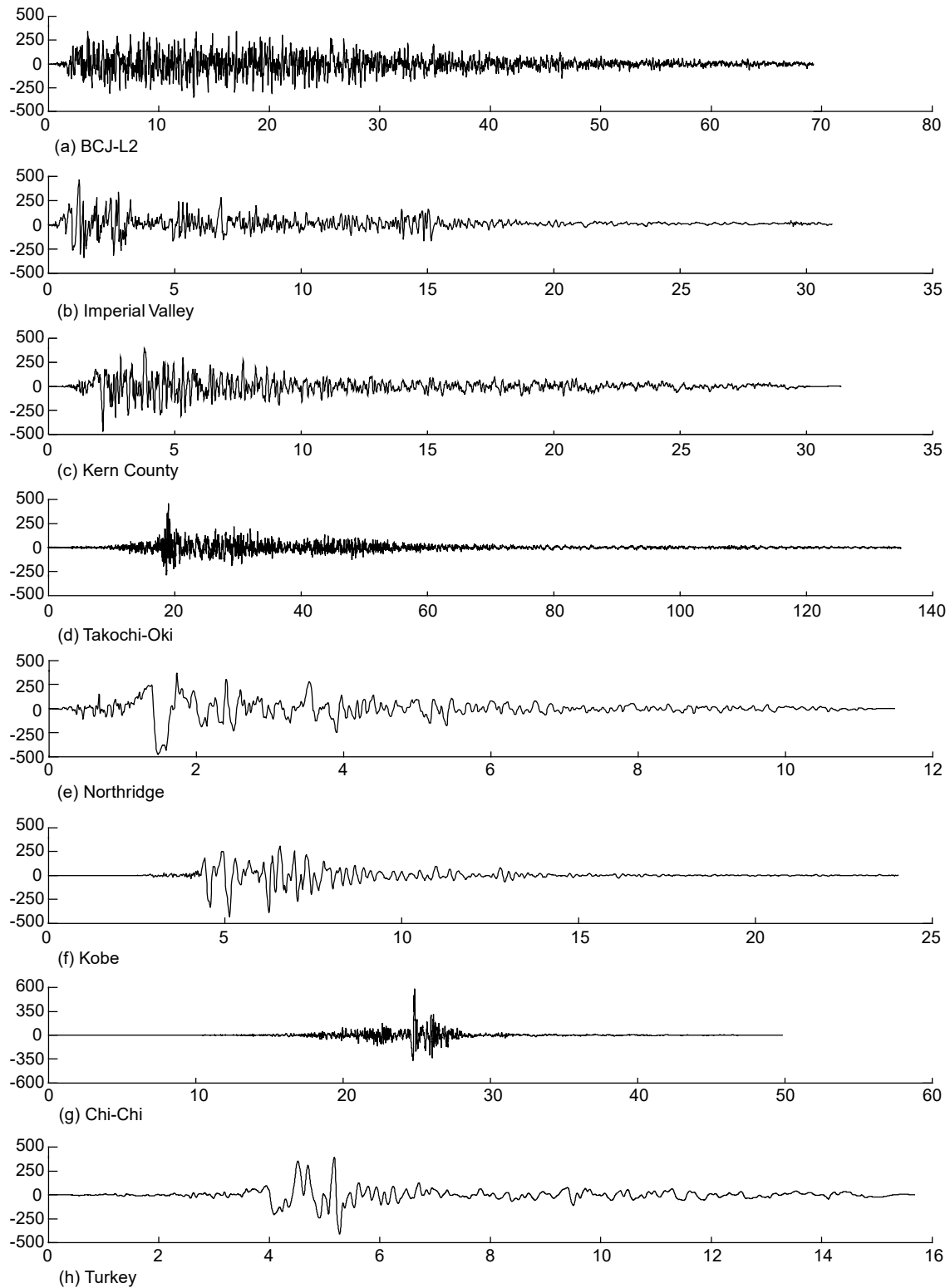
Fig. 4.2 Scaled acceleration time history of chosen inputs
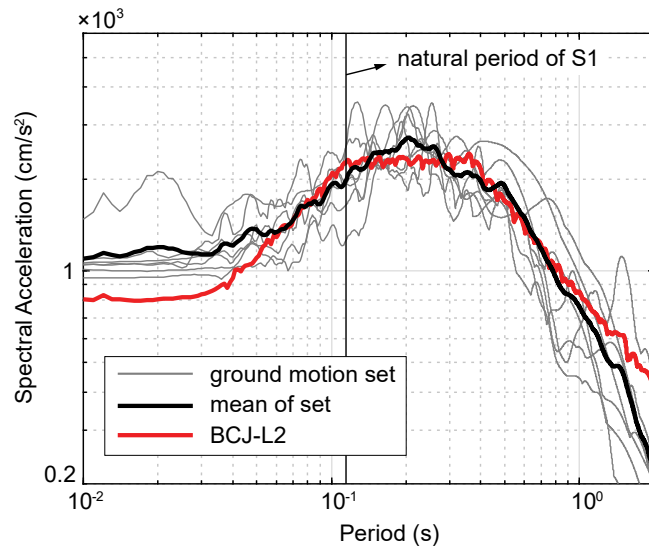
Fig. 4.3 Spectral acceleration of scaled chosen inputs

Table 4.1 Detail information of the chosen inputs

No.	event	year	station	Mw	R_{jb}(km)	Vs30(m/s)	PGA(g)	PGV(cm/s)	scale factor
1	BCJ-L2	—	—	—	—	—	0.36	—	2.22
2	Imperial Valley	1940	EI Centro#9	7	6	213	0.25	30	3.07
3	Kern County	1952	Taft Lincoln Sch.	7.4	38	385	0.17	16	6.03
4	Takochi-oki	1968	Hachinohe	8.3	—	—	0.24	18	4.52
5	Northridge	1994	Rinaldi Rec. St.	6.7	0	282	0.87	167.3	1.28
6	Kobe	1995	Kobe JMA	6.9	1	312	0.71	76	1.23
7	Chi-Chi	1999	TCU045	7.6	26	705	0.51	39	2.68
8	Kocaeli, Turkey	1999	Duzce	7.5	13.6	282	0.36	59	2.64

4.4 Influence of core-wood stiffness ratio α

4.4.1 Maximum displacement and shear force demand

(a)   (b)
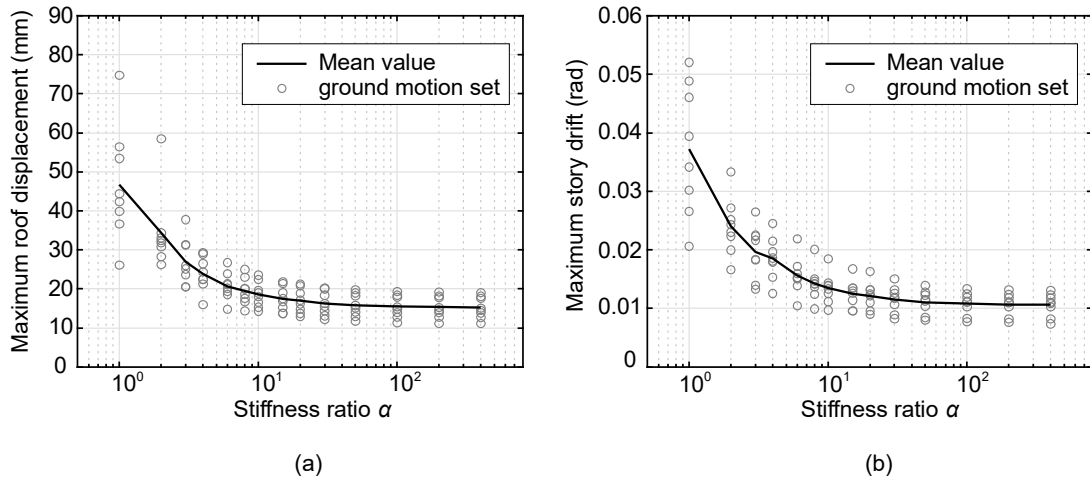
Fig. 4.4 Maximum displacement demands of numerical model versus various α; (a) roof displacement,

(b) story drift

(a)   (b)
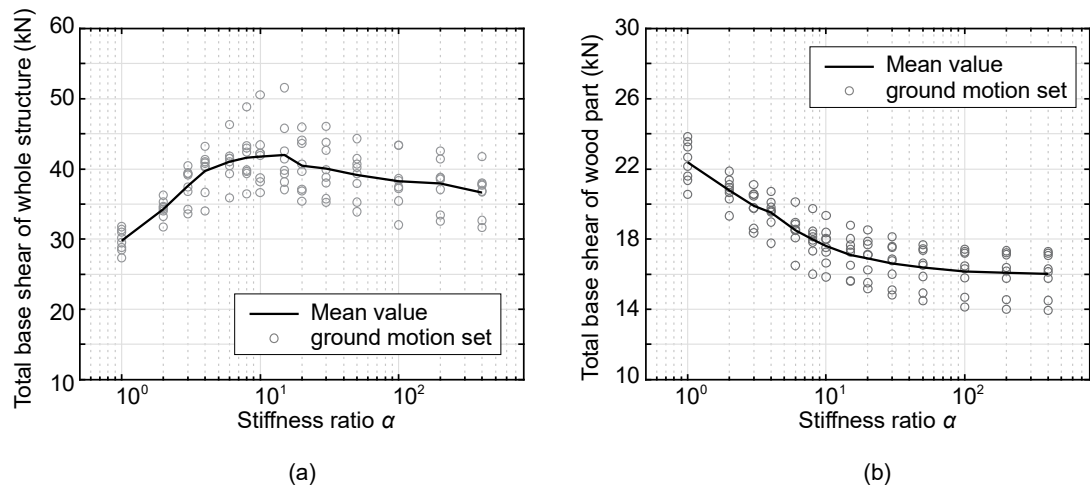
Fig. 4.5 Maximum shear demands of numerical model versus various α, (a) total base shear, (b) base

shear of wood part

Fig. 4.4 shows the displacement demands of the model with various stiffness ratio α, a constant

mass ratio β equals to 1 and a constant stiffness ratio δ equals to 1.05. At each stiffness ratio α, all

8 ground motions in Table 4.1 were used as the input. It is apparent that both the roof displacement and the maximum story drift decreased when the stiffness ratio α increased. The decrement slows down after the ratio is higher than 10 and level off when the ratio exceeds 50. Meanwhile, the difference between the different ground motion inputs narrows down as well. When the ratio α equals to 1, the peak value in the ground motion set of the maximum roof displacement is 2.9 times to the bottom value whereas the rate is 1.7 when the ratio α equals to 10. Notice that when the ratio α equals to 1, the model is a non-hybrid counterpart of the test specimen S1. The average story drift decrease around 60% when the core is 10 times stiffer than the wood part compared to the non-hybrid counterpart at the cost of an average 40% increment of the total base shear (Fig. 4.5(a)). The average total base shear increment then drops to 20% when the ratio α reached 400. The dropping is caused by the decrease of the natural period which leads to a lower spectral acceleration along with a lower response. When the ratio α is lower than 10, although the total base shear increases, the base shear of the wood part decreases instead, which indicated that increased base shear force was all sustained by the core part (Fig. 4.5(b)).

4.4.2 Maximum tension of connection
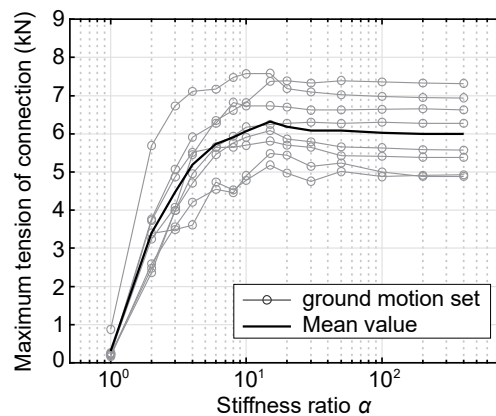
Fig. 4.6 Maximum tension of a single connection versus various α

Fig. 4.6 illustrates the maximum tension of a single connection during the simulation. The relationship between the tension with the ratio α is approximately double-linear and the inflection point is around $\alpha=10$.

4.4.3 Shear force distribution

(a)   (b)
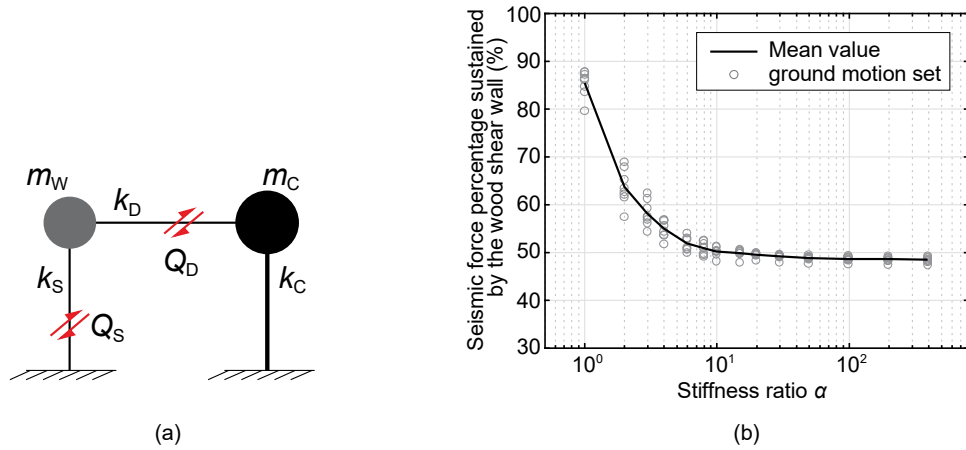
Fig. 4.7 (a) schematic diagram for force transfer, (b) seismic force percentage sustained by wood shear wall versus various α

(a)

(b)
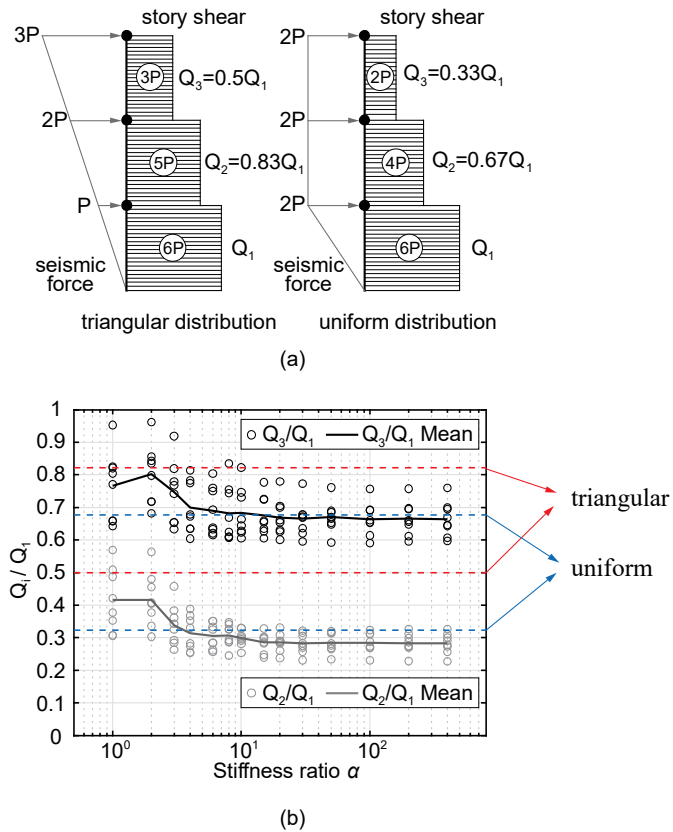
Fig. 4.8 Vertical shear force distribution, (a) theoretical, (b) numerical

4-8

Fig. 4.7 demonstrates the transfer of the seismic force generated by the wood part and the relative percentage sustained by the wood shear wall, in other words, the proportion of the shear force which is transferred to the ground through the wood shear wall (Q_S) in the total shear force generated from the wood part mass (Q_S+Q_D). The proportion decreases rapidly with the increase of the ratio α and keeps around 50% after the ratio reaches 10. This stable extremum of the percentage is effected by all the parameters of α, β, and δ which will be demonstrated in Section 4.6. The vertical shear force distribution of the wood part is shown in Fig. 4.8 where Q_i refers to the lateral shear force of the wood part in i-story. It is believed that the seismic force distribution changed from inverted-triangular to uniform while the ratio α increased. When the ratio α equals to 1, the model is a non-hybrid structure and, as expected, the shear force ratio Q_2/Q_1 and Q_3/Q_1 are in accordance with the triangular distribution. When the ratio α is higher than 10, the shear force ratio Q_2/Q_1 and Q_3/Q_1 decreased and are in accordance with the uniform distribution.

4.5 Influence mass ratio β and formal frequency ratio γ

4.5.1 Maximum roof displacement and base shear of wood part

Apart from the ratio α, the mass ratio β also could be different due to various structural design. With two various parameters, the influence of the parameters on the property of the hybrid structure is difficult to distinguish. A more intrinsic parameter is needed to define the difference between the wood part and the core part. Therefore, the formal frequency ratio γ is used to normalize the influence of α and β with a constant δ =1.05. The physical implication of the ratio γ is the vibration period ratio between the core part and the wood part. The higher the ratio, the greater the dynamic difference between the core part and the wood part. It should be pointed out that the ratio γ is not the exact period ratio between the two parts but has the same dimension with it. From Fig. 4.9 to Fig. 4.12, the displacement and force demands demonstrates a distinct and identical trend change regardless of the variation of the ratio β. For various inputs, the magnitude of the demands are different but the trends are the same: the demands decrease with the growth of the ratio γ and the decrease tendency nearly stops when the ratio γ is higher than 3. When PGA rises from 0.4g to 0.8g, the tendency doesn't change for all the inputs. It indicates that the proposed formal frequency ratio γ is stable for various design of the core part and different ground motions, therefore, the ratio γ is sufficient to distinguish the dynamic difference between the core part and the wood part.

(a) BCJ-L2

(b) Imperial Valley

(c) Kern County

(d) Takochi-Oki

(e) Northridge

(f) Kobe

(g) Chi-Chi

(h) Turkey
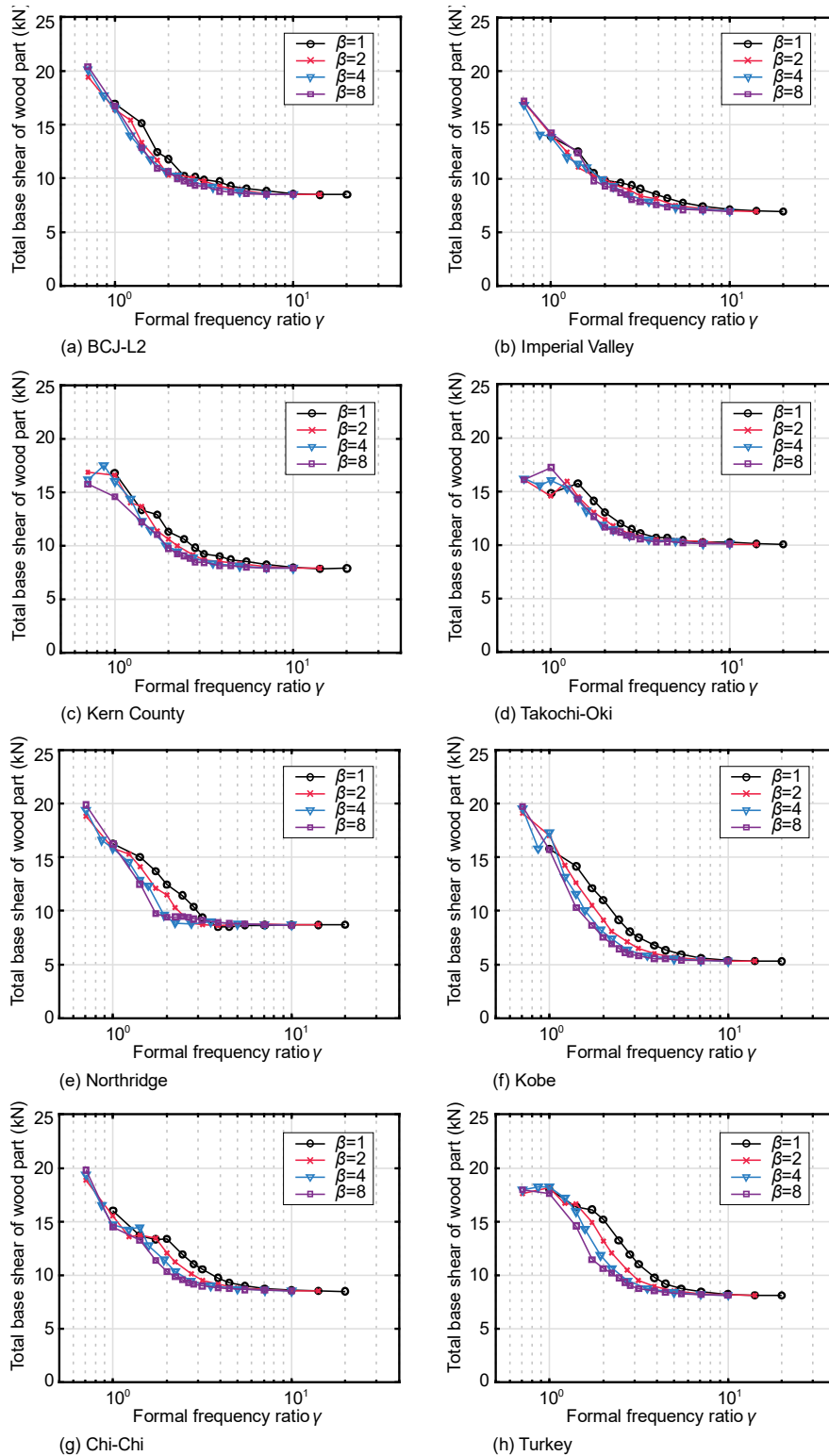
Fig. 4.9 Maximum roof displacement versus various γ, PGA=0.4g
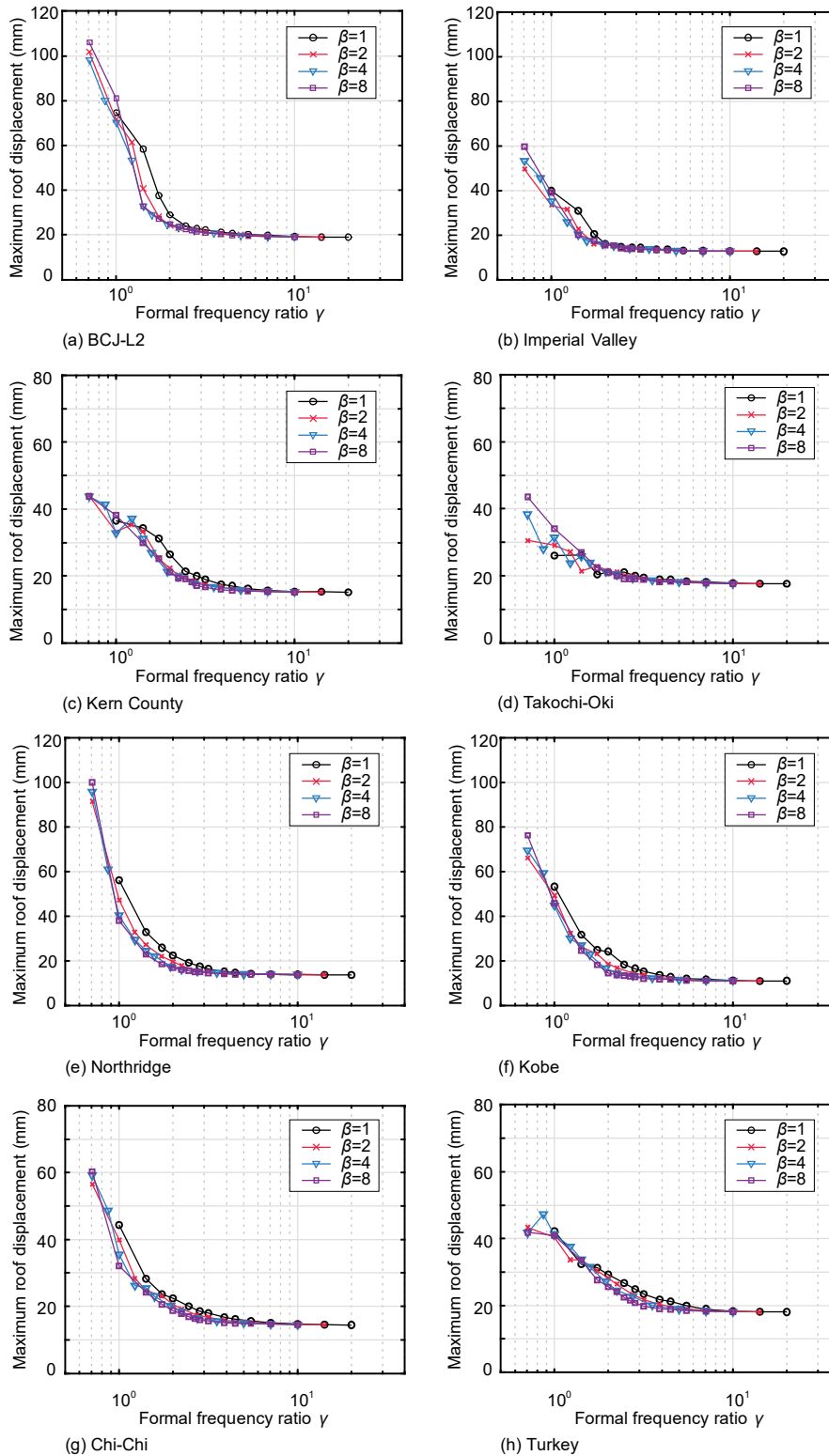
Fig. 4.10 Maximum roof displacement versus various γ, PGA=0.8g

(a) BCJ-L2

(b) Imperial Valley

(c) Kern County

(d) Takochi-Oki

(e) Northridge

(f) Kobe

(g) Chi-Chi

(h) Turkey
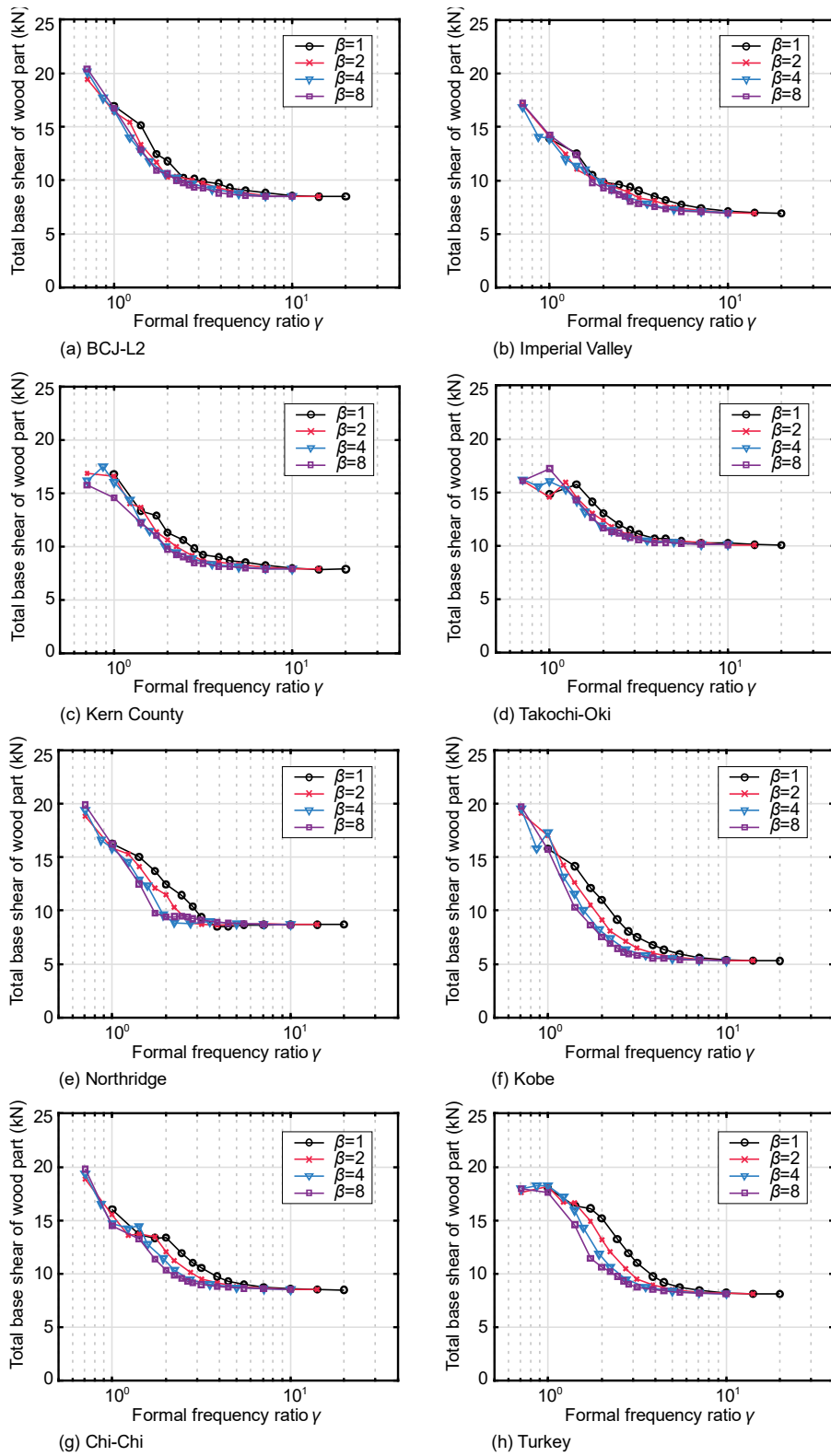
Fig. 4.11 Maximum base shear of wood part versus various γ, PGA=0.4g
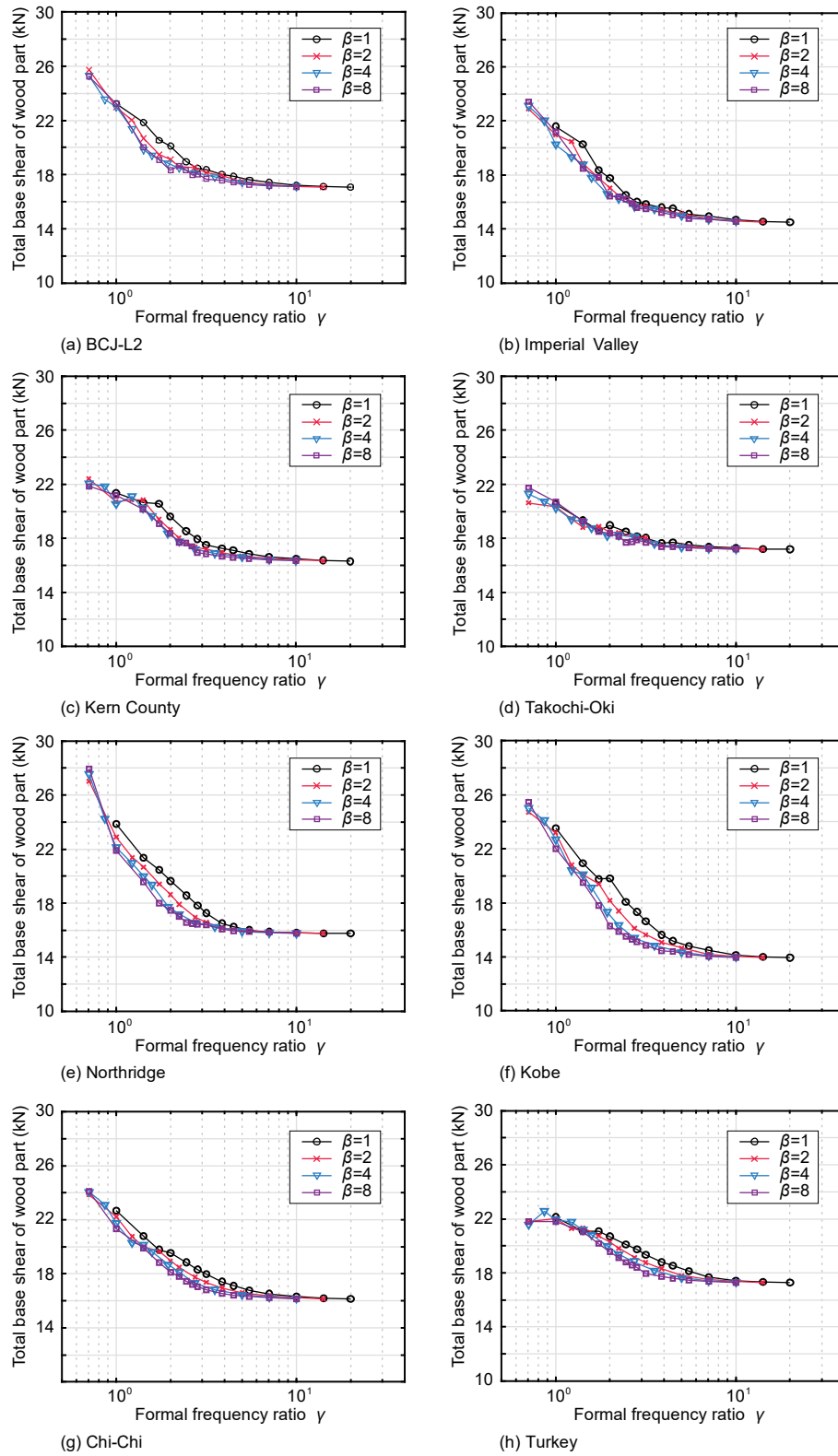
Fig. 4.12 Maximum base shear of wood part versus various γ, PGA=0.8g

4.5.2 Shear force distribution

In Fig. 4.13 and Fig 4.14, the seismic force percentage is discrete when γ is smaller than 3 and with the increase of γ, the percentage come to a constant value 50% which is believed to have a close relationship with the ratio δ=1.05 used here. It is apparent that the seismic performance of the wood part is susceptible to the minor ratio γ. When the ratio γ is higher than 3, its influence on the performance was limited. For most of the ground motions, the stable percentage is around 50% except for the Chi-Chi earthquake whose stable percentage is 58% (Fig. 4.13(b), Fig. 4.14(b)). For each ground motion, when the PGA rises from 0.4g to 0.8g, the stable shear force percentage does not have a distinct change. Therefore, in the seismic design of the wooden hybrid structure, the formal frequency ratio γ is recommended to be higher than 2 or 3 to achieve a steady and predictable performance regardless of the various design of the core part and the different inputs.

(a) BCJ-L2

(b) Imperial Valley

(c) Kern County

(d) Takochi-Oki

(e) Northridge

(f) Kobe

(g) Chi-Chi

(h) Turkey
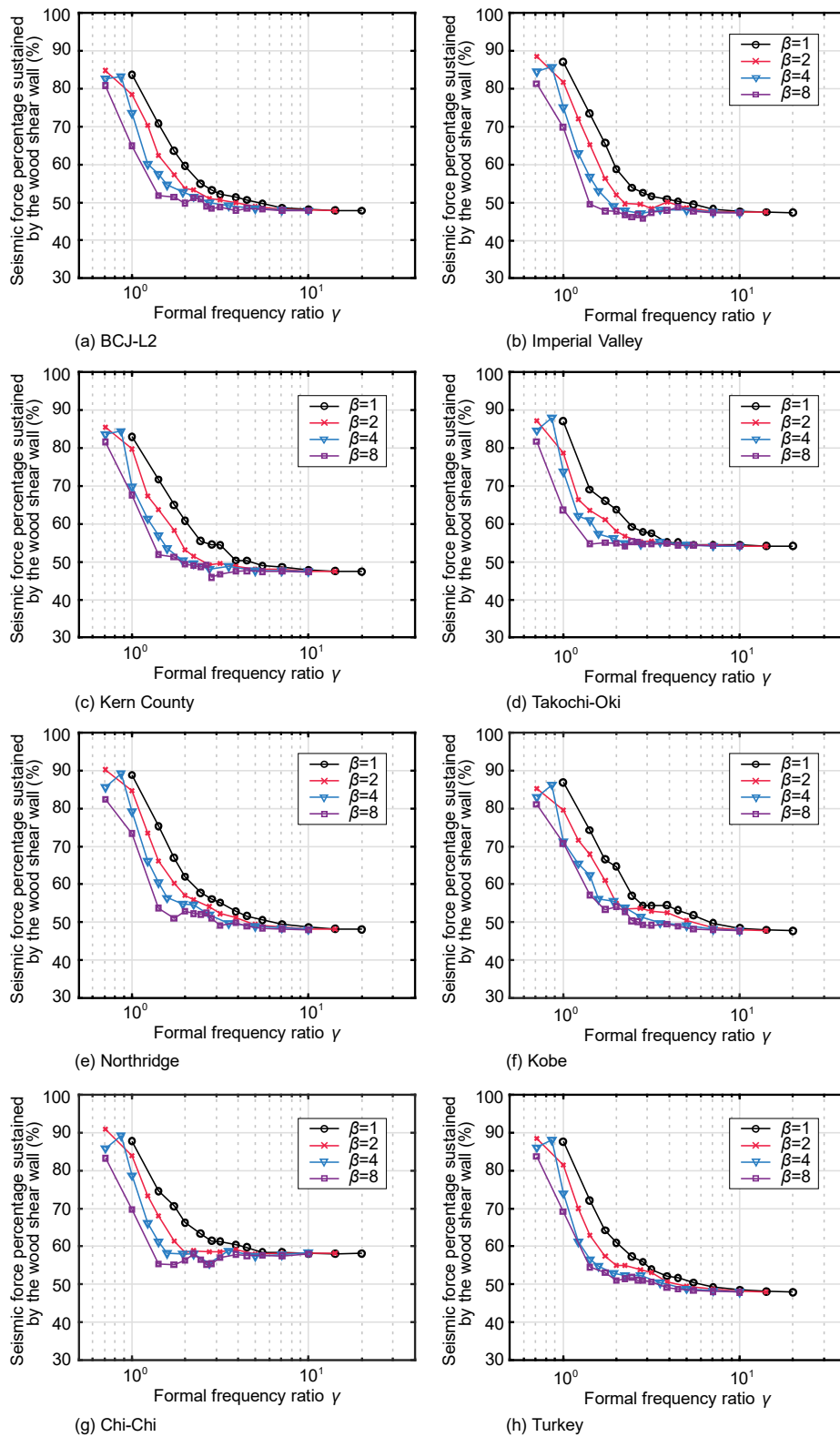
Fig. 4.13 Seismic force percentage sustained by wood shear wall versus various γ, PGA=0.4g

(a) BCJ-L2

(b) Imperial Valley

(c) Kern County

(d) Takochi-Oki

(e) Northridge

(f) Kobe

(g) Chi-Chi

(h) Turkey

Fig. 4.14   Seismic force percentage sustained by wood shear wall versus various γ, PGA=0.8g

4.6 Influence of diaphragm-wall stiffness ratio δ

In this section the mass ratio β of the numerical model is constantly 3 which is same with shaking table specimen S1 and since the results of different inputs are roughly similar only the results of BCJ-L2 is presented.

Fig. 4.15(a) shows the maximum story drift versus the diaphragm to shear wall stiffness ratio δ. The influence of δ is evident since the average maximum drift decreases nearly 50% when δ changes from 1 to 2. The acceleration amplification factor also decreases rapidly with the increase of δ in Fig. 4.15(b). It is worth noting that the total base shear versus δ has different trend for various α (Fig. 4.15(c)). When α=23 and 50 the base shear increases along with δ, whereas an opposite trend is observed when α = 200 and 400. The inconsistency was caused by the change of the natural period. When α was high, which means the core part was rigid enough, the increase of δ could reduce the period of the first mode by increasing the total stiffness of the hybrid structure. According to the spectrum of the inputs, the natural period may shift to the ascent stage and consequently mitigate the seismic response. The change of the natural period is also reflected on the connection force in Fig. 4.15(d) where the same inconsistency is found for 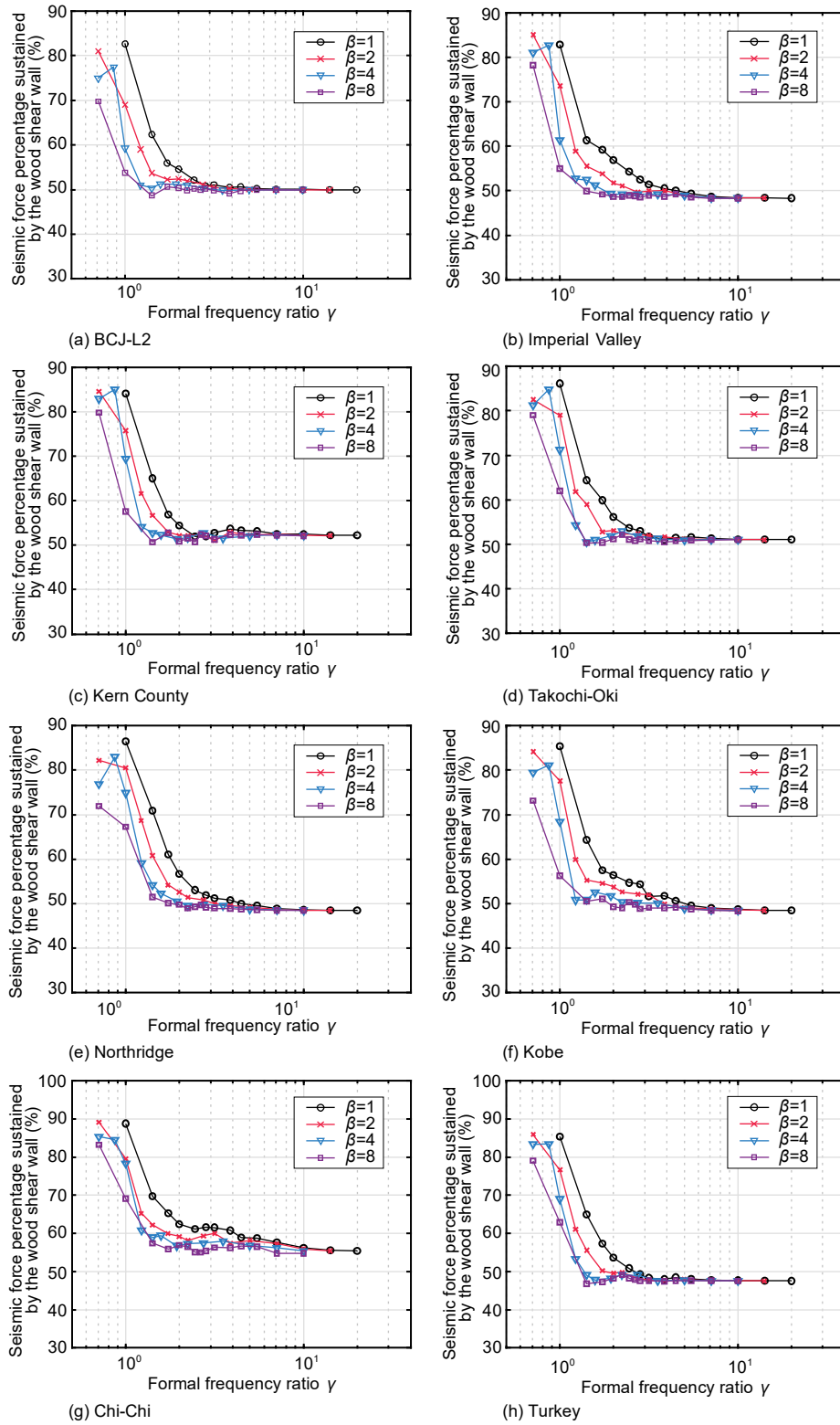low and high α. In general, the diaphragm to shear wall stiffness ratio was recommended to locate in range from 2 to 4 which would mitigate the seismic response while limiting excessive growth of the seismic shear in the base and connection. If the core part was rigid enough ($\alpha \geq 200$), the ratio δ could also be higher than 50 to achieve the same mitigation influence.

Considering the force transfer mechanism between the shear wall and diaphragm, the ratio δ was supposed to have a major impact on the distribution of shear force between the wood part and the core part. In the seismic analysis for normal structure, the seismic force of the shear members is usually distributed by the relative stiffness of the member. However, in the horizontal hybrid structure, the situation was slightly different. Fig. 4.16 demonstrates the shear force proportion between the shear wall and diaphragm. The value distributed directly by stiffness between the shear wall and diaphragm have a large deviation from the numerical analysis (Num.) especially for a relatively small α. The reason was that the diaphragm and the core part could participate into a joint vibration when the core was not extremely rigid, in which case they could be considered as springs in series whose stiffness was much smaller that the diaphragm itself. Therefore, the shear force distribution between the shear wall and the diaphragm is modified considering the influence of the core part as follows:

$$\rho = \frac{k_S}{k_S + k_0} = \frac{1}{1/(\beta/\alpha + 1/\delta) + 1} \tag{4.5}$$
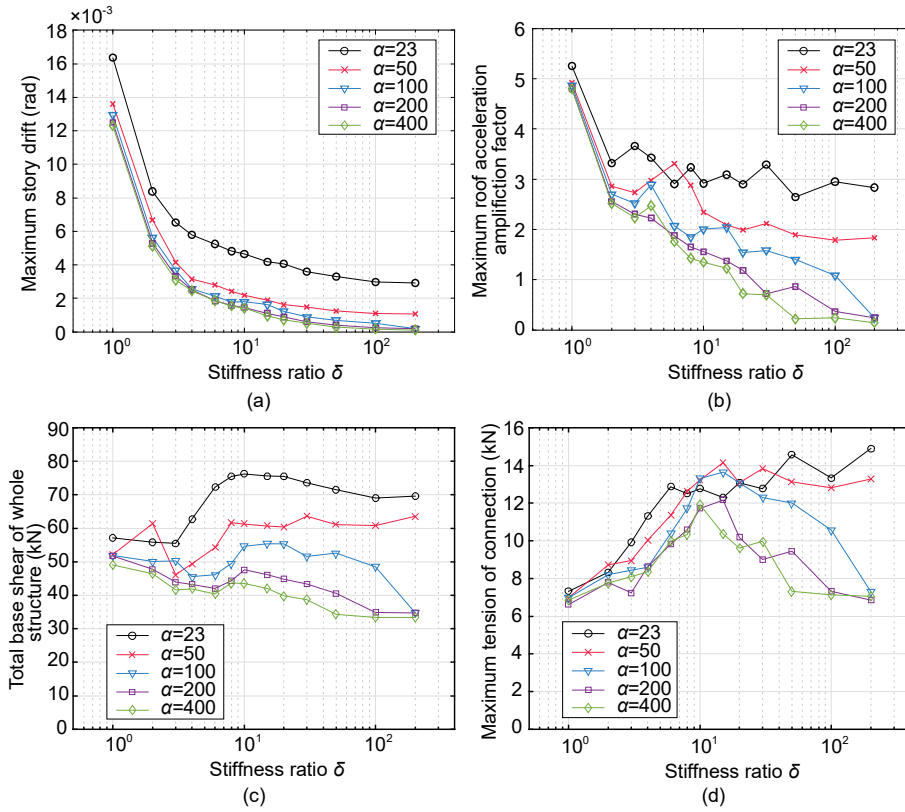
Fig. 4.15 Maximum demand of numerical model versus various δ when subjected to BCJ-L2 with PGA=0.8g, (a) story drift, (b) roof acceleration amplification factor, (c) total base shear, (d) tension of single connection

$$k_0 = \frac{1}{1/k_D + 1/k_C'} \tag{4.6}$$

$$k_C' = k_C/\beta \tag{4.7}$$

in which ρ is the seismic force percentage sustained by the wood shear wall; k_0 is the series stiffness of the diaphragm and the core part; k_C' is the stiffness of the core part normalized by the mass ratio β. The good match between the results calculated from Eq. (4.5)-(4.7) (Cal.) and the ones from the numerical analysis (Num.) indicated that the modification process was efficient (Fig. 4.15).
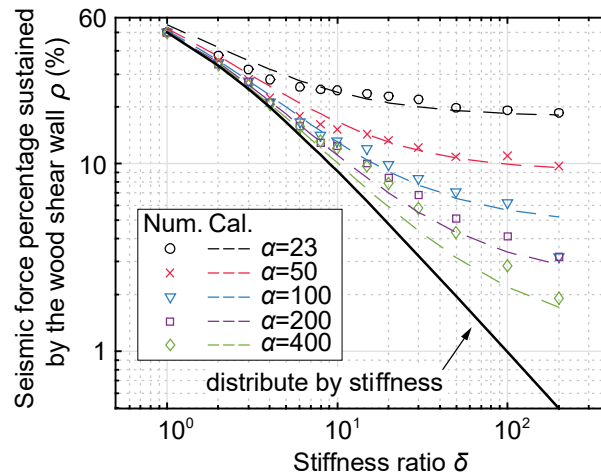
Fig. 4.16 Prediction of seismic force percentage sustained by the wood shear wall

4.7 Conclusion

To extend the understanding of the seismic performance of the wooden horizontal hybrid structure. Parameter analysis was also conducted to study the influence of several concerned parameters based on the built numerical model. The main contributions of this investigation are as follows:

- Increase of the core-wood stiffness ratio could significantly mitigate the seismic response of the hybrid structure at the cost of increasing seismic shear at the connection and the total base shear. The increased base shear was all sustained by the core part. Meanwhile the vertical shear distribution of the wood part would change from inverted-triangular to uniform. Increase of the diaphragm-wall stiffness ratio could also mitigate the seismic response yet obviously magnify the force demand of the connection. However, if the core part was rigid enough, further increase of the diaphragm-wall stiffness ratio would reduce the seismic response while limiting excessive growth of the seismic shear in the base and connection.

- The formal frequency ratio was an efficient indicator to distinguish the seismic difference between the wood part and the core part. In the seismic design of horizontal hybrid structure, the ratio was recommended to be higher than 2 or 3 to achieve a steady and predictable performance regardless of the various design of the core part.

- The shear force distribution between the wood shear wall and diaphragm was affected by both the diaphragm-wall stiffness ratio and the core-wood stiffness ratio. The proposed equation provided an effective prediction on the shear force distribution compared with the conventional distribution by relative stiffness.

5 Simplified method for evaluation seismic loading of wooden horizontal hybrid structure

5.1 Introduction

The concept of hybrid structure has marked one of the useful developments for elevating seismic safety of structural systems since it combines the advantages of different materials and building types. Wooden horizontal hybrid structure, as a novel kind therein, has shown some beneficial features in improving the seismic performance compared to the traditional lightweight wood structure. The representative type of the wooden horizontal hybrid structure studied in this research is shown in Fig. 5.1. The wood part is a multi-story lightweight wood frame with lateral shear resistance member. And it is horizontally connected to the relative rigid core part, which is built with steel frame, concrete frame or concrete shear wall system. In a symmetric design the wood parts are separated by the core parts in the length of the building. The earthquake input direction studied in this research is vertical to the length of the building since the wood part is a complex multi-degree-of-freedom system in that direction. During the earthquake, the seismic force derived from the wood part is transferred in two ways: one way through the lateral shear member (wood shear wall or moment-resisting frame) to the ground; the other way through the diaphragm to the core part. In addition, the gravities of the two parts are sustained by their respective vertical components. The irregularity of horizontal stiffness usually causes torsion in seismic scenario for traditional building type (Fig. 5.1(c)). However in this wooden horizontal hybrid type, the wooden flexible diaphragm suppress the torsion vibration of the whole building, resulting in the major shear deformation of the diaphragm itself (Fig. 5.1(d)). Also, the preferred symmetric design provides further suppression on the torsion vibration. Therefore, the wood part could be simplified into a 2D frame in which only the shear deformation is concerned (Fig. 5.1(b)).

The characteristics of structure with flexible diaphragm and rigid core has been studied by several researchers. Kim and White (2004) investigated the results of shaking table tests on a half-scale one-story reinforced masonry building with a flexible diaphragm and based on the test, a simplified multiple-degree-of-freedom approach was proposed and corresponding model calibration process was performed to provide accurate prediction of the dynamic response. Lee et al. (2007) found that in structures with flexible diaphragm as the diaphragm became more flexible, the contribution of higher mode tended to be increasing, and a mode based method was proposed to estimate the inter-story drift of low-rise structures with flexible diaphragm. Humar and Popovski (2013) presented the linear and nonlinear seismic response of large-scale single-story building with flexible diaphragms. Koliou *et al*. (2016a, b) studied the collapse performance of
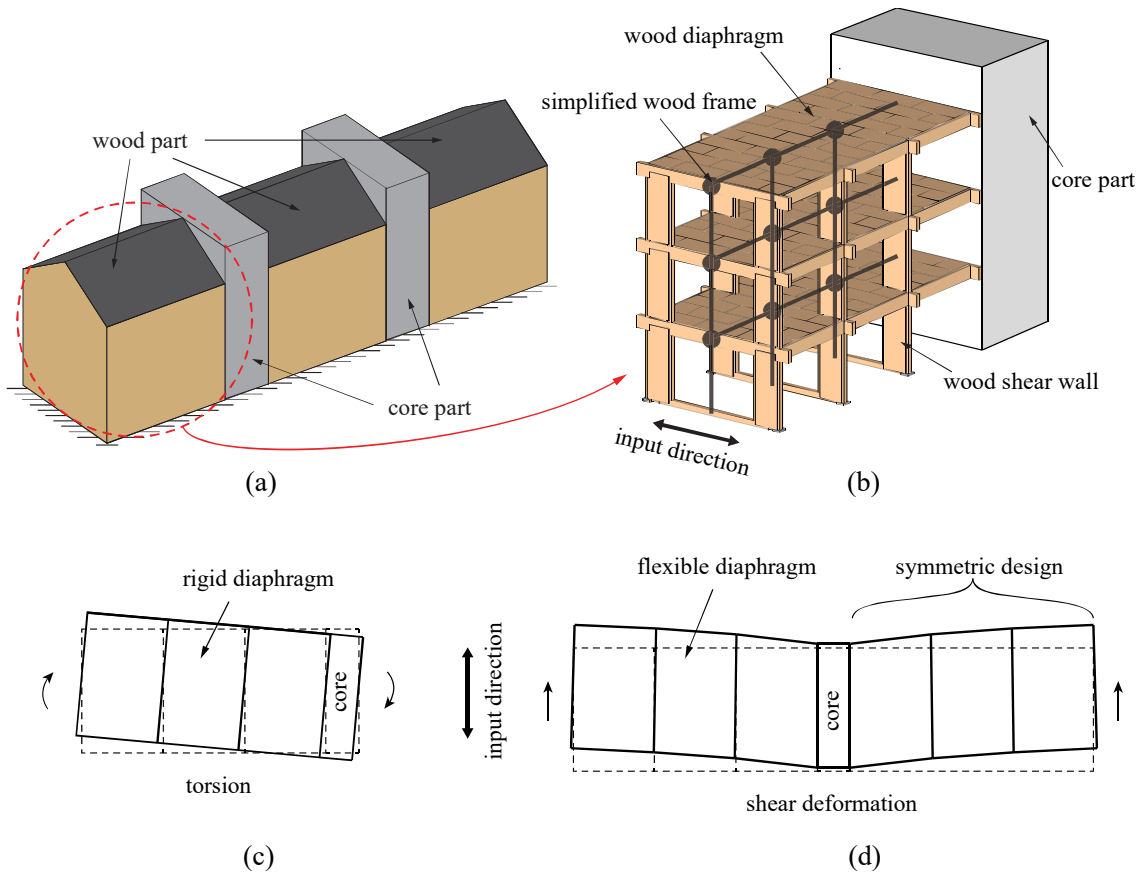
Fig. 5.1 Typical type of wooden horizontal hybrid structure (a) general layout; (b) one kind of detailed design of the wood part and the possible simplified frame; and relative deformation mechanism (c) building with rigid diaphragm; (d) building with flexible diaphragm and symmetric design

the rigid wall-flexible diaphragm system and proposed a seismic design approach to account for flexible roof diaphragm response by distributing yielding in the roof diaphragm as the predominant inelastic response under extreme ground shaking.

Notwithstanding these findings, a simple procedure is still required to estimate the seismic force for the horizontal hybrid structure, especially in the preliminary linear design stage. In earthquake engineering practice, equivalent lateral force (ELF) method has been widely used for the linear seismic analysis. Although the ELF method has strict prerequisites and the results are approximate, it has been absorbed into the build codes of many counties (ICBO 1997, CEN 2004, Ministry of Construction 2005, ASCE 2010) on account of the convenience during the linear seismic design. However, due to the inherent lateral irregularity in both mass and stiffness, wooden horizontal hybrid structure is theoretically difficult to be analyzed by the ELF method. To estimate the seismic force of the wooden horizontal hybrid structure, a new approximation is

developed in this study by using the theory of ELF method and the proposed dual equivalent lateral force (DELF) method is tested by the case study of the shaking table test conducted in Chapter 2. It is shown that the DELF method is sufficient to provide a reasonable estimation of the seismic force for the linear seismic design.

5.2 Equivalent lateral force method

5.2.1 Basis and feature of ELF method

Firstly, the standard procedure of the ELF method is derived and demonstrated since the DELF method is based on it. The basis and some features of the ELF method is list blow (FEMA 2007):

1. Use empirical period of vibration;

2. Use smoothed response spectrum;

3. Compute total base shear V as if single degree of freedom;

4. Distribute V along height assuming regular geometry;

5. Method if based on fist mode response;

6. Provide a reasonable estimate of the envelope of story shear, not to provide accurate estimates of story force;

5.2.2 Procedure of ELF method

Step 1: Calculate the total base shear.

$$V = C_{s}W \tag{5.1}$$

$$C_{s} = S_{a}(T_{1}) \tag{5.2}$$

$$W = C_{p}Mg \tag{5.3}$$

Where

V = total design base shear;

W = total effective seismic weight;

C_{s} = seismic response coefficient of hybrid structure;

S_{a} = spectral acceleration of the concerned ground motion, 5% damping used in this paper;

T_{1} = the natural period of the structure;

C_{p} = participation factor of the total weight of the structure, set to 85% in this paper;

g = gravity acceleration, set to 9.8m/s^{2} in this paper
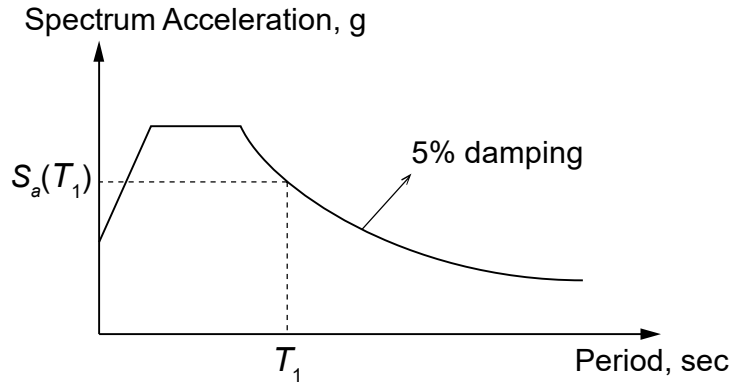
Fig. 5.2 Spectral acceleration used in ELF method

In ELF method, the base shear is simply the spectral acceleration times the weight of the building. The acceleration S_a is determined from the 5% damped elastic spectrum as shown in Fig. 5.2 while T is the natural period of the structure. There is one thing to point out that in ASCE 10, the first mode effective mass is assumed to be equal to total seismic mass M. It means that the modal participation factor for the first mode is assumed to be 1.0 and that 100% of the weight is assigned to the first mode. However, in the building law of some country, such as China, the weight used for the calculation of the base shear in the ELF method is set to 85% of the total weight (Ministry of Construction 2005). The reduction of the factor is to take the influence of the higher mode in the multiple-degree-of-freedom system into consideration. In that condition, the seismic weight is not totally assigned to the first mode to calculate the total base shear. For the wooden horizontal hybrid structure in this study, the dynamic freedom in the concerned input direction is multiple degree and the higher model may participate into the vibration to some extent. Therefore, in the following calculation of the ELF and DELF method, the participation factor of the weight is set to 85%.

   Step 2: Distribute the seismic shear along the height of the structure.

$$F_n = C_n V \tag{5.4}$$

$$F_n = \frac{h_n}{h} d_r \omega_1^2 \frac{w_n}{g} \tag{5.5}$$

$$V = \sum_{n=1}^{N} F_n = \frac{d_r \omega_1^2}{hg} \sum_{n=1}^{N} h_n w_n \tag{5.6}$$

$$C_n = \frac{w_n h_n}{\sum_{i=n}^{N} w_n h_n} \tag{5.7}$$

where

F_n = lateral seismic force of n-story;

d_r = displacement of the roof;

C_n = vertical distribution factor of n-story;

W_n = seismic weight of n-story;

h_n = height of n-story;

N = number of stories.

While distributing the shear along the height of the structure, the implicit assumption is that the first mode shape is a straight line and the total acceleration can be approximated as the displacements times the frequency squared as depicted in Fig. 5.3. Given the displacement at any height, the acceleration is determined and the inertial force are combined to provide the total base shear.
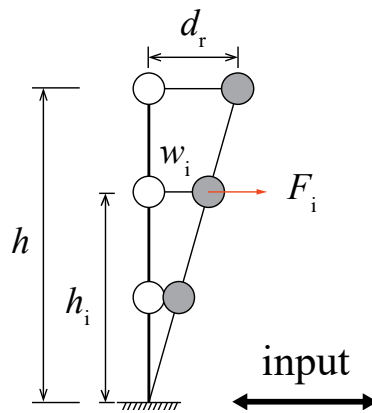
Fig. 5.3 Distribution of shear force in ELF method

5.3 Dual equivalent lateral force method

5.3.1 Assumption and feature of DELF method

The DELF method is difficult to be conducted and testified on a real horizontal hybrid building at this stage, considering the absence of engineering practice and seismic record. As an alternative approach, shaking table test on the horizontal hybrid structure is an ideal analysis object with its controllable condition and detailed record. Therefore, one of the test specimens S1 is chosen from the conducted shaking table test in Appendix C to illustrate the whole procedure of the DELF method. The chosen test specimen is a typical horizontal hybrid structure. The wood part is a 3-story, 3-bay wood frame with two shear panels at each frame of all the 3 stories (Fig. C.2). The story stiffness and seismic mass of the wood part are approximately uniform along the height and the length. The modal analysis in Chapter 2 indicated that the shape of the first mode is approximately straight line in both the height and the length for the wood part (Fig. 2.4). The displacement of wood part decreases linearly from the roof to the base and from the outer frame to the core part, respectively. Given the assumption that the acceleration can be approximated as the displacement times the frequency squared, the ELF method could be conducted in the hybrid structure with a proportionate seismic force distributed on the wood part.

The core part is a rigid steel frame which has high lateral stiffness along the input direction. In the test specimen, the stiffnesses of the wood shear wall and the wood diaphragm were quite close, and the stiffness of the core part was nearly 23 times greater than the wood part which is applicable for the DELF method. According to the parameter analysis in Chapter 4, the response of the wood part is stable and exonerative to the influence of the various magnitude of the inputs as the core part is define as rigid. Meanwhile the change of the core part would not affect the seismic force distribution between the core part and the wood part. In this condition, the response of the wood part and the core part could be analyzed separately.

For the DELF method, firstly, the hybrid structure should be simplified as a 2D frame which is perpendicular to the concerned input direction (Fig. 5.4(1)). When the hybrid structure is subjected to the seismic scenario in the concerned direction, the wood part vibrates as a two-edge-constrained plate (Yamazaki and Sakata 2016). The main idea of the DELF method is to separate the complex vibration mechanism of the wood part into two distinct components: one is the vibration of an ordinary independent wood frame, namely, Substructure A (Fig. 5.4(b)); the other one is the vibration of a horizontally oblique wood frame, namely, Substructure B (Fig. 5.4(c)). The separation itself is arbitrary and has no distinct theoretical argument, however, the basic structural implication exists: restrains of the wood part are released respectively and the responses of the corresponding substructures are combined to get the response of the original fully restrained

wood part. In Substructure A, the restraint of the core part is released; in Substructure B, the restraint of the ground is released and the rigid core part could be considered as the ground while the diaphragm is regarded as the shear wall of the frame. Both substructures are then simplified to a simple lumped mass system and evaluated by the ELF method, respectively (Fig. 5.4(d, e)). Naturally, the assumptions of the ELF method restrain the scope of this study. Different building code proposes specific limitations of using the ELF method, but most general limitations are structure regularity and its height or period. Therefore, the hybrid structure studied here should be a low-rise building in both height and length, also the wood part could be divided into regular story levels with uniform or approximately uniform mass and stiffness along the vertical and horizontal orientation. It is worth noting that the core part in Substructure B is assumed to act as the ground which could provide equal acceleration along the height, however, since the core part is not perfectly rigid the actual acceleration is always higher on the upper story which makes the DELF method inevitably underestimate the seismic demands of the upper story. In fact, the parameter analysis in Chapter 4 indicated that the formal frequency ratio between the core part and the wood part should be higher than 3 to make sure that the fundamental mode vibration of the wood part was not notably affected by the vibration of the core part.

There exists another concern about the connection between the wood part and the core part. Experiment indicated that the connection may suffer from severe damage when the hybrid structure is subjected to major earthquakes (Isoda *et al*. 2017). However for the ELF and DELF method, the involved design stage is the minor earthquake during which the whole hybrid structure is supposed to be linear including the connection. Regardless of the use of damper or seismic isolation device at the connection part, the shear stiffness of the connection should be much higher than the diaphragm. In that condition, the assumption about approximately perfect fixity between the wood part and the core part is reasonable and the Substructure B could be evaluated by the ELF method. After the ELF analyses of Substructure A and Substructure B are finished, the seismic force of each story is distributed to each lumped node by the weight of the node mass (Fig. 5.4(f, g)). Then the seismic force of these two substructures are combined by the stiffness of the relative vertical force transfer element: the wood shear wall in Substructure A and the diaphragm in Substructure B (Fig. 5.4(h)). The weighted geometric mean is used here and the weight factor represents the period difference between the substructures and the original wood part. Higher stiffness of vertical force transfer element means closer period with the original wood part and the higher participation in the fundamental vibration.
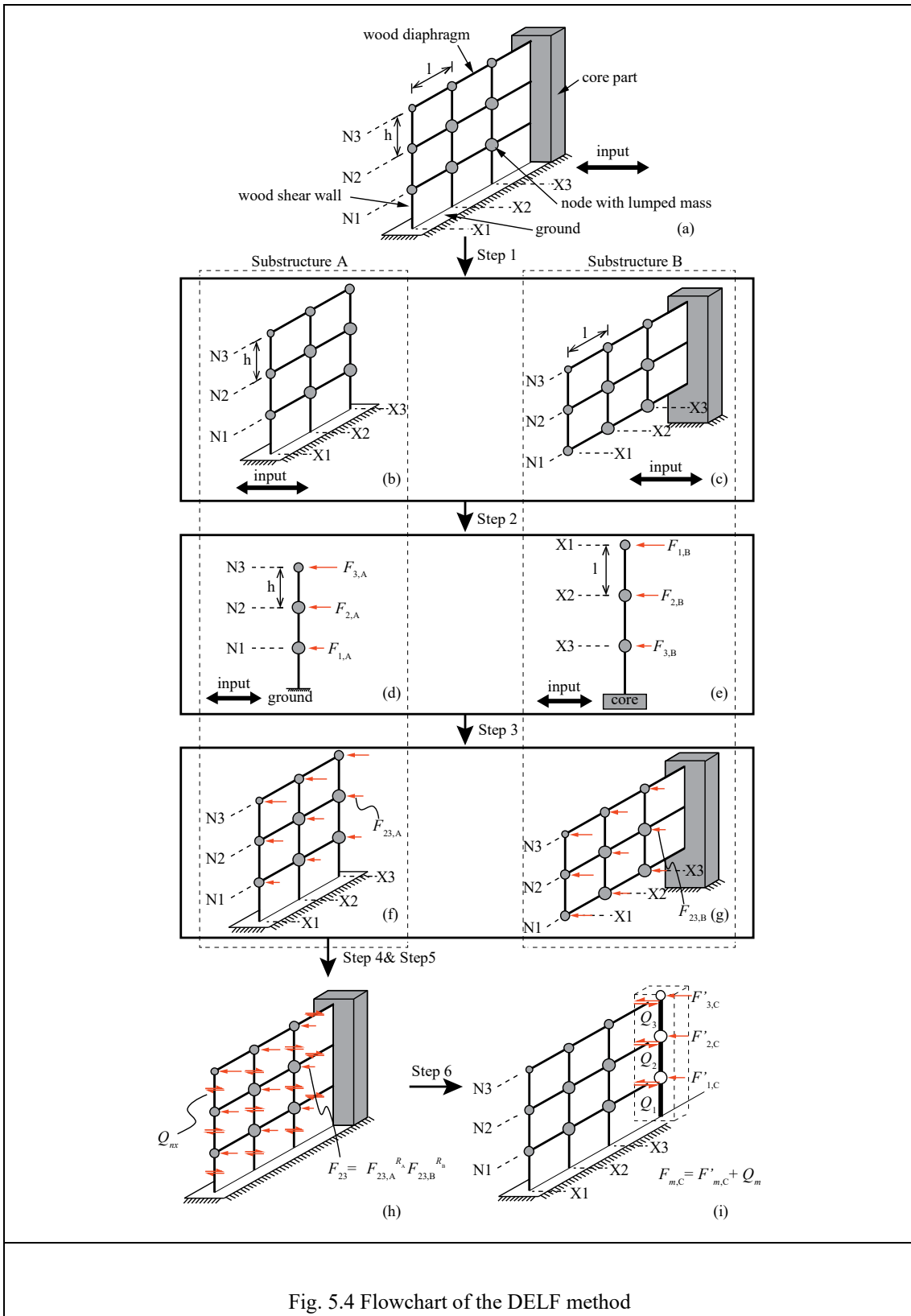
Fig. 5.4 Flowchart of the DELF method

5.3.2 Procedure of DELF method

The DELF method shown in Fig. 5.4 is summarized in the following procedure:

Step 1: The wooden horizontal structure is separated into two substructures in which the constraint of the core part and the ground is released respectively (Fig. 5.4(a-c)).

Step 2: Regardless of the gravity force, the substructures could be considered as structures with uniformly distributed mass and stiffness, which are applicable to the ELF method. For Substructure A, the standard ELF analysis is carried out by Eqs. (5.8)-(5.10) (Fig. 5.4 (d)),

$$F_{n,A} = C_{n,A} V_W \tag{5.8}$$

$$V_W = C_S W_W \tag{5.9}$$

$$C_{n,A} = \frac{w_{n,A} h_{n,A}}{\sum_{n=1}^{N_A} w_{n,A} h_{n,A}} \tag{5.10}$$

where

$F_{n,A}$ = lateral seismic force of n-story in Substructure A;

W_W = total effective seismic weight of the wood part;

$C_{n,A}$ = vertical distribution factor of n-story in Substructure A;

$w_{n,A}$ = seismic weight of n-story of the wood part in Substructure A;

V_W = total design base shear;

$h_{n,A}$ = height of n-story in Substructure A;

N_A = number of stories in Substructure A.

It should be pointed out that when defining C_s the period used should be the one of the original hybrid structure rather than the one of the Substructure A or B. Besides, for Substructure A and B, the three parameter in Eq. (5.9) are the same, therefore, V_W, C_S and W_W are not separated with subscript A and B.

Step3: For Substructure A, once the ELF analysis of each substructure is finished, the seismic force of each story is distributed to the respective nodes by the lumped seismic mass by Eq. (5.11) (Fig. 5.4(f)),

$$F_{nx,A} = \frac{w_{nx}}{w_n} F_{n,A} \tag{5.11}$$

where

$F_{nx,A}$ = lateral seismic force of the node at n-story, x-frame in Substructure A;

w_{nx} = seismic weight of the node at n-story, x-frame.

Repeat Step 2 and Step 3 for Substructure B to get the seismic force $F_{mx,\mathrm{B}}$ at each node (Fig. 5.4(e, g)). It is worth noting that the subscript n and x are consistent in Substructure A and B since the n and x refer to the n-story and x-frame in the original hybrid structure (Fig. 5.4(a)). Although Substructure B is rotated in Step 2 (Fig. 5.4(c)), the location of m and x is mapping with the original hybrid structure to avoid any misunderstanding.

Step 4: The seismic forces at the same node of Substructure A and B are combined using the weighted geometric mean by Eqs. (5.12)-(5.14) (Fig. 5.4(h)),

$$F_{nx} = F_{nx,\mathrm{A}}{}^{R_\mathrm{A}} F_{nx,\mathrm{B}}{}^{R_\mathrm{B}} \tag{5.12}$$

$$R_\mathrm{A} = \frac{\sqrt{K_\mathrm{s}}}{\sqrt{K_\mathrm{s}} + \sqrt{K_\mathrm{d}}} \tag{5.13}$$

$$R_\mathrm{B} = \frac{\sqrt{K_\mathrm{d}}}{\sqrt{K_\mathrm{s}} + \sqrt{K_\mathrm{d}}} \tag{5.14}$$

where

F_{nx} = combined seismic force of the node at m-story, x-frame in the original structure;

$R_{\mathrm{A/B}}$ = the weighting factor of Substructure A/B;

K_s = the stiffness of the wood shear wall;

K_d = the stiffness of the diaphragm.

Step 5: Apply the combined force F_{mn} on the original hybrid structure statically to get the estimated seismic shear force Q_{mn} of the shear wall and diaphragm in the wood part (Fig. 5.4(h)).

Step 6: Once the DELF analysis of the wood part is completed, the core part could be analyzed independently by using the standard ELF method. Accordingly, the shear force of the core part is the arithmetical combination of the ELF method result and the shear force transferred from the wood part through the diaphragm which could be obtained from Step 5 as shown in Eq. (5.15).

$$F_{n,\mathrm{C}} = F'_{n,\mathrm{C}} + Q_n \tag{5.15}$$

Where

$F_{n,\mathrm{C}}$ = combined seismic force of the node at n-story in the core part;

$F'_{n,\mathrm{C}}$ = seismic force of the node at n-story in the core part calculated using ELF method;

Q_n = shear force transferred to the core part though the diaphragm of n-story

The core part in the shaking table test specimen is a 3-story steel frame with an opening on one side (Fig. C.5). The main purpose of the steel frame is to provide a strong stiffness in and vertical to the input direction. The accurate internal force of the steel frame is not clear since no direct

measurement setup is implemented on the steel frame to record its internal force or displacement. While the indirect process such as integration of acceleration may provide unreliable result and mislead the analysis and the evolvement of the test. As a consequence, the calculation of the seismic force of the core part is not covered in the DELF method.

5.4 Modal response method

5.4.1 Natural mode and frequency
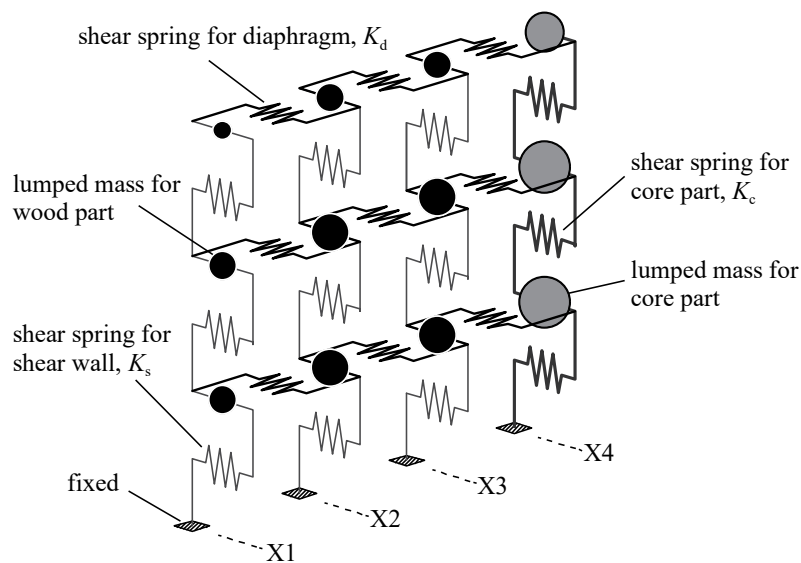
Fig. 5.5 Linear model to calculate the fundamental mode of vibration for MRS method

Apart from the DELF method, modal response spectrum (MRS) method is also used in this paper to evaluate the shear force of the specimen to provide an alternative prediction. The MRS method is conducted based on the linear model shown in Fig. 5.5. The mode of the linear model is calculated according to the eigenvalue equation Eq. (5.16),

$$\left[\boldsymbol{k} - \omega_j^2 \boldsymbol{m} \right] \boldsymbol{\Phi}_j = \boldsymbol{0} \tag{5.16}$$

$$
\boldsymbol{k} =
\begin{pmatrix}
k_{11} & k_{12} & \boldsymbol{0} & k_{1(X+1)} & \boldsymbol{0} & \boldsymbol{0} \\
k_{21} & k_{22} & \ddots & \boldsymbol{0} & \ddots & \boldsymbol{0} \\
\boldsymbol{0} & \ddots & \ddots & \ddots & \boldsymbol{0} & k_{(J-X)X} \\
k_{(X+1)1} & \boldsymbol{0} & \ddots & \ddots & \ddots & \boldsymbol{0} \\
\boldsymbol{0} & \ddots & \boldsymbol{0} & \ddots & k_{(J-1)(J-1)} & k_{(J-1)J} \\
\boldsymbol{0} & \boldsymbol{0} & k_{X(J-X)} & \boldsymbol{0} & k_{J(J-1)} & k_{JJ}
\end{pmatrix}
\tag{5.17}
$$

$$
\boldsymbol{m} =
\begin{pmatrix}
M_1 & & & \boldsymbol{0} \\
& \ddots & & \\
& & M_i & \\
& & & \ddots \\
\boldsymbol{0} & & & M_I
\end{pmatrix}
=
\begin{pmatrix}
m_{11} & & & \boldsymbol{0} \\
& \ddots & & \\
& & m_{nx} & \\
& & & \ddots \\
\boldsymbol{0} & & & m_{NX}
\end{pmatrix}
\tag{5.18}
$$

Where

$\boldsymbol{k}$ = stiffness matrix of the linear model;

$\boldsymbol{m}$ = mass matrix of the linear model;

M_i = seismic mass of node i;

m_{mx} = seismic mass of node at m-story, x-frame;

ω_j = frequency of jth mode of the linear model;

Φ_j = jth mode of the linear model

The freedom J of the model equals to N times X in which the N and X refers to the number of story and frame in the linear model, respectively. On the other hand, the number of the node I is also equals to N times X and each node provide a single freedom in the concerned direction. Once the $\boldsymbol{k}$ and $\boldsymbol{m}$ are defined, the frequency ω_j could be solved by Eq.5.19,

$$
\det\left[\boldsymbol{k} - \omega_j^2 \boldsymbol{m}\right] = 0
\tag{5.19}
$$

Then bring ω_j into eigenvalue equation Eq. (5.16) and the mode of the linear model Φ_j could be

obtained.

5.4.2 Definition of seismic force in MRS

The seismic force of node i for mode j F_{ij} is calculated according to Eq. (5.20) and Eq. (5.21),

$$F_{ji} = M_i \gamma_j \Phi_{ji} S_a(T_j) \tag{5.20}$$

$$\gamma_j = \frac{\{\Phi_j\}^T [m]\{1\}}{\{\Phi_j\}^T [m]\{\Phi_j\}} \tag{5.21}$$

Where

γ_j = participation factor for mode j;

$S_a(T_j)$ = spectral acceleration at the period of mode j

Once the lateral seismic force at node i is defined, the internal shear force of the model could be calculated using static analysis. The maximum response of the model for mode j is S_j and the total response S could be evaluated by SRSS method in Eq. (5.22),

$$S = \sqrt{\sum S_j^2} \tag{5.22}$$

5.5 Case study

Case study is performed based on the proposed DELF method. Several structures are studied. Case1 is the chosen test specimen S1 shown in Fig. C.2. The stiffnesses of the shear wall and diaphragm are derived from the measured initial stiffness of the shaking table test specimen (Appendix C). The value of the lumped mass is also calculated directly from the test specimen. Case2 to Case6 is a hypothetical structure which has the same configuration with Case1 except the diaphragm stiffness, which is from 2 to 10 times the one of Case1. For the horizontal hybrid structure, the potential design of the diaphragm may include wood panel, steel deck or concrete panel. Therefore, the stiffness of the diaphragm may change in a wide range due to different design. The given difference between the two cases is to investigate the stability of the DELF method under various diaphragm design. Case7 to Case12 have an exactly uniform distribution of the node mass and the diaphragm to shear wall stiffness ratio changes from 1 to 10. To study the applicability of the DELF method for building with different stories, Case13 to Case20 are defined. Case13 to Case16 are 2-story model with a uniform distribution of node mass and Case17
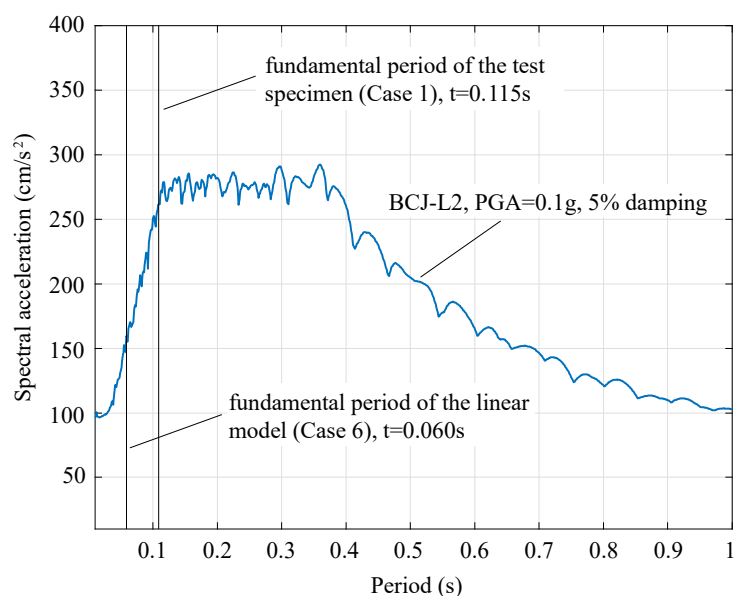
Fig. 5.6 Spectral acceleration of the scaled BCJ-L2 wave and the fundamental period of

Case 1 and Case 2

to Case20 are 1-story mode with a uniform distribution of node mass. Meanwhile the stiffness of the core part in the linear model is set to 1000 times higher than the shear wall to get an ideal rigid core part in all the cases. Table 5.1 demonstrates the detailed parameter used in the DELF and MRS.

In the shaking table test in Chapter 2, the specimen was subjected to the time-scaled BCJ-L2 wave (BRI 1992) with increasing peak ground acceleration (PGA) from 0.1g to 0.8g. To compare with the test results, the same time-scaled BCJ-L2 wave is chosen as the design ground motion in the DELF method. The PGA of the BCJ-L2 wave is set to 0.1g, at which level the hybrid structure is verified to be linear and suitable for the DELF method. The spectral acceleration of the BCJ-L2 wave is shown in Fig. 5.6. To avoid the tedious calculation procedure, the seismic response coefficient C_S in Eq. (5.9) is arbitrarily set to the spectral acceleration of the design ground motion at the fundamental period of the test specimen, instead of a comprehensive consideration of building importance, site class, seismic hazard, etc. Fundamental periods of Case1 and Case6 are depicted in Fig. 5.6. The relative spectral accelerations are used as the C_S in the DELF method. Moreover, the total effective seismic weight W was set to 85% of the total weight of the building considering the horizontal hybrid structure is a multiple-degree-of-freedom system (Ministry of Construction 2005). The simplification of C_S and reduction of W seems to be reasonable in terms

of the expected match in the following results.

Meanwhile, modal response spectrum (MRS) approach (Chopra A.K. 1995) is also performed using the eigenvalue derived from a simplified linear model as shown in Fig. 5.5. The relative parameters used in MRS are the same with DELF as shown in Table 5.1. Since the models of the cases are low-rise buildings whose story is under 3, only the fundamental mode of vibration is used in the MRS.

Table 5.1 Structural weight (N) and shear stiffness (N/mm) used in DELF and MRS

Case	story	frame	δ	mass	$w12\ w13$ $w22\ w23$	$w11\ w21$	$w32\ w33$	$w31$	$w41\ w42$	$w43$	Ks	Kd	Kc
Case1	3	4	1.07	S1	3283	1754	2146	1117	6693	5282	1250	1313	1.25E+06
Case2	3	4	2	S1	3283	1754	2146	1117	6693	5282	1250	2500	1.25E+06
Case3	3	4	4	S1	3283	1754	2146	1117	6693	5282	1250	5000	1.25E+06
Case4	3	4	6	S1	3283	1754	2146	1117	6693	5282	1250	7500	1.25E+06
Case5	3	4	8	S1	3283	1754	2146	1117	6693	5282	1250	10000	1.25E+06
Case6	3	4	10	S1	3283	1754	2146	1117	6693	5282	1250	12500	1.25E+06
Case7	3	4	1	uniform	3283	3283	3283	3283	6693	5282	1250	1250	1.25E+06
Case8	3	4	2	uniform	3283	3283	3283	3283	6693	5282	1250	2500	1.25E+06
Case9	3	4	4	uniform	3283	3283	3283	3283	6693	5282	1250	5000	1.25E+06
Case10	3	4	6	uniform	3283	3283	3283	3283	6693	5282	1250	7500	1.25E+06
Case11	3	4	8	uniform	3283	3283	3283	3283	6693	5282	1250	10000	1.25E+06
Case12	3	4	10	uniform	3283	3283	3283	3283	6693	5282	1250	12500	1.25E+06

Table 5.1 Structural weight (N) and shear stiffness (N/mm) used in DELF and MRS

Case	story	frame	δ	mass	$w11\ w12\ w13$	$w21\ w22\ w23$	$w41\ w42$	$w43$	K_s	K_d	K_c
Case13	2	4	1	uniform	3283	3283	6693	5282	1250	1250	1.25E+06
Case14	2	4	2	uniform	3283	3283	6693	5282	1250	2500	1.25E+06
Case15	2	4	6	uniform	3283	3283	6693	5282	1250	7500	1.25E+06
Case16	2	4	10	uniform	3283	3283	6693	5282	1250	12500	1.25E+06
Case17	1	4	1	uniform	3283	—	6693	5282	1250	1250	1.25E+06
Case18	1	4	2	uniform	3283	—	6693	5282	1250	2500	1.25E+06
Case19	1	4	6	uniform	3283	—	6693	5282	1250	7500	1.25E+06
Case20	1	4	10	uniform	3283	—	6693	5282	1250	12500	1.25E+06

5.5.1 Model with 3 stories

The results of the DELF and MRS analysis for model with 3 stories are demonstrated in Fig. 5.7. It could be seen that for Case1 the result of the shaking table test is also depicted. The listed values refer to the peak shear force of the shear walls and the diaphragms connected to the core part. The error between the test results and the prediction of the MRS and DELF method is also depicted in Fig. 5.7(a). The error is defined by Eq. (5.23).

$$error = \frac{MRS \text{ or } DELF\text{-}Test}{Test} \times 100\% \tag{5.23}$$

The accordance of the peak shear forces is satisfactory for both the shear wall and the diaphragm. The shear force of the wood shear wall gives a margin of error with nearly 10% between the DELF and the test in the 1st and 2nd story. The agreement of the diaphragm is also acceptable especially in the concerned soft segment. The soft segment refers to the shear wall of the 1st story and the diaphragm connected to the core part where the deformations of those shear components are much higher than other parts of the hybrid structure. Meanwhile, the error of the total wood base shear is 1% which is astonishingly precise for the preliminary design. The main discrepancy between the DELF analysis and the test is focusing on the 3rd story where the error is increasing from X1 to X3. This error derived from the inherent limitation of the ELF method in which the response of the upper story could be underestimated to some extent, depending on the configuration of the building. Some building codes attempt to amend that underestimation by introducing an additional seismic force at the top of the building (Ministry of Construction 2005, ICBO 1997). While in DELF method the underestimation occurred in the area which is of little importance compared with the soft segment, therefore, no additional force was involved here. It is worth noting that although the MRS method tended to somehow overestimate the seismic shear in the 1st and 2nd story, the results of DELF and MRS method are of comparable quality through all the stories. It adds weight to the idea that the combination of the vibration of the two substructure is equivalent to the fundamental mode of the original wood part, which verifies the rationality of the DELF method.

From Case 2, only the results of DELF and MRS method are presented since there is no corresponding test (Fig. 5.7(b)). The disparity between DELF and MRS method increased compared with Case 1, especially in the 3rd story. The increase of the diaphragm stiffness would change the vibration shape of the fundamental mode which could not be fully compensated by the weighting factor in the DELF method. When the stiffness ratio δ increases from 2 to 8, the shape of the model changes apparently. The displacement of the 3rd floor begin to decrease while

(a) Case1

(b) Case2

(c) Case3

Fig. 5.7 Peak shear force of the shear wall and diaphragm by DELF, MRS and shaking table test result, PGA=0.1g, unit:N, (a) Case1, δ=1.05, (b) Case2, δ=2, (c) Case3, δ=4
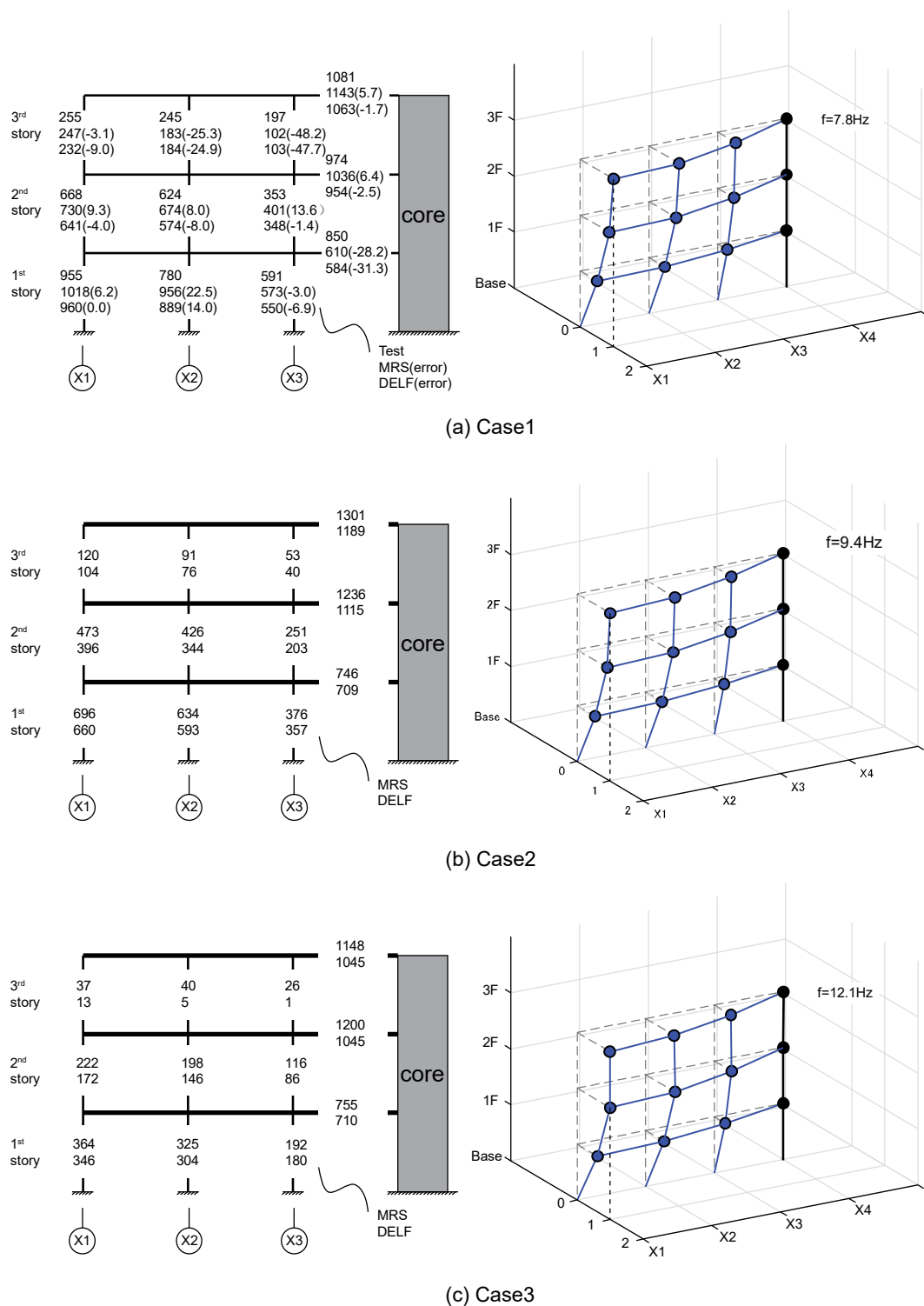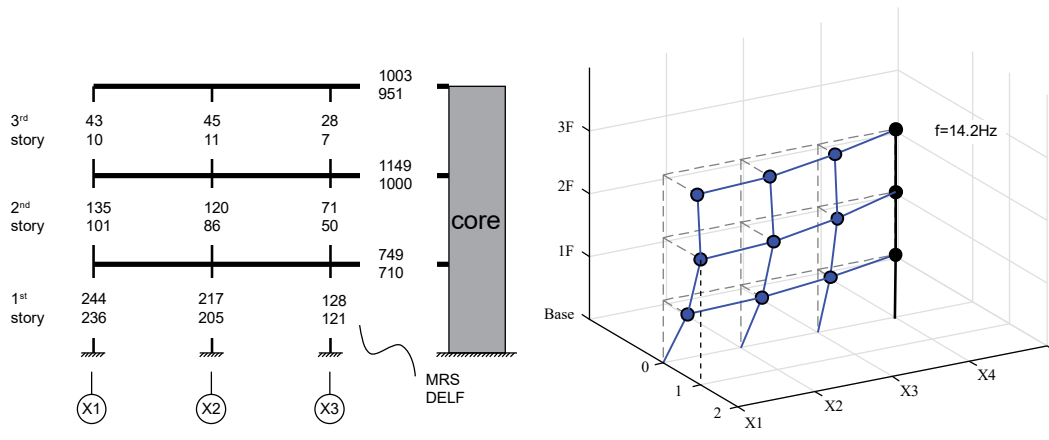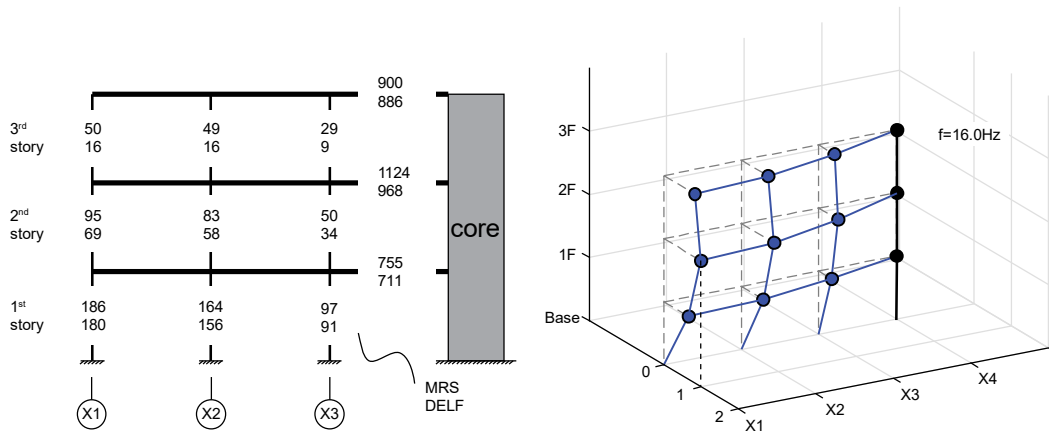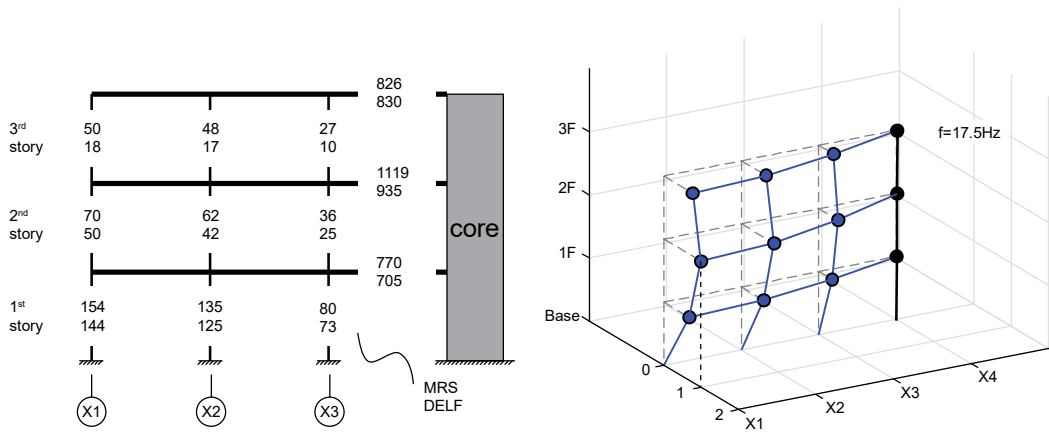
(d) Case4

(e) Case5

(f) Case6

Fig. 5.7 Peak shear force of the shear wall and diaphragm by DELF, MRS and shaking table test result, PGA=0.1g, unit:N, (d) Case4, δ=6, (e) Case5, δ=8, (f) Case6, δ=10

Table 5.2 Shear force error between the DELF and MRS method (3-story, mass same with S1)

Case	shear wall									diaphragm		
	1F			2F			3F			3F	2F	1F
	X1	X2	X3	X1	X2	X3	X1	X2	X3			
Case1	-5.8%	-7.4%	-5.2%	-12.5%	-15.4%	-13.9%	-9.9%	-11.5%	-18.0%	-7.2%	-8.0%	-5.2%
Case2	-5.2%	-6.4%	-5.0%	-16.3%	-19.4%	-19.2%	-13.4%	-17.1%	-26.2%	-8.7%	-10.1%	-5.0%
Case3	-5.0%	-6.4%	-6.1%	-22.6%	-25.8%	-26.5%	-66.7%	-88.4%	-95.7%	-9.0%	-12.9%	-6.0%
Case4	-3.4%	-5.0%	-5.3%	-25.0%	-28.3%	-29.3%	-78.1%	-75.2%	-74.7%	-5.1%	-12.9%	-5.2%
Case5	-3.6%	-5.3%	-5.9%	-27.3%	-30.6%	-31.6%	-67.3%	-67.8%	-68.5%	-1.5%	-13.8%	-5.8%
Case6	-6.2%	-7.9%	-8.8%	-30.7%	-33.8%	-34.8%	-66.0%	-67.1%	-68.2%	0.1%	-16.5%	-8.7%

error =(DELF-MRS)/MRS × 100%

the one of the 2nd floor reach the peak value. The reason is that the mass is not uniformly distributed in the model, the mass of the 2nd floor and 1st floor is higher than the 3rd floor. When the stiffness of the diaphragm increases, the seismic acceleration is easier to transfer from the core part to the higher floor and the accompanying seismic force provide higher demand in the 2nd floor. The direction of the displacement in the 3rd floor is reversed to the 1st and 2nd story. The DELF method is powerless to catch the shape of this kind of vibration. Table 5.2 demonstrates the detailed error between the result of DELF and MRS method. It is apparent that when the stiffness of the diaphragm increases, the errors in the 2nd and 3rd floor increase as well. When the ratio δ is higher than 4, the errors in the 3rd floor are higher than 50%. Nevertheless, in the concerned soft segment, the results of the DELF and MRS method are close and acceptable at the level of construction engineering. The prediction of the DELF method in 1st floor is stable when the δ increases and the error with MRS method is under 10% with all aspects. And the errors of the diaphragm connected to the core part are under 15%. It should also be pointed out that the DELF underestimate the shear force for nearly all the shear wall and diaphragm. It may be caused by the deduction of the seismic mass in the calculation.

Fig. 5.8 shows the results of the DELF and MRS analysis for model with uniform mass distribution. The mode shape of the models are different from the ones with same mass distribution of S1. When the stiffness of the diaphragm increase for 1 to 10, the shape of the fundamental mode basically remains constant. The displacement decreases from 3rd floor to 1st floor and from X1 to X3, respectively and the value is nearly linear for the decrease. As for the difference between DELF and MRS method, the trend is similar with the cases which have the same mass distribution of S1. The errors increase with the stiffness ratio δ and the discrepancies between the DELF and MRS method increase from the 1st floor to 3rd floor. Unlike the cases with S1 mass distribution, the DELF method seems to overestimate the shear force in the 1st floor while underestimate the upper floors. On the other hand, the errors of the concerned soft segment remains a relative low level. In general, the DELF method provides a reasonable prediction of the base seismic force and connection shear force with the same accuracy of the MRS method but lesser computing work for the wooden hybrid structure.
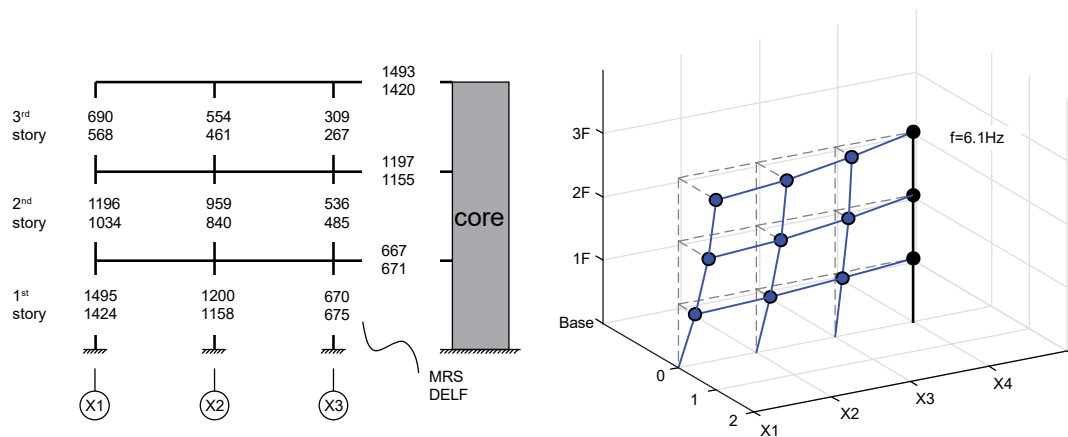
(a) Case7

(b) Case8
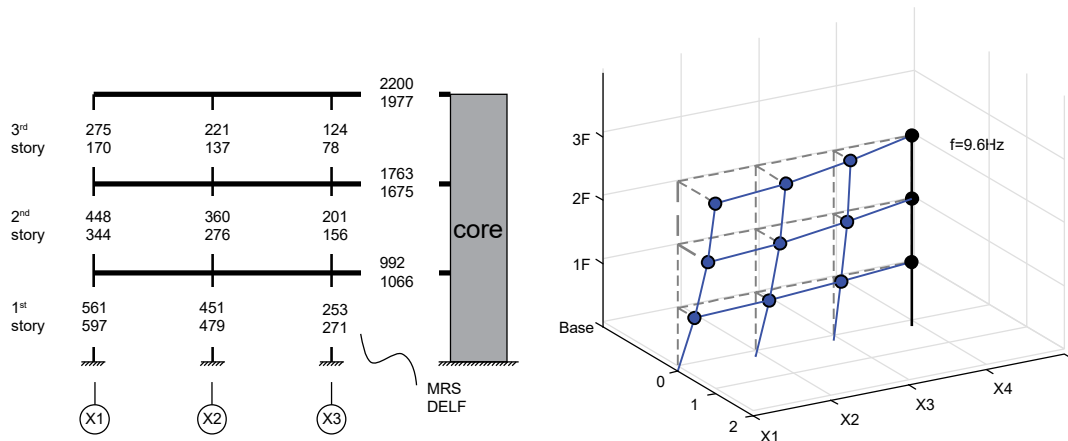
(c) Case9

Fig. 5.8 Peak shear force of the shear wall and diaphragm by DELF and MRS, PGA=0.1g, unit:N, (a) Case7, δ=1, (b) Case8, δ=2, (c) Case9, δ=4
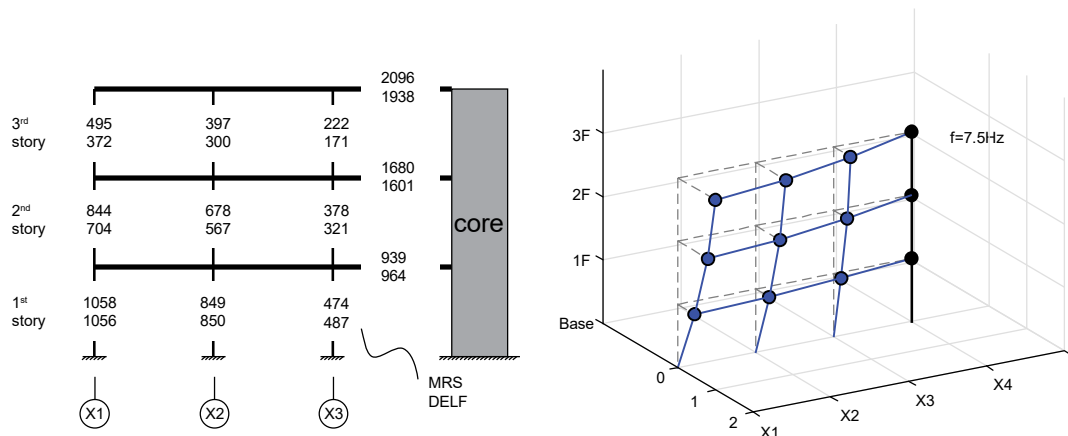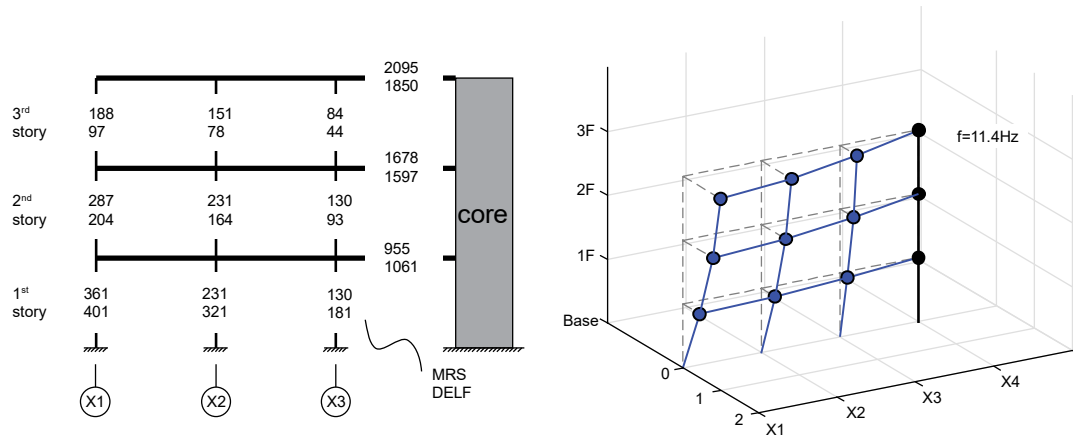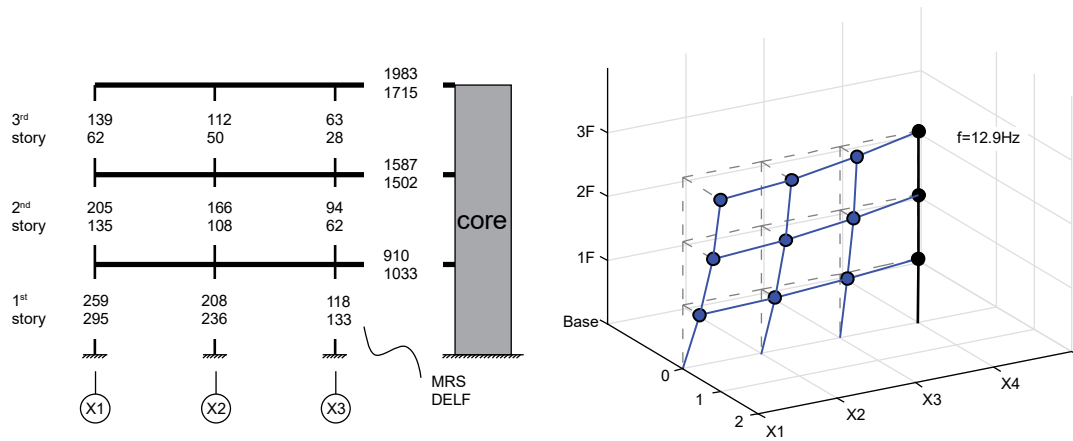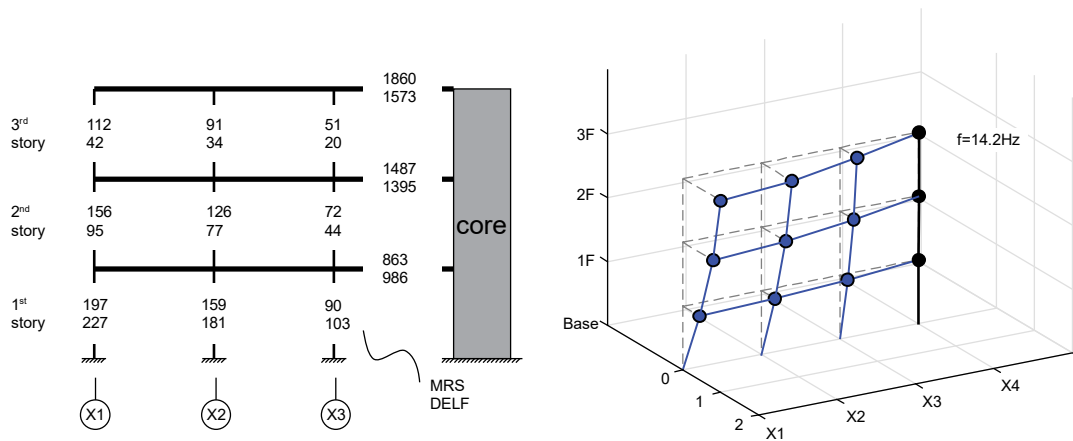
(d) Case10

(e) Case11

(f) Case12

Fig. 5.8 Peak shear force of the shear wall and diaphragm by DELF and MRS, PGA=0.1g, unit:N, (d) Case10, δ=6, (e) Case11, δ=8, (f) Case12, δ=10

Table 5.3 Shear force error between the DELF and MRS method (3-story, uniform mass)

Case	shear wall									diaphragm		
	1F			2F			3F					
	X1	X2	X3	X1	X2	X3	X1	X2	X3	3F	2F	1F
Case7	-4.8%	-3.4%	0.6%	-13.5%	-12.4%	-9.5%	-17.8%	-16.7%	-13.8%	-4.8%	-3.5%	0.6%
Case8	-0.1%	0.2%	2.6%	-16.6%	-16.4%	-15.0%	-24.8%	-24.5%	-23.1%	-7.5%	-4.7%	2.6%
Case9	6.5%	6.1%	7.2%	-23.2%	-23.4%	-22.8%	-37.9%	-38.0%	-37.3%	-10.1%	-5.0%	7.4%
Case10	11.1%	10.3%	10.7%	-28.9%	-29.2%	-28.8%	-48.6%	-48.7%	-48.1%	-11.7%	-4.8%	11.1%
Case11	14.0%	12.9%	12.9%	-34.2%	-34.4%	-34.0%	-55.9%	-56.0%	-55.3%	-14.8%	-11.0%	-5.8%
Case12	15.1%	13.8%	13.4%	-39.1%	-39.3%	-38.8%	-62.7%	-62.7%	-61.9%	-15.4%	-6.2%	14.2%

error =(DELF-MRS)/MRS × 100%

5.5.2 Model with 2 stories

Fig. 5.9 shows the results of the DELF and MRS analysis for model with 2 stories. When the stiffness ratio δ increased, the mode shape of the model basically remains the same. Meanwhile the frequency of the model increased as expected. As the stiffness ratio δ increased, the shear force sustained by the diaphragm increased as well when the one sustained by the shear wall decreased. However for Case15 and Case16, the shear force of the diaphragm decreases while the stiffness of the diaphragm increased. The reason is that due to the increase of the frequency, the period of the model moves from the acceleration constant area to the acceleration sensitive area where the value of the spectral acceleration is negative relative to the frequency. Therefore, the decreased acceleration provides a smaller demand for Case16. As shown in Table 5.4, the error of the concerned soft segment is satisfactory. The absolute errors of the 1st floor and the diaphragm connected to the core are under 10% for all the four cases. For the 2nd floor, the DELF method underestimate the shear force generally and the absolute value of the error increased when the stiffness of the diaphragm increased.

Table 5.4 Shear force error between the DELF and MRS method (2-story)

Case	shear wall						diaphragm	
	1F			2F				
	X1	X2	X3	X1	X2	X3	2F	1F
13	-7.5%	-5.9%	-0.8%	-14.6%	-13.2%	-9.1%	-3.7%	-0.8%
14	-5.1%	-4.8%	-2.1%	-18.2%	-17.9%	-16.2%	-7.1%	-2.1%
15	2.5%	1.8%	2.2%	-30.0%	-30.3%	-30.0%	-8.8%	2.4%
16	6.2%	5.2%	4.9%	-39.9%	-40.2%	-39.9%	-10.1%	5.1%

error =(DELF-MRS)/MRS × 100%

5.5.3 Model with 1 story

Fig. 5.10 shows the results of the DELF and MRS analysis for model with 1 story and Table 5.4 demonstrates the relative error. The changing trend of the mode shape is similar to the model with 2 stories. The increase of the diaphragm stiffness does not have an observable change on the mode shape but the increase of the fundamental frequency of the model. It should be pointed that in Case7, the absolute value of the error decrease from X1 to X3. It means the implicit displacement of the DELF method is not as linear as the ones in MRS method. The deformation shape of the DELF method is more curved and the deformation discrepancy between the X1 and X2 are

smaller than the one in the mode shape. On the whole, the error is satisfactory with all the absolute value under 10%.

Table 5.5 Shear force error between the DELF and MRS method (1-story)

Case	shear wall			diaphragm
	X1	X2	X3	
17	-11.9%	-9.7%	-3.0%	-3.0%
18	-9.2%	-8.7%	-5.2%	-5.2%
19	-7.4%	-8.2%	-7.6%	-7.6%
20	-6.1%	-7.1%	-7.2%	-7.2%

error =(DELF-MRS)/MRS × 100%

(a) Case13

(b) Case14

(c) Case15

(d) Case16

Fig. 5.9 Peak shear force of the shear wall and diaphragm by DELF and MRS, PGA=0.1g, unit:N, (a) Case13, δ=1, (b) Case14, δ=2, (c) Case15, δ=6, (d) Case16, δ=10
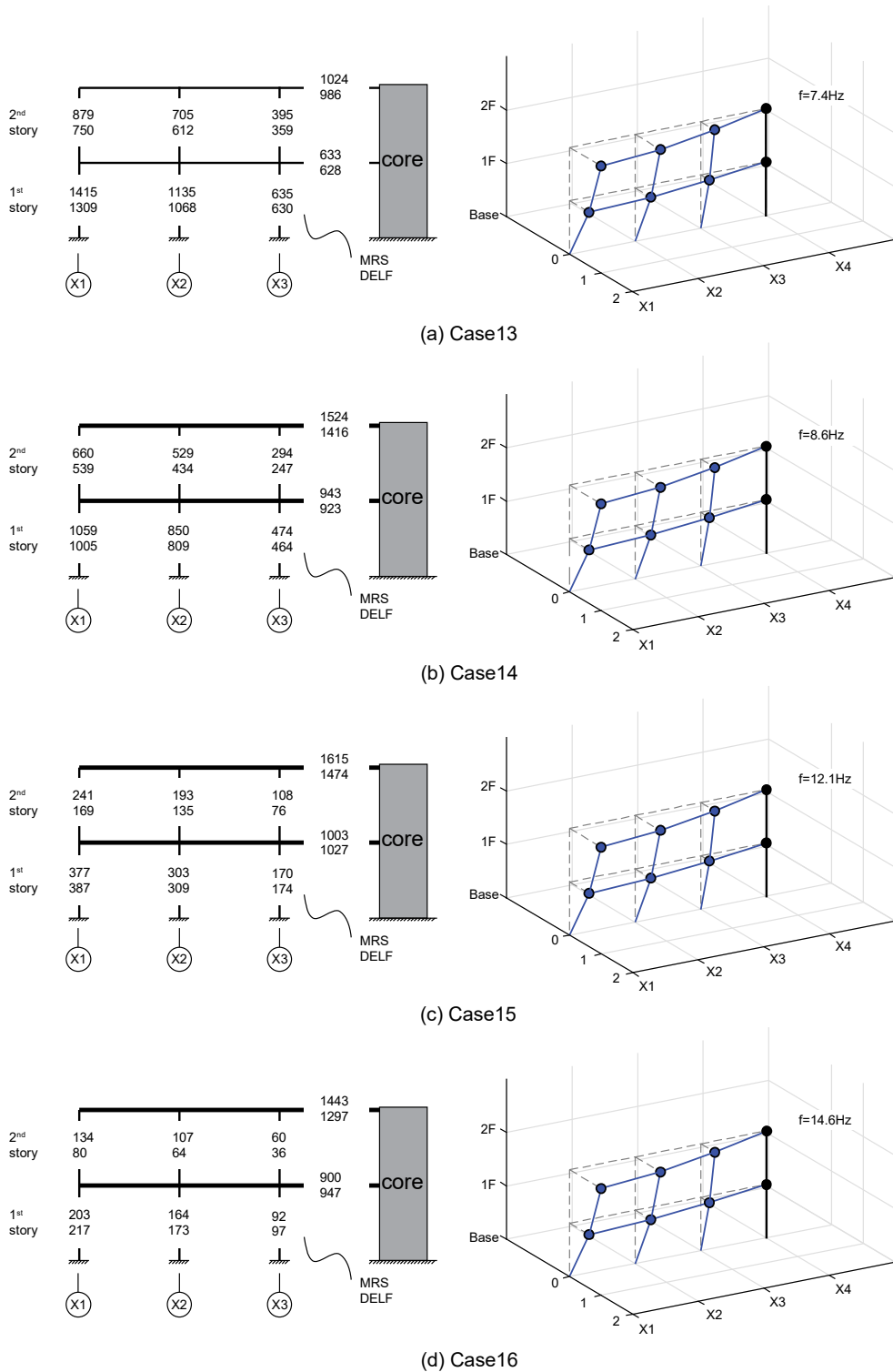
(a) Case17

(b) Case18
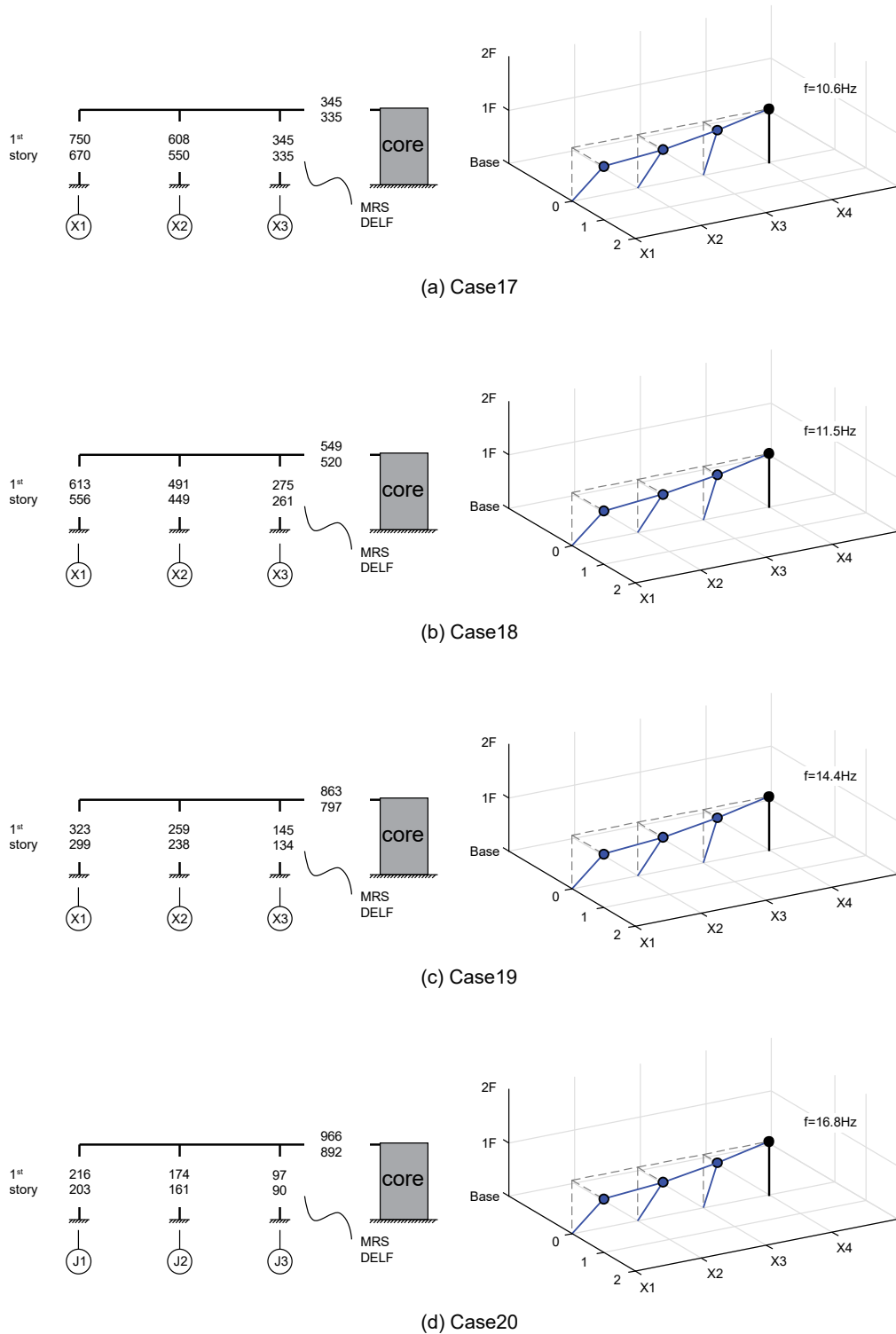
(c) Case19

(d) Case20

Fig. 5.10 Peak shear force of the shear wall and diaphragm by DELF and MRS, PGA=0.1g, unit:N, (a) Case17, δ=1, (b) Case18, δ=2, (c) Case19, δ=6, (d) Case20, δ=10

5.6 Conclusion

A simplified method has been proposed for the estimation of the seismic shear force for the preliminary linear design of low-rise wooden horizontal hybrid structure. This method requires the knowledge and prerequisites of the equivalent lateral force method and therefore has the succeeded advantages and limitations. The proposed dual equivalent lateral force method could be sufficient to predict the approximate seismic shear force if the wooden part has a relatively uniform distribution of stiffness and mass. The calculation procedure is also straightforward and could be conducted manually. However, the DELF method has done a poor job predicting the shear force in the upper story. The seismic shear of the shear wall is underestimated by up to 55% in the top story. Accordingly, additional roof seismic load may be necessary for the DELF method. Besides, the increase of stiffness difference between the shear wall and the diaphragm in the wood part could affect the accuracy of the DELF method.

There should also be pointed out that in the case study the seismic response coefficient is set to the spectral acceleration arbitrarily which eventually gives a reasonable result. While in the engineering practice, the seismic response coefficient is of great concern, since it is related to various factors and could have great influence on the ELF and DELF analysis result. Meanwhile, further study is required for the sensitivity of the concerned parameter.

6   Conclusions

Chapter 2 presents the shaking table tests of 1/3-scale wood horizontal hybrid structure, whose structural properties were in compliance with the prototype developed by AIJ. Following conclusion are extracted:

- Due to the limitation of the shaking table and the omission of the transferred-to-core shear force, the design of the specimens in this chapter was verified to be relatively conservative. However, the proposed target-drift-based design process could be feasible if the transferred-to-core shear force was taken into consideration.

- The increase of the diaphragm stiffness substantially improved the seismic performance of the test specimen along with the higher demands for the connection and the core part. In addition, the concept of concentrated shear wall at one side was practicable and sufficient but the corresponding specimen was more vulnerable to severe earthquake scenarios. Furthermore, the influences of these design features also verified that the shear force transfer between the wood part and the core part was related to the stiffness layout of the shear wall and diaphragm.

- High-than-normal story acceleration amplification observed in the tests was caused by the conservative design and the potential bullwhip effect as well as the high height-width ratio in the input direction. The energy consumption system or seismic isolation system was expected to alleviate the high acceleration amplification and improve the seismic performance of the structure.

- The connection between the wood part and the core part was reliable and hold well in the tests. In view of the tensile-shear stress status, the stiffness layout of the shear wall and diaphragm as well as the eccentricity of the structure need to take into consideration to make a more comprehensive design for the connection.

Chapter 3 demonstrates the numerical model built for the shaking table test specimen in *OpenSees*. The response of the numerical model is compared with the result of the shaking table test. Following conclusion are extracted:

- The *MSAWS* material is sufficient to catch the elastic and plastic performance of the shear wall and diaphragm in different stage. However, discrepancy occurs especially when the inputs are minor.

- The built 3D numerical model is adequate to predict the seismic performance of the wooden horizontal hybrid structure, including the displacement and shear force demands during medium and severe earthquake scenarios.

Chapter 4 presents the parameter analysis based on the built numerical simulation. Several concerned parameter are studied to extend the understanding of the seismic performance of the wooden horizontal hybrid structure. Following conclusion are extracted:

● Increase of the core-wood stiffness ratio could significantly mitigate the seismic response of the hybrid structure at the cost of increasing seismic shear at the connection and the total base shear. The increased base shear was all sustained by the core part. Meanwhile the vertical shear distribution of the wood part would change from inverted-triangular to uniform. Increase of the diaphragm-wall stiffness ratio could also mitigate the seismic response yet obviously magnify the force demand of the connection. However, if the core part was rigid enough, further increase of the diaphragm-wall stiffness ratio would reduce the seismic response while limiting excessive growth of the seismic shear in the base and connection.

● The formal frequency ratio was an efficient indicator to distinguish the seismic difference between the wood part and the core part. In the seismic design of horizontal hybrid structure, the ratio was recommended to be higher than 2 or 3 to achieve a steady and predictable performance regardless of the various design of the core part.

● The shear force distribution between the wood shear wall and diaphragm was affected by both the diaphragm-wall stiffness ratio and the core-wood stiffness ratio. The proposed equation provided an effective prediction on the shear force distribution compared with the conventional distribution by relative stiffness.

Chapter 5 proposed a simplified method to evaluate the seismic shear force in the wooden horizontal hybrid structure. Following conclusion are extracted:

● The proposed dual equivalent lateral force method could be sufficient to predict the approximate seismic shear force if the wooden part has a relatively uniform distribution of stiffness and mass. The calculation procedure is also straightforward and could be conducted manually.

● For structure no more than 3 stories, the proposed dual equivalent lateral force method is sufficient to predict the base shear with a deviation within 10% compared with the modal response spectrum method.

● The proposed dual equivalent lateral force method has done a poor job predicting the shear force in the upper story. The seismic shear of the shear wall is underestimated by up to 55% in the top story. Accordingly, additional roof seismic load may be necessary for the DELF method. Besides, the increase of stiffness difference between the shear wall and the diaphragm in the wood part could affect the accuracy of the DELF method.

Appendix A   Photograph credit

Fig 1.2 Innovative Housing, Inc, Cornerstone Condominiums, Portland, OR, USA. Credit: *William Wilson Architects*. Source: http://www.wwarchitects.com

Fig 1.3(a) OGAL Plaza, Iwata, Japan. Credit: *Inayama Masahiro*. Source: Inayama Masahiro, Technical issues and future direction in structural design. Japan Housing and Wood Technology Center: House and Timber, 2014, 37(433): 18-21 (in Japanese).

Fig 1.3(b) OGAL Plaza, Iwata, Japan. Credit: *Shiwa Public Library*. Source: http://lib.town.shiwa.iwate.jp/index.html

Fig 1.4 FondAction CSN office building, Quebec, Canada. Credit: (a) *Louise Leblanc*, (b) *Nordic Engineered Wood*. Source: Dagenais C, Desjardins R. Cases Studies of Performance-based Design for Mid-Rise Wood Constructions in Quebec (Canada). Proceedings of the 12th World Conference for Timber Engineering, Auckland, New Zealand, 2012.

Fig 1.5 Eiko Gakuen High School, Kamakura, Japan. Credit: *Eiko Gakuen High School*. Source: http://ekh.jp/en/about/equipment/index.html

Apart from the photograph given above, the rest of the photographs contained in this paper are credited to *SAKATA Laboratory*, *Department of Architecture and Building Engineering*, *Tokyo Institute of Technology*.

Appendix B   Detail information of the pilot experiment

A total number of 6 specimens were tested in the pilot experiment under quasi-static load. Fig. B.1 shows the design configuration of the specimens. Three shear wall specimens and three diaphragm specimens were tested. The shear walls were constructed with plywood panels (t=9mm) and nails (d=2.1mm, L=32mm, @50mm), and the diaphragms were constructed with plywood panels (t=12mm) and nails (d=2.1mm, L=32mm, @33mm for D33, @50mm for D50, @50mm for D100).
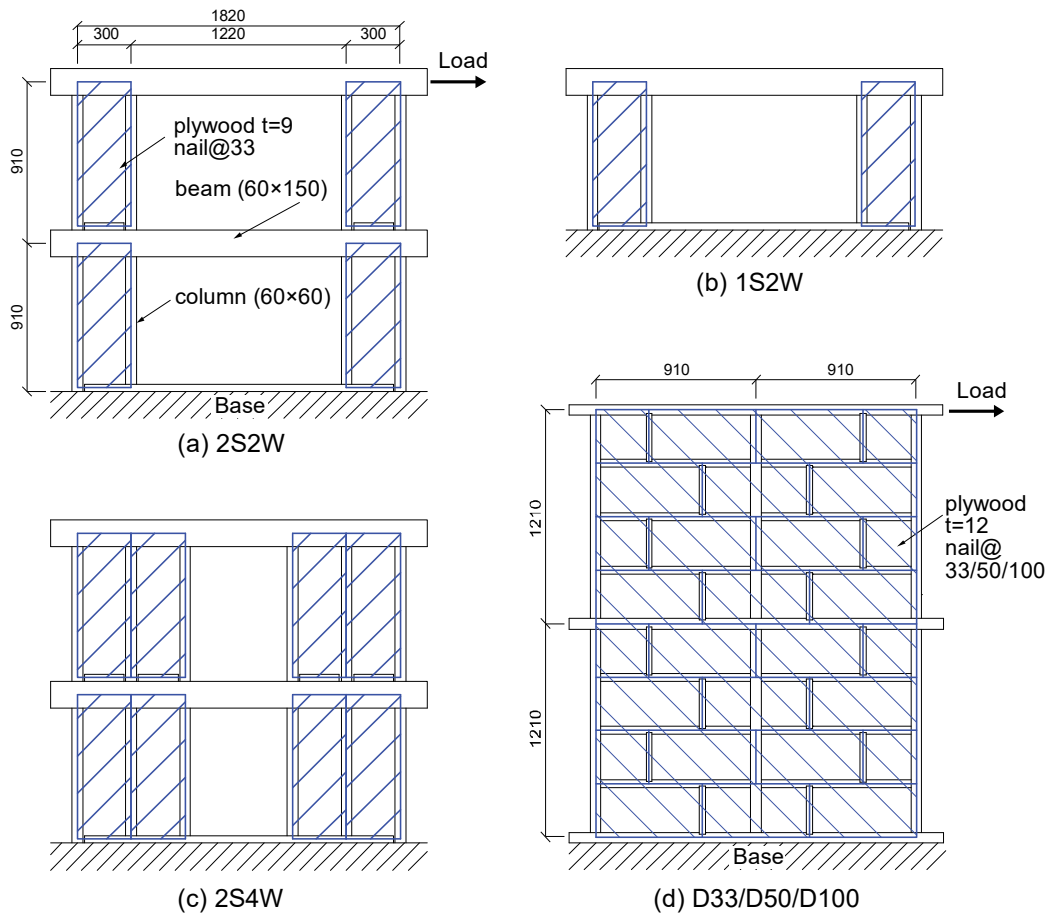
Fig. B.1 Design of specimens in the pilot experiment (dimensions in millimeters), (a-c) shear wall, (d)diaphragm

Thread steel bar (Φ 6)

Screw cap
Steel gasket

Tenon

150

60

Tenon

(a) beam-beam joint

(b) beam-column joint

Square steel bar

Shear ring

Steel plate

60

60

(c) base-column joint
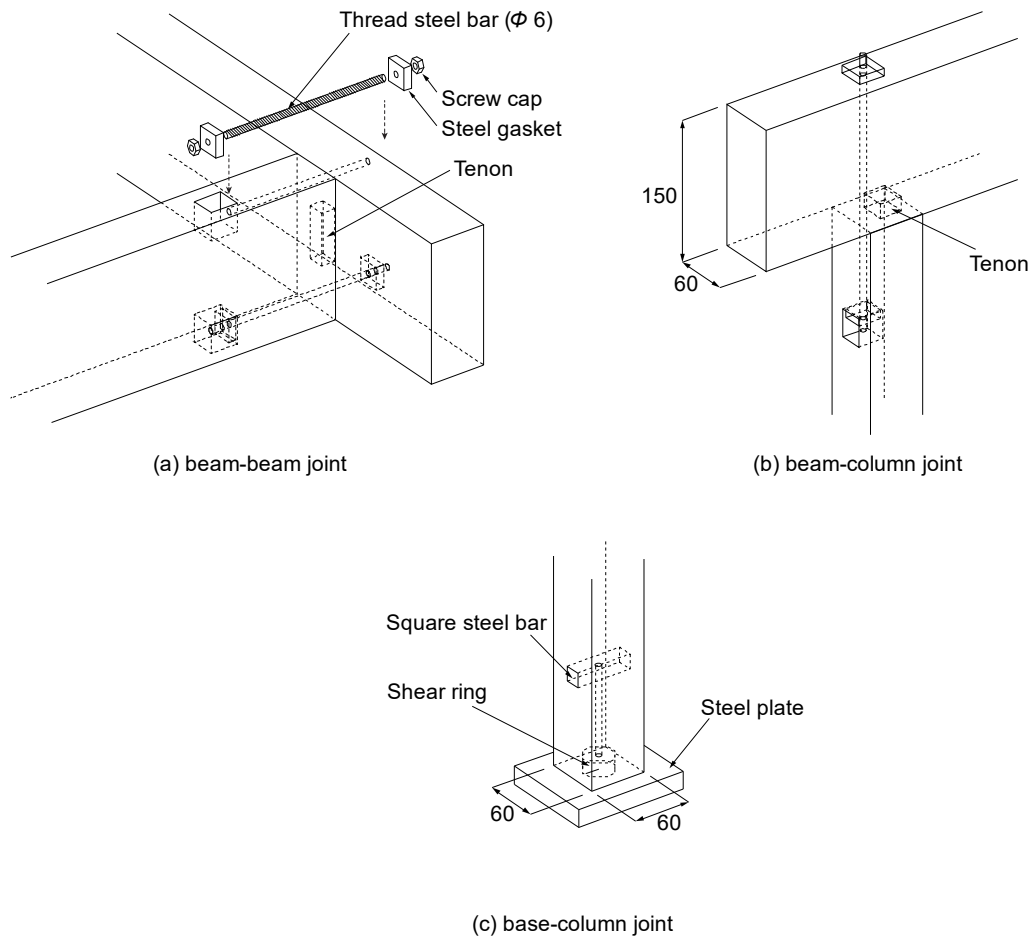
Fig. B.2 Design details of joints in the specimen (dimensions in millimeters)

(a) load pattern

(b) force-drift response
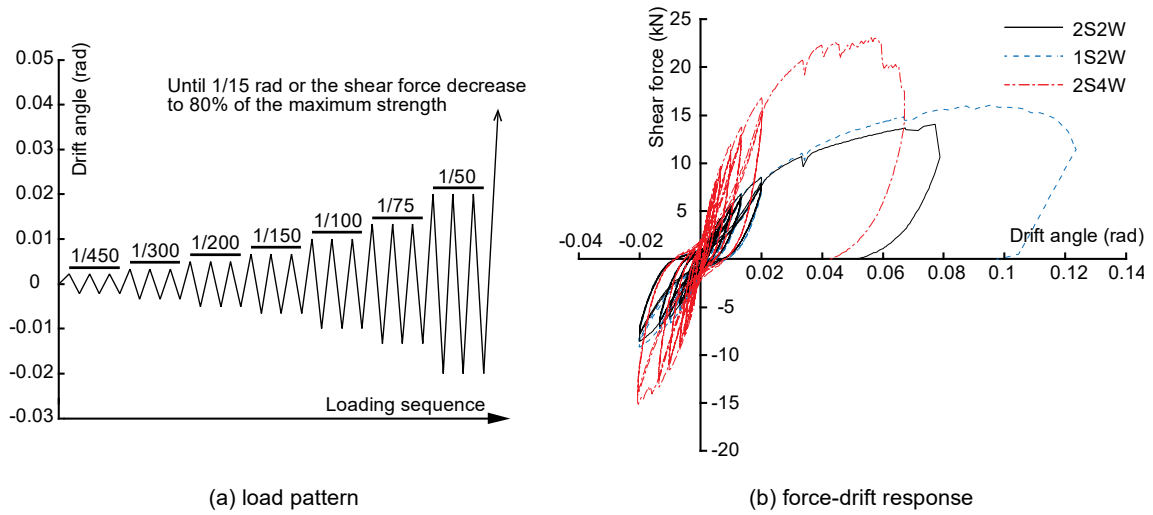
Fig. B.3 Load pattern and the force-drift response of the shear wall in the pilot experiment

(a) load pattern

(b) force-drift response
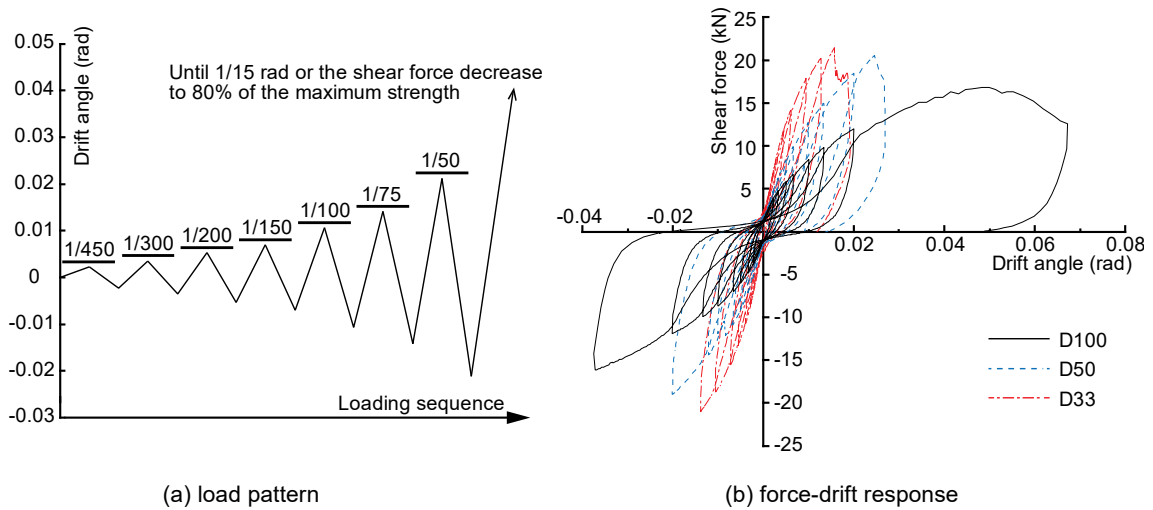
Fig. B.4 Load pattern and the force-drift response of the diaphragm in the pilot experiment
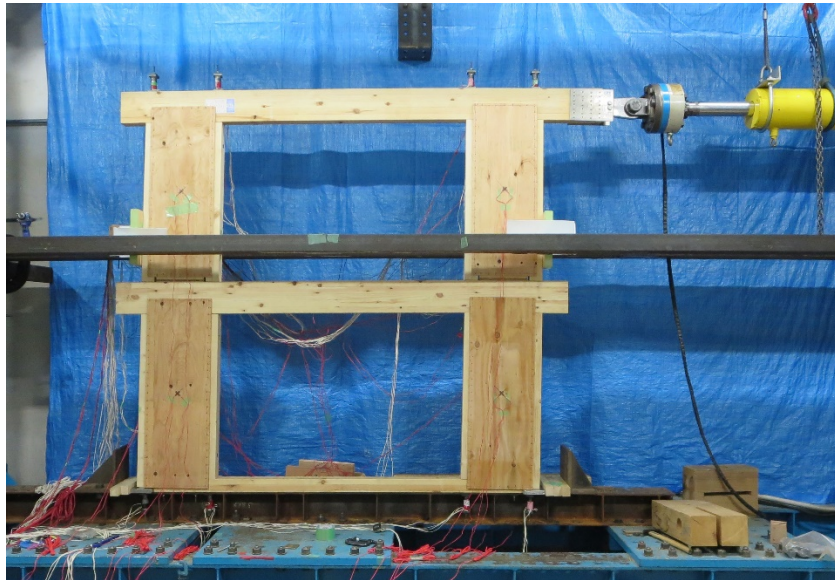
Fig. B.5 Deformation pattern of the specimen 2S2W at the drift of 1/50 rad
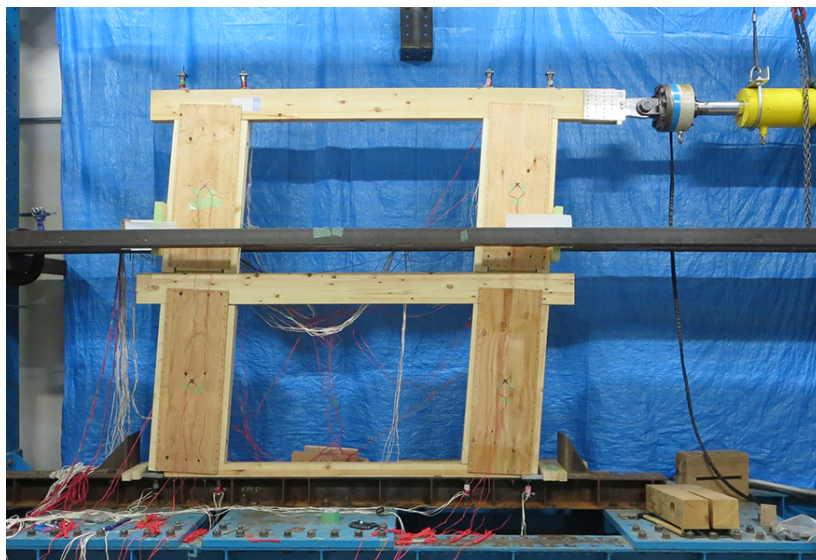
Fig. B.6 Deformation pattern of the specimen 2S2W at the drift of 1/15 rad
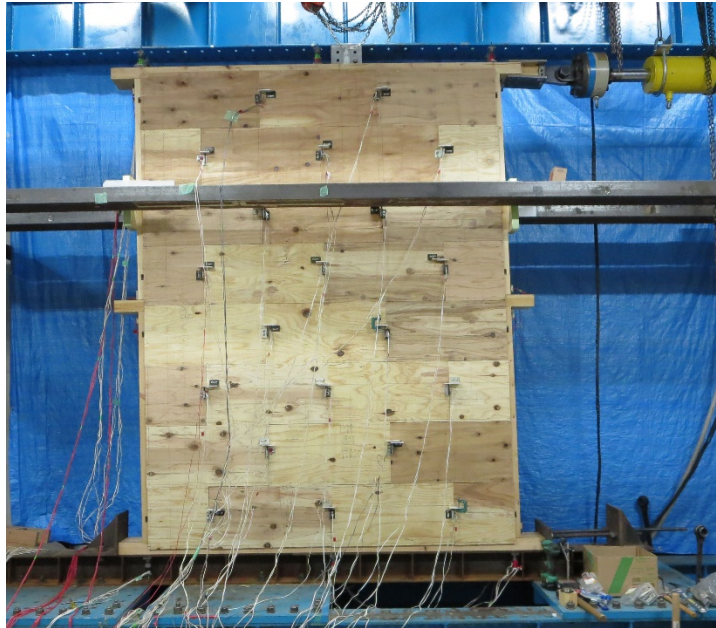
Fig. B.7 Deformation pattern of the specimen D100 at the drift of 1/50 rad
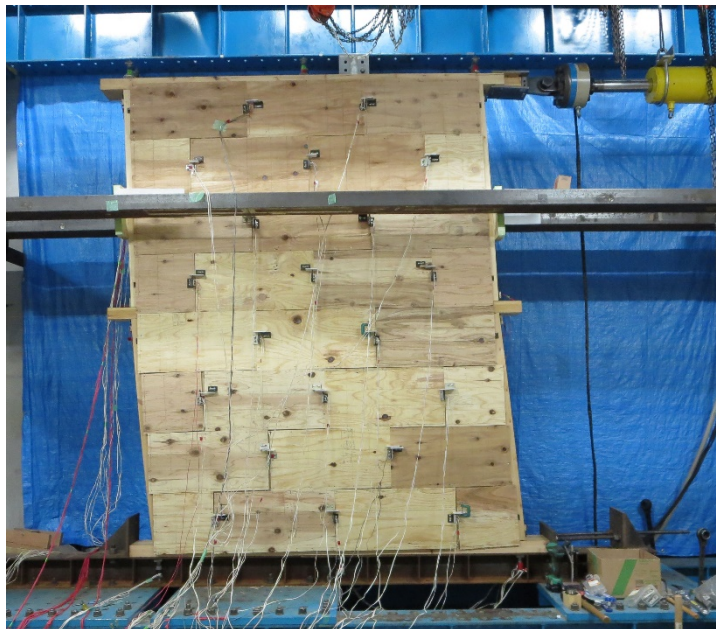
Fig. B.8 Deformation pattern of the specimen D100 at the drift of 1/10 rad

Appendix C   Detail information of the 1/3-scaled shaking table test

Specimen configuration
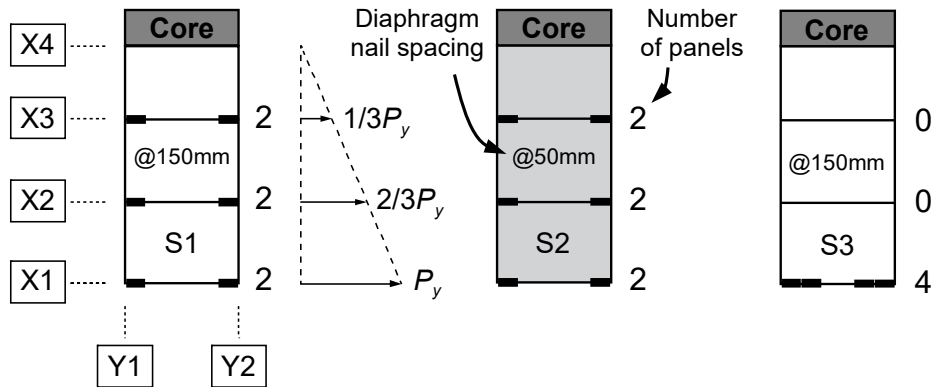
Fig. C.1   Configuration of specimens and distribution of design base shear force in S1

Three specimens, Specimen No.1, Specimen No.2 and Specimen No.3 (S1, S2&S3) were designed referring to the structural characteristics of the prototype in Fig 1.6. The configurations of S1, S2 and S3 is shown in Fig. C.1. Unlike a traditional wooden structure in which the diaphragm is usually considered as rigid slab, the diaphragm of horizontal hybrid structure was part of the force transfer system and hence the stiffness was of interest to the designers. So in S1 and S2, the stiffness of the diaphragm was different by changing the nail spacing to investigate the corresponding influence. In addition, the public facilities generally require large inner space, therefore S3 had no inner shear wall but doubled the ones at the side frame.

Fig. C.2 shows the S1 on the shaking table. Table C.1 lists the scale factors used in this experiment (Harris and Sabnis 1999). It should be pointed out that considering the capacity of the shaking table, the specimens designed in this experiment were not exactly 1/3-scale from the prototype dimension. The length and width of the wood part were around 1/7 of the prototype and the story height of the specimen was 1/3 of the common light wood structure in Japan. Meanwhile, the building elements of the specimens, such as beam and column, were 1/3-scale from the actual element to satisfy the similitude requirement in Table C.1. The design of the specimen aimed to grasp the typical feature of the horizontal hybrid structure such as the prototype, which is a multi-story, light-weight wooden frame connected to a rigid core at one end horizontally, rather than a reduce-scale copy of the prototype. The 3-story, 3-bay wood frames were built by glulam beams and columns, with section size of 60 × 150mm and 60 × 60mm, respectively (Table C.2). The beams and columns were connected by thread steel bar (SS400, 6 mm) and screw cap through the
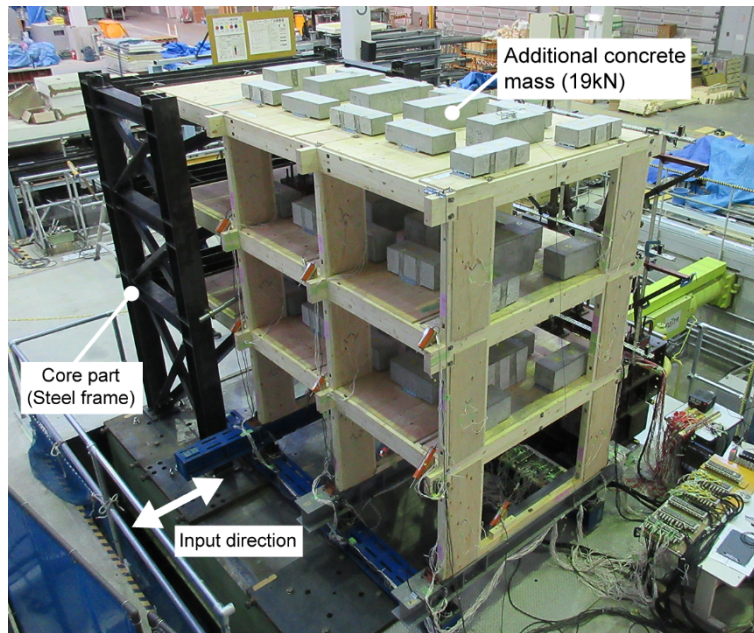
Fig. C.2 Design details of wood-core joint

Table C.1 Scale factors of the test

Quantity	Scale factor	Value
Length	S_L	1/3
Stress	S_σ	1/1
Gravitational acceleration	$S_a^{\,g}$	1/1
Force	$S_F = S_L^2\, S_\sigma$	1/9
Gravity mass	$S_M^{\,g} = S_F\,(S_a^{\,g})^{-1}$	1/9
Seismic mass	$S_M^{\,s} = S_M^{\,g}$	1/9
Seismic acceleration	$S_a^{\,s} = S_F\,(S_M^{\,s})^{-1}$	1/1
Time	$S_t = (S_L)^{1/2}(S_a^{\,s})^{1/2}$	$1/\sqrt{3}$

Table C.2 Specification of specimen members

Member	Material Grades	Dimension (mm)	Young's modulus (GPa)	Yield/ Bending Strength (MPa)
Connection Bar	SS400 (JIS)	$\Phi\,6$	200	245
Column	Homogeneous, E95-F315 (JAS)	60×60	9.5	31
Beam	Symmetric, E105-F300 (JAS)	60×150	10.5	30
Plywood	Class 2 (JAS)	9 for shear wall 12 for diaphragm	5.0 4.0	— —
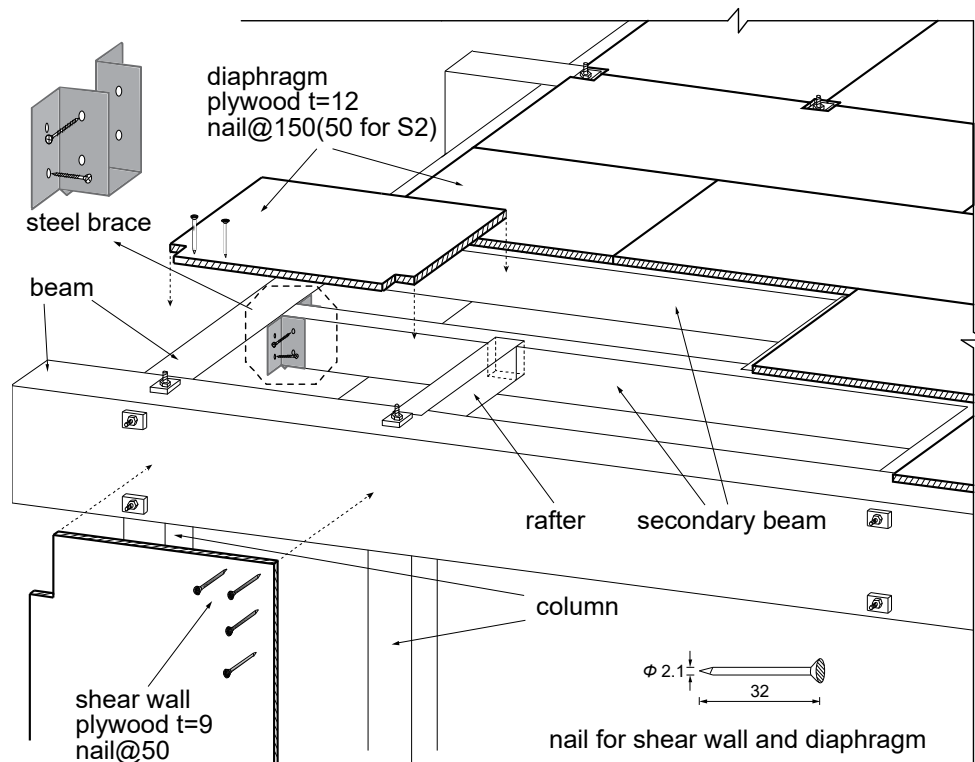
Fig. C.3 Layout of shear wall and diaphragm at the roof (in mm)

precast holes in the wood elements, which were the same with the pilot experiment in Appendix B (Fig. B.2). The joints between column and beam were supposed to be moment free, if not, to have limited moment resistance capacity compared with the shear wall, which was verified in the later experiment results. The shear walls in all the specimens were constructed with plywood panels (t=9mm) and nails (d=2.1mm, L=32mm, @50mm), and the diaphragms were constructed with plywood panels (t=12mm) and nails (d=2.1mm, L=32mm, @150mm for S1&3, @50mm for S2). The detailed layout of the shear wall and diaphragm is depicted in Fig. C.3. Several concrete bricks were fastened on each floor as additional mass, with a total weight of 19kN. The detailed design procedure of the additional weight is shown in Chapter 2.

To simulate the concrete core part of the prototype, the wood specimen was connected to a steel frame which had a high stiffness along the input direction. SS400 steel type was used for the frame. The connection between two parts is shown in Fig. C.4. Since the stiffness of the wood part was much smaller than the concrete core in the prototype, the vibration of the 1st mode was supposed to focus on the wood part and the failure would first occur in the wood part and wood-concrete connection. In this condition, the concrete core was designed to provide high lateral and

H-200×200×8×12
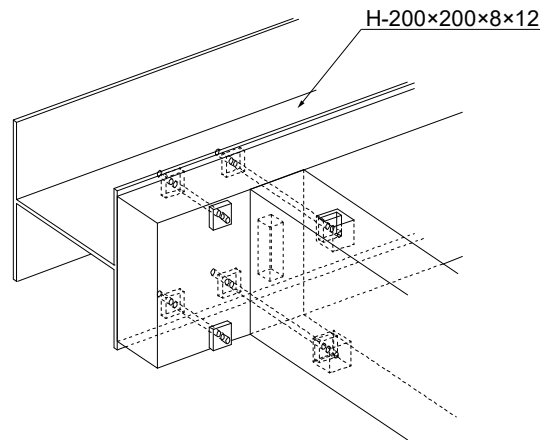
Fig. C.4 Design details of wood-core joint

torsional strength rather than to be an energy consumption part, while the steel frame of the specimens was presumed to act the same way during the tests. The connection was designed to be rigid enough to transfer the shear force and moment effectively between the two parts. Since the specimen was designed through the proposed design process rather directly scaled from the prototype, the detailed layout of the connection in the specimen was different from the prototype. The potential failure mechanism of the wood-concrete connection, therefore, was not included in this paper in view of that the tensile damage of concrete may be the main cause of the connection failure.

In general, the specimens were believed to be representative of wood horizontal hybrid structures which have large plane irregularity due to different lateral stiffness between the disparate parts included.

Measurement setup

Nearly 120 sensors were mounted on the specimens to build the measurement system. Uniaxial accelerometers and draw-wire displacement sensors were fixed on each floor and each frame. Force transducers were mounted at the joints between the wood frame and steel frame as well as the joints between the wood frame and the shaking table. On each shear wall, a pair of orthogonal strain transducers was attached on the plywood panel to measure the shear strain. The detailed arrangement of measurement equipment is shown in Fig. C.5. Next to the specimen, on the shaking table stood a steel tower to install the laser displacement sensor. However, during the tests, the tower had a non-negligible vibration which made the records of the laser displacement sensor unreliable. So the displacements of the specimen were mainly acquired from the draw-wire displacement sensor between each floor.

(a) front view

(b) side view

(c) top view

Mark	Symbol	Measurement Sensor
◄--◄--	D_L	Laser Displacement Sensor
╱	D_W	Draw-wire Displacement Sensor
●→ ◎	A_i	Uniaxial Accelerometer
∧	δ	Strain Gauge
⇒	Q	Shear Force Transducer
⇅	D_R	Relative Displacement Sensor
▮	N	Axial Force Transducer
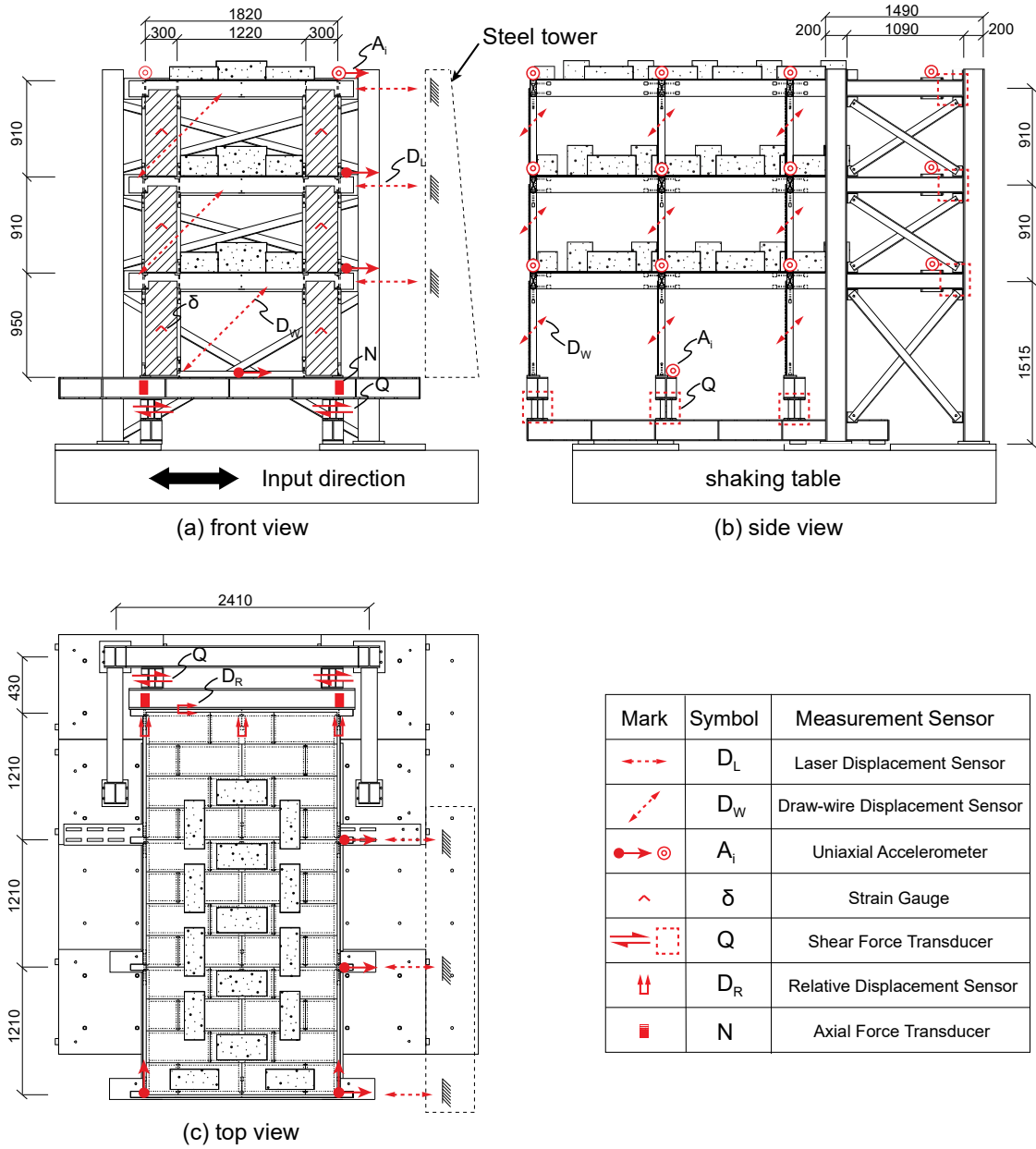
Fig. C.5 Overall dimension and measurement setup of S1 (in mm)

Input ground motion and test procedure

The input ground motions were BCJ-L2 waves with increasing PGA intensity from 0.1g to 0.8g, which represent moderate to severe earthquake scenarios. The BCJ-L2 wave is one of the simulation ground motions specified by the Building Center of Japan. It is developed, at 5% damping ratio, to have the same response spectral shape with the design spectrum in Japanese Building Code (BCJ 2016). The BCJ-L2 wave used in this paper is designed for a solid site with shear wave velocity higher than 400m/s (BRI 1992). The duration of BCJ-L2 wave is scaled to 0.58 times of the original one to satisfy the similitude requirement in Table C.1. Fig. C.6(a) is the time history of 0.4g BCJ-L2 wave used in this experiment and Fig. C.6(b) illustrates the response spectrum of BCJ-L2 and the design spectrum. Before and after each ground motion input, white noise tests were conducted to analyze the dynamic properties of the specimens. The PGA amplitude of the white noise was 0.05g, with a frequency range from 0.01 to 30 Hz. Each specimen was subjected to the same test sequence in Table C.3. WN and EQ represent white noise and BCJ-L2 wave input respectively. All the inputs used in this experiment were transversely unidirectional as shown in Fig. C.5.

(a) time history	(b) accleration spectrum
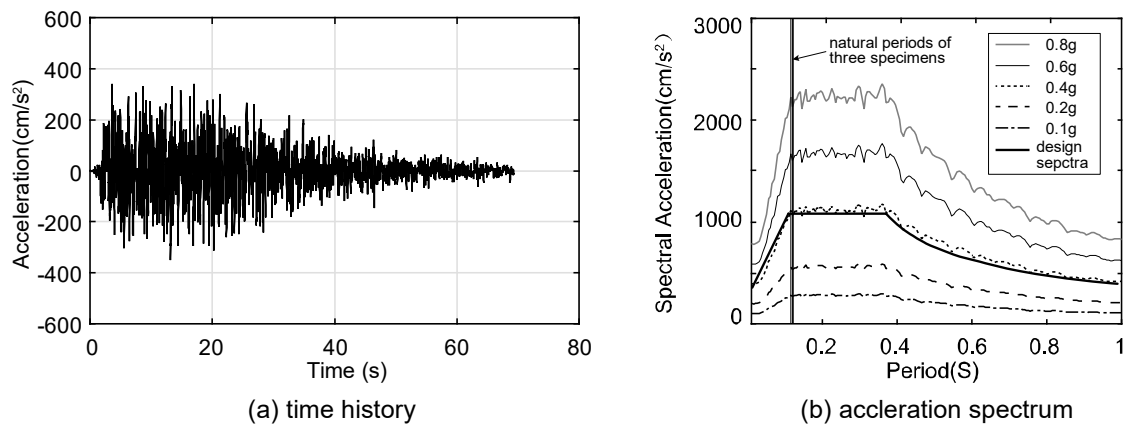
Fig. C.6 Time history and acceleration spectrum of scaled BCJ-L2

Table C.3 Test sequence

Sequence	1	2	3	4	5	6	7	8	9	10	11
Input	WN	EQ1	WN	EQ2	WN	EQ3	WN	EQ4	WN	EQ5	WN
PGA(g)	0.05	0.1	0.05	0.2	0.05	0.4	0.05	0.6	0.05	0.8	0.05

WN : white noise

EQ# : BCJ-L2 wave

Appendix D   Subroutine of *MSAWS* material

The script of MSAWSMaterial.cpp :

```
/* ********************************************************************* **
**    OpenSees - Open System for Earthquake Engineering Simulation    **
**          Pacific Earthquake Engineering Research Center        **
**                                                **
**                                                **
** (C) Copyright 1999, The Regents of the University of California    **
** All Rights Reserved.                                **
**                                                **
** Commercial use of this program without express permission of the   **
** University of California, Berkeley, is strictly prohibited.  See    **
** file 'COPYRIGHT'  in main directory for information on usage and    **
** redistribution,  and for a DISCLAIMER OF ALL WARRANTIES.        **
**                                                **
** Developed by:                                      **
**   Frank McKenna (fmckenna@ce.berkeley.edu)              **
**   Gregory L. Fenves (fenves@ce.berkeley.edu)             **
**   Filip C. Filippou (filippou@ce.berkeley.edu)            **
**                                                **
** ********************************************************************* */

// $Revision: 1.4 $
// $Date: 2010-02-04 20:12:15 $
// $Source: /usr/local/cvs/OpenSees/SRC/material/uniaxial/SAWSMaterial.cpp,v $
// Written: Patxi (Converted from FORTRAN code originally written by Bryan
Folz)
// Created: June 2006
// Description: This file contains the class definition for
// SAWSMaterial.  SAWSMaterial provides the implementation
// of a one-dimensional hysteretic model develeped as part of
// the CUREe Caltech wood frame project.
// Reference: Folz, B. and Filiatrault, A. (2001). "SAWS - Version 1.0,
// A Computer Program for the Seismic Analysis of Woodframe Structures",
// Structural Systems Research Project Report No. SSRP-2001/09,
// Dept. of Structural Engineering, UCSD, La Jolla, CA .

// MSAWSMaterial: 1.0, modified from SAWSMaterial by Wu Di in 2017-03-03
// MSAWSMaterial added a new parameter to control the stiffness of the
pinching part.
// Reference: Wu Di


#include <stdlib.h>
#include "MSAWSMaterial.h"
#include <OPS_Globals.h>
#include <math.h>
#include <float.h>
#include <Channel.h>
#include <classTags.h>
#include <iostream>
#include <elementAPI.h>
#ifdef  USRDLL
#define OPS Export extern "C" _declspec(dllexport)
#elif  MACOSX
#define OPS_Export extern "C" __attribute__((visibility("default")))
#else
#define OPS_Export extern "C"
#endif
```

```
static int numMSAWSMaterials = 0;

OPS Export void *
OPS_MSAWSMaterial()
{
  if (numMSAWSMaterials == 0) {

    OPS Error("MSAWSMaterial unaxial material - Written by Paxti Uriz, Exponent
2009¥n", 1);
        numMSAWSMaterials=1;
  }

  // Pointer to a uniaxial material that will be returned
  UniaxialMaterial *theMaterial = 0;

  int   iData[1];
  double dData[12];
  int numData = 1;

  if (OPS_GetIntInput(&numData, iData) != 0) {
    opserr << "WARNING invalid uniaxialMaterial MSAWSMaterial tag" << endln;
    return 0;
  }

  numData = 12;
  if (OPS_GetDoubleInput(&numData, dData) != 0) {
    opserr << "Invalid Args want: uniaxialMaterial SAWS tag? F0? FI? dU? S0?"
<< endln;
    opserr << "   R1? R2? R3? R4? alpha? beta?" << endln;
    return 0;
  }

  // Parsing was successful, allocate the material
  theMaterial = new MSAWSMaterial(iData[0],
                                  dData[0], dData[1], dData[2],
                                  dData[3], dData[4], dData[5],
                                  dData[6], dData[7], dData[8],
                                  dData[9], dData[10], dData[11]);

  if (theMaterial == 0) {
    opserr << "WARNING could not create uniaxialMaterial of type
MSAWSMaterial¥n";
    return 0;
  }

  return theMaterial;
}

MSAWSMaterial::MSAWSMaterial(int tag,
                        double f0, double fI, double dU, double s0,
                        double r1, double r2, double r3, double r4,
                        double A, double B, double G, double D):
UniaxialMaterial(tag, 0),
F0(f0), FI(fI), DU(dU), S0(s0), R1(r1), R2(r2), R3(r3), R4(r4),
ALPHA(A), BETA(B), gama(G), delta(D)
{

  TOL   = 1.0E-8 ;  //  Tolerance for bi-section search.

  LPATH  = 1;
  cLPATH = 1;
```

```cpp
    LPPREV  = 1;
    cLPPREV = 1;
    IYPLUS  = 0;
    IYMINS  = 0;

    DOLD   = 0.0;
    FOLD   = 0.0;
    DUNP   = 0.0;
    FUNP   = 0.0;
    DUNM   = 0.0;
    FUNM   = 0.0;
    DMAXP  = 0.0;
    FMAXP  = 0.0;
    DMAXM  = 0.0;
    FMAXM  = 0.0;
    SP     = 0.0;
    R4M=0.0;
    R4P=0.0;

    STIFF  = S0;

    // Initialize history variables
    this->revertToStart();
    this->revertToLastCommit();

}

MSAWSMaterial::MSAWSMaterial()
  :UniaxialMaterial(0, 0),
   F0(0.0), FI(0.0), DU(0.0), S0(0.0), R1(0.0), R2(0.0), R3(0.0), R4(0.0),
   ALPHA(0.0), BETA(0.0), gama(0.0), delta(0.0)
{

}

MSAWSMaterial::~MSAWSMaterial()
{
  // Nothing to do
}

int
MSAWSMaterial::setTrialStrain(double strain, double strainRate)
{

  // Set the initial parameters from the commited stage
  DISPL  = strain;
  LPATH  = cLPATH;
  LPPREV = cLPPREV;
  IYPLUS = cIYPLUS;
  IYMINS = cIYMINS;
  DOLD   = cDOLD;
  /*FOLD   = cFOLD;*/
  DUNP   = cDUNP;
  FUNP   = cFUNP;
  DUNM   = cDUNM;
  FUNM   = cFUNM;
  DMAXP  = cDMAXP;
  FMAXP  = cFMAXP;
  DMAXM  = cDMAXM;
  FMAXM  = cFMAXM;
  SP     = cSP;
   /*R4P    = cR4P;
```

```
R4M    = cR4M;*/

int foundStateFlag = 0 ;
int checkThisStateFlag = 0;

// The following has been converted from SAWS (originally written in
//    FORTRAN by Bryan Folz), converted by Patxi Uriz 6/12/2006
/* -----------------------------------------------------------------------
 *      SUBROUTINE HYSTR CALCULATES THE FORCE-DISPLACEMENT RESPONSE
 *      BASED ON A MODIFIED STEWART HYSTERETIC MODEL. IN THIS MODEL THE
 *      ENVELOPE CURVE IS THE FOSCHI EXPONENTIAL CURVE WITH A LINEAR
 *      SOFTENING BRANCH. FORCE AND STIFFNESS ARE RETURNED FOR AN
 *      INPUTTED DISPLACEMENT.
 *-----------------------------------------------------------------------
 */

/*  SUBROUTINE HYSTR (DISPL, FORCE, STIFF, JFLAG)
    IMPLICIT DOUBLE PRECISION (A - H, O - Z)
    COMMON /H01/ LPATH, LPPREV, IMODE, IYPLUS, IYMINS
    COMMON /H02/ F0, FI, DU, S0, R1, R2, R3, R4, ALPHA, BETA,gama, delta
    COMMON /H03/ DOLD, DUNP, FUNP, DUNM, FUNM, DMAXP, FMAXP, DMAXM,
    FMAXM, SP
*/

int IFLAG = 0   ;   // Looping flag to capture infinite loop.
int JFLAG = 0   ;
int IMODE = 3   ;   //  Full hysteretic response permitted.

// Determine ultimate force FU, corresponding to DU.

FAC1 = F0 + (R1 * S0 * DU);
FAC2 = 1.0 - exp(-S0*DU/F0);
FU = FAC1 * FAC2;

/* Check if DISPL > DF.  If so, there is no capacity left in the
   connector: set FORCE = 0, STIFF = 0 and LPATH = 0.

   Corrected DF1 failure displacement criterion
   McDonald 9/20/05

   DF1 = (FU - FI - (R2*S0*DU)) / (S0*(R4 - R2))
*/

DF1 = (FU + FI - (R2*S0*DU)) / (S0*(R4 - R2));
DF = DF1;
DF2 = DU - (FU/(R2*S0));
if (DF2 < DF1 )
  DF = DF2 ;
if ( fabs(DISPL) >= DF || LPATH == 0) {
  // Reduce the force and stiffness to a small number
  FORCE = 1.0e-8*DISPL;
  STIFF = 1.0e-8;
  LPATH = 0 ;
  opserr << "Strain too large" << endln;
  return 0;
}

/*  For the static analysis option (IMODE = 1 or 2) the load
    displacement response remains on the envelope curve.
    The option of IMODE set to 1 or 2 is used in the CASHEW program.
*/
```

```
  if (IMODE ==  2) {
    if (DISPL >= 0.0) {
      if  (DISPL <= DU) {
         FAC1 = F0 + (R1 * S0 * fabs(DISPL));
         FAC2 = 1.0 - exp(-S0*fabs(DISPL)/F0);
         FAC3 = 1 - FAC2;
         FORCE = FAC1 * FAC2;
         STIFF = (FAC1 * (S0/F0) * FAC3) + (R1 * S0 * FAC2);
         return 0;
      } else if  (DISPL > DU) {
         D0 = DU - (FU/(R2*S0));
         if (DISPL >= D0) {
           // Reduce the force and stiffness to a small number
           FORCE = 1.0e-8*DISPL;
           STIFF = 1.0e-8;
           return 0;
         }
         FORCE = FU + (R2*S0*(DISPL - DU));
         STIFF = R2 * S0;
         return 0;
      }

    } else if (DISPL <  0.0) {

      if (DISPL >= -DU) {
         FAC1 = F0 + (R1 * S0 * fabs(DISPL));
         FAC2 = 1.0 - exp(-S0*fabs(DISPL)/F0);
         FAC3 = 1 - FAC2;
         FORCE = -FAC1 * FAC2;
         STIFF = (FAC1 * (S0/F0) * FAC3) + (R1 * S0 * FAC2);
         return 0;
      } else if (DISPL < -DU) {
         D0 = (FU/(R2*S0)) - DU;
         if (DISPL <= D0) {
           // Reduce the force and stiffness to a small number
           FORCE = 1.0e-8*DISPL;
           STIFF = 1.0e-8;
           return 0;
         }
         FORCE = -FU + (R2*S0*(DISPL + DU));
         STIFF = R2 * S0;
         return 0;
      }
    }
  }


  //if (LPATH == 5)
  //  DINT2 = - DINT2;
  //
  //DY = F0 / S0;

  // Find R40 (using bi-section search). the tangent point of LPATH5/7 with
LPATH 2

  DA = 0.0;
  DB = 2.0 * DU;
  DIFF = TOL + 1.0;
  while (fabs(DIFF) > TOL) {
          DINT1 = (DA + DB) / 2.0;
          FAC1 = F0 + (R1 * S0 * fabs(DINT1));
```

```
        FAC2 = 1.0 - exp(-S0*fabs(DINT1) / F0);
        Fun1 = R1*S0*(1.0 - exp(-S0*fabs(DINT1) )/ F0);
        Fun2 = (F0 + (R1 * S0 * fabs(DINT1)))*S0*exp(-S0*fabs(DINT1) / F0) /
F0; // Fun1+Fun2 is tangent function of the backbone curve
        Fun3 = (FAC1*FAC2 - FI) / fabs(DINT1);
                DIFF = Fun1 + Fun2 - Fun3;

        if (DIFF <= 0.0) {
                DB = DINT1;
        }
        else {
                DA = DINT1;
        }
  }
  DINT1 = fabs(DINT1);
  Fun3 = (FAC1*FAC2 - FI) / fabs(DINT1);
  R40 = fabs(Fun3)/S0;
  if (LPATH == 5)
  DINT1 = - DINT1;
   DY = F0 / S0;

  // // Find DINT8 (using bi-section search).  the tangent point of LPATH 2
with Line with k=3
  // DA = 0.0;
  //DB = 2.0 * DU;
  //DIFF = TOL + 1.0;
  //if (R3<1.0) {
  //while (fabs(DIFF) > TOL) {
        // DINT8 = (DA + DB) / 2.0;
        // FAC1 = F0 + (R1 * S0 * fabs(DINT8));
        // FAC2 = 1.0 - exp(-S0*fabs(DINT8) / F0);
        // Fun1 = R1*S0*(1.0 - exp(-S0*fabs(DINT8) )/ F0);
        // Fun2 = (F0 + (R1 * S0 * fabs(DINT8)))*S0*exp(-S0*fabs(DINT8) / F0)
/ F0; // Fun1+Fun2 is tangent function of the backbone curve
        // Fun3 = R3*S0;
                // DIFF = Fun1 + Fun2 - Fun3;

        // if (DIFF <= 0.0) {
                // DB = DINT8;
        // }
        // else {
                // DA = DINT8;
        // }
  //}
  //DINT8 = fabs(DINT8);}
  //else {
        // DINT8=0.0;
  //}




  // ------------------------------------------
  // NEED TO DEAL WITH THIS PESKY 'GO TO' BUSINESS,
  // TRY WHILE LOOP, INSTEAD
  // Edited by Patxi 6/12/2006
  // 100 CONTINUE;
  while (foundStateFlag == 0 ) {
```

```
  // if we are looping through, and looking for the right state,
  // we need to stop at all LPATH checks
  checkThisStateFlag = 0;

  IFLAG = IFLAG + 1;

  if (IFLAG > 10) {
    JFLAG = 1;
    foundStateFlag = 1;
    return 0;
  }

  //=============================================================
  /*
   *     LPATH = 1: Load-displacement response is on the non-linear
   *               (exponential) segment of the backbone curve.
   *               Unloading occurs along LPATH 1.
   */
  if (LPATH == 1  && foundStateFlag == 0 && checkThisStateFlag == 0) {
                /*  Find DINT2 (using bi-section search).*/

DA = 0.0;
DB = 2.0 * DU;
DIFF = TOL+1.0;

while ( fabs(DIFF) > TOL ) {
  //10 DINT2 = (DA + DB) / 2.0D0;
  DINT2 = (DA + DB) / 2.0;
  FAC1 = F0 + (R1 * S0 * fabs(DINT2));
  FAC2 = 1.0 - exp(-S0*fabs(DINT2)/F0);
  FAC3 = FI + (R4 * S0 * DINT2);
  DIFF = (FAC1 * FAC2) - FAC3;

  if (DIFF >= 0.0) {
    DB = DINT2;
  } else {
    DA = DINT2;
  }
}
DINT2 = fabs(DINT2);

    DLIM = 1.05 * fabs(DINT2);

    if ( (DISPL >= 0.0) && (DISPL <= DLIM)) {

        FAC1 = F0 + (R1 * S0 * fabs(DISPL));
        FAC2 = 1.0 - exp(-S0*fabs(DISPL)/F0);
        FAC3 = 1 - FAC2;
        FORCE = FAC1 * FAC2;
        STIFF = (FAC1 * (S0/F0) * FAC3) + (R1 * S0 * FAC2);
        DOLD = DISPL;
        FOLD = FORCE;
        foundStateFlag = 1;
        return 0;

    } else if  ( (DISPL < 0.0) && (DISPL >= (-DLIM)) ) {

        FAC1 = F0 + (R1 * S0 * fabs(DISPL));
        FAC2 = 1.0 - exp(-S0*fabs(DISPL)/F0);
        FAC3 = 1 - FAC2;
        FORCE = -FAC1 * FAC2;
        STIFF = (FAC1 * (S0/F0) * FAC3) + (R1 * S0 * FAC2);
```

```
      DOLD = DISPL;
      /*FOLD = FORCE;*/
      foundStateFlag = 1;
      return 0;

  } else {

      LPATH = 2;
      LPPREV = 1;

  }

}

//=====================================================================
/*
 *    LPATH = 2: Load-displacement response is on the non-linear
 *              (exponential) segment of the backbone curve.
 */
if ( LPATH == 2 && foundStateFlag == 0 && checkThisStateFlag == 0) {

  if (fabs(DISPL) <= DU) {

     if (fabs(DISPL) >= fabs(DOLD)) {

       FAC1 = F0 + (R1 * S0 * fabs(DISPL));
       FAC2 = 1.0 - exp(-S0*fabs(DISPL)/F0);
       FAC3 = 1 - FAC2;

       if (DISPL >= 0.0) {

         FORCE = FAC1 * FAC2;
         IYPLUS = 1;
         DUNP = DISPL;
         FUNP = FORCE;
         DMAXP = BETA * DUNP;
         FAC1 = F0 + (R1 * S0 * DMAXP);
         FAC2 = 1.0 - exp(-S0*DMAXP/F0);
         FMAXP = FAC1 * FAC2;

         if (FMAXP > FU) {

           FMAXP = FU;

         }

       } else {

         FORCE = -FAC1 * FAC2;
         IYMINS = 1;
         DUNM = DISPL;
         FUNM = FORCE;
         DMAXM = BETA * DUNM;
         FAC1 = F0 + (R1 * S0 * fabs(DMAXM));
         FAC2 = 1.0 - exp(-S0*fabs(DMAXM)/F0);
         FMAXM = -FAC1 * FAC2;

         if (FMAXM < (-FU)) {

           FMAXM = -FU;

         }
```

```
        }

        STIFF = (FAC1 * (S0/F0) * FAC3) + (R1 * S0 * FAC2);
        DOLD = DISPL;
        /*FOLD = FORCE;*/
        LPPREV = 2;
        foundStateFlag = 1;
        return 0;

      } else {

        LPATH = 4 ;  //Unloading off LPATH 2.

      }

   } else {

      LPATH = 3;    //Loading continues on LPATH 3.

   }

}


// ===================================================================
/*
 *    LPATH = 3: Load-displacement response is on the second segment
 *              of the backbone curve
 *               (hardening or softening response).
 */
if (LPATH == 3 && foundStateFlag == 0 && checkThisStateFlag == 0 ) {

  /* Corrected D6 - displacement where hysteresis slope intersects R2*S0
     McDonald 9/20/05

     D6 = ((FU - FI) - (R2*S0*DU)) / (S0*(R4-R2))
  */

  D6 = ((FU + FI) - (R2*S0*DU)) / (S0*(R4-R2));

  if (DISPL > D6) {

     if (fabs(DISPL) >= fabs(DOLD)) {

       FORCE = FU + (R2*S0*(DISPL - DU));
       STIFF = R2 * S0;
       DOLD = DISPL;
       /*FOLD = FORCE;*/
       DUNP = DISPL;
       FUNP = FORCE;
       DMAXP = BETA * DUNP;
       FMAXP = FU + (R2*S0*(DMAXP - DU));
       LPATH  = 3;
       LPPREV = 3;
       foundStateFlag = 1;
       return 0;

     } else {

       LPATH = 4;
       LPPREV = 3;
```

```
      checkThisStateFlag = 1;
      // GO TO 100;

   }

} else if  (DISPL < -D6) {

   if (fabs(DISPL) >= fabs(DOLD)) {

     FORCE = -FU + (R2*S0*(DISPL + DU));
     STIFF = R2 * S0;
     DOLD = DISPL;
    /* FOLD = FORCE;*/
     DUNM = DISPL;
     FUNM = FORCE;
     DMAXM = BETA * DUNM;
     FMAXM = -FU + (R2*S0*(DMAXM + DU));
     LPATH  = 3;
     LPPREV = 3;
     foundStateFlag = 1;
     return 0;

   } else {

     LPATH = 4;
     LPPREV = 3;
     checkThisStateFlag = 1;
     //GO TO 100;

   }

}

if (fabs(DISPL) >= fabs(DOLD) && checkThisStateFlag == 0) {

   if (DISPL > 0.0) {

     D0 = DU - (FU/(R2*S0));

     if (DISPL >= D0) {

       LPATH = 3;
       LPPREV = 3;
       // Reduce the force and stiffness to a small number
       FORCE = 1.0e-8*DISPL;
       STIFF = 1.0e-8;
       foundStateFlag = 1;
       return 0;
     }

     IYPLUS = 1;
     FORCE = FU + (R2*S0*(DISPL - DU));
     STIFF = R2 * S0;
     DOLD = DISPL;
    /* FOLD = FORCE;*/
     DUNP = DISPL;
     FUNP = FORCE;
     DMAXP = BETA * DUNP;
     FMAXP = FU + (R2*S0*(DMAXP - DU));
     LPPREV = 3;
     foundStateFlag = 1;
     return 0;
```

```
    } else if  (DISPL < 0.0 && checkThisStateFlag == 0) {

     D0 = (FU/(R2*S0)) - DU;

     if (DISPL <= D0) {

       LPATH = 3;
       // Reduce the force and stiffness to a small number
       FORCE = 1.0e-8*DISPL;
       STIFF = 1.0e-8;
       foundStateFlag = 1;
       return 0;

     }

     IYMINS = 1;
     FORCE = -FU + (R2*S0*(DISPL + DU));
     STIFF = R2 * S0;
     DOLD = DISPL;
    /* FOLD = FORCE;*/
     DUNM = DISPL;
     FUNM = FORCE;
     DMAXM = BETA * DUNM;
     FMAXM = -FU + (R2*S0*(DMAXM + DU));
     LPPREV = 3;
     foundStateFlag = 1;
     return 0;

    }

  } else if ( checkThisStateFlag == 0) {

     LPATH = 4;  // Unloading off LPATH 4

  }

}


// ======================================================
/*
 * LPATH = 4: Load-displacement response is unloading off
 *            the backbone curve (LPATH 2 or 3).
 */
if (LPATH == 4 && foundStateFlag == 0 && checkThisStateFlag == 0) {

  if ((DOLD < 0.0) && (DISPL >= 0.0)) {

     LPPREV = 4;
     LPATH = 13;
     checkThisStateFlag = 1;
     //GO TO 100;

  }

  if ((DOLD > 0.0) && (DISPL <= 0.0) && checkThisStateFlag == 0) {

     LPPREV = 4;
     LPATH = 14;
     checkThisStateFlag = 1;
     //GO TO 100
```

```
        }

    if (DISPL >= 0.0 && checkThisStateFlag == 0) {
                R4P = R4*pow((DU/ DUNP),gama);
                if (R4P >= R40){
                        R4P = R40;}
                else{
                        R4P = R4*pow((DU / DUNP), gama);
                        if(R4P>R4M && R4M!=0.0){
                                R4P=R4M;
                        }
                }
        dZero = DUNP - (FUNP/(R3*S0));
        DINT1P = (FI - (R3*S0*dZero))/(S0*(R4P - R3)); // the section point of
LPATH 4 and LPATH 5

        if (DISPL >= DINT1P) {

          FORCE = R3*S0*(DISPL - dZero);

          if (FORCE >=FUNP) {

            LPPREV = 4;
            LPATH = 2;
            checkThisStateFlag = 1;
            //GO TO 100

          }
           LPPREV = 4;
          STIFF = R3 * S0;
          DOLD = DISPL;
          /*FOLD = FORCE;*/
          foundStateFlag = 1;
          return 0;

        } else {
    LPPREV = 4;
        LPATH = 5;
        checkThisStateFlag = 1;
        }

    } else if ( checkThisStateFlag == 0) {

                R4M = R4*pow((DU / fabs(DUNM)), gama);
                if(R4M >= R40){
                        R4M = R40;
                } else {
                        R4M = R4*pow((DU / fabs(DUNM)), gama);
                        if(R4M>R4P){
                                R4M=R4P;
                        }
                }

        dZero = DUNM - (FUNM/(R3*S0));
        DINT1M = (-FI - (R3*S0*dZero))/(S0*(R4M - R3));


        if (DISPL <= DINT1M) {

          FORCE = R3*S0*(DISPL - dZero);
```

```
            if (FORCE <=FUNM) {

              LPPREV = 4;
              LPATH = 2;
              checkThisStateFlag = 1;
              //GO TO 100

            }
            /* LPPREV = 4;*/
            STIFF = R3 * S0;
            DOLD = DISPL;
            /*FOLD = FORCE;*/
            foundStateFlag = 1;
            return 0;

        } else {
  LPPREV = 4;
        LPATH = 7;
  checkThisStateFlag = 1;
        }
    }
  }


  //====================================================
  /*
   * LPATH = 5: Load-displacement response is unloading or
   *          reloading on the pinched curve
   *          (for negative forces).
   */
  if (LPATH == 5 && foundStateFlag == 0 && checkThisStateFlag == 0) {

    //c Corrected McDonald 9/20/05
    //c      DINT4 = (-FU + FI + (R2*S0*DU))/(S0*(R4 - R2))
    //DINT4 = (-FU + FI + (R2*S0*DU))/(S0*(R4 - R2));
              R4P = R4*pow((DU/ DUNP),gama);
        if (R4P >= R40 && R40!=0.0){
              R4P = R40;
        }else {
              R4P = R4*pow((DU / DUNP), gama);
              if(R4P>R4M && R4M!=0.0){
                           R4P=R4M;
                     }
        }

          /*  Find DINT2 (using bi-section search).*/

 DA=0.0;
 DB=fabs(DINT1);
 DIFF=TOL+1.0;
 if (R4P!=R40) {
 while (fabs(DIFF) > TOL ) {
   DINT2 = (DA + DB) / 2.0;

   FAC1 = F0 + (R1 * S0 * fabs(DINT2));
   FAC2 = 1.0 - exp(-S0*fabs(DINT2)/F0);
   FAC3 = FI + (R4P * S0 * DINT2);
   DIFF = (FAC1 * FAC2) - FAC3;
   if (DIFF >= 0.0) {
     DB = DINT2;
```

```
   } else {
     DA = DINT2;
   }

  }

 DINT2 = -fabs(DINT2);

 }else{
        DINT2=-fabs(DINT1);
 }
/*  Find DINT4 (using bi-section search).*/
  R4L=((fabs(FU)-FI)/DU)/S0;
         DA=fabs(DINT1);
 DB=DU;
 DIFF=TOL+1.0;
        if (R4P>=R4L) {    //calculate the crossing point of the LPATH 5 and
2 use bio-section
                 while (fabs(DIFF) > TOL ) {
   DINT4 = (DA + DB) / 2.0;
   FAC1 = F0 + (R1 * S0 * fabs(DINT4));
   FAC2 = 1.0 - exp(-S0*fabs(DINT4)/F0);
   FAC3 = FI + (R4P * S0 * DINT4);
   DIFF = (FAC1 * FAC2) - FAC3;
   if (DIFF <= 0.0) {
     DB = DINT4;
   } else {
     DA = DINT4;
   }
  }
 DINT4 = -fabs(DINT4);
         } else {
               DINT4 = (-FU + FI + (R2*S0*DU))/(S0*(R4P - R2));//calculate the
crossing point of the LPATH 5 and 3
         }


    if ((DISPL <= DINT4)&&(R4P>=R4L)) {

       LPATH = 2;
       LPPREV = 5;
       checkThisStateFlag = 1;

    }
          if ((DISPL <= DINT4)&&(R4P<R4L)) {

       LPATH = 3;
       LPPREV = 5;
       checkThisStateFlag = 1;

    }

    if ((LPPREV == 5) && (DISPL > DOLD)  && checkThisStateFlag == 0 ) {

       LPATH = 9;

    } else if ( checkThisStateFlag == 0) {

       if (IYMINS == 1) {

         if (DMAXM != 0.0)
           SP = delta*S0 * pow((DY/fabs(DMAXM)),ALPHA);
```

D-14

```
        } else {

          SP = delta*S0;

        }
        R4P = R4*pow((DU / DUNP), gama);
        if (R4P >= R40){
                R4P = R40;}
        else {
                R4P = R4*pow((DU / DUNP), gama);
                if(R4P>R4M&& R4M!=0.0){
                                R4P=R4M;
                        }
        }
        DINT3 = (-FI - FMAXM + (SP*DMAXM))/(SP - (R4P*S0));//the section point
of LAPTH 5 and LPATH 6

        if (DISPL >= DINT2) {
                R4P = R4*pow((DU / DUNP), gama);
                if (R4P >= R40) {
                        R4P = R40;}
                else {
                        R4P = R4*pow((DU / DUNP), gama);
                        if(R4P>R4M&& R4M!=0.0){
                                R4P=R4M;
                          }
                }
          FORCE = -FI + (R4P*S0*DISPL);
          STIFF = R4P * S0;
          DOLD = DISPL;
         /* FOLD = FORCE;*/
          LPPREV = 5;
          foundStateFlag = 1;

          return 0;

        } else if  ((DISPL < DINT2) && (IYMINS == 0)) { //IYMINS is used to
define the first loop

          LPPREV = 5;
          LPATH = 1;
          checkThisStateFlag = 1;
          //GOTO 100
        } else if  ((DISPL < DINT2) &&  (DISPL >= DINT3)) {
                R4P = R4*pow((DU / DUNP), gama);
                if (R4P >= R40) {
                        R4P = R40;}
                else {
                        R4P = R4*pow((DU / DUNP), gama);
                        if(R4P>R4M&& R4M!=0.0){
                                R4P=R4M;
                          }
                }
                        /* FAC1 = F0 + (R1 * S0 * fabs(DISPL));
          FAC2 = 1.0 - exp(-S0*fabs(DISPL)/F0);
          if (-FI + (R4M*S0*DISPL)<= -FAC1*FAC2) {
                FORCE = -FAC1*FAC2;
          }else{
                FORCE = -FI + (R4M*S0*DISPL);}*/
          FORCE = -FI + (R4P*S0*DISPL);
          STIFF = R4P * S0;
```

```
        DOLD = DISPL;
        /*FOLD = FORCE;*/
        LPPREV = 5;
        foundStateFlag = 1;
        return 0;
      } else {
        LPPREV=5;
        LPATH = 6;
    checkThisStateFlag = 1;
      }

    }

  }

  //=================================================
  /*
   *    LPATH = 6: Load-displacement response is reloading from the
   *              pinched curve (LPATH 5) to the backbone curve
   *              (LPATH 2 or 3).
   */

  if (LPATH == 6 && foundStateFlag == 0 && checkThisStateFlag == 0) {

    DINT6=(FMAXM+FU-R2*S0*DU-SP*DMAXM)/(R2*S0-SP); //the crossing point of
LPATH 6 and 3
    if ((LPPREV == 6) && (DISPL > DOLD)) {

      LPATH = 11;

    } else {

      if ((DISPL >= DMAXM)&&(DMAXM>=DINT6)) {

        SP = delta*S0 * pow((DY/fabs(DMAXM)),ALPHA);
      /*  FAC1 = F0 + (R1 * S0 * fabs(DISPL));
        FAC2 = 1.0 - exp(-S0*fabs(DISPL)/F0);*/
         FORCE = FMAXM + (SP*(DISPL - DMAXM));
              /*if (FORCE <= -FAC1*FAC2) {
                  FORCE = -FAC1*FAC2;
             }else{
                  FORCE = FORCE;}*/
         STIFF = SP;
         DOLD = DISPL;
        /* FOLD = FORCE;*/
         LPPREV = 6;
         foundStateFlag = 1;
         return 0;

      } else if ((DISPL >= DINT6)&&(DMAXM<DINT6)) {

      /* FAC1 = F0 + (R1 * S0 * fabs(DISPL));
        FAC2 = 1.0 - exp(-S0*fabs(DISPL)/F0);*/
              SP = delta*S0 * pow((DY/fabs(DMAXM)),ALPHA);
       FORCE = FMAXM + (SP*(DISPL - DMAXM));
              /*if (FORCE <= -FAC1*FAC2) {
                  FORCE = -FAC1*FAC2;
             }else{
                  FORCE = FORCE;}*/
         STIFF = SP;
         DOLD = DISPL;
        /* FOLD = FORCE;*/
```

```
        LPPREV = 6;
        foundStateFlag = 1;
        return 0;

      }else {
  LPPREV = 6;
        LPATH = 2;
        checkThisStateFlag = 1;
        //GOTO 100

      }

    }

  }

  //========================================================
  /*
   *    LPATH = 7: Load-displacement response is unloading or
   *              reloading on the pinched curve
   *              (for positive forces).
   */

  if (LPATH == 7 && foundStateFlag == 0 && checkThisStateFlag == 0) {

    //c Corrected McDonald 9/20/05
    //c      DINT4 = (FU - FI - (R2*S0*DU))/(S0*(R4 - R2))
              R4M = R4*pow((DU / fabs(DUNM)), gama);
        if (R4M >= R40){
              R4M = R40;}
        else {
              R4M = R4*pow((DU / fabs(DUNM)), gama);
              if(R4M>R4P && R4P!=0.0){
                           R4M=R4P;
                      }
        }
      /* Find DINT2 (using bi-section search).*/ //calculate the LEFT crossing
point of the LPATH 7 and 2 use bio-section

 DA=0.0;
 DB=fabs(DINT1);
 DIFF=TOL+1.0;
 if (R4M!=R40) {
 while (fabs(DIFF) > TOL ) {
   DINT2 = (DA + DB) / 2.0;

   FAC1 = F0 + (R1 * S0 * fabs(DINT2));
   FAC2 = 1.0 - exp(-S0*fabs(DINT2)/F0);
   FAC3 = FI + (R4M * S0 * DINT2);
   DIFF = (FAC1 * FAC2) - FAC3;
   if (DIFF >= 0.0) {
     DB = DINT2;
   } else {
     DA = DINT2;
   }
 }
 DINT2 =fabs(DINT2);
 }else{
        DINT2=fabs(DINT1);
 }
/* Find DINT4 (using bi-section search).*/
        R4L=((fabs(FU)-FI)/DU)/S0;
```

```
        DA=fabs(DINT1);
 DB=DU;
 DIFF=TOL+1.0;
          if (R4M>=R4L) {    //calculate the RIGHT crossing point of the LPATH
7 and 2 use bio-section
                while (fabs(DIFF) > TOL ) {
   DINT4 = (DA + DB) / 2.0;
   FAC1 = F0 + (R1 * S0 * fabs(DINT4));
   FAC2 = 1.0 - exp(-S0*fabs(DINT4)/F0);
   FAC3 = FI + (R4M * S0 * DINT4);
   DIFF = (FAC1 * FAC2) - FAC3;
   if (DIFF <= 0.0) {
     DB = DINT4;
   } else {
     DA = DINT4;
   }
 }
 DINT4 = fabs(DINT4);
        } else {
             DINT4 = (FU - FI - (R2*S0*DU))/(S0*(R4M - R2)); //the crossing
point of LPATH 7 and 2
        }


    if ((DISPL >= DINT4)&&(R4M>=R4L)) {

       LPPREV = 7;
       LPATH = 2;
       checkThisStateFlag = 1;

    }
          if ((DISPL >= DINT4)&&(R4M<R4L)) {

       LPPREV = 7;
       LPATH = 3;
       checkThisStateFlag = 1;

    }

    if ((LPPREV == 7) && (DISPL < DOLD) && checkThisStateFlag == 0 ) {

       LPATH = 10;

    } else if ( checkThisStateFlag == 0 ) {

       if (IYPLUS == 1) {

         if (DMAXP != 0.0)
           SP = delta*S0 * pow((DY/DMAXP),ALPHA);

       } else {

         SP = delta*S0 ;

       }
       R4M = R4*pow((DU / fabs(DUNM)), gama);
       if (R4M >= R40){
               R4M = R40;}
       else {
               R4M = R4*pow((DU / fabs(DUNM)), gama);
               if(R4M>R4P && R4P!=0.0){
                               R4M=R4P;
```

```
                            }
        }
        DINT3 = (FI - FMAXP + (SP*DMAXP))/(SP - (R4M*S0)); //the section point
of LPATH 8 and 7
        /*if (DINT4 <= DINT3) {
                DINT3=DINT4;
        }*/

        if (DISPL <= DINT2) {
                R4M = R4*pow((DU / fabs(DUNM)), gama);
                if (R4M >= R40){
                        R4M = R40;}
                else {
                        R4M = R4*pow((DU / fabs(DUNM)), gama);
                        if(R4M>R4P && R4P!=0.0){
                                R4M=R4P;
                        }
                }

          FORCE = FI + (R4M*S0*DISPL);
          STIFF = R4M * S0;
          DOLD = DISPL;
/*   FOLD = FORCE;*/
          LPPREV = 7;
          foundStateFlag = 1;


          return 0;

        } else if  ((DISPL > DINT2) &&  (IYPLUS == 0)) {

          LPPREV = 7;
          LPATH = 1;
          checkThisStateFlag = 1;
          //GOTO 100

        } else if ((DISPL > DINT2) && (DISPL <= DINT3)) {
                R4M = R4*pow((DU / fabs(DUNM)), gama);
                if (R4M >= R40){
                        R4M = R40;}
                else {
                        R4M = R4*pow((DU / fabs(DUNM)), gama);
                        if(R4M>R4P && R4P!=0.0){
                                R4M=R4P;
                        }
                }
            /*FAC1 = F0 + (R1 * S0 * fabs(DISPL));
          FAC2 = 1.0 - exp(-S0*fabs(DISPL)/F0);
          if (FI + (R4M*S0*DISPL)>= FAC1*FAC2) {
                  FORCE = FAC1*FAC2;
          }else{
                  FORCE = FI + (R4M*S0*DISPL);}*/
                FORCE = FI + (R4M*S0*DISPL);
          STIFF = R4M * S0;
          DOLD = DISPL;
/*   FOLD = FORCE;*/
          LPPREV = 7;
          foundStateFlag = 1;

          return 0;

        } else {
```

```
        LPPREV = 7;
        LPATH = 8;
checkThisStateFlag = 1;
        }

    }

  }

  //==============================================================
  /*
   *     LPATH = 8: Load-displacement response is reloading from the
   *                pinched curve (LPATH 7) to the backbone curve
   *                (LPATH 2 or 3).
   */

  if (LPATH == 8 && foundStateFlag == 0 && checkThisStateFlag == 0) {
                DINT6=(FMAXP-FU+R2*S0*DU-SP*DMAXP)/(R2*S0-SP);

    if ((LPPREV == 8) && (DISPL < DOLD)  ) {

       LPATH = 12;

      } else  {

        if  ((DISPL <= DMAXP)&&(DMAXP<=DINT6)) {
          SP = delta*S0 * pow((DY/fabs(DMAXP)),ALPHA);
                      /* FAC1 = F0 + (R1 * S0 * fabs(DISPL));
        FAC2 = 1.0 - exp(-S0*fabs(DISPL)/F0);*/
         FORCE = FMAXP + (SP*(DISPL - DMAXP));
              /*if (FORCE >= FAC1*FAC2) {
                FORCE = FAC1*FAC2;
            }else{
                FORCE = FORCE;}*/
         STIFF = SP;
         DOLD = DISPL;
              /*       FOLD = FORCE;*/
         LPPREV = 8;
          foundStateFlag = 1;
         return 0;

        } else if  ((DISPL <= DINT6)&&(DMAXP>DINT6)) {

       /* FAC1 = F0 + (R1 * S0 * fabs(DISPL));
        FAC2 = 1.0 - exp(-S0*fabs(DISPL)/F0);*/
             SP = delta*S0 * pow((DY/fabs(DMAXP)),ALPHA);
         FORCE = FMAXP + (SP*(DISPL - DMAXP));
              /*if (FORCE >= FAC1*FAC2) {
                FORCE = FAC1*FAC2;
            }else{
                FORCE = FORCE;}*/
         STIFF = SP;
         DOLD = DISPL;
              /*       FOLD = FORCE;*/
         LPPREV = 8;
          foundStateFlag = 1;
         return 0;

        }else {
              /*LPPREV = 8;*/
         LPATH = 2;
```

```
        checkThisStateFlag = 1;
         // GOTO 100

          }
        }
   }


   //=====================================================
   /*
    *     LPATH = 9: Load-dispalcement response is between the two
    *                pinched curves (LPATH 5 and 7).
    */
   if (LPATH == 9 && foundStateFlag == 0 && checkThisStateFlag == 0) {
               R4M = R4*pow((DU /fabs(DUNM)), gama);
               if (R4M >= R40){
                     R4M = R40;}
               else {
                     R4M = R4*pow((DU /fabs(DUNM)), gama);
                     if(R4M>R4P){
                             R4M=R4P;
                       }
               }
     FOLD = -FI + (R4P*S0*DOLD);
     DUPPER = (FOLD - FI - (R3*S0*DOLD))/(S0*(R4M - R3));//the section point
between LPATH 9 and 7
     DLOWER = DOLD;

              /* Find DINT11 the section point between LPATH 9 and 8*/
        SP = delta*S0 * pow((DY/fabs(DMAXP)),ALPHA);
        DINT3 = (FI - FMAXP + (SP*DMAXP))/(SP - (R4M*S0)); //the section
point of LPATH 8 and 7
     DINT11= (FMAXP-FOLD+DOLD*R3*S0-SP*DMAXP)/(R3*S0-SP); //the section point
between LPATH 9 and 8
if (DINT11 >=DUPPER && DUPPER>=  DINT3 ) {
       DUPPER = DINT11;}

     if (DISPL <= DLOWER) {

       LPATH = 5;
       LPPREV = 9;
       checkThisStateFlag = 1;
       //GO TO 100

     } else if  ((DISPL > DLOWER) && (DISPL <=DUPPER)) {
       FORCE = FOLD + (R3*S0*(DISPL - DLOWER));
       STIFF = R3 * S0;
       foundStateFlag = 1;
       return 0;

     }else {

       LPATH = 7;
        LPPREV = 9;
        checkThisStateFlag = 1;
       //GOTO 100;

     }

   }

   //=============================================================
```

```
    /*
     *     LPATH = 10: Load-displacement response is between the
     *               two pinched curves (LPATH 7 and 5).
     */

    if (LPATH == 10 && foundStateFlag == 0 && checkThisStateFlag == 0) {
                R4P = R4*pow((DU / fabs(DUNP)), gama);
                if (R4P >= R40){
                        R4P = R40;}
                else {
                        R4P = R4*pow((DU / fabs(DUNP)), gama);
                        if(R4P>R4M){
                                R4P=R4M;
                        }
                } //the stiffness according to the DUNM
     FOLD = FI + (R4M*S0*DOLD);
         DUPPER = DOLD;
     DLOWER = (FOLD + FI - (R3*S0*DOLD))/(S0*(R4P - R3));
          // /* Find DINT11 the section point between LPATH 10 and 6*/
          SP = delta*S0 * pow((DY/fabs(DMAXM)),ALPHA);
          DINT3 = (-FI - FMAXM + (SP*DMAXM))/(SP - (R4P*S0));//the section
point of LAPTH 5 and LPATH 6
     DINT11= (FMAXM-FOLD+DOLD*R3*S0-SP*DMAXM)/(R3*S0-SP);//the section point
between LPATH 10 and 6

if (DINT11 <=DLOWER && DLOWER<= DINT3) {
        DLOWER = DINT11;}


    if (DISPL <= DLOWER) {

        LPATH = 5;
        LPPREV = 10;
        checkThisStateFlag = 1;
        //GO TO 100

    } else if  ((DISPL > DLOWER) && (DISPL < DUPPER)) {

        FORCE = FOLD + (R3*S0*(DISPL - DUPPER));
        STIFF = R3 * S0;
        foundStateFlag = 1;
        return 0;

    }else {

        LPATH = 7;
        LPPREV = 10;
        checkThisStateFlag = 1;
        //GOTO 100

    }

    }

    //============================================================
    /*
     *     LPATH = 11: Load-displacement response is unloading off the
     *               reloading curve (LPATH 6).
     */

    if (LPATH == 11 && foundStateFlag == 0 && checkThisStateFlag == 0) {
                R4P = R4*pow((DU / DUNP), gama);
```

```
        if (R4P >= R40){
                R4P = R40;}
        else {
                R4P = R4*pow((DU / DUNP), gama);
                if(R4P>R4M){
                                R4P=R4M;
                        }
        }
    SP = delta*S0 * pow((DY/fabs(DMAXM)),ALPHA);
    DINT3 = (-FI - FMAXM + (SP*DMAXM))/(SP - (R4P*S0));//the section point of
LPATH 5 and 6

    if ((LPPREV == 5) && (DISPL <= DINT3)) {

       LPATH = 6;
       LPPREV = 11;
       checkThisStateFlag = 1;
       //GO TO 100

    } else {
                R4M = R4*pow((DU / fabs(DUNM)), gama);
                if (R4M >= R40){
                        R4M = R40;}
                else {
                        R4M = R4*pow((DU / fabs(DUNM)), gama);
                        if(R4M>R4P){
                                R4M=R4P;
                        }
                }
       FOLD = FMAXM + (SP*(DOLD - DMAXM));
       DLOWER = DOLD;
       DUPPER = (FOLD - FI - (R3*S0*DLOWER))/(S0*(R4M - R3));

       if (DISPL >= DUPPER) {
       LPATH=7;
         LPPREV = 11;
         checkThisStateFlag = 1;
         //GO TO 100

       } else if  ((DISPL > DLOWER) && (DISPL < DUPPER)) {

         FORCE = FOLD + (R3*S0*(DISPL - DLOWER));
         STIFF = R3 * S0;
         foundStateFlag = 1;
         return 0;

        } else {

         LPATH = 6;
         LPPREV = 11;
          checkThisStateFlag = 1;
         //GOTO 100

        }
      }
    }

  //============================================================
  /*
   *    LPATH = 12: Load-displacement response is unloading off the
   *               reloading curve (LPATH 8).
   */
```

```
if (LPATH == 12 && foundStateFlag == 0 && checkThisStateFlag == 0) {
            R4M = R4*pow((DU / fabs(DUNM)), gama);
            if(R4M >= R40){
                    R4M = R40;}
            else {
                    R4M = R4*pow((DU / fabs(DUNM)), gama);
                    if(R4M>R4P){
                            R4M=R4P;
                    }
            }
  SP = delta*S0 * pow((DY/DMAXP),ALPHA);

  DINT3 = (FI - FMAXP + (SP*DMAXP))/(SP - (R4M*S0));

  if ((LPPREV == 7) && (DISPL >= DINT3)) {

     LPATH = 8;
     LPPREV = 12;
     checkThisStateFlag = 1;
     //GO TO 100

  } else {
            R4P = R4*pow((DU / fabs(DUNP)), gama);
            if (R4P >= R40){
                    R4P = R40;}
            else {
                    R4P = R4*pow((DU / fabs(DUNP)), gama);
                    if(R4P>R4M){
                            R4P=R4M;
                    }
            }
     FOLD = FMAXP + (SP*(DOLD - DMAXP));
     DUPPER = DOLD;
     DLOWER = (FOLD + FI - (R3*S0*DUPPER))/(S0*(R4P - R3));

     if (DISPL <= DLOWER) {
       LPATH = 5;
       LPPREV = 12;
       checkThisStateFlag = 1;
       //GO TO 100

     } else if ((DISPL > DLOWER) && (DISPL < DUPPER)) {

       FORCE = FOLD + (R3*S0*(DISPL - DUPPER));
       STIFF = R3 * S0;
       foundStateFlag = 1;
       return 0;

      } else {

        LPATH = 8;
        LPPREV = 12;
         checkThisStateFlag = 1;
        //GOTO 100

       }

   }

}

//============================================================
```

```
/*
 *    LPATH = 13: Load-displacement response following LPATH 3 when
 *                displacement goes from negative to positive.
 */
if (LPATH == 13 && foundStateFlag == 0 && checkThisStateFlag == 0) {
            R4M = R4*pow((DU / fabs(DUNM)), gama);
            if (R4M >= R40){
                    R4M = R40;}
            else {
                    R4M = R4*pow((DU / fabs(DUNM)), gama);
                    if(R4M>R4P){
                            R4M=R4P;
                      }
            }
  dZero = DUNM - (FUNM/(R3*S0));
  DINT5= (-FI - (R3*S0*dZero))/(S0*(R4M - R3));

  if (DISPL < DINT5) {

     LPPREV = 13;
     FORCE = R3*S0*(DISPL - dZero);

     if (FORCE < FMAXM) {

       LPATH = 1;
       checkThisStateFlag = 1;
       //GO TO 100

     }

     STIFF = R3 * S0;
     DOLD = DISPL;
     /*FOLD = FORCE;*/
     foundStateFlag = 1;
     return 0;

  } else {

     LPPREV = 13;
     LPATH = 7;
     checkThisStateFlag = 1;
     //GO TO 100

  }

}

// ================================================================
/*
 *    LPATH = 14: Load-displacement response following LPATH 4 when
 *                displacement goes from positive to negative.
 */
if (LPATH == 14 && foundStateFlag == 0 && checkThisStateFlag == 0) {
            R4P = R4*pow((DU / DUNP), gama);
            if (R4P >= R40){
                    R4P = R40;}
            else {
                    R4P = R4*pow((DU / DUNP), gama);
                    if(R4P>R4M){
                            R4P=R4M;
                      }
            }
```

```
        dZero = DUNP - (FUNP/(R3*S0));
        DINT5= (FI - (R3*S0*dZero))/(S0*(R4P - R3));

        if (DISPL > DINT5) {

            LPPREV = 14;
            FORCE = R3*S0*(DISPL - dZero);

            if (FORCE > FMAXP) {

                LPATH = 1;
                checkThisStateFlag = 1;
                //GO TO 100

            }

            STIFF = R3 * S0;
            DOLD = DISPL;
            /*FOLD = FORCE;*/
            foundStateFlag = 1;
            return 0;

        } else {

            LPPREV = 14;
            LPATH = 5;
            checkThisStateFlag = 1;
            //GO TO 100

        }

    }

  }
return 0;

}


double
MSAWSMaterial::getStrain(void)
{
  return DISPL;
}

double
MSAWSMaterial::getStress(void)
{
  return FORCE;
}

double
MSAWSMaterial::getTangent(void)
{
  return STIFF;
}


double
MSAWSMaterial::getInitialTangent(void)
{
  return S0;
```

```cpp
}

int
MSAWSMaterial::commitState(void)
{
  cDISPL  = DISPL;
  cFORCE  = FORCE;
  cSTIFF  = STIFF;
  cLPATH  = LPATH;
  cLPPREV = LPPREV;
  cIYPLUS = IYPLUS;
  cIYMINS = IYMINS;
  cDOLD   = DOLD;
  /*cFOLD   = FOLD;*/
  cDUNP   = DUNP;
  cFUNP   = FUNP;
  cDUNM   = DUNM;
  cFUNM   = FUNM;
  cDMAXP  = DMAXP;
  cFMAXP  = FMAXP;
  cDMAXM  = DMAXM;
  cFMAXM  = FMAXM;
  cSP     = SP;
  return 0;
}

int
MSAWSMaterial::revertToLastCommit(void)
{
  DISPL = cDISPL;
  FORCE = cFORCE;
  STIFF = cSTIFF;
  LPATH = cLPATH;
  LPPREV= cLPPREV;
  IYPLUS = cIYPLUS;
  IYMINS = cIYMINS;
  DOLD   = cDOLD;
  //FOLD   = cFOLD;
  DUNP   = cDUNP;
  FUNP   = cFUNP;
  DUNM   = cDUNM;
  FUNM   = cFUNM;
  DMAXP  = cDMAXP;
  FMAXP  = cFMAXP;
  DMAXM  = cDMAXM;
  FMAXM  = cFMAXM;
  SP     = cSP;
  /* R4P   = cR4P;
  R4M    = cR4M;*/
  return 0;
}

int
MSAWSMaterial::revertToStart(void)
{
  DISPL  = cDISPL =0.0;
  FORCE = cFORCE = 0.0;
  STIFF = cSTIFF = S0 ;
  LPATH = cLPATH = 1  ;
  LPPREV = cLPPREV = 1  ;
  IYPLUS = cIYPLUS = 0  ;
  IYMINS = cIYMINS = 0  ;
```

```
  DOLD = cDOLD = 0.0;
  /* FOLD = cFOLD = 0.0;*/
  DUNP = cDUNP = 0.0;
  FUNP = cFUNP = 0.0;
  DUNM = cDUNM = 0.0;
  FUNM = cFUNM = 0.0;
  DMAXP = cDMAXP = 0.0;
  FMAXP = cFMAXP = 0.0;
  DMAXM = cDMAXM = 0.0;
  FMAXM = cFMAXM = 0.0;
  SP = cSP = 0.0;
   /*R4P = cR4P = 0.0;
  R4M = cR4M = 0.0;*/
  return 0;
}

UniaxialMaterial*
MSAWSMaterial::getCopy(void)
{
  MSAWSMaterial *theCopy = new MSAWSMaterial (this->getTag(),
                                              F0, FI, DU, S0,
                                              R1, R2, R3, R4,
                                              ALPHA, BETA, gama, delta);

  theCopy->cDISPL  = this->cDISPL;
  theCopy->cFORCE  = this->cFORCE;
  theCopy->cSTIFF  = this->cSTIFF;
  theCopy->cLPATH  = this->cLPATH;
  theCopy->cIYPLUS = this->cIYPLUS;
  theCopy->cIYMINS = this->cIYMINS;
  theCopy->cDOLD   = this->cDOLD;
  /*theCopy->cFOLD   = this->cFOLD;*/
  theCopy->cDUNP   = this->cDUNP;
  theCopy->cFUNP   = this->cFUNP;
  theCopy->cDUNM   = this->cDUNM;
  theCopy->cFUNM   = this->cFUNM;
  theCopy->cDMAXP  = this->cDMAXP;
  theCopy->cFMAXP  = this->cFMAXP;
  theCopy->cDMAXM  = this->cDMAXM;
  theCopy->cFMAXM  = this->cFMAXM;
  theCopy->cSP     = this->cSP;
 /* theCopy->cR4P    =this->cR4P;
  theCopy->cR4M    =this->cR4M;*/

  return theCopy;
}

int
MSAWSMaterial::sendSelf(int commitTag, Channel &theChannel)
{
  int res = 0;

  static Vector dataVec(30);

  dataVec(0) = this->getTag();
  dataVec(1) = F0;
  dataVec(2) = FI;
  dataVec(3) = DU;
  dataVec(4) = S0;
  dataVec(5) = R1;
  dataVec(6) = R2;
  dataVec(7) = R3;
```

```cpp
  dataVec(8) = R4;
  dataVec(9) = ALPHA;
  dataVec(10) = BETA;
  dataVec(11) = cDISPL;
  dataVec(12) = cSTIFF;
  dataVec(13) = cFORCE;
  dataVec(14) = cLPATH;
  dataVec(15) = cLPPREV;
  dataVec(16) = cIYPLUS;
  dataVec(17) = cIYMINS;
  dataVec(18) = cDOLD;
  dataVec(19) = cDUNP;
  dataVec(20) = cFUNP;
  dataVec(21) = cDUNM;
  dataVec(22) = cFUNM;
  dataVec(23) = cDMAXP;
  dataVec(24) = cFMAXP;
  dataVec(25) = cDMAXM;
  dataVec(26) = cFMAXM;
  dataVec(27) = cSP;

  dataVec(28) = gama;
  dataVec(29) = delta;

  /*dataVec(30) = cR4P;
  dataVec(31) = cR4M;*/

  //dataVec(30) = cFOLD;
  res = theChannel.sendVector(this->getDbTag(), commitTag, dataVec);
  if (res < 0)
    opserr << "MSAWSMaterial::sendSelf() - failed to send data\n";


  return res;
}

int
MSAWSMaterial::recvSelf(int commitTag, Channel &theChannel,
                        FEM_ObjectBroker &theBroker)
{
  int res = 0;

  static Vector dataVec(30);
  res = theChannel.recvVector(this->getDbTag(), commitTag, dataVec);

  if (res < 0) {
      opserr << "MSAWSMaterial::recvSelf() - failed to receive data\n";
      return res;
  }
  else {
    this->setTag((int)dataVec(0));
    F0     = dataVec(1);
    FI     = dataVec(2);
    DU     = dataVec(3);
    S0     = dataVec(4);
    R1     = dataVec(5);
    R2     = dataVec(6);
    R3     = dataVec(7);
    R4     = dataVec(8);
    ALPHA  = dataVec(9);
    BETA   = dataVec(10);
    cDISPL = dataVec(11);
```

```
   cSTIFF  = dataVec(12);
   cFORCE  = dataVec(13);
   cLPATH  = int(dataVec(14));
   cLPPREV = int(dataVec(15));
   cIYPLUS = int(dataVec(16));
   cIYMINS = int(dataVec(17));
   cDOLD   = dataVec(18);
   cDUNP   = dataVec(19);
   cFUNP   = dataVec(20);
   cDUNM   = dataVec(21);
   cFUNM   = dataVec(22);
   cDMAXP  = dataVec(23);
   cFMAXP  = dataVec(24);
   cDMAXM  = dataVec(25);
   cFMAXM  = dataVec(26);
   cSP     = dataVec(27);
        gama = dataVec(28);
        delta = dataVec(29);
        /*cR4P    = dataVec(30);
        cR4M    = dataVec(31);*/
        /* cFOLD  = dataVec(30);*/
   // set the trial values
   FORCE  = cFORCE;
   DISPL  = cDISPL;
        STIFF  = cSTIFF;
   LPATH  = cLPATH;
   LPPREV = cLPPREV;

  }

  return res;
}

void
MSAWSMaterial::Print(OPS_Stream &s, int flag)
{

        s << "MSAWSMaterial, tag: " << this->getTag() << endln;
        s << "F0: " << F0 << endln;
        s << "FI: " << FI << endln;
        s << "DU: " << DU << endln;
        s << "S0: " << S0 << endln;
        s << "R1: " << R1 << endln;
        s << "R2: " << R2 << endln;
        s << "R3: " << R3 << endln;
        s << "R4: " << R4 << endln;
        s << "ALPHA: " << ALPHA << endln;
        s << "BETA: " << BETA << endln;
        s << "gama: " << gama << endln;
        s << "delta: " << delta << endln;
        s << "  stress: " << FORCE << " tangent: " << STIFF << endln;
}
```

Appendix E *OpenSees* **script of numerical simulation**

The script of the numerical simulation :

```
wipe
puts "system"
model basic -ndm 3 -ndf 6
puts "node"
set h 0.95;  #height
set s 1.82;  #width
set l 1.21;  #length
set h2 [expr $h+0.91];
set h3 [expr $h+0.91*2];
set s2 [expr $s*2];
set s3 [expr $s*3];
set l2 [expr $l*2];
set l3 [expr $l*3];

# ------------wood part-----------------

node 1 0 0 0
node 2 $s 0 0
node 3 $s 0 $h
node 4 $s 0 $h
node 5 $s 0 $h
node 6 $s 0 $h2
node 7 $s 0 $h2
node 8 $s 0 $h2
node 9 $s 0 $h3
node 10 $s 0 $h3
node 11 0 0 $h3
node 12 0 0 $h3
node 13 0 0 $h2
node 14 0 0 $h2
node 15 0 0 $h2
node 16 0 0 $h
node 17 0 0 $h
node 18 0 0 $h
node 19 $s 0 $h
node 20 $s $l $h
node 21 0 0 $h
node 22 0 $l $h
node 23 $s 0 $h2
node 24 $s $l $h2
node 25 0 0 $h2
node 26 0 $l $h2
node 27 $s 0 $h3
node 28 $s $l $h3
node 29 0 0 $h3
node 30 0 $l $h3

node 101 0 $l 0
node 102 $s $l 0
node 103 $s $l $h
node 104 $s $l $h
node 105 $s $l $h
node 106 $s $l $h2
node 107 $s $l $h2
node 108 $s $l $h2
node 109 $s $l $h3
node 110 $s $l $h3
```

```
node 111 0 $l $h3
node 112 0 $l $h3
node 113 0 $l $h2
node 114 0 $l $h2
node 115 0 $l $h2
node 116 0 $l $h
node 117 0 $l $h
node 118 0 $l $h
node 119 $s $l $h
node 120 $s $l2 $h
node 121 0 $l $h
node 122 0 $l2 $h
node 123 $s $l $h2
node 124 $s $l2 $h2
node 125 0 $l $h2
node 126 0 $l2 $h2
node 127 $s $l $h3
node 128 $s $l2 $h3
node 129 0 $l $h3
node 130 0 $l2 $h3

node 201 0 $l2 0
node 202 $s $l2 0
node 203 $s $l2 $h
node 204 $s $l2 $h
node 205 $s $l2 $h
node 206 $s $l2 $h2
node 207 $s $l2 $h2
node 208 $s $l2 $h2
node 209 $s $l2 $h3
node 210 $s $l2 $h3
node 211 0 $l2 $h3
node 212 0 $l2 $h3
node 213 0 $l2 $h2
node 214 0 $l2 $h2
node 215 0 $l2 $h2
node 216 0 $l2 $h
node 217 0 $l2 $h
node 218 0 $l2 $h
node 219 $s $l2 $h
node 220 $s $l3 $h
node 221 0 $l2 $h
node 222 0 $l3 $h
node 223 $s $l2 $h2
node 224 $s $l3 $h2
node 225 0 $l2 $h2
node 226 0 $l3 $h2
node 227 $s $l2 $h3
node 228 $s $l3 $h3
node 229 0 $l2 $h3
node 230 0 $l3 $h3

#-----------core part--------------

node 301 0 $l3 0
node 302 $s $l3 0
node 303 $s $l3 $h
node 304 $s $l3 $h
node 305 $s $l3 $h
node 306 $s $l3 $h2
node 307 $s $l3 $h2
node 308 $s $l3 $h2
```

```
node 309 $s $l3 $h3
node 310 $s $l3 $h3
node 311 0 $l3 $h3
node 312 0 $l3 $h3
node 313 0 $l3 $h2
node 314 0 $l3 $h2
node 315 0 $l3 $h2
node 316 0 $l3 $h
node 317 0 $l3 $h
node 318 0 $l3 $h
#
node 1001 0 0 0
node 1002 $s 0 0
node 1101 0       $l 0
node 1102 $s $l 0
node 1201 0       $l2 0
node 1202 $s $l2 0
node 1301 0       $l3 0
node 1302 $s $l3 0

puts "restrain"
fix 1001 1 1 1 1 1 1;
fix 1002 1 1 1 1 1 1;
fix 1101 1 1 1 1 1 1 ;
fix 1102 1 1 1 1 1 1 ;
fix 1201 1 1 1 1 1 1 ;
fix 1202 1 1 1 1 1 1 ;
fix 1301 1 1 1 1 1 1 ;
fix 1302 1 1 1 1 1 1 ;
fix 401 1 1 1 1 1 1;
fix 402 1 1 1 1 1 1;
fix 501 1 1 1 1 1 1;
fix 502 1 1 1 1 1 1;

puts "mass"
mass 4 95.0 95.0 95.0 10.16 40.26 51.95
mass 7 95.0 95.0 95.0 10.16 40.26 51.95
mass 10 61.75 61.75 61.75 6.1 25.29 31.23
mass 11 61.75 61.75 61.75 6.1 25.29 31.23
mass 14 95.0 95.0 95.0 10.16 40.26 51.95
mass 17 95.0 95.0 95.0 10.16 40.26 51.95
mass 104 168.0 168.0 168.0 18.20 80.53 99.38
mass 107 168.0 168.0 168.0 18.20 80.53 99.38
mass 110 109.0 109.0 109.0 11.13 49.58 61.57
mass 111 109.0 109.0 109.0 11.13 49.58 61.57
mass 114 168.0 168.0 168.0 18.20 80.53 99.38
mass 117 168.0 168.0 168.0 18.20 80.53 99.38
mass 204 164.2 164.2 164.2 18.20 80.53 99.38
mass 207 156.0 156.0 156.0 18.20 80.53 99.38
mass 210 104.5 104.5 104.5 11.13 49.58 61.57
mass 211 104.5 104.5 104.5 11.13 49.58 61.57
mass 214 156.0 156.0 156.0 18.20 80.53 99.38
mass 217 164.2 164.2 164.2 18.20 80.53 99.38

mass 304 380.1 380.1 380.1 0 0 0
mass 317 380.1 380.1 380.1 0 0 0
mass 307 340.1 340.1 340.1 0 0 0
mass 314 340.1  340.1 340.1 0 0 0
mass 310 270.1 270.1 270.1 0 0 0
mass 311 270.1 270.1 270.1 0 0 0

puts "transf"
```

```
geomTransf PDelta 1 1 0 0;# wood column/steel truss 2
geomTransf PDelta  2 0 0 1;
geomTransf PDelta  3 0 0 1;#steel truss
geomTransf PDelta  4 0 1 0; #steel column/beam

puts "element-beam&column"
set AC [expr 0.06*0.06];
set AB [expr 0.06*0.15];
set E 9500.0E13;# ragid
set G 1.5e10;# ragid
set JC [expr 0.141*0.06*pow(0.06,3)];# the torsional moment of the section
set JB [expr 0.249*0.15*pow(0.06,3)];
set Iyc [expr pow(0.06,4)/12];
set Izc [expr pow(0.06,4)/12];
set Iyb [expr 0.6*pow(0.15,3)/12]; #the second moment
set Izb [expr 0.15*pow(0.06,3)/12];
#element elasticBeamColumn $eleTag $iNode $jNode $A    $E   $G    $J    $Iy   $Iz
$transfTag
element elasticBeamColumn 1 1 18 $AC $E $G $JC $Iyc $Izc 1
element elasticBeamColumn 2 2 3 $AC $E $G $JC $Iyc $Izc 1
element elasticBeamColumn 3 17 4 $AB $E $G $JB $Iyb $Izb 2
element elasticBeamColumn 4 5 6 $AC $E $G $JC $Iyc $Izc 1
element elasticBeamColumn 5 14 7 $AB $E $G $JB $Iyb $Izb 2
element elasticBeamColumn 6 16 15 $AC $E $G $JC $Iyc $Izc 1
element elasticBeamColumn 7 8 9 $AC $E $G $JC $Iyc $Izc 1
element elasticBeamColumn 8 11 10 $AB $E $G $JB $Iyb $Izb 2
element elasticBeamColumn 9 13 12 $AC $E $G $JC $Iyc $Izc 1
element elasticBeamColumn 10 19 20 $AB $E $G $JB $Iyb $Izb 3
element elasticBeamColumn 11 21 22 $AB $E $G $JB $Iyb $Izb 3
element elasticBeamColumn 12 23 24 $AB $E $G $JB $Iyb $Izb 3
element elasticBeamColumn 13 25 26 $AB $E $G $JB $Iyb $Izb 3
element elasticBeamColumn 14 27 28 $AB $E $G $JB $Iyb $Izb 3
element elasticBeamColumn 15 29 30 $AB $E $G $JB $Iyb $Izb 3

element elasticBeamColumn 101 101 118 $AC $E $G $JC $Iyc $Izc 1
element elasticBeamColumn 102 102 103 $AC $E $G $JC $Iyc $Izc 1
element elasticBeamColumn 103 117 104 $AB $E $G $JB $Iyb $Izb 2
element elasticBeamColumn 104 105 106 $AC $E $G $JC $Iyc $Izc 1
element elasticBeamColumn 105 114 107 $AB $E $G $JB $Iyb $Izb 2
element elasticBeamColumn 106 116 115 $AC $E $G $JC $Iyc $Izc 1
element elasticBeamColumn 107 108 109 $AC $E $G $JC $Iyc $Izc 1
element elasticBeamColumn 108 111 110 $AB $E $G $JB $Iyb $Izb 2
element elasticBeamColumn 109 113 112 $AC $E $G $JC $Iyc $Izc 1
element elasticBeamColumn 110 119 120 $AB $E $G $JB $Iyb $Izb 3
element elasticBeamColumn 111 121 122 $AB $E $G $JB $Iyb $Izb 3
element elasticBeamColumn 112 123 124 $AB $E $G $JB $Iyb $Izb 3
element elasticBeamColumn 113 125 126 $AB $E $G $JB $Iyb $Izb 3
element elasticBeamColumn 114 127 128 $AB $E $G $JB $Iyb $Izb 3
element elasticBeamColumn 115 129 130 $AB $E $G $JB $Iyb $Izb 3

element elasticBeamColumn 201 201 218 $AC $E $G $JC $Iyc $Izc 1
element elasticBeamColumn 202 202 203 $AC $E $G $JC $Iyc $Izc 1
element elasticBeamColumn 203 217 204 $AB $E $G $JB $Iyb $Izb 2
element elasticBeamColumn 204 205 206 $AC $E $G $JC $Iyc $Izc 1
element elasticBeamColumn 205 214 207 $AB $E $G $JB $Iyb $Izb 2
element elasticBeamColumn 206 216 215 $AC $E $G $JC $Iyc $Izc 1
element elasticBeamColumn 207 208 209 $AC $E $G $JC $Iyc $Izc 1
element elasticBeamColumn 208 211 210 $AB $E $G $JB $Iyb $Izb 2
element elasticBeamColumn 209 213 212 $AC $E $G $JC $Iyc $Izc 1
element elasticBeamColumn 210 219 220 $AB $E $G $JB $Iyb $Izb 3
element elasticBeamColumn 211 221 222 $AB $E $G $JB $Iyb $Izb 3
element elasticBeamColumn 212 223 224 $AB $E $G $JB $Iyb $Izb 3
```

```
element elasticBeamColumn 213 225 226 $AB $E $G $JB $Iyb $Izb 3
element elasticBeamColumn 214 227 228 $AB $E $G $JB $Iyb $Izb 3
element elasticBeamColumn 215 229 230 $AB $E $G $JB $Iyb $Izb 3

element elasticBeamColumn 301 301 318 $AC $E $G $JC $Iyc $Izc 1
element elasticBeamColumn 302 302 303 $AC $E $G $JC $Iyc $Izc 1
element elasticBeamColumn 303 317 304 $AB $E $G $JB $Iyb $Izb 2
element elasticBeamColumn 304 305 306 $AC $E $G $JC $Iyc $Izc 1
element elasticBeamColumn 305 314 307 $AB $E $G $JB $Iyb $Izb 2
element elasticBeamColumn 306 316 315 $AC $E $G $JC $Iyc $Izc 1
element elasticBeamColumn 307 308 309 $AC $E $G $JC $Iyc $Izc 1
element elasticBeamColumn 308 311 310 $AB $E $G $JB $Iyb $Izb 2
element elasticBeamColumn 309 313 312 $AC $E $G $JC $Iyc $Izc 1

#------------------------elastic frame------------------------
puts "beam&column joint"
#uniaxialMaterial ElasticMultiLinear 1 -strain -0.03 -0.005 0.0 0.005 0.03 -
stress -2275.0 -1025.0 0.0 1025.0 2275.0
uniaxialMaterial ElasticMultiLinear 9 -strain [expr -0.03/$h] [expr -0.005/$h]
0.0 [expr 0.005/$h]  [expr 0.03/$h] -stress [expr -2275.0/4] [expr -1025.0/4]
0.0 [expr 1025.0/4] [expr 2275.0/4];
uniaxialMaterial ElasticMultiLinear 99 -strain [expr -0.03/$h] [expr -
0.005/$h] 0.0 [expr 0.005/$h]  [expr 0.03/$h] -stress [expr -3350.0/4] [expr -
2050.0/4] 0.0 [expr 2050.0/4] [expr 3350.0/4];
uniaxialMaterial Elastic 1 1.0;

element zeroLength 16 18 17 -mat 9 1 9 -dir 4 5 6 -orient 1 0 0 0 1 0
element zeroLength 17 3 4 -mat 9 1 9 -dir 4 5 6 -orient 1 0 0 0 1 0
element zeroLength 18 4 5 -mat 9 1 9 -dir 4 5 6 -orient 1 0 0 0 1 0
element zeroLength 19 17 16 -mat 9 1 9 -dir 4 5 6 -orient 1 0 0 0 1 0
element zeroLength 20 6 7 -mat 9 1 9 -dir 4 5 6 -orient 1 0 0 0 1 0
element zeroLength 21 15 14 -mat 9 1 9 -dir 4 5 6 -orient 1 0 0 0 1 0
element zeroLength 22 7 8 -mat 9 1 9 -dir 4 5 6 -orient 1 0 0 0 1 0
element zeroLength 23 14 13 -mat 9 1 9 -dir 4 5 6 -orient 1 0 0 0 1 0
element zeroLength 24 9 10 -mat 9 1 9 -dir 4 5 6 -orient 1 0 0 0 1 0
element zeroLength 25 12 11 -mat 9 1 9 -dir 4 5 6 -orient 1 0 0 0 1 0
element zeroLength 26 4 19 -mat 9 9 1 -dir 4 5 6 -orient 1 0 0 0 1 0
element zeroLength 27 20 104 -mat 9 9 1 -dir 4 5 6 -orient 1 0 0 0 1 0
element zeroLength 28 17 21 -mat 9 9 1 -dir 4 5 6 -orient 1 0 0 0 1 0
element zeroLength 29 22 117 -mat 9 9 1 -dir 4 5 6 -orient 1 0 0 0 1 0
element zeroLength 30 7 23 -mat 9 9 1 -dir 4 5 6 -orient 1 0 0 0 1 0
element zeroLength 31 24 107 -mat 9 9 1 -dir 4 5 6 -orient 1 0 0 0 1 0
element zeroLength 32 14 25 -mat 9 9 1 -dir 4 5 6 -orient 1 0 0 0 1 0
element zeroLength 33 26 114 -mat 9 9 1 -dir 4 5 6 -orient 1 0 0 0 1 0
element zeroLength 34 10 27 -mat 9 9 1 -dir 4 5 6 -orient 1 0 0 0 1 0
element zeroLength 35 28 110 -mat 9 9 1 -dir 4 5 6 -orient 1 0 0 0 1 0
element zeroLength 36 11 29 -mat 9 9 1 -dir 4 5 6 -orient 1 0 0 0 1 0
element zeroLength 37 30 111 -mat 9 9 1 -dir 4 5 6 -orient 1 0 0 0 1 0
element zeroLength 50 1001 1 -mat 9 1 9 -dir 4 5 6 -orient 1 0 0 0 1 0
element zeroLength 51 1002 2 -mat 9 1 9 -dir 4 5 6 -orient 1 0 0 0 1 0

element zeroLength 116 118 117 -mat 9 1 9 -dir 4 5 6 -orient 1 0 0 0 1 0
element zeroLength 117 103 104 -mat 9 1 9 -dir 4 5 6 -orient 1 0 0 0 1 0
element zeroLength 118 104 105 -mat 9 1 9 -dir 4 5 6 -orient 1 0 0 0 1 0
element zeroLength 119 117 116 -mat 9 1 9 -dir 4 5 6 -orient 1 0 0 0 1 0
element zeroLength 120 106 107 -mat 9 1 9 -dir 4 5 6 -orient 1 0 0 0 1 0
element zeroLength 121 115 114 -mat 9 1 9 -dir 4 5 6 -orient 1 0 0 0 1 0
element zeroLength 122 107 108 -mat 9 1 9 -dir 4 5 6 -orient 1 0 0 0 1 0
element zeroLength 123 114 113 -mat 9 1 9 -dir 4 5 6 -orient 1 0 0 0 1 0
element zeroLength 124 109 110 -mat 9 1 9 -dir 4 5 6 -orient 1 0 0 0 1 0
element zeroLength 125 112 111 -mat 9 1 9 -dir 4 5 6 -orient 1 0 0 0 1 0
element zeroLength 126 104 119 -mat 9 9 1 -dir 4 5 6 -orient 1 0 0 0 1 0
```

```
element zeroLength 127 120 204 -mat 9 9 1 -dir 4 5 6 -orient 1 0 0 0 1 0
element zeroLength 128 117 121 -mat 9 9 1 -dir 4 5 6 -orient 1 0 0 0 1 0
element zeroLength 129 122 217 -mat 9 9 1 -dir 4 5 6 -orient 1 0 0 0 1 0
element zeroLength 130 107 123 -mat 9 9 1 -dir 4 5 6 -orient 1 0 0 0 1 0
element zeroLength 131 124 207 -mat 9 9 1 -dir 4 5 6 -orient 1 0 0 0 1 0
element zeroLength 132 114 125 -mat 9 9 1 -dir 4 5 6 -orient 1 0 0 0 1 0
element zeroLength 133 126 214 -mat 9 9 1 -dir 4 5 6 -orient 1 0 0 0 1 0
element zeroLength 134 110 127 -mat 9 9 1 -dir 4 5 6 -orient 1 0 0 0 1 0
element zeroLength 135 128 210 -mat 9 9 1 -dir 4 5 6 -orient 1 0 0 0 1 0
element zeroLength 136 111 129 -mat 9 9 1 -dir 4 5 6 -orient 1 0 0 0 1 0
element zeroLength 137 130 211 -mat 9 9 1 -dir 4 5 6 -orient 1 0 0 0 1 0
element zeroLength 150 1101 101 -mat 9 1 9 -dir 4 5 6 -orient 1 0 0 0 1 0
element zeroLength 151 1102 102 -mat 9 1 9 -dir 4 5 6 -orient 1 0 0 0 1 0


element zeroLength 216 218 217 -mat 9 1 9 -dir 4 5 6 -orient 1 0 0 0 1 0
element zeroLength 217 203 204 -mat 9 1 9 -dir 4 5 6 -orient 1 0 0 0 1 0
element zeroLength 218 204 205 -mat 9 1 9 -dir 4 5 6 -orient 1 0 0 0 1 0
element zeroLength 219 217 216 -mat 9 1 9 -dir 4 5 6 -orient 1 0 0 0 1 0
element zeroLength 220 206 207 -mat 9 1 9 -dir 4 5 6 -orient 1 0 0 0 1 0
element zeroLength 221 215 214 -mat 9 1 9 -dir 4 5 6 -orient 1 0 0 0 1 0
element zeroLength 222 207 208 -mat 9 1 9 -dir 4 5 6 -orient 1 0 0 0 1 0
element zeroLength 223 214 213 -mat 9 1 9 -dir 4 5 6 -orient 1 0 0 0 1 0
element zeroLength 224 209 210 -mat 9 1 9 -dir 4 5 6 -orient 1 0 0 0 1 0
element zeroLength 225 212 211 -mat 9 1 9 -dir 4 5 6 -orient 1 0 0 0 1 0
element zeroLength 226 204 219 -mat 9 9 1 -dir 4 5 6 -orient 1 0 0 0 1 0
element zeroLength 227 220 304 -mat 9 9 1 -dir 4 5 6 -orient 1 0 0 0 1 0
element zeroLength 228 217 221 -mat 9 9 1 -dir 4 5 6 -orient 1 0 0 0 1 0
element zeroLength 229 222 317 -mat 9 9 1 -dir 4 5 6 -orient 1 0 0 0 1 0
element zeroLength 230 207 223 -mat 9 9 1 -dir 4 5 6 -orient 1 0 0 0 1 0
element zeroLength 231 224 307 -mat 9 9 1 -dir 4 5 6 -orient 1 0 0 0 1 0
element zeroLength 232 214 225 -mat 9 9 1 -dir 4 5 6 -orient 1 0 0 0 1 0
element zeroLength 233 226 314 -mat 9 9 1 -dir 4 5 6 -orient 1 0 0 0 1 0
element zeroLength 234 210 227 -mat 9 9 1 -dir 4 5 6 -orient 1 0 0 0 1 0
element zeroLength 235 228 310 -mat 9 9 1 -dir 4 5 6 -orient 1 0 0 0 1 0
element zeroLength 236 211 229 -mat 9 9 1 -dir 4 5 6 -orient 1 0 0 0 1 0
element zeroLength 237 230 311 -mat 9 9 1 -dir 4 5 6 -orient 1 0 0 0 1 0
element zeroLength 250 1201 201 -mat 9 1 9 -dir 4 5 6 -orient 1 0 0 0 1 0
element zeroLength 251 1202 202 -mat 9 1 9 -dir 4 5 6 -orient 1 0 0 0 1 0



puts "spring"
#K0-K5 follow the Fig 2.17 on page 39 of paper02 units N,M,Pa
#for shearwall
#-------------------------------X1--------------------------------------
set F0 6325.5; #N
set F1 475.0
set S0 1254.4e3;#N/m
set S1 32.5e3
set S2 150.0e3
set S3 1190.3e3
set S4 15.0e3
set DU 0.100; #m
set alpha 0.5
set beta 1.1
set gama 1.2
set delta 0.9
#R0-R4 follow the fig of opensees SAWS guide
set R1 [expr $S1/$S0]
set R2 [expr -$S2/$S0]
set R3 [expr $S3/$S0]
set R4 [expr $S4/$S0]
```

```
# the shearwall parameters need to be turned into element parameters
set p1 [expr (pow($s,2)+pow($h,2))/(2*pow($s,2))];
set coss [expr $s/(sqrt(pow($s,2)+pow($h,2)))];
set sins [expr $h/(sqrt(pow($s,2)+pow($h,2)))];
set p2 [expr 1/(2*$coss)];
set sF0 [expr $p2*$F0];
set sF1 [expr $p2*$F1];
set sDU [expr $coss*$DU];
set sS0 [expr $p1*$S0];

uniaxialMaterial MSAWSMaterial 1002 $sF0 $sF1 $sDU $sS0 $R1 $R2 $R3 $R4 $alpha
$beta $gama $delta;

#-------------------------------X2-------------------------------------
uniaxialMaterial MSAWSMaterial 2002 $sF0 $sF1 $sDU $sS0 $R1 $R2 $R3 $R4 $alpha
$beta $gama $delta;

#-------------------------------X3-------------------------------------
uniaxialMaterial MSAWSMaterial 3002 $sF0 $sF1 $sDU $sS0 $R1 $R2 $R3 $R4 $alpha
$beta $gama $delta;
#uniaxialMaterial MFatigueMaterial 2 1002 -m -0.54
puts "sw spring done!"

#for diaphragm

#-------------------------------F3-------------------------------------
set dF0 5486.7; #N
set dF1 650.0
set dS0 1336.0e3;#N/m
set dS1 143.3e3
set dS2 150.0e3
set dS3 2000.6e3
set dS4 30.0e3; #
set dDU 0.045;#m
set dalpha 0.3
set dbeta 1.1
set dgama 1.2
set ddelta 1.0
#R0-R4 follow the fig of opensees SAWS guide
set dR1 [expr $dS1/$dS0]
set dR2 [expr -$dS2/$dS0]
set dR3 [expr $dS3/$dS0]
set dR4 [expr $dS4/$dS0]
#the shearwall parameters need to be turned into element parameters
set dp1 [expr (pow($s,2)+pow($l,2))/(2*pow($s,2))];
set dcosd [expr $s/(sqrt(pow($s,2)+pow($l,2)))];
set dsind [expr $l/(sqrt(pow($s,2)+pow($l,2)))];
set dp2 [expr 1/(2*$dcosd)];
set dF0 [expr $dp2*$dF0];
set dF1 [expr $dp2*$dF1];
set dDU [expr $dcosd*$dDU];
set dS0 [expr $dp1*$dS0];
uniaxialMaterial MSAWSMaterial 3003 $dF0 $dF1 $dDU $dS0 $dR1 $dR2 $dR3 $dR4
$dalpha $dbeta $dgama $ddelta

#---------------------------------F1-----------------------------------
uniaxialMaterial MSAWSMaterial 1003 $dF0 $dF1 $dDU $dS0 $dR1 $dR2 $dR3 $dR4
$dalpha $dbeta $dgama $ddelta

#---------------------------------F2-----------------------------------
uniaxialMaterial MSAWSMaterial 2003 $dF0 $dF1 $dDU $dS0 $dR1 $dR2 $dR3 $dR4
$dalpha $dbeta $dgama $ddelta
```

```
#uniaxialMaterial MFatigueMaterial 3 1003 -m -0.54

puts "dia spring done!"
# how to define the area? area -mat
element twoNodeLink 38 17 2 -mat 1002 1 1 1 1 1 -dir 1 2 3 4 5 6 -orient 0 1 0
element twoNodeLink 39 1 4 -mat 1002 1 1 1 1 1 -dir 1 2 3 4 5 6 -orient 0 1 0
element twoNodeLink 40 14 4 -mat 1002 1 1 1 1 1 -dir 1 2 3 4 5 6 -orient 0 1 0
element twoNodeLink 41 17 7 -mat 1002 1 1 1 1 1 -dir 1 2 3 4 5 6 -orient 0 1 0
element twoNodeLink 42 11 7 -mat 1002 1 1 1 1 1 -dir 1 2 3 4 5 6 -orient 0 1 0
element twoNodeLink 43 14 10 -mat 1002 1 1 1 1 1 -dir 1 2 3 4 5 6 -orient 0 1
0
puts "1002 done!"
element twoNodeLink 44 4 117 -mat 1003 1 1 1 1 1 -dir 1 2 3 4 5 6 -orient 0 0
1
element twoNodeLink 45 17 104 -mat 1003 1 1 1 1 1 -dir 1 2 3 4 5 6 -orient 0 0
1
puts "1003 done!"
element twoNodeLink 46 7 114 -mat 2003 1 1 1 1 1 -dir 1 2 3 4 5 6 -orient 0 0
1
element twoNodeLink 47 14 107 -mat 2003 1 1 1 1 1 -dir 1 2 3 4 5 6 -orient 0 0
1
puts "2003 done!"
element twoNodeLink 48 10 111 -mat 3003 1 1 1 1 1 -dir 1 2 3 4 5 6 -orient 0 0
1
element twoNodeLink 49 11 110 -mat 3003 1 1 1 1 1 -dir 1 2 3 4 5 6 -orient 0 0
1
puts "3003 done!"

element twoNodeLink 138 117 102 -mat 2002 1 1 1 1 1 -dir 1 2 3 4 5 6 -orient 0
1 0
element twoNodeLink 139 101 104 -mat 2002 1 1 1 1 1 -dir 1 2 3 4 5 6 -orient 0
1 0
element twoNodeLink 140 114 104 -mat 2002 1 1 1 1 1 -dir 1 2 3 4 5 6 -orient 0
1 0
element twoNodeLink 141 117 107 -mat 2002 1 1 1 1 1 -dir 1 2 3 4 5 6 -orient 0
1 0
element twoNodeLink 142 111 107 -mat 2002 1 1 1 1 1 -dir 1 2 3 4 5 6 -orient 0
1 0
element twoNodeLink 143 114 110 -mat 2002 1 1 1 1 1 -dir 1 2 3 4 5 6 -orient 0
1 0
element twoNodeLink 144 104 217 -mat 1003 1 1 1 1 1 -dir 1 2 3 4 5 6 -orient 0
0 1
element twoNodeLink 145 117 204 -mat 1003 1 1 1 1 1 -dir 1 2 3 4 5 6 -orient 0
0 1
element twoNodeLink 146 107 214 -mat 2003 1 1 1 1 1 -dir 1 2 3 4 5 6 -orient 0
0 1
element twoNodeLink 147 114 207 -mat 2003 1 1 1 1 1 -dir 1 2 3 4 5 6 -orient 0
0 1
element twoNodeLink 148 110 211 -mat 3003 1 1 1 1 1 -dir 1 2 3 4 5 6 -orient 0
0 1
element twoNodeLink 149 111 210 -mat 3003 1 1 1 1 1 -dir 1 2 3 4 5 6 -orient 0
0 1

element twoNodeLink 238 217 202 -mat 3002 1 1 1 1 1 -dir 1 2 3 4 5 6 -orient 0
1 0
element twoNodeLink 239 201 204 -mat 3002 1 1 1 1 1 -dir 1 2 3 4 5 6 -orient 0
1 0
element twoNodeLink 240 214 204 -mat 3002 1 1 1 1 1 -dir 1 2 3 4 5 6 -orient 0
1 0
element twoNodeLink 241 217 207 -mat 3002 1 1 1 1 1 -dir 1 2 3 4 5 6 -orient 0
1 0
element twoNodeLink 242 211 207 -mat 3002 1 1 1 1 1 -dir 1 2 3 4 5 6 -orient 0
```

```
1 0
element twoNodeLink 243 214 210 -mat 3002 1 1 1 1 1 -dir 1 2 3 4 5 6 -orient 0
1 0
element twoNodeLink 244 204 317 -mat 1003 1 1 1 1 1 -dir 1 2 3 4 5 6 -orient 0
0 1
element twoNodeLink 245 217 304 -mat 1003 1 1 1 1 1 -dir 1 2 3 4 5 6 -orient 0
0 1
element twoNodeLink 246 207 314 -mat 2003 1 1 1 1 1 -dir 1 2 3 4 5 6 -orient 0
0 1
element twoNodeLink 247 214 307 -mat 2003 1 1 1 1 1 -dir 1 2 3 4 5 6 -orient 0
0 1
element twoNodeLink 248 210 311 -mat 3003 1 1 1 1 1 -dir 1 2 3 4 5 6 -orient 0
0 1
element twoNodeLink 249 211 310 -mat 3003 1 1 1 1 1 -dir 1 2 3 4 5 6 -orient 0
0 1


puts "steel core frame"

uniaxialMaterial Elastic 98 1.0e13;
#set p1 [expr (pow($s,2)+pow($h,2))/(2*pow($s,2))];
#set S0 1250.0e3
set NN 23;     #the ratio bewteen the core and the shear wall
set F0 [expr 6325.5*$NN]; #N
set F1 [expr 475.0*$NN]
set S0 [expr 1254.4e3*$NN];#N/m
set S1 [expr 32.5e3*$NN]
set S2 [expr 150.0e3*$NN]
set S3 [expr 1190.3e3*$NN]
set S4 [expr 15.0e3*$NN]
set DU 0.100; #m
set alpha 0.5
set beta 1.1
set gama 1.2
set delta 0.9
#R0-R4 follow the fig of opensees SAWS guide
set R1 [expr $S1/$S0]
set R2 [expr -$S2/$S0]
set R3 [expr $S3/$S0]
set R4 [expr $S4/$S0]
# the shearwall parameters need to be turned into element parameters
set p1 [expr (pow($s,2)+pow($h,2))/(2*pow($s,2))];
set coss [expr $s/(sqrt(pow($s,2)+pow($h,2)))];
set sins [expr $h/(sqrt(pow($s,2)+pow($h,2)))];
set p2 [expr 1/(2*$coss)];
set sF0 [expr $p2*$F0];
set sF1 [expr $p2*$F1];
set sDU [expr $coss*$DU];
set sS0 [expr $p1*$S0];

uniaxialMaterial MSAWSMaterial 10000 $sF0 $sF1 $sDU $sS0 $R1 $R2 $R3 $R4
$alpha $beta $gama $delta;

element twoNodeLink 338 317 302 -mat 10000 1 1 1 1 1 -dir 1 2 3 4 5 6 -orient
0 1 0
element twoNodeLink 339 301 304 -mat 10000 1 1 1 1 1 -dir 1 2 3 4 5 6 -orient
0 1 0
element twoNodeLink 340 314 304 -mat 10000 1 1 1 1 1 -dir 1 2 3 4 5 6 -orient
0 1 0
element twoNodeLink 341 317 307 -mat 10000 1 1 1 1 1 -dir 1 2 3 4 5 6 -orient
0 1 0
element twoNodeLink 342 311 307 -mat 10000 1 1 1 1 1 -dir 1 2 3 4 5 6 -orient
0 1 0
```

```
element twoNodeLink 343 314 310 -mat 10000 1 1 1 1 1 -dir 1 2 3 4 5 6 -orient
0 1 0

element zeroLength 316 318 317 -mat 98 1 98 -dir 4 5 6 -orient 1 0 0 0 1 0
element zeroLength 317  303 304 -mat 98 1 98 -dir 4 5 6 -orient 1 0 0 0 1 0
element zeroLength 318 304 305 -mat 98 1 98 -dir 4 5 6 -orient 1 0 0 0 1 0
element zeroLength 319 317 316 -mat 98 1 98 -dir 4 5 6 -orient 1 0 0 0 1 0
element zeroLength 320 306 307 -mat 98 1 98 -dir 4 5 6 -orient 1 0 0 0 1 0
element zeroLength 321 315 314 -mat 98 1 98 -dir 4 5 6 -orient 1 0 0 0 1 0
element zeroLength 322 307 308 -mat 98 1 98 -dir 4 5 6 -orient 1 0 0 0 1 0
element zeroLength 323 314 313 -mat 98 1 98 -dir 4 5 6 -orient 1 0 0 0 1 0
element zeroLength 324 309 310 -mat 98 1 98 -dir 4 5 6 -orient 1 0 0 0 1 0
element zeroLength 325 312 311 -mat 98 1 98 -dir 4 5 6 -orient 1 0 0 0 1 0
element zeroLength 350 1301 301 -mat 98 1 98 -dir 4 5 6 -orient 1 0 0 0 1 0
element zeroLength 351 1302 302 -mat 98 1 98 -dir 4 5 6 -orient 1 0 0 0 1 0


#--------------element---------------------

puts "equal dof"
equalDOF 17 18 1 2 3
equalDOF 4 3 1 2 3
equalDOF 4 5 1 2 3
equalDOF 17 16 1 2 3
equalDOF 7 6 1 2 3
equalDOF 14 15 1 2 3
equalDOF 7 8 1 2 3
equalDOF 14 13 1 2 3
equalDOF 10 9 1 2 3
equalDOF 11 12 1 2 3
equalDOF 4 19 1 2 3
equalDOF 104 20 1 2 3
equalDOF 17 21 1 2 3
equalDOF 117 22 1 2 3
equalDOF 7 23 1 2 3
equalDOF 107 24 1 2 3
equalDOF 14 25 1 2 3
equalDOF 114 26 1 2 3
equalDOF 10 27 1 2 3
equalDOF 110 28 1 2 3
equalDOF 11 29 1 2 3
equalDOF 111 30 1 2 3
equalDOF 1001 1 1 2 3
equalDOF 1002 2 1 2 3

equalDOF 117 118 1 2 3
equalDOF 104 103 1 2 3
equalDOF 104 105 1 2 3
equalDOF 117 116 1 2 3
equalDOF 107 106 1 2 3
equalDOF 114 115 1 2 3
equalDOF 107 108 1 2 3
equalDOF 114 113 1 2 3
equalDOF 110 109 1 2 3
equalDOF 111 112 1 2 3
equalDOF 104 119 1 2 3
equalDOF 204 120 1 2 3
equalDOF 117 121 1 2 3
equalDOF 217 122 1 2 3
equalDOF 107 123 1 2 3
equalDOF 207 124 1 2 3
equalDOF 114 125 1 2 3
equalDOF 214 126 1 2 3
```

```
equalDOF 110 127 1 2 3
equalDOF 210 128 1 2 3
equalDOF 111 129 1 2 3
equalDOF 211 130 1 2 3
equalDOF 1101 101 1 2 3
equalDOF 1102 102 1 2 3

equalDOF 217 218 1 2 3
equalDOF 204 203 1 2 3
equalDOF 204 205 1 2 3
equalDOF 217 216 1 2 3
equalDOF 207 206 1 2 3
equalDOF 214 215 1 2 3
equalDOF 207 208 1 2 3
equalDOF 214 213 1 2 3
equalDOF 210 209 1 2 3
equalDOF 211 212 1 2 3

equalDOF 204 219 1 2 3
equalDOF 304 220 1 2 3
equalDOF 217 221 1 2 3
equalDOF 317 222 1 2 3
equalDOF 207 223 1 2 3
equalDOF 307 224 1 2 3
equalDOF 214 225 1 2 3
equalDOF 314 226 1 2 3
equalDOF 210 227 1 2 3
equalDOF 310 228 1 2 3
equalDOF 211 229 1 2 3
equalDOF 311 230 1 2 3
equalDOF 1201 201 1 2 3
equalDOF 1202 202 1 2 3

equalDOF 317 318 1 2 3
equalDOF 304 303 1 2 3
equalDOF 304 305 1 2 3
equalDOF 317 316 1 2 3
equalDOF 307 306 1 2 3
equalDOF 314 315 1 2 3
equalDOF 307 308 1 2 3
equalDOF 314 313 1 2 3
equalDOF 310 309 1 2 3
equalDOF 311 312 1 2 3
equalDOF 1301 301 1 2 3
equalDOF 1302 302 1 2 3
#

#-------------------------eigen analysis----------------------------------
puts "eigen analysis"
if { [file exists output] == 0 } {

  file mkdir output;

}
set n 10; # the orders of the mode you want to calculate
for {set i 1} {$i<=$n} {incr i} {
set filename eigen$i
append filename _node.out
recorder Node -file output/$filename -node 1 2 4 7 10 11 14 17 101 102 104 107
110 111 114 117 201 202 204 207 210 211 214 217 304 307 310 311 314 317 401
402 404 407 410 411 414 417 501 502 504 507 510 511 514 517  -dof 1 2  "eigen
$i"
```

```
}

set numModes 40; # the total dof
set lambda [eigen $numModes] ;#-genBandArpack,-fullGenLapack
set eigen "Eigens.txt"
set Eigens [open $eigen "w"]
puts $Eigens " $lambda"
close $Eigens
record
puts "eigen ananlysis successed"


#------------------------rayleigh damping wood-------------------------------
--------
set xDamp 0.06; # the damping ratio
set nEigenI 1;
set nEigenJ 2;
set lambdaN [eigen [expr $nEigenJ]];
set lambdaI [lindex $lambdaN [expr $nEigenI-1]];
set lambdaJ [lindex $lambdaN [expr $nEigenJ-1]];
set omegaI [expr pow($lambdaI,0.5)];
set omegaJ [expr pow($lambdaJ,0.5)];
set alphaM [expr $xDamp*(2.0*$omegaI*$omegaJ)/($omegaI+$omegaJ)];
set betaKcurr [expr 2.0*$xDamp/($omegaI+$omegaJ)];
#rayleigh $alphaM $betaKcurr 0 0;
region 1 -nodeRange 1 400 -nodeRange 1000 1100 -rayleigh $alphaM $betaKcurr  0
0
#------------------------rayleigh damping steel------------------------------
set xDamp 0.02; # the damping ratio
set nEigenI 1;
set nEigenJ 2;
set lambdaN [eigen [expr $nEigenJ]];
set lambdaI [lindex $lambdaN [expr $nEigenI-1]];
set lambdaJ [lindex $lambdaN [expr $nEigenJ-1]];
set omegaI [expr pow($lambdaI,0.5)];
set omegaJ [expr pow($lambdaJ,0.5)];
set alphaM [expr $xDamp*(2.0*$omegaI*$omegaJ)/($omegaI+$omegaJ)];
set betaKcurr [expr 2.0*$xDamp/($omegaI+$omegaJ)];
region 2 -nodeRange 400 600 -rayleigh $alphaM $betaKcurr 0 0
#---------------------------------------------------------------------------
puts "recorder"

recorder Node -file output/node_dis.out -time -node 4 7 10 104 107 110 204 207
210  -dof 1 2 disp;
recorder Node -file output/node_acc.out -time -node 4 7 10 104 107 110 204 207
210 -dof 1 2 accel;
recorder Node -file output/nodes_dis.out -time -node 404 417 407 414 410 411  -
dof 1 2 disp;
recorder Node -file output/nodes_acc.out -time -node 404 417 407 414 410 411  -
dof 1 2 accel;

recorder Node -file output/node310_dis.out -time -node 310  -dof 1 2 disp;
recorder Node -file output/node307_dis.out -time -node 307  -dof 1 2 disp ;
recorder Node -file output/node304_dis.out -time -node 304  -dof 1 2 disp ;
recorder Node -file output/node310_acc.out -time -node 310  -dof 1 2 accel;
recorder Node -file output/node307_acc.out -time -node 307  -dof 1 2 accel;
recorder Node -file output/node304_acc.out -time -node 304  -dof 1 2 accel;

recorder Element -file output/ele38_f.out -time -ele 38  force;
recorder Element -file output/ele39_f.out -time -ele 39  force;
recorder Element -file output/ele40_f.out -time -ele 40  force;
recorder Element -file output/ele41_f.out -time -ele 41  force;
```

```
recorder Element -file output/ele42_f.out -time -ele 42  force;
recorder Element -file output/ele43_f.out -time -ele 43  force;
recorder Element -file output/ele44_f.out -time -ele 44  force;
recorder Element -file output/ele45_f.out -time -ele 45  force;
recorder Element -file output/ele46_f.out -time -ele 46  force;
recorder Element -file output/ele47_f.out -time -ele 47  force;
recorder Element -file output/ele48_f.out -time -ele 48  force;
recorder Element -file output/ele49_f.out -time -ele 49  force;

recorder Element -file output/ele138_f.out -time -ele 138  force;
recorder Element -file output/ele140_f.out -time -ele 140  force;
recorder Element -file output/ele142_f.out -time -ele 142  force;
recorder Element -file output/ele144_f.out -time -ele 144  force;
recorder Element -file output/ele146_f.out -time -ele 146  force;
recorder Element -file output/ele148_f.out -time -ele 148  force;

recorder Element -file output/ele238_f.out -time -ele 238  force;
recorder Element -file output/ele240_f.out -time -ele 240  force;
recorder Element -file output/ele242_f.out -time -ele 242  force;
recorder Element -file output/ele244_f.out -time -ele 244  force;
recorder Element -file output/ele246_f.out -time -ele 246  force;
recorder Element -file output/ele248_f.out -time -ele 248  force;
# axial force
recorder Element -file output/ele210_f.out -time -ele 210  force;
recorder Element -file output/ele211_f.out -time -ele 211  force;
recorder Element -file output/ele212_f.out -time -ele 212  force;
recorder Element -file output/ele213_f.out -time -ele 213  force;
recorder Element -file output/ele214_f.out -time -ele 214  force;
recorder Element -file output/ele215_f.out -time -ele 215  force;

recorder Element -file output/ele15_f.out -time -ele 15  force;
recorder Element -file output/ele115_f.out -time -ele 115  force;
recorder Element -file output/ele13_f.out -time -ele 13  force;
recorder Element -file output/ele113_f.out -time -ele 113  force;
recorder Element -file output/ele11_f.out -time -ele 11  force;
recorder Element -file output/ele111_f.out -time -ele 111  force;

recorder Element -file output/ele440_f.out -time -ele 440  force;
recorder Element -file output/ele441_f.out -time -ele 441  force;
recorder Element -file output/ele442_f.out -time -ele 442  force;
recorder Element -file output/ele443_f.out -time -ele 443  force;
recorder Element -file output/ele444_f.out -time -ele 444  force;
recorder Element -file output/ele445_f.out -time -ele 445  force;
recorder Element -file "Damage.out" -time -ele 38 material 2 damage

#-----------------------load gravity---------------------------------
puts "gravity"
pattern Plain 1 Linear {
load  4 0.E+00 0.E+00 -882 0.E+00 0.E+00 0.E+00
load  7 0.E+00 0.E+00 -882 0.E+00 0.E+00 0.E+00
load  10 0.E+00 0.E+00 -556.15 0.E+00 0.E+00 0.E+00
load  11 0.E+00 0.E+00 -556.15 0.E+00 0.E+00 0.E+00
load  14 0.E+00 0.E+00 -882 0.E+00 0.E+00 0.E+00
load  17 0.E+00 0.E+00 -882 0.E+00 0.E+00 0.E+00
load  104 0.E+00 0.E+00 -1646.4 0.E+00 0.E+00 0.E+00
load  107 0.E+00 0.E+00 -1646.4 0.E+00 0.E+00 0.E+00
load  110 0.E+00 0.E+00 -1068.2 0.E+00 0.E+00 0.E+00
load  111 0.E+00 0.E+00 -1068.2 0.E+00 0.E+00 0.E+00
load  114 0.E+00 0.E+00 -1646.4 0.E+00 0.E+00 0.E+00
load  117 0.E+00 0.E+00 -1646.4 0.E+00 0.E+00 0.E+00
load  204 0.E+00 0.E+00 -1658.16 0.E+00 0.E+00 0.E+00
load  207 0.E+00 0.E+00 -1577.8 0.E+00 0.E+00 0.E+00
```

```
load  210 0.E+00 0.E+00 -1073.1 0.E+00 0.E+00 0.E+00
load  211 0.E+00 0.E+00 -1073.1 0.E+00 0.E+00 0.E+00
load  214 0.E+00 0.E+00 -1577.8 0.E+00 0.E+00 0.E+00
load  217 0.E+00 0.E+00 -1658.16 0.E+00 0.E+00 0.E+00
load  304 0.E+00 0.E+00 -588.98 0.E+00 0.E+00 0.E+00
load  317 0.E+00 0.E+00 -588.98 0.E+00 0.E+00 0.E+00
load  307 0.E+00 0.E+00 -588.98 0.E+00 0.E+00 0.E+00
load  314 0.E+00 0.E+00 -588.98 0.E+00 0.E+00 0.E+00
load  310 0.E+00 0.E+00 -588.98 0.E+00 0.E+00 0.E+00
load  311 0.E+00 0.E+00 -588.98 0.E+00 0.E+00 0.E+00
}
puts "gravity analysis"
constraints Transformation
numberer Plain
system BandGeneral
test EnergyIncr 1.0e-6 200
algorithm Newton
integrator LoadControl 0.5
analysis Static
analyze 10


loadConst -time 0.0
puts "timehistory analysis"
puts "load"
set IDloadTag 1001; #tag of node 1001
set num 5;    #the interpolation number of the original record
set iGMfile "GM3-5.txt"; # the ground motion used as input, pga=350gal,
dt=0.01s
set iGMdirection "1";  #the direction of inout: 1 for x,2 for y
set PGA 0.8;         #the PGA of the input 9.8*0.6/350=0.0168
if {$iGMfile=="GM3-5.txt"} { ; # dt=0.002, 34645*3 ,unit cm/s^2 max 350
set iGMfact "[expr $PGA*9.8/350]"   ; #the factor to calibrate the pga of the
original record
} elseif {$iGMfile=="GM3-5table.txt"} { ; #% dt=0.002, 39675*3 ,unit cm/s^2
max 739
set iGMfact "[expr $PGA*9.8/739]" ;
}
set dt [expr 0.01/$num];         #the new dt
foreach GMdirection $iGMdirection GMfile $iGMfile GMfact $iGMfact {
incr IDloadTag;
set GMfatt [expr 1*$GMfact];
set AccelSeries "Series -dt $dt -filePath $GMfile -factor $GMfatt";
pattern UniformExcitation $IDloadTag $GMdirection -accel $AccelSeries;
 } ;
puts "analysis"
constraints Transformation
integrator Newmark 0.5 0.25
#integrator CentralDifference
numberer Plain
system UmfPack
analysis Transient
#test EnergyIncr 1.0e-8 100 2
test NormDispIncr 1.0e-6 100 2
algorithm Newton

# use different algorithm to implement the analysis
set ok 0;
if {$iGMfile=="GM3-5.txt"} { ;#% dt=0.002, 34645*3 ,unit cm/s^2 max 350
set step [expr 6929*$num*3]    ; #the factor to calibrate the pga of the
original record
} elseif {$iGMfile=="GM3-5table.txt"} { ; #% dt=0.002, 39675*3 ,unit cm/s^2
```

```
max 739
set step [expr 39675*3];
}

set maxTime [expr $step*$dt]
set currentTime 0
set currentStep 1
while {$ok==0&&$currentTime<$maxTime} {

  set ok [analyze 1 $dt];
# if analysis was not successfull
# 1st change to modified newton
    if {$ok!=0} {
    puts "regular newton failed.. lets try modified newton for this step"
    test NormDispIncr  1.0e-8 100 2;
    algorithm ModifiedNewton
    set ok [analyze 1 $dt]
    test EnergyIncr 1.0e-8 100 2; #back to newton
    algorithm Newton
            };
#2nd change to initial stiffness Newton
    if {$ok!=0} {
    puts "Modified newton failed.. lets try an initial stiffness for this
step";
    test NormDispIncr  1.0e-8 100 2
    algorithm Newton -initial
    set ok [analyze 1 $dt]
        if {$ok==0} {
        puts "Initial stiffness works... back to regular newton";
        test NormDispIncr  1.0e-8 100 2
        algorithm Newton
                } elseif { $ok!=0 } {
          puts "ModifiedNewton and Initial stiffness both failed... please
try something else";
          test NormDispIncr  1.0e-8 100 2;
          algorithm Newton
                            }
            }
#3nd change to krylov-newton Newton
if {$ok!=0} {
    puts " lets try krylov-newton for this step"
    test NormDispIncr  1.0e-6 100 2;
    algorithm KrylovNewton
    set ok [analyze 1 $dt]
    test NormDispIncr  1.0e-8 100 2; #back to newton
    algorithm Newton
            };
#4nd change to Newton with Line Search
if {$ok!=0} {
    puts " lets try newton with line search for this step"
    test NormDispIncr  1.0e-6 1000 2;
    algorithm NewtonLineSearch
    set ok [analyze 1 $dt]
    test NormDispIncr  1.0e-8 100 2; #back to newton
    algorithm Newton
            };
#5nd change to Secant Newton
if {$ok!=0} {
    puts " lets try secant newton with line search for this step"
    test NormDispIncr  1.0e-6 1000 2;
    algorithm SecantNewton
    set ok [analyze 1 $dt]
```

```
        test NormDispIncr  1.0e-8 100 2; #back to newton
        algorithm Newton
                };
#5nd change to BFGS
if {$ok!=0} {
        puts " lets try BFGS for this step"
        test EnergyIncr 1.0e-6 10 2;
        algorithm BFGS
        set ok [analyze 1 $dt]
        test EnergyIncr 1.0e-8 100 2; #back to newton
        algorithm Newton
                };
#6nd change to Broyden
if {$ok!=0} {
        puts " lets try Broyden for this step"
        test EnergyIncr 1.0e-6 10 2;
        algorithm Broyden
        set ok [analyze 1 $dt]
        test EnergyIncr 1.0e-8 100 2; #back to newton
        algorithm Newton
                };

set currentTime [getTime]
set currentStep [expr $currentStep+1]
puts $currentStep
}

if {$ok==0} {
        puts "Time history analysis completed SUCCESSFULLY";
            } else {
        puts "Time history analysis completed FAILED";
}
```

Bibliography

Ahmadi, B. H., and Saka, M. P. (1993). "Behavior of composite timber-concrete floors." *Journal of Structural Engineering*, 119(11), 3111–3130.

ASCE (2010). *ASCE/SEI-7-10 Minimum Design Loads for Buildings*. American Society of Civil Engineers, Reston, VA.

BCJ (2016). *The Building Standard Law of Japan*. [in Japanese.] Building Center of Japan, Tokyo, Japan.

BRI (1992). "The technical guidance for the build of design earthquake input." [in Japanese.] Building Center of Japan, Building Research Institute, Tokyo, Japan.

Canada Wood Group (2017). "Wood-concrete hybrid construction." Accessed May 4, 2017. <http://www.canadawood.cn/downloads/pdf/tl/EngNo9-Wood−ConcreteHybridConstruction.pdf>.

Ceccotti, A., Sandhaas, C., Okabe, M., Yasumura, M., Minowa, C., and Kawai, N. (2013). "SOFIE project - 3D shaking table test on a seven-storey full-scale cross-laminated timber building." *Earthquake Engineering & Structural Dynamics*, 42(13), 2003–2021.

CEN. (2004). *Eurocode 8, Design of Structures for Earthquake Resistance-Part 1: General Rules, Seismic Actions, and Rules for Buildings (EN 1998-1:2004)*. Comité Européen de Normalisation, Brussels.

Charney, F. A. (2008). "Unintended consequences of modeling damping in structures." *Journal of Structural Engineering*, 134(4), 581–592.

Chopra, A. K. (1995). *Dynamics of Structures, Theory and Applications to Earthquake Engineering*. Prentice-Hall, Englewood Cliffs, NJ.

Christovasilis, I. P., Filiatrault, A., and Wanitkorkul, A. (2009). *Shaking Table Testing of a Full-Scaled Two-Story Light-Frame Wood Building: Neeswood Benchmark Test*. Technical Rep. MCEER-09-005. Buffalo, NY: State University of New York, Buffalo.

FEMA (2000). *PreStandard and Commentary for the Seismic Rehabilitation of Buildings (FEMA 356)*. Federal Emergency Management Agency, Washington, D.C.

FEMA (2003). *NEHRP Recommended Provisions for Seismic Regulations, for New Buildings and Other Structures (FEMA 450)*. Federal Emergency Management Agency, Washington, D.C.

FEMA (2007). *NEHRP Recommended Provisions for Seismic Regulations, for New Buildings and Other Structures: Training and Instructional Materials (FEMA 451B)*. Federal Emergency Management Agency, Washington, D.C.

FEMA (2009). *Quantification of Building Seismic Performance Factors (FEMA P695)*. Federal Emergency Management Agency, Washington, D.C.

Filiatrault, A., Christovasilis, I. P., Wanitkorkul, A., and van de Lindt, J. W. (2009). "Experimental seismic response of a full-scale light-frame wood building." *Journal of Structural Engineering*, 136(3), 246–254.

Folz, B., and Filiatrault, A. (2001). "Cyclic analysis of wood shear walls." *Journal of Structural Engineering*, 127(4), 433–441.

Gelfi, P., Giuriani, E., and Marini, A. (2002). "Stud shear connection design for composite concrete slab and wood beams." *Journal of Structural Engineering*, 128(12), 1544–1550.

Goertz, C., Mollaioli, F., and Tesfamariam, S. (2017). "Energy based seismic design of a timber core-wall multi-storey hybrid building." *Proceedings of 16th World Conference on Earthquake Engineering*, Santiago.

Harris, H. G., and Sabnis, G. (1999). *Structural Modeling and Experimental Techniques*. CRC Press, Boca Raton, Fl.

Hiyama, S. (2016). "Study on dynamic behavior of wooden horizontal hybrid structure." [in Japanese.] M.S. thesis, Tokyo Institute of Technology, Tokyo, Japan.

Humar, J., and Popovski, M. (2013). "Seismic response of single-storey buildings with flexible diaphragms." *Canadian Journal of Civil Engineering*, 40(9), 875–886.

ICBO (1997). *Uniform Building Code*. International Conference of Building Officials, Whittier, California.

Inayama, M., Koshihara, M., Kawahara, S., and et al. (2012). "Introduction of the structural prototype of wood school building." [in Japanese.] *Annual Convention of AIJ*, Tokai, Japan.

ICC (2006). *International Building Code*. International Code Council, Falls Church, VA.

Ishida, Y., Sakata, H., Takase, Y., Maida, Y., and Sato, T. (2018). "3D FEM analysis of post-installed adhesive anchors under combined stress: stress transmission mechanism and mechanical behavior of the joints for external seismic retrofitting Part 1" [in Japanese.] *Journal of Structural and Construction Engineering, Architectural Institute of Japan*, 83(751), 1307–1317.

Isoda, H., Kawai, N., Koshihara, M., Araki, Y., and Tesfamariam, S. (2017). "Timber-reinforced concrete core hybrid system: shake table experimental test." *Journal of Structural Engineering*, 143(1), 04016152.

Isoda, H., and Tesfamariam, S. (2016). "Connections for timber-concrete hybrid building: experimental and numerical model results." *Journal of Performance of Constructed Facilities*, 30(5), 04016024.

JHWTC (2008). *Allowable Stress Design Method for Framework Construction of Wooden House.* [in Japanese.] Japan Housing and Wood Technology Center, Tokyo.

JISC (2015). *Rolled Steels for General Structure (JIS G 3101).* [in Japanese.] Technical Committee on Steel Standards, Japanese Industrial Standards Committee, Tokyo.

Kaushik, K., and Tannert, T. (2017). "Feasibility study of a novel tall concrete-wood hybrid system." *Proceedings of Structures Congress 2017*, Denver, Colorado, 411–418.

Kim, S.-C., and White, D. W. (2004). "Nonlinear analysis of a one-story low-rise masonry building with a flexible diaphragm subjected to seismic excitation." *Engineering Structures*, 26(14), 2053–2067.

Koliou, M., Filiatrault, A., Kelly, D. J., and Lawson, J. (2016a). "Distributed yielding concept for improved seismic collapse performance of rigid wall-flexible diaphragm buildings." *Journal of Structural Engineering*, 142(2), 04015137.

Koliou, M., Filiatrault, A., Kelly, D. J., and Lawson, J. (2016b). "Buildings with rigid walls and flexible roof diaphragms. II: evaluation of a new seismic design approach based on distributed diaphragm yielding." *Journal of Structural Engineering*, 142(3), 04015167.

Lee, H. J., Kuchma, D., and Aschheim, M. A. (2007). "Strength-based design of flexible diaphragms in low-rise structures subjected to earthquake loading." *Engineering Structures*, 29(7), 1277–1295.

MAFF (2007). *Japanese Agricultural Standard for Glued Laminated Timber (JAS No. 1152).* [in Japanese.] Ministry of Agriculture, Forestry and Fisheries, Tokyo.

MAFF (2008). *Japanese Agricultural Standard for Plywood (JAS No. 1751).* [in Japanese.] Ministry of Agriculture, Forestry and Fisheries, Tokyo.

Matsushima, Y. (1995). *Research of Ground Motions Used for Dynamic Analysis of High-Rise Buildings.* [in Japanese.] Research Assistant Report of Japanese Building Center.

Ministry of Construction (1980). *Commentary on the Structural Calculation Based on the Revised Enforcement Order: Building Standard Law.* [in Japanese.] Building Center of Japan, Ministry of Construction, Housing Bureau, and Building Research Institute, Tsukuba, Japan.

Ministry of Construction (2003). *Code of Wood Structure Design (GB 50005-2003).* [in Chinese.] China Architecture and Building Press: Beijing, China.

Ministry of Construction (2005). *Code for Seismic Design of Buildings (GB 50011-2005).* [in Chinese.] China Architecture and Building Press, Beijing, China.

Mortazavi, P., and Humar, J. (2016). "Consideration of diaphragm flexibility in the seismic design of one-story buildings." *Engineering Structures*, 127, 748–758.

Mortazavi, P., and Humar, J. (2017). "Seismic design of single-story buildings with a nonlinear flexible roof diaphragm." *Proceedings of 16th World Conference on Earthquake Engineering*, Santiago.

NRCC. (2005). *National Building Code of Canada*. Canadian Commission on Building and Fire Codes, National Research Council of Canada, Ottawa, Ontario, Cananda.

PEER (2015). *OpenSees: Open System for Earthquake Engineering Simulation*. Pacific Earthquake Engineering Research Center, Berkeley, CA.

Sawada, S. (2016). "Experimental study on dynamic behavior of wooden horizontal hybrid structure." [in Japanese.] M.S. thesis, Tokyo Institute of Technology, Tokyo, Japan.

Steinberg, E., Selle, R., and Faust, T. (2003). "Connectors for timber-lightweight concrete composite structures." *Journal of Structural Engineering*, 129(11), 1538–1545.

Tomasi, R., Sartori, T., Casagrande, D., and Piazza, M. (2015). "Shaking table testing of a full-scale prefabricated three-story timber-frame building." *Journal of Earthquake Engineering*, 19(3), 505–534.

Tsuji, T., and Isoda, H. (2012). "Lateral force distribution and behavior of mixed structure of wood and reinforced concrete." [in Japanese.] *Journal of Japan Association for Earthquake Engineering*, 12(1).

Xiong, H., and Jia, G. (2008). "Research on seismic behavior of wood concrete hybrid structure system." *Proceedings of the 14th World Conference on Earthquake Engineering*, Beijing, China.

Yamazaki, Y., and Sakata, H. (2016). "Simplified modeling method and seismic force evaluation of building structures involving stiff cores: study on dynamic behavior of wooden horizontal hybrid structure Part 1." [in Japanese.] *Journal of Structural and Construction Engineering, Architectural Institute of Japan*, 720, 291–301.

Zhou, L., Ni, C., Chui, Y.-H., and Chen, Z. (2014). "Seismic performance of a hybrid building system consisting of a light wood frame structure and a reinforced masonry core." *Journal of Performance of Constructed Facilities*, 28(6), A4014013.

Acknowledgements

thanks for the fun you bring to me. It really means a lot for a foreign student who live alone in Japan.

2019.02.12
In Tokyo